Photochemical Methods for Arene Functionalization and Lignin Depolymerization

by

Timothy M. Monos

A dissertation submitted in partial fulfillment
of the requirements for the degree of
Doctor of Philosophy
(Chemistry)
in the University of Michigan
2018

Doctoral Committee

Professor Corey Stephenson, Chair
Professor John Montgomery
Assistant Professor Corinna Schindler
Professor Levi Thompson

Timothy M. Monos

tmonos@umich.edu

ORCID iD: 0000-0002-0599-1566

DEDICATION

To Emma, Mom, Dad and Andrew

ACKNOWLEDGEMENTS

I am greatly indebted to kind and patient mentorship of many in order to develop into a scientist and thinker competent enough to compile this monograph. First, I must thank Prof. Corey Stephenson for allowing me the opportunity to train in his lab. His consistent dedication to meeting to discuss research, current and classic literature and the study of formulating scientific arguments in writing gives me the confidence to move forward in my career in synthetic chemistry. He has been generous with supporting travel to conferences and professional development opportunities, both of which return focus and enthusiasm for lab work. I am also grateful to Prof. Corinna Schindler, for advising me in my first semester, participating in my thesis committee, and seeing through two NSF GRFP applications. I have also had the pleasure of teaching for and taking classes from Prof. John Montgomery. Thank you, Prof. Levi Thompson, for graciously joining my thesis committee. Finally, thank you to Dr. Kaid Harper for some key discussions about photochemistry that helped bring about some of the described chemistry.

Graduate school has introduced me to a swath of tenacious, dedicated and intelligent coworkers. I first would like to thank Rory McAtee and Alex Sun for their extensive help with writing and designing attractive chemdraws. Thank you to them and my other co-authors on publications: Gabe Magallanes, Leanne Sebren and Jim Devery. The scientific and personal mentorship I have received from John Nguyen, Bryan Matsuura, Joel Beatty, Mitch Keylor, Zac Garlets has been first rate and will not be easily forgotten. Post-doctoral support from James Douglas, Liz Swift, Daryl Staveness, Verner Loftstrand, Markus Karkas, Milena Cycz, Irene Bosque-Martinez,

Christian Malapit and Jim Devery has also been crucial in my achievements. I am thankful for a supportive cohort including Ahlam Armaly, Emilia Grosso, Paul Riehl, Yvonne Deporre, Melissa Lee, Eric Wiensch, Hillary Kerchner, Kendra Souther, Bijay Bhattarai and Jia Hui Tay. Thank you to the remainder of my co-workers from Corey and Corinna's labs including: Dirk Alpers, Taylor Sodano, Kevin Romero, Matthew Galliher, Ted McClain, James Collins, Hannah Vonesh, Cheng Yang, Xu Zhu, Martin Sevrin, Theresa Williams, Lara Cala, Vikram Shende, Alex Golonka, Jake Ludwig, James Annand, Rebecca Watson, Haley Albright, Chris McAtee, Dan Nasrallah and Marc Becker, you all have made this time memorable.

I would like to thank my friends and family outside of UM Chemistry. Thank you to my parents for supporting me and giving me the motivation to pursue a career in basic science research. Thank you to Emma, my wife, who boldly accepted my marriage proposal and has tackled the responsibilities of being the wife of a Ph.D. candidate. In the short course of five years, we have matured and grown in various directions, but am happily in love and admiring of your capacity to care for me. I look forward to returning the support as you embark on your own journey in graduate school starting this coming fall. Thank you to the remainder of my family, including my brother Andrew, my parents' in-law Hans and Carol, as well as the extended Monos-Holland and Bietsch families who have cheered me on from day one. Finally, I would like to thank my friends from Crossfit Lily, David Nims, Ernesto Witsitt, and Andrea Veltri for making Ann Arbor a town to enjoy.

I must also thank my mentors from the University Connecticut for encouraging my aspirations to pursue a graduate degree. These people include Prof. James Stuart, Dr. Anthony Provatas, Dr. Nicholas Leadbeater, Dr. Christopher Kelly, Dr. Trevor Hamlin and Dr. Michael Mercadante.

TABLE OF CONTENTS

LIST OF FIGURES

LIST OF TABLES

LIST OF ABBREVIATIONS

AcrH – 9,10-dihydroacridine

ADME - absorption, distribution, metabolism and excretion

ATRA – atom transfer radical addition

BDMAP - 1,6-bis(dimethylamino)pyrene

BNAH - Benzyl-1,4-dihydronicotinamide

BNA^+ – Benzylnicotinamdium cation

BT - 2-phenyl-dihydrobenzothaizoline

CAN - Ceric ammonium nitrate

CHD - 1,4-cyclohexadiene

CPO-biscyclopropanecarbonyl peroxide

CzIPN - 2,4,5,6-Tetra(9H-carbazol-9-yl)isophthalonitrile

DABCO - 1,4-diazabicyclo[2.2.2]octane

DCA - 9,10-dicyanoanthracene

$dF(CF_3ppy)_2$ = 2-(2,4-difluorophenyl)-5-trifluoromethyl pyridine

DHA - Dihydroacridine

DIPEA - diisopropylethylamine

DMF – dimethylformamide

DMSO – dimethylsulfoxide.

Dppb - 1,4-Bis(diphenylphosphino)butane

EDA – electron donor-acceptor

HEH - Hantszch's Ester

HOMO - highest occupied molecular orbital

*i*PrOH - isopropyl alcohol

$Ir(ppy)_3$ - Facial Iridium *tris*-phenylpyridine complex

LP - Lignin peroxidase

LUMO - lowest unoccupied molecular orbital

NADH - Nicotinamide adenine dinucleotide

SCE - Standard calomel electrode

*t*BPA - *tertiary*-butyl peracetate

TFA – trifluoroacetic acid or trifluoroacetate

TFAA – trifluoroacetic anhydride

TIPS-EBX - 1-[(Triisopropylsilyl)ethynyl]-1,2-benziodoxol-3(1H)-one

US DOE - United States Department of Energy

UV – Ultra-violet

Φ - Quantum Yield, chemical or photophysical

λ - Reorganization energy post electron transfer (Marcus Theory), or wavelength of light

ABSTRACT

The current demands of synthetic organic chemistry necessitate the generation of new molecules, for applications as materials and medicines, in a sustainable and energy efficient manner. Visible light photochemistry as a synthetic technology offers unique benefits to organic synthesis by converting abundantly available light energy into chemical energy through the reliable photophysical processes of specific organic dyes and organometallic complexes. Chemoselectivity and operational simplicity are central reaction designs of visible light promoted photoredox catalysis, as the selective excitation of the catalyst can occur at ambient termperature and pressure in the presence of many organic molecules. From the photoexcited state, a catalyst can engage in redox or energy transfer processes with organic molecules to generate reactive intermediates useful in organic synthesis.

Synthetically valuable functionalities such as the trifluoromethyl radical and aryl radicals have evaded the development of simple and environmentally benign synthetic methods. To render inert functionalities reactive, redox auxiliaries can be employed. Redox auxiliaries contain a redox labile functionality capable of interating with an excited state photocatalyst, as well as a predictably fragmentable pair of bonds; reagent design in this capacity harnesses both an enthalpic and entropic free energy contributions to generate the desired high energy intermiedate.

The efforts described herein summarize the application of visible light photocatalysis, and photochemistry for the synthesis of functionalized arenes and chemoselective C–X bond reduction for biomass valorization. These methods are unified through similar mechanistic hypotheses that begin with a photo-promoted redox transformation between a catalyst and substrate and finish with a critical bond fragmentation event to realize the desired product. To provide a broad summary of the context of this reaction design, Chapter 1 is a summary of the design priciples of visible light photoredox catalysis and the relevance of fragmentable redox auxiliaries. Chapter 2 supports the broad background of Chapter 1 by describing a simple and rapid synthesis of one class of visible light photoredox catalysts, the $Ir(III)^{+}$ polypyridyl complexes. Chapter 3 details the study of ketyl regulated C–X bond fragmentations as applied to the reduction of the β–O–4 bond in lignin biomass. Chapter 4 recounts a new method for alkene aminoarylation which employs arylsulfonamides as the sole reagent for amination and arylation. Lastly, Chapter 5 describes the development of a non-covalently associated electron donor-acceptor complex that is photoactivated for the trifluoromethylation of arenes.

Chapter 1: Redox Auxiliaries for Radical Generation in Photoredox Catalysis

* Portions of this chapter have been published in Monos, T.M.; Stephenson C.R.J. Photoredox Catalysis of Iridium(III)-Based Photosensitizers. In Iridium(III) in Optoelectronics and Photonics Applications; Zysman-Coleman, E., Ed.1; John Wiley and Sons: Pondicherry, 2017; Vol. 2; p 541.

1.1 Introduction: Photocatalysis Significance and Design Principles

For more than 100 years, chemical synthesis has afforded medicines and materials that define the developed world.[1] With an ever-growing concern of the permanent impact of the energy and material consumption involved in creating society's comforts, new chemical transformations hold the key to sustainable and benign utilization of Earth's elemental resources. While the focus of contemporary organic chemistry is efficiency and economy[2], photochemistry has long exemplified the tenets of "green" chemistry. By harnessing Earth's most abundant and accessible energetic resource – ultra-violet and visible light – photochemical reagents and catalysts offer the key to continued chemical synthesis.[3] Credited as the originator of photochemical research, Giacomo Ciamician noted in 1912 the revolutionary impact of harnessing photonic energy for chemical transformations[4]:

"It is thus possible that using the irradiation energy might become interesting in another way. When all of the coal will have been burnt, it may become necessary to resort to exploiting light energy for the progress of society."

In the century following Ciamician's seminal proof of the photochemical conversion of carvone (**1.1**) to carvone camphor (**1.2**)[5] (Figure 1), photochemistry has become developed into a versatile reactivity paradigm for the formation of C–C bonds and the interchanging of carbon oxidation

states in the form of functional group manipulations.[6] In one sense, photochemistry can be employed for stoichiometric excitation of an organic motif to access a reactive intermediate useful in processes such as photocycloadditions, electrocyclizations, the Norrish reactions, di-π-methane rearrangements and β–fragmentations.[7] This paradigm generally involves excitation with ultra-violet (UV) light, the equivalent of 70-100 kcal/mol and the most broadly use for the activation of ketones[8], enones[9], azides[10], arenes[11], extended π-systems, donor-acceptor π-π or n-π interacting systems. While the use of UV light provides highly exergonic elec tronic activations, many organic molecules undergo additional and unselective reactivity with this energy. The additional requirements for utilizing operationally safe photoreactors and the arguable unpredictable nature of photochemistry has deterred many from employing this technique for synthesis.

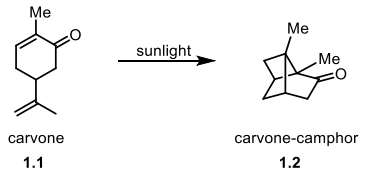

Figure 1: Photochemical Conversion of Carvone to Carvone-Camphor

The transformational improvement upon standard UV-photochemical reactivity is visible light photocatalysis.[12,13,14,15] The exchange of UV for visible light irradiation significantly mitigates the safety requirements of photochemistry, while catalysts enable chemoselective reactivity competitive with many UV photolysis methods. Visible light excitation imparts 40-65 kcal/mol, significantly less than UV excitation, however, photocatalysts convert irradiation to chemical energy through either energy sensitization or redox quenching, thus enabling the transformation of reactive motifs on small molecules akin to direct irradiation.

The combination of polypyridyl ligands and late transition metals such as Osmium, Ruthenium and Iridium produce visible light sensitive complexes exceptionally capable of reversible electron

transfer from both the ground and excited state.[16,17] Photosensitized electron transfer is understood to occur through a mechanism that begins with the absorption of a photon of visible light energy (Figure 2A-B, **1.3**-**1.3***). This promotes an electron from a metal centered t_{2g} orbital to a ligand centered π* orbital in what is formally recognized as a metal-to-ligand charge transfer (MLCT). Spin-orbit coupling between metal center and ligand enhances intersystem crossing from the singlet to the triplet multiplicity creating a long-lived excited state photoactivated complex.[18] By comparison, organic dyes lack a metal center for significant spin relaxation to a triplet state and exhibit shorter excited state lifetimes, while photochemical reactivity can occur at the singlet photoexcited state.[15] The photoexcited charge-separated state exhibits enhanced reactivity compared to the ground state, and in the presence of a specific chemical environment, can acquire or release an electron to form $\mathbf{1.3}^{-}$ or $\mathbf{1.3}^{+}$. The acquisition of an electron from a molecule containing a donor functionality represents a reductive quenching event (Figure 2D), whereas the release of an electron to a molecule containing an acceptor functionality (Figure 2C), represents an oxidative quenching event. After either redox quenching event, the ground state complex is still reactive, looking to reconstitute a normal electronic valence. The combination of excited state quenching and turnover electron transfer allow these complexes to enable redox neutral processes, as well as net oxidative or reductive reactions. Lastly, in the absence of outer sphere electron transfer, energy transfer processes can occur.[19–27] Importantly, energy transfer and electron transfer are decoupled quenching phenomena; ligand electronics and structure largely govern electron transfer properties, while metal identity distinguishes different energy transfer catalysts (Figure 3) (see Chapter 2). Finally, in the absence of a quenching species, the dissipation of excitation energy can occur through fluorescence or radiationless decay, reconstituting the ground state photosensitizer.

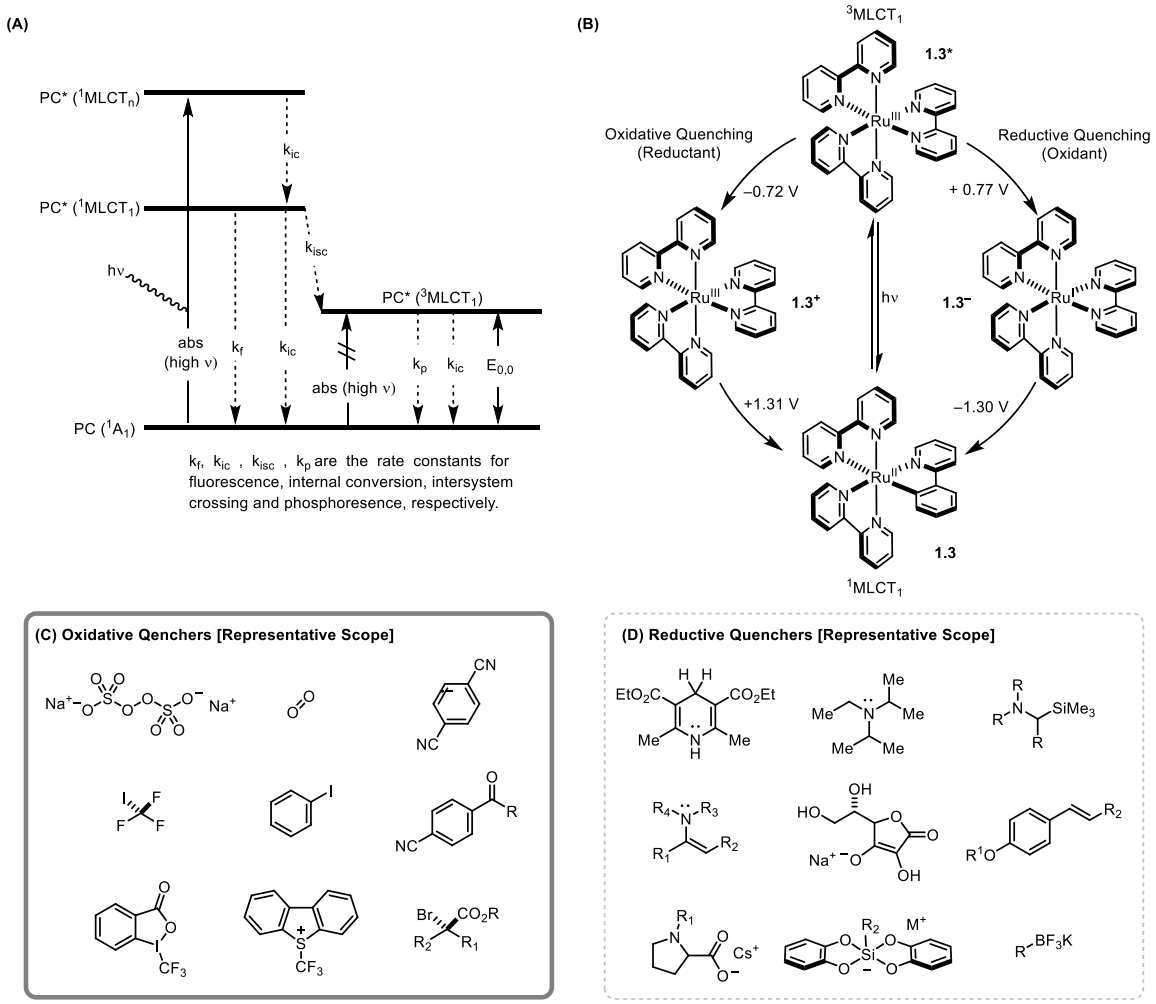

Figure 2: Photoredox Catalysis Photophysics (A) Jablonski diagram for photoredox photophysical processes (B) The photoredox catalytic cycle of Ru(bpy)3Cl2 (C) Representative Scope of Oxidative Quenchers (D) Representative Scope of Reductive Quenchers

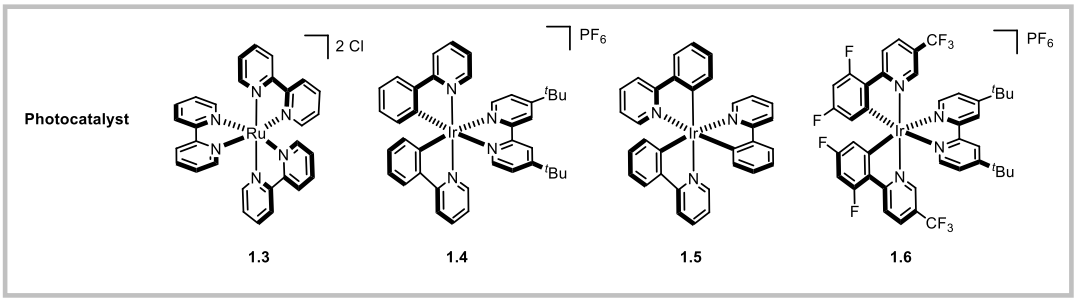

Triplet Excited State Energy	47 kcal/mol	50 kcal/mol	58 kcal/mol	60 kcal/mol
Excited State Oxidation Potential	–0.81 V vs SCE Ru(III/II*)	–0.96 V vs SCE Ir(III/II*)	–1.73 V vs SCE Ir(III/II*)	–0.89 V vs SCE Ir(III/II*)

Figure 3: Excited State Energy Transfer and Electron Transfer are decoupled events at a single photocatalyst

One contributing factor for the adaptation of many synthetic methodologies using photoredox catalysts stems from the predictable nature of electron transfer between an excited complex and an organic substrate. Firstly, the excited state redox potentials of a given photoredox catalyst are predicted by the summation of the electrochemical half reaction and the excited state energy of the catalyst (Figure 2B).[28] Notably, the photoexcited redox couples are both larger in magnitude, and reversed in polarity, enabling a greater range of reactivity within the short time span of the excited state. With knowledge of the excited state redox reactivity of a given photoredox reagent, favorable electron transfer with a substrate molecule can be determined by solving for the E_{cell} of an electron transfer event (Figure 4).

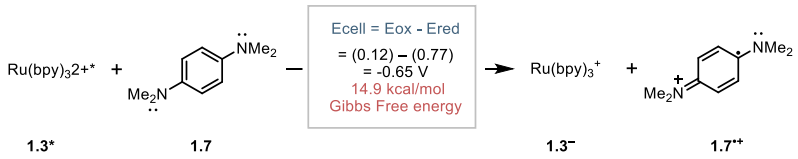

Figure 4: Predicting redox quenching of a photoexcited species

Many factors affect the electrochemical measurement of a ground state redox potential including solvent identity and polarity, supporting electrolyte identity and concentration, and the composition of the electrodes. Despite a relative variance experimental conditions, recorded electrochemical potentials provide a first-order approximation of the feasibility of a photochemical electron transfer step.

To formally demonstrate a photochemical quenching event, a Stern-Volmer analysis must be performed.[29] In this experiment, differences in a chromophore's excited state fluorescence signal intensity are measurably augmented in the presence of various concentrations of a redox or energetic quenching reagent. This relationship exhibits a linear relationship between the emission intensity ratio (I_0/I) to the concentration of quencher [Q] (Equation 1):

$$\frac{I_o}{I} = 1 + k_q \tau_o [Q] \qquad \textbf{Equation (1)}$$

where k_q is the rate of quenching, and τ_o is the lifetime of the photosensitizer in the excited state, and thus provides a linear means of observing the rate of excited state quenching. Time-resolved quenching studies provide a means of determining a pre-association between sensitizer and quencher[30], and further demonstrate the utility of photophysical analysis in the development of new catalytic reactions. Importantly, quenching studies do not prove the identity of the quenching event, rather, only the existence.

Lastly, kinetic considerations are key design factors that can both promote or prevent photoredox reactivity. One key event, back electron transfer, is a deleterious and unavoidable characteristic of photochemical electron transfer. While difficult to prove, and unnecessary in the case of new reactivity elucidation, documented examples of back electron transfer exist. In 1980, Darwent and Kalyanasundaram recorded both successful electron transfer and back electron transfer between $Ru(bpy)_3^{2+}$ and several quinone derivatives.[31] From steady-state Stern-Volmer quenching, $Ru(bpy)_3^{2+}$ was quenched by the benzoquinones at a rate of $3\text{-}6 \times 10^9$ $M^{-1}s^{-1}$. However, conducting time-resolved studies, the formation of dissociated ions from the initial electron transfer products was significantly less than another proven quencher, methyl viologen. From these studies the authors concluded columbic attraction between the $Ru(III)^+$ cation and the benzoquinone radical anion ($BQ^{\bullet -}$) precluded ionic dissociation and back electron transfer was the predominant process. In contrast, both methyl viologen (MV^{2+}) and Ru(II) are both cationic after electron transfer, thus columbic repulsion produces a larger population of separated ions in solution.

1.2 Application of Visible Light Photocatalysis in Radical Fragmentation Reactions

1.2.1 The Synthetic Utility of Fragmentation Reactions

The strategic implementation of a fragmentation, whether radical or polar, has long existed as a valued synthetic strategy in natural product, pharmaceutical and polymer synthesis.[32,33,34] A fragmentable synthon is based upon functional groups exhibiting a large enthalpic value for the cleavage, or release, from a molecular scaffold. Fragmentable motifs include the cyclopropane and butane hydrocarbons and corresponding heterocycles, peroxide O–O bonds, azine N=N bonds, C–X bonds (X = I, Br, Cl, NH_3^+, SR_3^+, RBF_3^-). In a seminal example Eschenmoser demonstrated the synthetic efficiency in a polar fragmentation design by heating carboxylated **1.8** to 175°C, enable the release of one mole of CO_2 and forming macrolactone **1.9**. Conformational analysis of the starting material **1.8**, reveals this molecule is ideally posed for the observed Grob fragmentation because the acetal oxygens effectively weaken the C–O bond of the sulfonate ester through the n $\rightarrow \sigma^* + \sigma_{C-c} \rightarrow \sigma_{C-o}^*$ orbital overlap (Figure 5). Gauche alignment between the carboxylate and acetal likely establish the large thermodynamic barrier to activation, as a near *syn*-elimination is required to fragment the starting material. Ultimately, a stepwise decarboxylation, carbanion formation and Grob fragmentation reveals the macrolide with impeccable olefin stereoselectivity.[35,36] In addition to thermal decarboxylation, Mulzer has highlighted the prevalence of tertiary alcohol deprotonation as a common method for triggering a Grob reaction for the synthesis of natural products.[32]

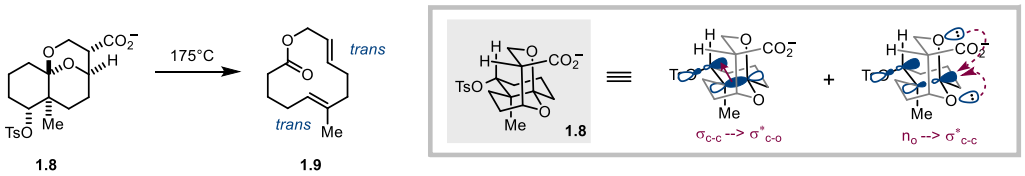

Figure 5: Polar Grob Fragmentation to form (5-E, 8-Z)-6-methyl-5,8-undecadien-11-olide

While many successful demonstrations of thermal fragmentation reactions exist, radical fragmentation reactions offer a chemoselectively orthogonal entry to the same reactivity. This can be advantageous as radical activation can be triggered through the fragmentation of an auxiliary functional handle or redox reactions that leave polar functionalities unperturbed. The most prevalent examples of auxiliary decomposition arise from Barton's reagents such as the thiohydroxamic acid ester[37], xanthate ester[38], and hydroxyphthalimide ester reduction[51] (Figure 6). In the case of the sulfur ester reagents, tributyltin radical addition to the sulfur atom weakens the adjacent N–O bond causing fragmentation. Once the carboxyl radical is generated, decarboxylation is entropically favored revealing a carbon centered radical poised for H-atom trapping from a reductant in solution. The utilization of the xanthate ester deoxygenation protocol was demonstrated on a complex scaffold by Wood and co-workers in the synthesis of the Phomoidride core (Figure 7).[39] A sterically hindered alcohol **1.10** prevents reduction by hydride reagents due to a sterically blocked C–O σ* molecular orbital, however, radical activation of xanthate ester and triethylborane/O_2/H_2O provides the deoxygenated product **1.11** in good yield by targeting the xanthate auxiliary. Interestingly, the tricyclic scaffold limits secondary fragmentation to provide **1.12**, and bimolecular H-atom transfer prevails as the faster process.

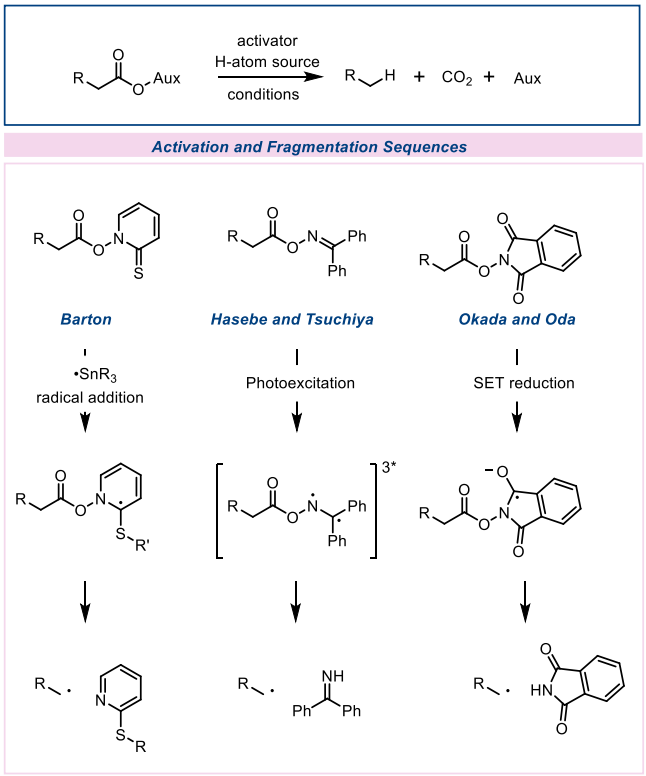

Figure 6: Ester Derivatives for Radical Generation

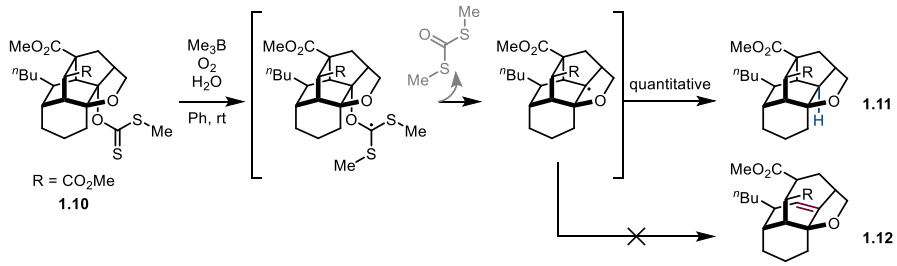

Figure 7: Wood's Deoxygenation of Phomoidride Core

with Tin-Free Barton Deoxygenation Method

1.2.2 Early Visible Light Redox Catalysis

The first visible light photocatalyzed methods derived significant inspiration from biological chemistry, in the use of dihydropyridines as reductants for several functional groups. 1,4-dihydropyridines (**1.13-15**), as modeled after nicotinamide adenine dinucleotide (NADH), serves as an excellent chemoselective reductant. Single electron oxidation (0.5-0.8, HEH = 0.72 V vs. SCE)[40], a process attainable by many ground state and photosensitized oxidants[41], weakens the

para-C–H bond and generates an irreversible single electron reductant. Fragmentation of the *para*-C–H bond favorably provides aromaticity to the pyridine substructure and rationalizes the driving force of this half reaction. Fundamental studies by Fukuzumi[40] and Savéant[42], respectively, demonstrated that formal H-atom loss by a dihydropyridine radical cation does not occur by H-atom transfer (Figure 8). Upon formation of the amine radical cation of a dihydropyridine (**1.13**$^{\bullet+}$), deprotonation occurs in concert with single electron transfer to furnish an α–amino radical (or vinylagous α–aminoradical) (**1.13**$^{\bullet}$). Additionally, carbonyl reduction by an amine radical cation occurs by deprotonation and electron transfer to the carbonyl. In this case, a carbonyl substrate can serve as the base, but often carbonyl reduction reaction conditions include added acid to neutralize the anionic ketyl radical intermediate and facilitate electron transfer, thus there are multiple basic sites including the ketyl radical, pyridine product and conjugate base in solution to accommodate acid generation.

Kellogg and co-workers were the first to realize dihydropyridines as reductive quenchers of photoexcited $Ru(bpy)_3^{2+}$ (Figure 9).[43] Mired by a sluggish reaction between Hantzsch Ester (HEH) and α–ketosulfonium salts (**1.17**), the employment of visible light and $Ru(bpy)_3Cl_2$ rapidly altered reactivity to provide selectively reduced ketones and oxidized Me-HE (**1.16**$^{+}$). In the absence of photochemical additives, **1.16** was observed to partially reduce keto-sulfonium salts until the concentration of starting material is sufficiently low, and then cross-hydrogen transfer between 1,4-dihdyropyridines to make a regioisomeric mixture of 1,4 and 1,2-dihydropyridines (**1.16:1.18**). However, when substoichiometric $Ru(bpy)_3^{2+}$ is included and the reaction solution is irradiated, the two reactants react favorably to fully reduce the sulfonium starting material, and not form 1,2-dihydropyridine byproducts. No mechanism was postulated by the authors, however, the simplicity

of using a “room light”, or neon fluorescent lamp, foreshadowed the operational simplicity attributable to visible light photocatalysis.

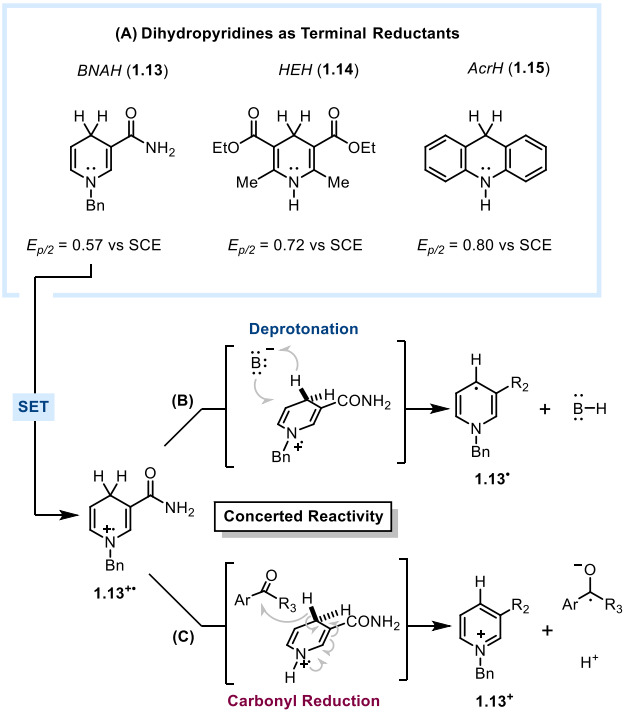

Figure 8: (A) Dihydropyridines as terminal reductants and concerted reactivity investigated by (B) Savéant and (C) Fukuzumi

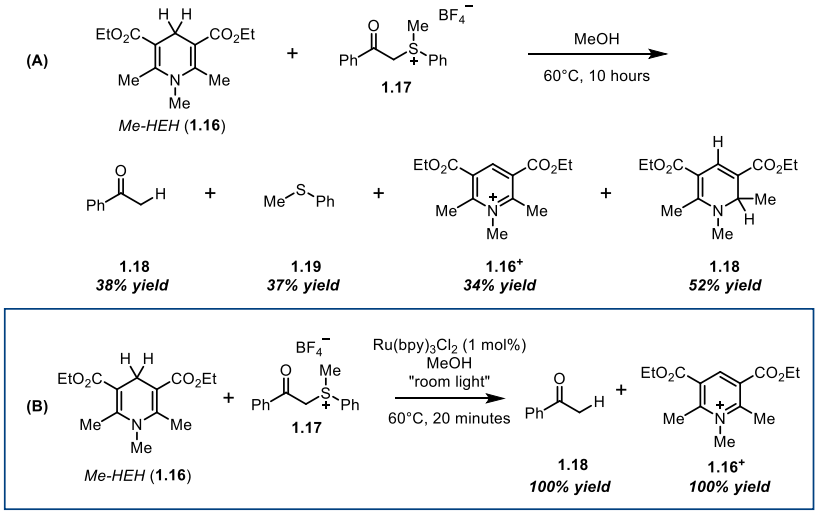

Figure 9: $Ru(bpy)_3Cl_2$ as an Additive to enhance rate of reactivity between dihyropyridines and α–keto sulfonium salts

Another chemical reaction lacking efficiency at elevated temperatures was the reduction of cinnamate esters by dihydropyridines (Figure 10).[44] Astutely postulating from Kellogg's work that $Ru(bpy)_3Cl_2$ was acting as a photoactivated redox reagent to oxidize the benzyl dihydropyridine, Pac and co-workers realized a photochemical cinnamate reduction similar to Kellogg. In this sense, from the photoexcited state, $Ru(bpy)_3^{2+*}$ and BNAH (**1.13**) undergo exergonic electron transfer to produce a $Ru(bpy)_3^{+}$ and radical cation, **1.13**$^{\bullet+}$. As discussed, single electron oxidation significantly acidifies the surrounding C–H bonds of the radical cation. Pac and coworkers found reduction yield to be responsive to solvent basicity, suggesting that **1.13**$^{\bullet+}$ is deprotonated and **1.13**$^{\bullet}$ along with $Ru(bpy)_3^{+}$ provide the two electrons necessary for reduction. Other reactivity observed in solution was the dimerization of **1.13** starting material and Giese addition to the cinnamate forming aminal products **1.23**. Different products were observed in the photocatalyzed reductions of diethylfumerate (**1.19**) and (*E*)-4-phenylbutenone (**1.22**) (Figure 10B). In the former case, the first reduction can occur from **1.13•** to form **1.19**$^{\bullet-}$. This is followed by a concerted electron and proton transfer from another molecule of **1.13** to form the β–ester enolate, which neutralizes quickly in solvent quantities of pyridine and methanol. Alternatively, 4-phenylbutenone is initially reduced through the same mechanism, however, the **1.22**$^{\bullet-}$ radical anion is stabilized by the phenyl group which allows it to couple through a radical-radical combination with another **1.13•**. The low yield of this process represents the challenge in radical-radical combination, as well as the subtle differences in radical kinetic and thermodynamically governed reactivity.[45] Later work by Pac and co-workers, elucidated reaction conditions with added Mg(II) salts could expand the scope of BNAH-olefin reductions as well as aryl ketone reductions.[46]

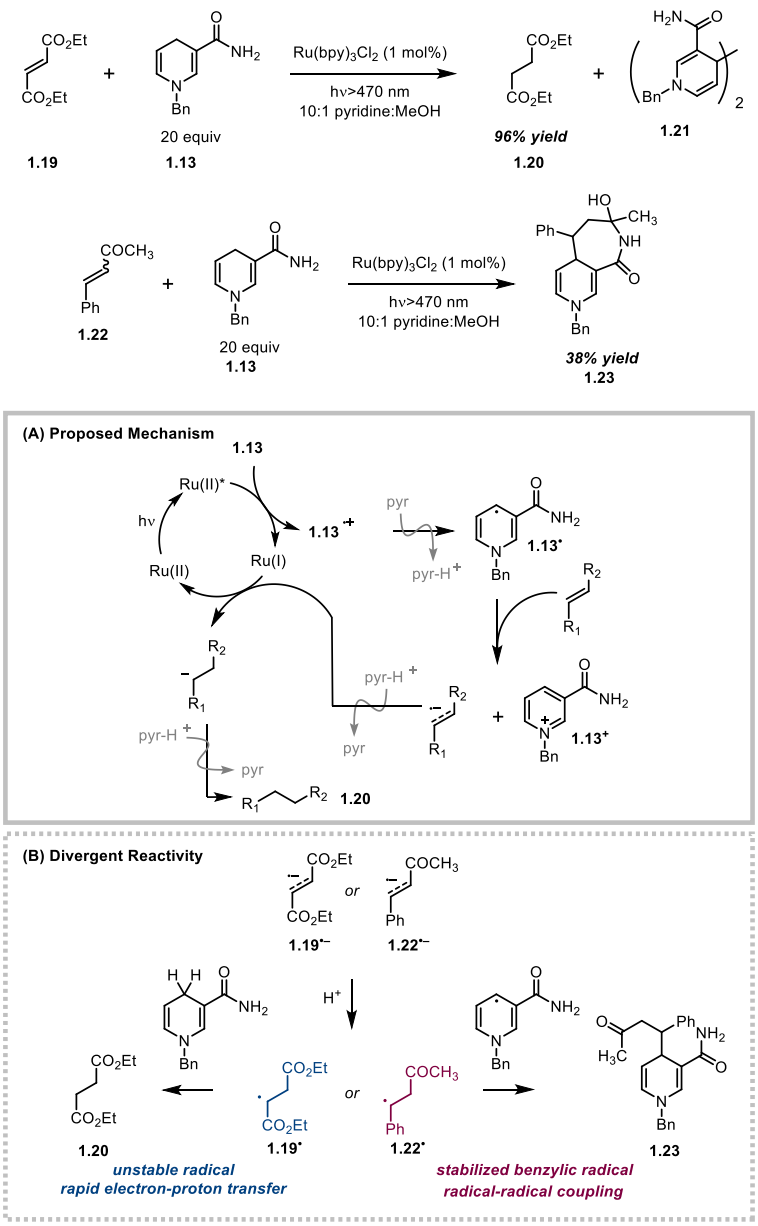

Figure 10 (A) Photocatalzed reduction of olefins with BNAH. (B) Proposed Mechanism (C) Divergent Reactivity between ethyl fumarate and ethyl cinnamate.

Observation of a substrate limitation to conjugated aryl-carbonyl motifs in photocatalyzed reductions using dihydropyridines was echoed in publications by Fukuzumi in the reduction of α-keto C–Br bonds (Figure 11).[37,47] In an investigation of the photocatalyzed hydrogen transfer reactivity of dihydropyridines to phenacylhalides (**1.24**), Fukuzumi et. al. found that rate of oxidative quenching observed between $Ru(bpy)_3^{2+}$ and the ketone substrate was dependent on the

electronic substitution of the arene, as well as presence of perchloric acid. When percholoric acid was included as an additive, both oxidative and reductive quenching of the $Ru(bpy)_3^{2+}$* excited state were possible; furthermore, oxidation of **1.15** results in an accumulation of **1.25•HBr**, which additionally facilitates this reaction. Notably, the rate of photochemical quenching between $Ru(bpy)_3^{2+}$ and different ketone substrates was enhanced by 2-3 orders of magnitude in the presence of a high concentration of perchloric acid.

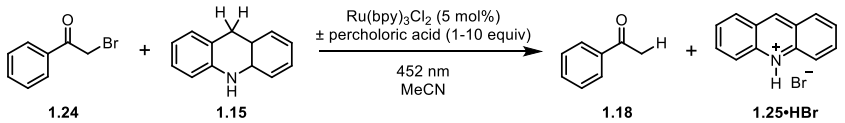

$Ru(bpy)_3^{2+*}$ Excited State Quenching

Phenacyl halide	k_{et} ($M^{-1}s^{-1}$) 1 eq $HClO_4$	6.6 eq $HClO_4$
p-$CNC_6H_4COCH_2Br$	2.6×10^7	1.5×10^8
$PhCOCH_2Br$	8.7×10^6	7.8×10^7
p-$OMeC_6H_4COCH_2Br$	7.9×10^7	3.3×10^8
$PhCOCH_2Cl$	2.9×10^6	1.6×10^7

Observed Reactivity

$HClO_4$ equiv	Acetophenone (%)	Acr-H^+ (%)
0	75	75
0.66	98	98
6.6	100	100

Figure 11: Acid-mediated, photocatalyzed phenacyl bromide reductions

Another early photocatalytic fragmentation reaction was developed by Okada and Oda for the reductive decarboxylation of carboxylic acids. The late 1980s marked significant experimentation in the development of ester auxiliaries enabling radical decarboxylation reactions (Figure 6). Towards this end, Barton's thiohydroxamic acid ester gained prominent design accolades for the utilization of a commercially available N-hydroxypyridine-2-thone and established knowledge of AIBN-tributyltinhydride reactivity.[37] Other approaches by Hasebe and Tsuchiya[48], as well as Okada and Oda offered photoactivated auxiliaries. Hasebe and Tsuchiya designed a benzophenone oxime ester, which upon photolysis could access the triplet diradical state of the benzophenone substructure to enact an N-O bond cleavage and decarboxylation. This in the presence of an H atom source, *t*-butyl mercaptan, provided the desired alkane products.

Okada and Oda also reported an N-O ester auxiliary, in the form of N-hydroxyphthalimide, which could be activated by single electron reduction. Given phthalimide lacks photosensitivity, as compared to benzophenone, electron donors such as 1,4-diazabicyclo[2.2.2]octane (DABCO)[49] and 1,6-bis(dimethylamino)pyrene (BDMAP)[50] were investigated for stoichiometric photochemical electron transfer (Figure 12). While these electron donors could facilitate the fragmentation and decarboxylation of **1.26**, UV irradiation was required. Additional limitations such as stoichiometric and superstoichiometric loadings of DABCO or BDMAP favored H-atom trapping, rather than C–C bond formation, as the highest yielding process. The photochemical yield of each decarboxylative functionalizations were described as moderate for BDMAP (0.1) and low for DABCO (0.001).

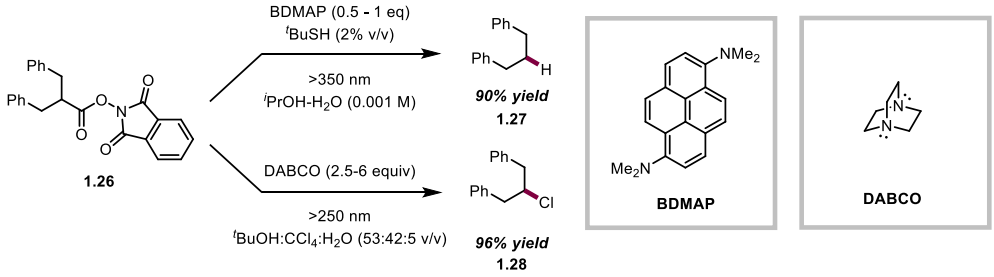

Figure 12: Okada and Oda early N-hydroxyphthalimide ester decarboxylation reactions

Following, Kellogg's reported use of $Ru(bpy)_3^{2+}$ as a visible light sensitive additive[43], Okada and Oda applied a similar this reaction design and observed significantly more chemoselective decarboxylation of the phthalimide N-oxide esters.[51] In contrast to the previous two methods, $Ru(bpy)_3^{2+}$ could be employed as a catalyst, transferring electrons from **1.13** to the *N*-hydroxyacid ester derivative to effect radical decarboxylation. The ensuing radical (primary, secondary or tertiary in nature) could then be trapped with either an H-atom additive or an acrylate system in a formal Giese reaction. The Giese reaction peaked at 69% yield (**1.30**), for a selective mono-functionalization of methylvinylketone and other acrylate traps (Figure 13). Unique to the

reduction of hydroxyphthalimide esters, water played a supporting role in promoting fragmentation by stabilizing the intermediate ketyl radical anion. This process exhibited a quantum yield of 1-2, signifying a substantially more efficient photochemical reduction of the ester derivative. The utility of $Ru(bpy)_3^{2+}$ as a photocatalyst was further demonstrated in the functionalization of alkyl radicals with reagents such as diphenyldiselenide (**1.33**), tetrachloromethane (**1.32**) and *t*-butyl mercaptan (**1.31**).

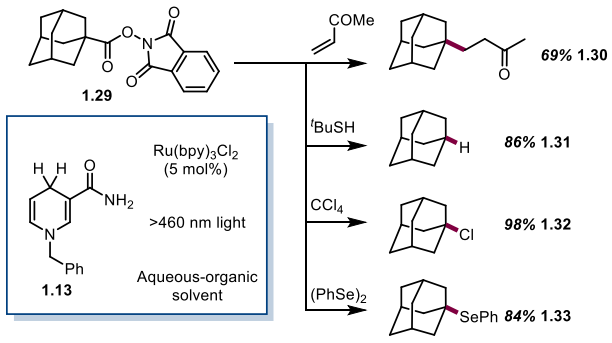

Figure 13: Photocatalyzed Radical Decarboxylation of *N*-hydroxyphthalimide esters for radical C–C, C–H and C–X bond formation.

Interestingly, the reductive decarboxylation of **1.29** to **1.31** exhibits a quantum yield of 15, likely operating through polarity-transfer radical reactivity, as documented by Roberts.[52,53] In polarity-transfer radical reactivity, the *t*-butyl mercaptan acts as a separate H-atom transfer catalyst because it exhibits a superior polarity match with both **1.13•** and **1.29** • than either reactant has with the other (Figure 14). This is reasonable as the *t*-butyl thiyl radical is anticipated to acquire negative charge in the transition state when reacting with the **1.13** starting material (Figure 14). Comparatively, the $\mathbf{1.29}^{\bullet-}$ cannot reasonably accommodate this charge in the transition state, thus it exhibits a kinetically slow reaction with **1.13**. Acrylate monofunctionalization occurs through this same kinetic rationale, namely, the α-ester radical has a matched polarity with **1.13** and can quickly transfer either an electron and a proton, or an H-atom, to form the observed product. Polarity reversal kinetic observations rarely hinder radical reactions Figure 14; however, when

designing a radical reaction, it is of significant benefit to consider the polarity matching of the reagents to enable a catalytic cycle.

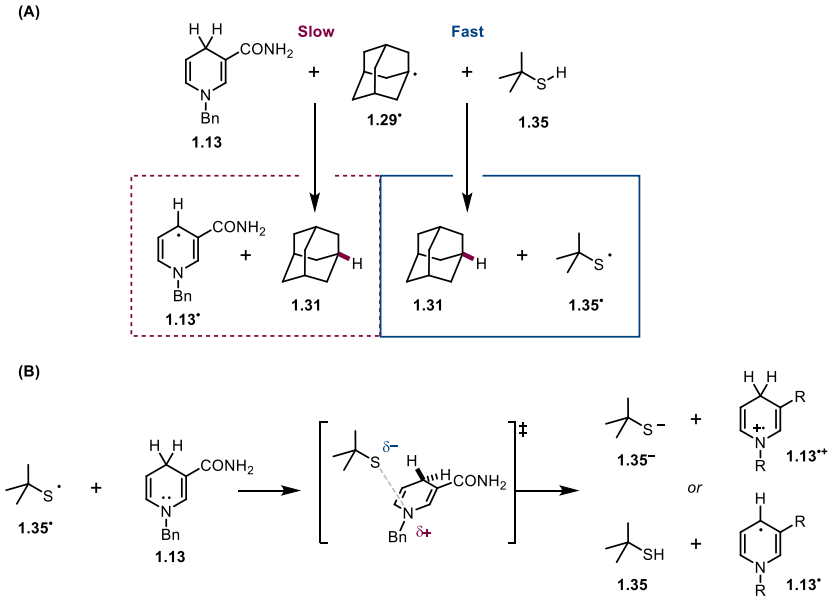

Figure 14: Polarity Matching in Radical Decarboxylation Reactions

(A) relative rate of reactivity of adamantane radical with BNAH and t-butyl mercaptan (B) Illustration of favorable transition state polarization between t-butyl thiyl radical and BNAH

One final thermal reaction that $Ru(bpy)_3^{2+}$ was found to enhance by accessing a photochemical reaction pathway was the Pschorr reaction, as investigated by Cano-Yelo and Deroziner.[54] In an initial investigation, stilbene diazonium salts (**1.36**) could be selectively activated via an oxidative quenching event with a photoexcited $Ru(bpy)_3^{2+}$ catalyst (Figure 15, quantitative yield). Importantly, the absorbance of **1.36** and $Ru(bpy)_3^{2+}$ are sufficiently separated such that low energy visible light was selective for $Rubpy_3^{2+}$ sensitization. Direct photolysis of the starting material could produce the desired phenanthrene (**1.37**), however, in significantly diminished yields and with a significant accumulation of amide (**1.38**, ***80%***). This result was in accordance with the finding that photolysis of arene diazonium salts produces a σ arene cation.[55] The $Ru(bpy)_3Cl_2$ mediated reaction was found to have a quantum yield ranging between 0.46-0.78, suggesting a prominent radical propagation pathway was not occurring despite the low reduction potential (-0.1

V vs SCE) of the diazonium substrate. Comparatively, the direct photolysis is a significantly less efficient reaction, with quantum yields measured between 0.06-0.175.

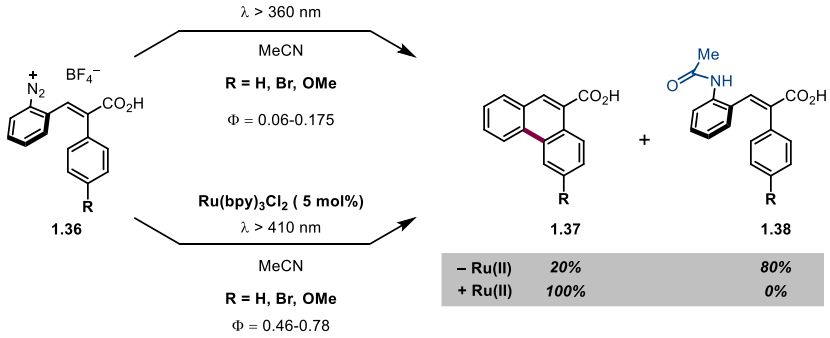

Figure 15: Photochemical Pschorr Reactions Investigated by Cano-Yelo and Deroziner.

Having realized the oxidative quenching of $Ru(bpy)_3^{2+}$* with arene diazonium salts, Cano-Yelo and Deroziner applied this oxidant to the net oxidation of benzylic alcohols.[56] In this study, the authors utilized *o*-diazo benzophenone (**1.39**) only to find that the cyclization reaction was significantly disfavored in comparison with intermolecular H-atom trapping from either the solvent or alcohol (**1.40**). The 3:1 ratio of H-atom trapping to cyclization was also observed for *o*-diazodiphenylether and *o*-diazodiphenylmethane under the same reaction conditions, highlighting the poor conformational alignment of the two aryl systems for reactivity at room temperature.[57] This noted difference in reactivity between the diazonium salt starting materials in the context of the Pschorr reaction indicates the highly reactive and unselective character of the aryl σ–radical.

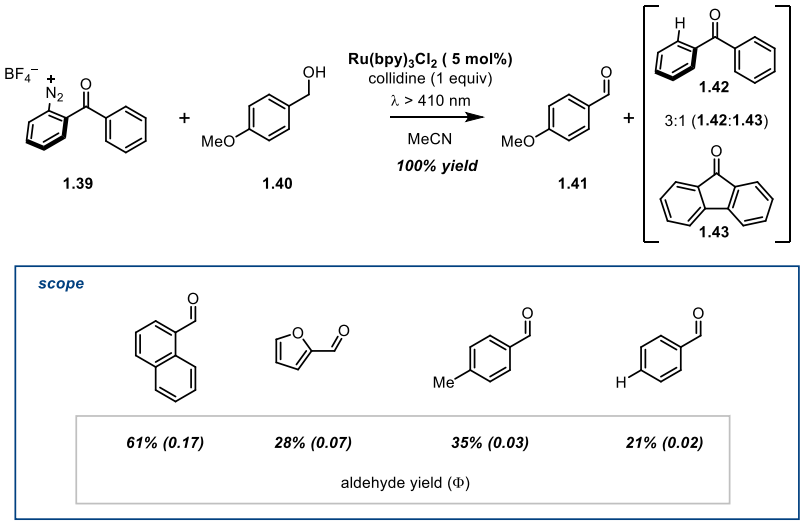

Figure 16: Oxidation of benzylic alcohols with 2-diazobenzophenone and Ru(II) photocatalysis

1.2.3 Contemporary Photocatalysis: Radical Fragmentation Examples

The following discussed examples of early visible light photocatalysis went under recognized in the synthetic community for reasons only one can speculate; however, in 2008 foundational demonstrations by Yoon[58], MacMillan[59] and Stephenson[60] revived the interest in using visible light for small molecule synthesis. These reactions showcased the operational simplicity of visible light irradiation over conventional ultra-violet photochemical reactions, in addition to preparing valued and complex molecules. The promulgation of these reactions as a renaissance in visible-light catalysis has been discussed extensively[12–1512], and the remainder of the discussion will be reserved for photocatalytic reactions employing a key redox auxiliary for radical generation.

For small organic molecules, single electron oxidation or reduction results in the formation of an unstable radical ion. This radical ion is disposed for a preliminary fragmentation event such as decarboxylation or strain-driven C–C bond homolysis. With a few exceptions[61,62], electron transfer from a donor molecule, through either inner or outer sphere, ionization and fragmentation is a step-

wise process; a concerted process would require a large reorganization energy (λ) at the instance of electron transfer, effectively slowing down the rate of electron transfer (Marcus inverted region).[63,64] As such, it is commonly accepted that a single redox change and fragmentation is a step-wise process and the most logical post electron transfer step. Nonetheless, many motifs and functionalities fail to participate in electron transfer with photoredox catalysts and synthesis requires the incorporation and utilization of a variety of different functional handles to forge C–C and C–X bonds. As such, a significant portion of research in photoredox catalysis has been devoted to the development of redox auxiliaries to attain the generation of desired radical intermediates. Redox auxiliaries typically involve a redox activation followed by two fragmentation processes to reveal radicals such as the trifluoromethyl radical, acyl radicals and carbon centered radicals with the extrusion of a discrete molecules like CO_2, SO_2, Hantzsch's pyridine or iodobenzene as innocuous by-products of the activation process. The following discussion is organized by the resultant radical of each auxiliary.

1.2.2.1 Alkyl Radical Generation

The resurgence of double fragmentation-based carbon radical generation reactivity was brought about by Overman and co-workers as a solution to the C_8-C_{14} configuration in Aplyviolene (Figure 17).[65] Prior work established that cuprate formation of **1.47** accomplished the challenging C–C bond formation in the natural product, however, not in the correct stereochemical configuration (**1.48**). Questioning whether the use of radical chemistry would alter the stereoselectivity of this transformation, Overman and co-workers sought to find a functional group tolerant, chemoselective radical generation method to enact a Giese-type reaction between **1.45** and **1.46.** By simply applying previously developed chemistry by Okada and Oda's methodology (Figure 13), **1.45** was appended to the phthalate auxiliary (**1.49**), and activated in the presence of HEH

(**1.14)** and $Ru(bpy)_3Cl_2$ (Figure 17C). Gratifyingly, this radical method coupled fragments **1.49** and **1.50** resurrected the synthesis by providing the desired epimer (**1.51**) of Aplyiolene (**1.44**). Overman and co-workers concluded that the steric profile of the alkyl cuprate reversed the natural configurational bias of fragment **1.45** for intermolecular bond formation, thus simplifying the cuprate to a nucleophilic radical, while reversing the stereoselectivity.

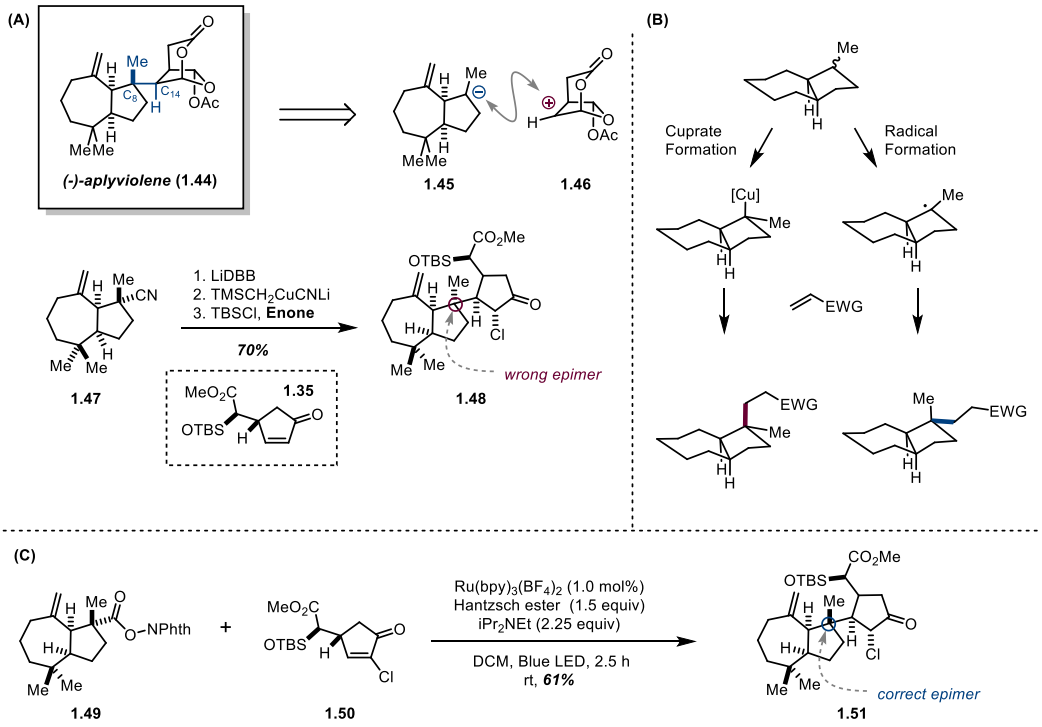

Figure 17: Overman's Synthesis of Aplyviolene using tertiary radical coupling

Enchanted by the success of radical generation from *N*-hydrophalamide esters, Overman and co-workers advanced the utility of this auxiliary by incorporating an oxylate (-COCO-) linker to source the carbon radicals from alcohols (**1.52** to **1.56**).[66] Tertiary radicals are often derived from alkyl halide precursors; however, preparation of these materials suffer from elimination reactions and rearrangements in complex scaffolds. Alcohols, as Overman argues, are a more stable counterparts to tertiary halides, and warranted investigation as radical precursors. In a single pot, *N*-hydrophthalimide can be selectively monoacylated by oxalyl chloride, followed by alcohol

incorporation of the opposite oxylate terminus. Soft deprotonation conditions to enable the second acylation were astutely implemented, leading to the formation of H-NEt_3 and H-DMAP, which could be filtered prior to the photocatalytic reaction.

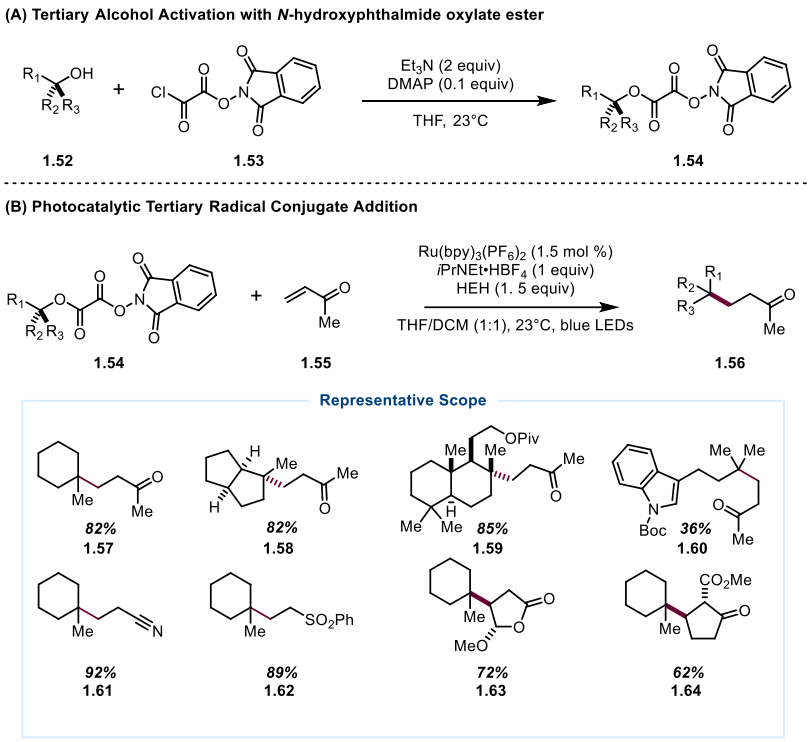

Figure 18: General procedure for radical conjugate addition

The optimized reaction conditions showcase a non-polar solvent choice with strong acid additive ($^{i}PrNEy_2$-HBF_4) to maximize conjugate addition of the radical to the acrylate species. A variety of tertiary alcohols bearing steroidal or carbocyclic skeletons were coupled in good yields to methyl vinyl ketone. Additionally, a variety of alkenes included acrylonitrile (**1.61**), dimethylfumarate (**1.58**), and 5-methoxyfuran-2-one (**1.63**) were successful coupling partners in this reaction. Two experiments were conducted to evaluate if the operative product forming step was H-atom transfer or reduction and protonation (Figure 19).[67] Firstly, **1.14-d** provided **1.57-d** in ***32%*** yield with >95% deuteration at the α–carbon. This result is in line with a second radical trapping experiment with α–substituted acrylonitriles (**1.65-66**). Based on the electronic identity

of the leaving group (-OBn or -Br), the reaction was observed to eliminate the electron poor substituent (Br) and retain the benzyl ether, suggesting that product formation likely proceeded through H-atom transfer. Lastly, the reaction was observed to progress slowly in the absence of photocatalyst, but still provided good yields. The collected evidence corroborates Okada and Oda's original findings while showcasing the sourcing of radicals from stable and available tertiary alcohols.

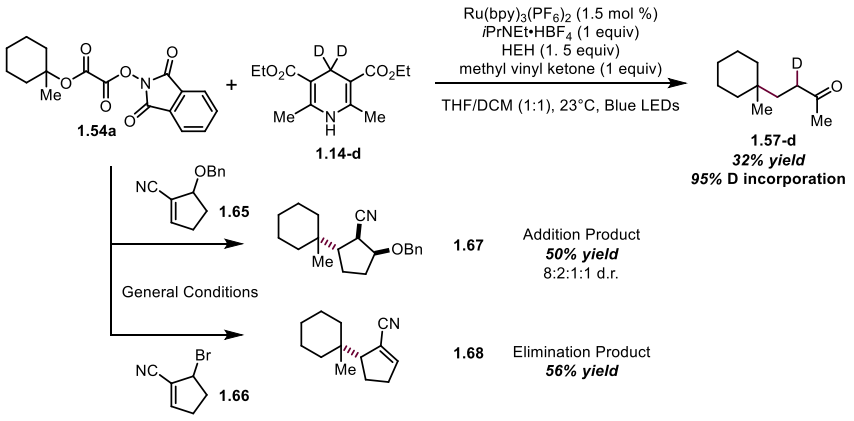

Figure 19: Studies on the fate of the α–ester radical in Overman's radical conjugate addition reaction

While Overman was concluding the mechanism studies of the *N*-hydrophthalimide oxylate esters, MacMillan et. al. had adapted another variant of this reaction in collaboration with Prof. Overman. Together, the combined research team realized the decarboxylative conjugate addition from an oxidative decarboxylation reaction (Figure 20).[68] Having developed a robust set of photocatalyzed carboxylate decarboxylation reactions[69], MacMillan was well suited to further elaborate upon and improve this methodology. Critically, formation of the oxylate cesium salts (**1.69**) improved upon the general stability of the tertiary radical precursors and simplified the synthesis. In the forward sense, these compounds could be decarboxylated in polar solvents containing water, with an oxidizing Ir(III) photocatalyst. By design, the photoexcited Ir(III) catalyst possessing an oxidation potential of +0.87 V vs SCE can oxidize an oxylate salt (**1.69**,

onset $E_{p/2}$ = 0.8 V/ peak = 1.28 V vs SCE), providing a driving force for a double decarboxylation and tertiary radical generation (Figure 20B). The tertiary radical favorably adds into the acrylate trap, and **1.71•** is reduced by an Ir(II) species to turn over the catalyst (ΔG = –17.9 kcal/mol). This method substantially improves upon Okada and Overman's methods through a redox neutral catalyst cycle and enables higher yields on challenging substrates. Similar to Overman's conditions, radical decarboxylation from secondary carbons exhibits a slow second decarboxylation (Figure 20D). In these instances, acyl radical addition to the acrylate trap can be observed. The stereoelectronic influence of an arene ring can reverse this effect for secondary and primary radicals.

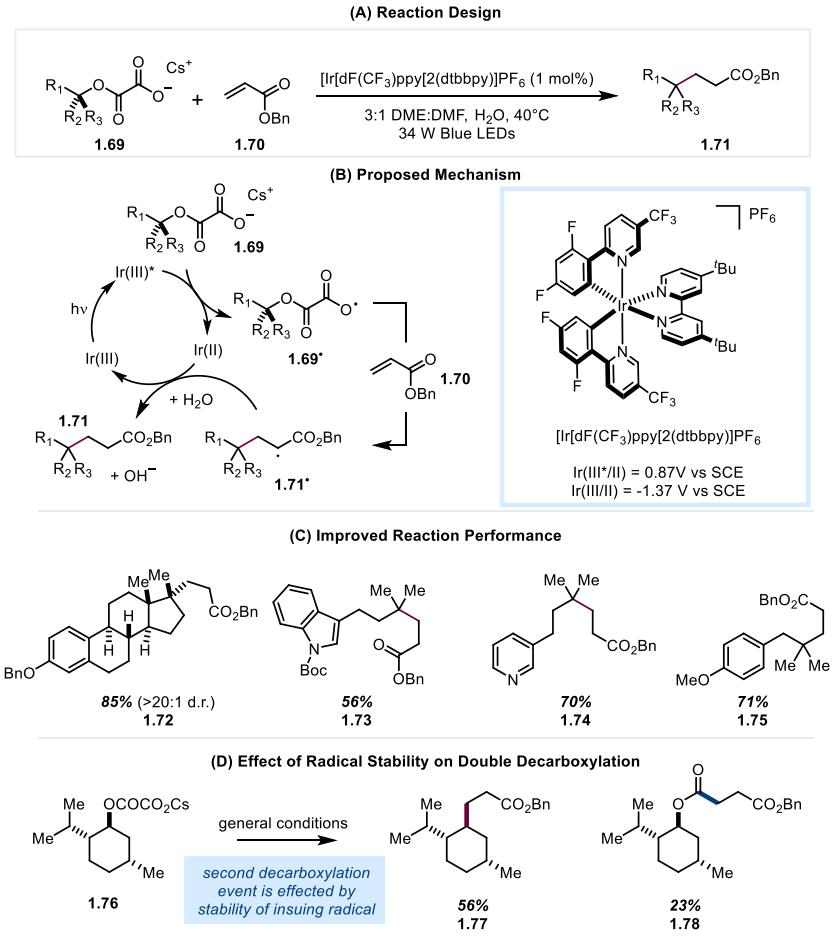

Figure 20: Improved Reactivity with MacMillan's Oxylate Decarboxylation Reaction

The *N*-hydroxyphalamide esters offer multiple entry points into radical chemistry based on the reductant employed. In the time since Overman and MacMillan's studies, methods employing low valent metals published by Jiao[70], Baran[71,72] and Weix[73] have demonstrated the utility of this redox auxiliary outside of photochemical catalysis. One unique example of a stoichiometric photoinduced radical generation between an *N*-hydroxyphalamide ester and a boron-ate reductant to borylate arenes was described by Glorious.[74] By mixing $B_2(pin)_2$ and pyridine an association complex forms (**1.80**) which can transfer an electron. Furthermore, Glorious and co-workers found that benzoate *N*-hydroxyesters exhibit a near visible absorption maximum and are capable of photoexcitation near 400 nm. Interaction between photoexcited benzoyloxy *N*-hydroxyphthalimide esters (**1.79**) and the association complex **1.80** transfers an electron within the lifetime of the **1.79** excited state and effect radical decomposition. The decomposition productively resolves in a functional group transformation from aryl-carboxylate to aryl boronic ester. This transformation was general across a variety of electronically distinct arene carboxylates and effective on elaborated scaffolds like herbicide diflufenican (**1.88**). To improve the reactivity of electron deficient benzoate esters, *N*-Hydroxytetrachlorophthalimide was used as the redox active ester. This enables both a better absorption of light and better acceptor functionality for electron transfer. This method, in light of the multitude of reductants that activate *N*-hydrophalalmide esters demonstrates the robust utility of redox active esters as auxiliaries in synthesis.[75]

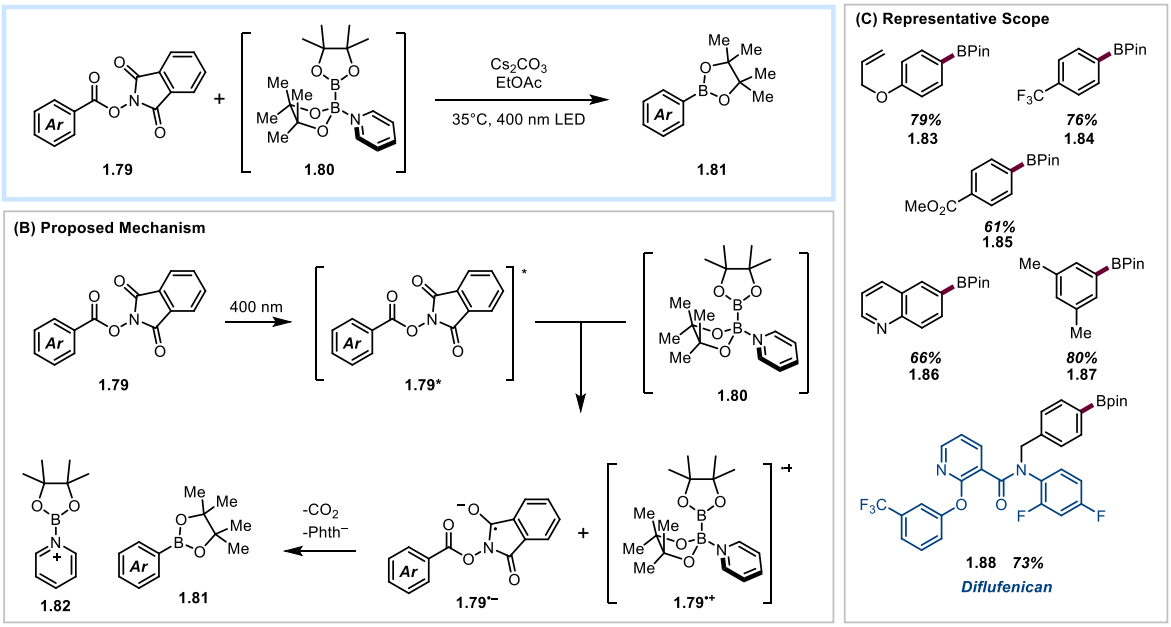

Figure 21: Electron transfer between photoexcited *N*-hydroxyphthalimide ester and boronic ester - pyridine complex

Another versatile and prominent redox active auxiliary is alkyl-dihydropyridine. This auxiliary effectively transforms aldehydes into alkyl radicals through the Hantzsch dihydropyridine synthesis (Figure 23). The resultant dihydropyridines are often solids, beneficial operation simplicity and handling. While the most common dihydropyridine is HEH, replacing formaldehyde for a substituted aldehyde generates a 1,4-dihydroalkylpyridine that extrudes a carbon radical upon oxidation. Molander and co-workers realized this reactivity by simply mixing persulfate and substituted HEH derivatives to find that alkyl-HEH derivatives (**1.53**) slowly reduce persulfate at room temperature.[76] The resultant radical could be trapped with a radical acceptor such as quinone or nitrogenous heterocycles. Moreover, photoredox catalysts such as $Ir(ppy)_3$ and 4-CzIPN have been used to enable the radical coupling, from alkyl-DHP derivatives, and cross-coupling reactions with various electrophiles.[77,78] DHP activation, however, does not require the use of a redox catalyst. Melchiorre and co-workers recently disclosed that alkyl DHPs (**1.89**, **1.93**) have a measurable absorption and Stokes shift, proving the existence of an excited triplet state (Figure 22).[79] Photoexcited alkyl DPHs can react with cyanoarenes and benzylic halides, to enable

the electron transfer, followed by fragmentation of a carbon centered radical, which productively couples with the acceptor molecule. Radical fragmentation of the alkyl group is favored over the H-aotm transfer because the C–C bond is elongated to accommodate the steric influence of the 3,4,5-trisubstituted naure of the alkyl HEH (Figure 22B). Furthermore, H-atom loss would produce a sterically congested pyridine derivative. Additionally, Melchiorre has demonstrated C–C bond formation with chiral iminium catalysis and alkyl dihydropyridines (Figure 22C). This proceeds in a slightly different fashion, in which the the iminium species is excited and undergoes a s reductive quenching event with the alkyl DHP.[80] The minor difference between the two reaction designs is manifest in the operative wavelength employed. The alkyl dihydropyridines are excited in the near UV range (~400 nm), whereas the iminium ions exhibit a red-shifted maximum absorption and can be excited at 420 nm. While alkyl dihydropyridine activation creates an equivalent of pyridine waste, the photochemical process is far less energy intensive compared to transition metal decarbonylation chemistry; future investigations to convert pyridine to dihydropyridines and regenerate alkyl-dihydropyridines will make this a formidable technology for C–C bond construction.

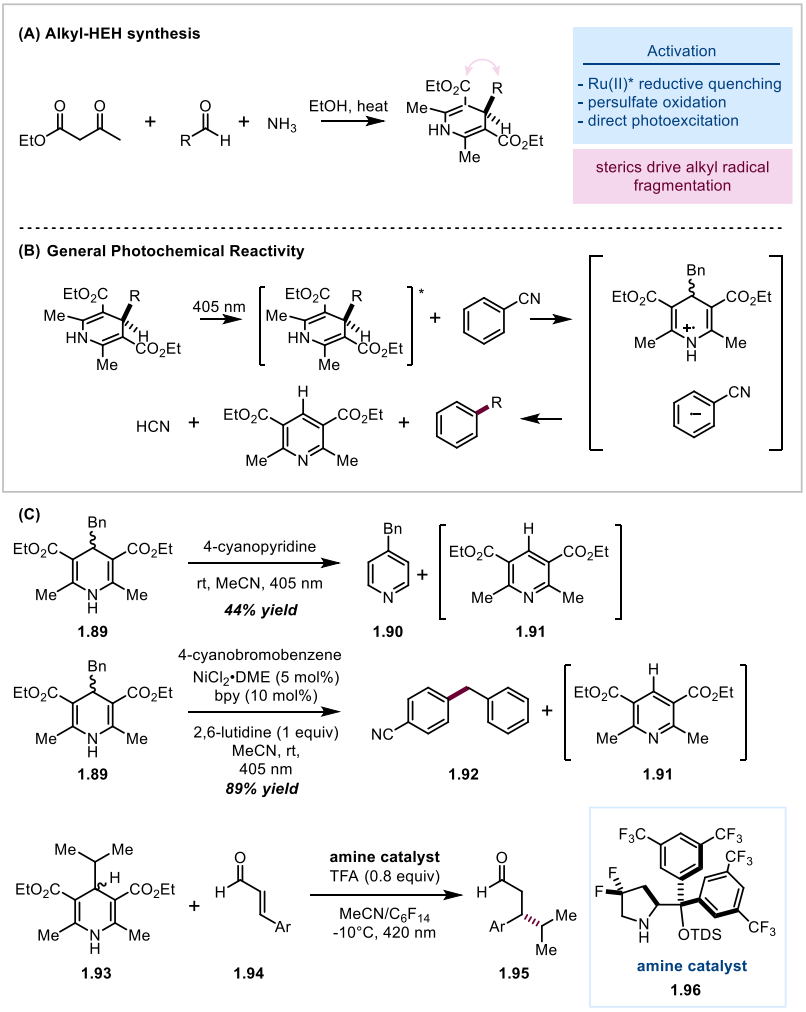

Figure 22: Melchiorre's photochemical investigations of photoexcited dihydropyridines as alkyl radical precursors

One key challenge in cabon radical reactivity is realizing small alkyl radical reactivity. While MacMillan, Overman, Molander and Melchiorre's examples (*vide supra*) provide direct access to tertiary and secondary carbon centered radicals, many are still interested in the generation of methyl, ethyl and cyclopropyl radicals for heterocycle functionalization. Radical heterocycle functionalization, notably investigated by Minsci from 1970-1990,[81] provides the most direct access for heterocycle alkylation; an approach greatly valued in pharmaceutical synthesis for late stage derivatization.[82] In the hit-to-lead paradigm of small molecule drug design, late stage functionalization allows for minute optimization of valued assets by modifying structural features

that can improve medicinal chemistry properties such as adsorption, metabolism, dispersion and excretion (ADME). DiRocco and co-workers at Merck realized a solution to this challenge by optimizing the reductive decomposition of *tert*-butyl peracetate (*t*BPA) for the radical methylation of pharmaceutically relevant heterocycles (Figure 23A).[83] This reaction was realized through high-throughput experimentation, on a 8x12 well plate, which enabled the screening of various photocatalysts and solvents. A key design feature, one conserved across many successful *N*-heterocycle radical alkylation reactions, is the use of excess acid (10 equiv of TFA). The acid additive works to activate the pyridine as well as the peroxyacetate, as electron transfer between the photoexcited catalyst and peroxide is endothermic (ΔG = 24.4 kcal/mol). Overall, the predicted reaction mechanism begins with an oxidative quenching event between photocatalyst ([Ir[dF(CF_3ppy)$_2$(dtbbpy]PF_6) and acid activated *t*BPA (Figure 23B). Electron transfer causes a reduction in the weak O–O bond, 119 kcal/mol,[84,85], followed by a second fragmentation of the *t*-butyl oxyl radical to acetone and methyl radical. Following the desired radical generation, radical alkylation of the *N*-heterocycle occurs, and product forms through oxidation by either the *t*BPA or catalyst turn-over (Ir(IV/III)). The reductive decomposition of *t*BPA was generalized to other acyl endoperoxides (Figure 23E). This allowed for selective generation of an ethyl radical from *tert*-amyl peracetate and biscycloprpanecarbonyl peroxide (CPO). The latter forms two equivalents of cyclopropyl radical through a double decarboxylation event. These radical methylation conditions were tested directly on known drugs to prove the generality of this transformation as a late-stage functionalize strategy. The yields are largely poor to moderate, reflecting both the challenge of methyl radical alkylation chemistry and *N*-heteroaromatic radical alkylation; yet, comparing other radical methylation methodologies developed by Baran[86], Molander[87] and Minisci[81], DiRocco's method was uniquely effective on the pharmaceutical Voriconazole (Figure 23D). This method

stands as a valued approach in medicinal chemistry, in which compound production is completed to provide the proof-of-concept in the most rapid manner possible.

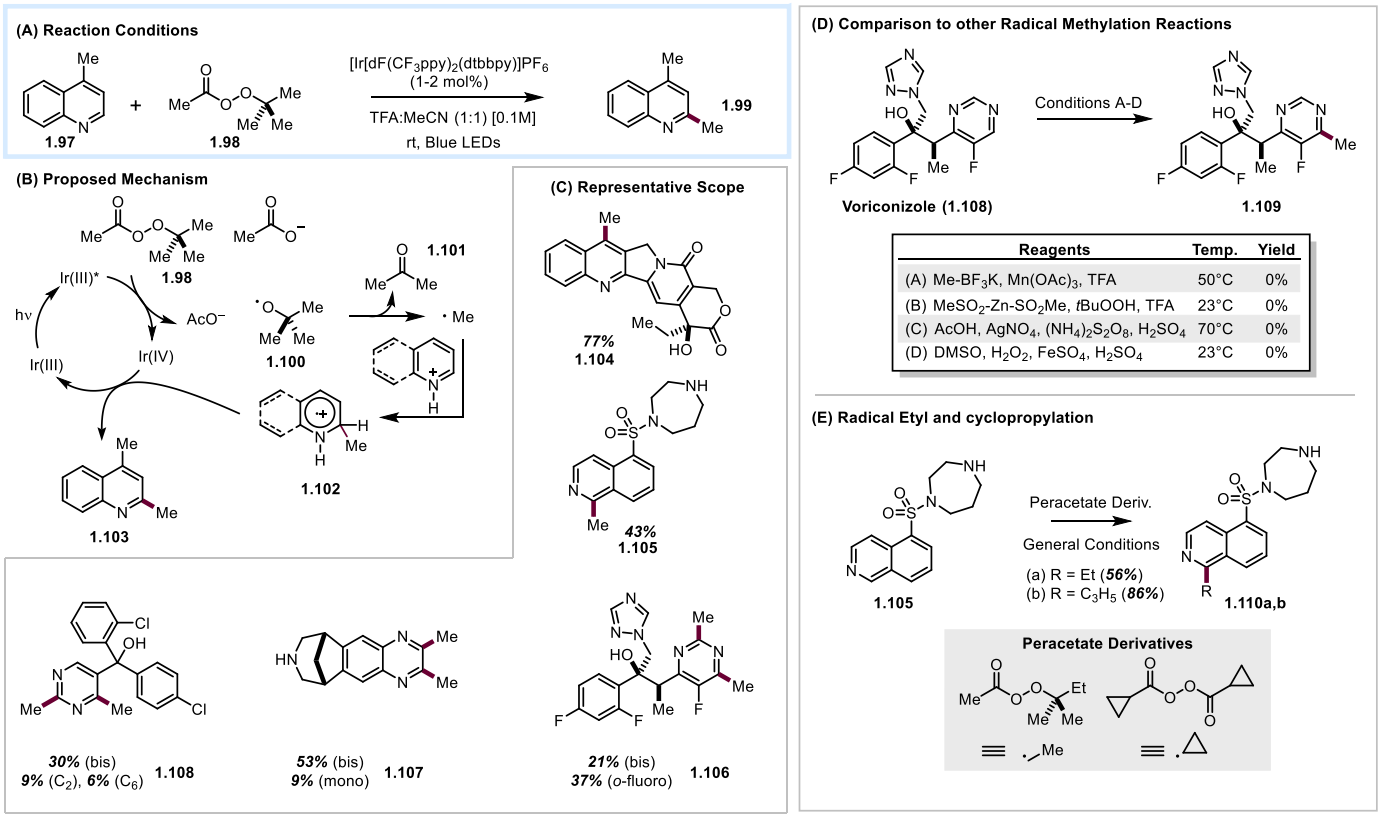

Figure 23: DiRocco's radical methylation from *t*-butylperacetate reduction

1.2.2.2 Nitrogen Centered Radicals:

Nitrogen centered radicals, particularly from a reductive activation event, is a highly advantageous reactive intermediate as it affords C–N bond formation events at arenes, alkenes as well as alkanes with varying selectivity.[88] Nitrogen centered radicals also exhibit competitive C–H abstraction to C–N bond formation, yet, many intramolecular examples for radical cyclizations have proven effective. Stoichiometric oxidation of amines and amides by bromine and chlorine afford haloamines and amides that are prone to decomposing into radical reactants. As such, a major effort in synthetic research has been to identify more stable and controllable redox auxiliaries to reveal the nitrogen centered radicals. With the advent of visible-light photochemistry

and catalysis, carboamination and hydroamination has become more accessible and controlled than ever before. The following is a discussion of the notable approaches for nitrogen radical photoactivation.

In the same vein as Okada, Sanford and co-workers realized the reduction of *N*-acyloxyphalamides as a facile entry into phalamidyl radical generation for arene amination (Figure 24).[89] To achieve a reversal in chemoselectivity for radical generation, Sanford utilized an acetate and other electron deficient substituents on the acetate portion of the *N*-acyloxyphalamide ester to discourage carboxyl radical formation and drive the formation of a nitrogen-centered radical (Figure 24A). This was not effective in the presence of a methyl substituent; however, when trifluoromethyl *N*-acyloxyphalamide was utilized, a high yield of the desired arene amination product was revealed. In turn, reducing trifluoromethylacyloxyphthalimide was effective for a range of different arene substrates containing both electron donating and withdrawing substituents, as well as heteroarenes. By relying on purely radical reactivity, regioisomeric distributions of arene amination products were observed; however, this methodology can rapidly generate aminated arenes at room temperature. Similar methods have been developed with N-bromo saccharin and bisulfonylated hydroxylamines.[90,91,92]

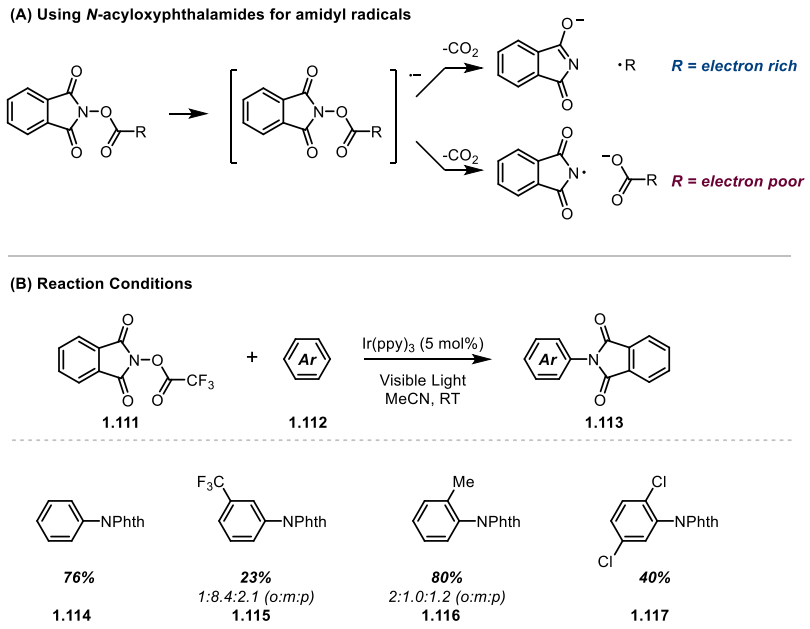

Figure 24: *N*-acyloxyphthalimide esters for Nitrogen Radical Generation

Hydroxylamine serves as a general precursor to amidyl radical chemistry, provided that acylation and sulfonylation reactions to differentially protect and mask these two nucleophilic atoms are available. Leveraging the utility of the weak N–O bond, MacMillan and co-workers realized the dinitrophenylsulfoxy group as an effective redox auxiliary to amidyl radical chemistry (Figure 25A).[93] Dinitrophenylsulfoxylated hydroxylamine (**1.118**) proved a competent radical amination reagent with the previously developed platform of enamine catalysis. In this reaction design, the enamine (**1.122**) is sufficiently electron donating while **1.118** is an activated electron acceptor. Simple visible light irradiation promotes either photoexcitation of **1.118**, or electron transfer within an association complex, to generate the radical cation **1.123**$^{\bullet+}$ and the radical anion of **1.118**$^{\bullet-}$. N-O bond cleavage reveals the desired amidyl radical (**1.125**) and favorably couples with an electron-rich enamide for C–N bond formation. This success of this reaction implies the catalytic cycle of the enamide formation is faster than N-O bond reduction and the enamide present at a significant concentration at the time of amidyl radical generation. Impressively, this reaction

produces high yields of enantioselectively aminated aldehydes without the use of an external photocatalyst. This allows for simple starting materials such as hydrocinammaldhyde to be transformed into chrial aminoalcohols and amino acids (**1.132**) in which the configuration of the C–N bond is determined by the configuration of the amine organocatalyst.

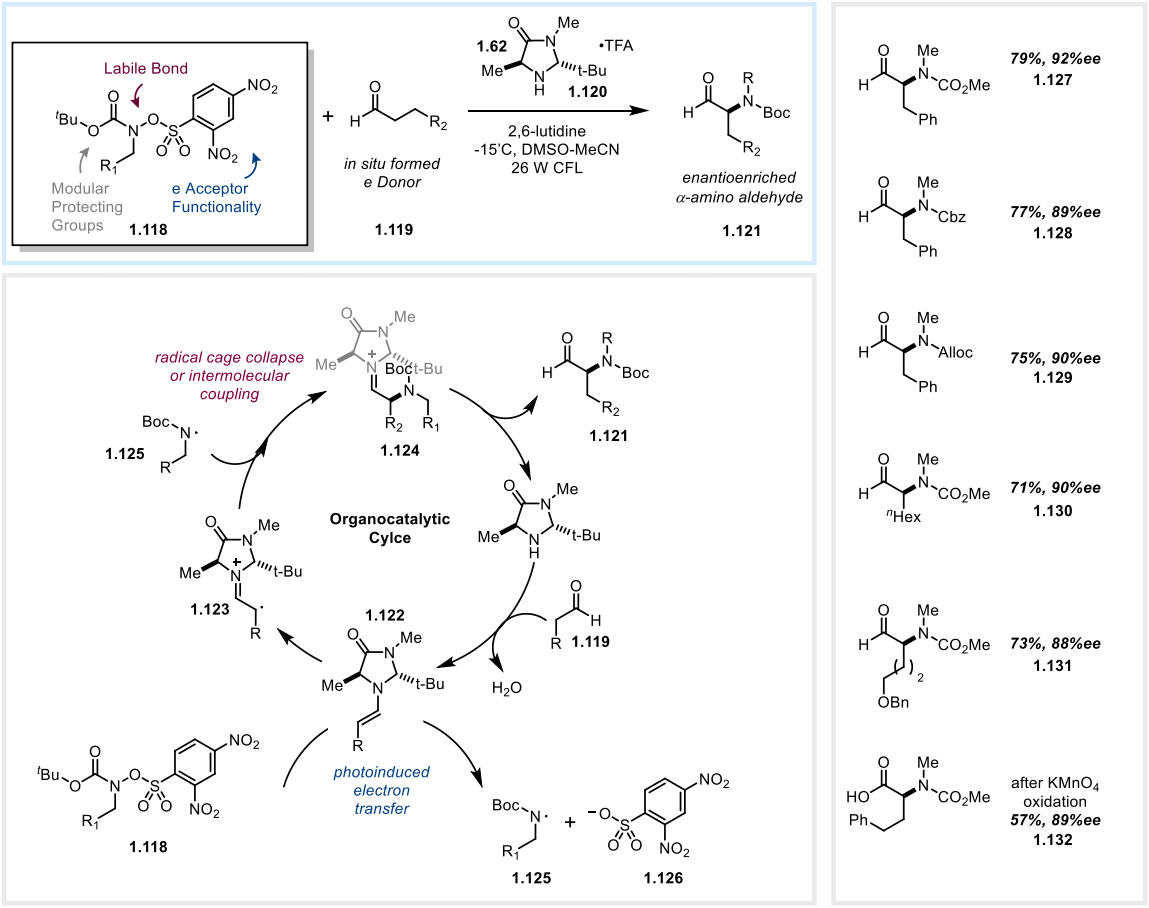

Figure 25: *N*-sulfonyloxy radical precursors for enantioselective aldehyde α–amination

Another N-O-acceptor design for nitrogen-centered radical chemistry has been developed by Lenori and co-workers. *O*-nitrophenyl hydroxylamine, capable of condensation with ketones to provide the corresponding *O*-nitrophenyl oxime (**1.133**), provides a different entry into iminyl radical chemistry (Figure 26A).[94] A key design feature of the acceptor functionality is the tunability of the arene portion to modulate the electron-deficiency and enthalpic barrier to

reduction and fragmentation. Utilizing this rationale, Lenori et. al. reason that 2,4-dinitrophenyl, as opposed to 4-cyano or 2,3,5,6-tetrafluorophenyl, oxime is best suited to participate in a photoredox catalyzed reaction with eosin Y. The first transformation realized with this redox auxiliary design was an intramolecular hydroamination reaction to form **1.135** (Figure 26B). In this instance, the 5-*exo*-trig radical cyclization of **1.134** outcompetes intermolecular H atom abstraction from the terminal reductant, 1,4-cyclohexadiene. A second transformation was developed for the hydroxyamination of alkenes (**1.136**) under redox neutral conditions, by removing the terminal reductant, CHD, and adding potassium carbonate as a weak base.[95] Finally, the *O*-dinitrophenyl oxime auxiliary can be activated by n-donation by trimethylamine. The association complex between triethylamine and the dinitrophenyl oxime exhibits a charge transfer band of <600 nm, allowing blue light to photoinitate the iminyl radical generation. Under these conditions, despite triethylamine being oxidized, the 5-*exo*-trig cyclization product traps the oxygen atom from the released dinitrophenyl auxiliary rather than an H-atom from the triethylamine radical cation (Figure 26C). Overall the triethylamine photoinitiated iminohydroxylation reaction productively affords good yields of the pentacyclic products in all cases.

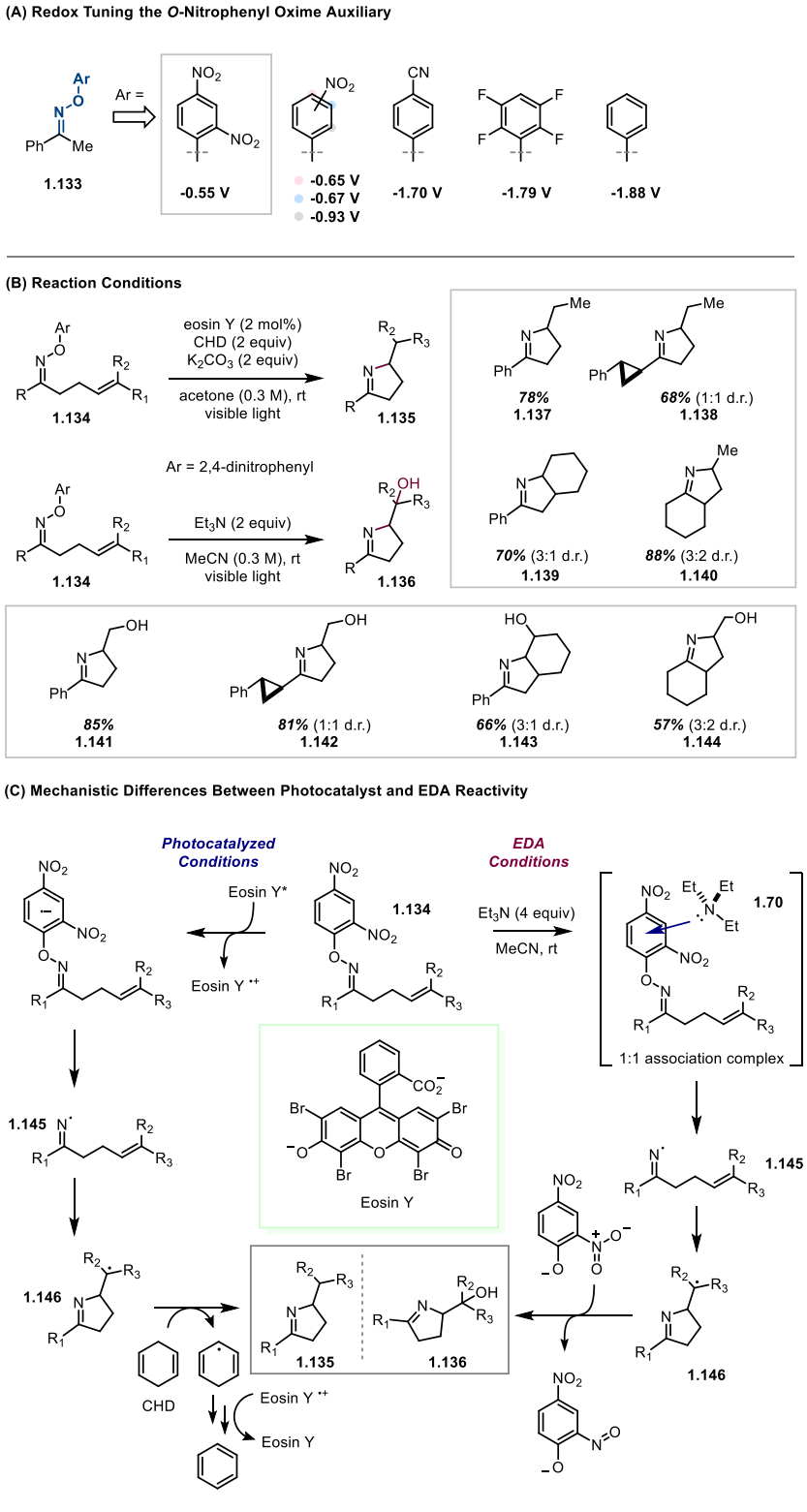

Figure 26: *O*-aryl oxime redox auxiliary for iminyl radical chemistry

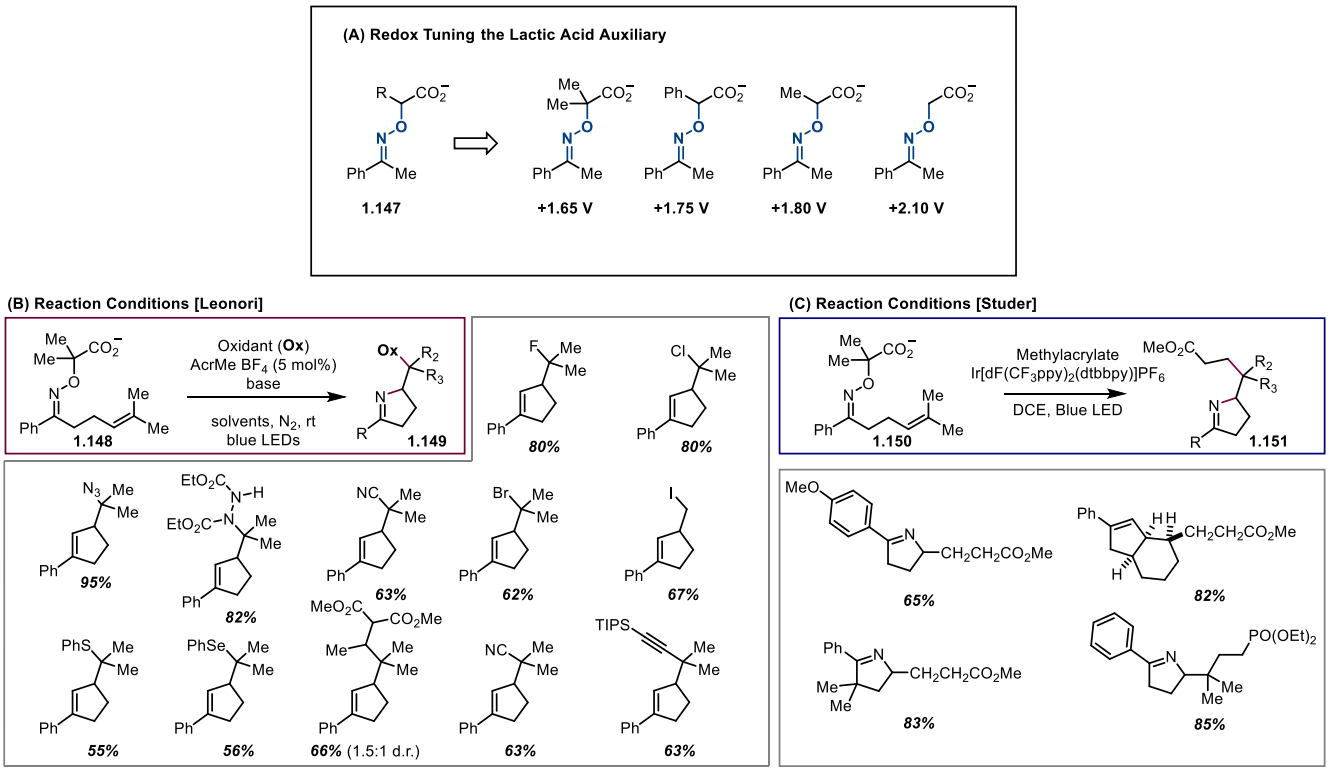

Figure 27: Reactivity of Lactic Acid redox auxiliary

With the aim of improving upon the reaction design of the *O*-dinitrophenyl oxime-iminyl radical generation protocol, Leonori investigated a visible light mediated iminyl radical generation method resulting from a reductive quenching event, rather than oxidative quenching. In this manner, the iminyl radical could be generated and the pentacyclic cyclization product could be trapped with a variety of radical terminating oxidants such as *N*-bromosuccinimide. This reversal in catalytic design also affords the catalyst turnover step as a reduction between a catalytic amount of reduced photocatalyst (PC–) and a stoichiometric amount of oxidant. The redox auxiliary to accomplish this was a lactic acid based oxime (**1.147**) (Figure 27A-B).[96] The reactivity of the auxiliary can be modified by the structure of the α-oxime carboxylic acid, varying over a 700 mV range in oxidation potential based on the other α—substituents of the carboxylic acid. In practice, this allowed Leonori and co-workers to study the same 5-*exo*-trig cyclization in which the different imidation products were defined by the external oxidant added in solution. The designed reaction

was highly effective over a range of different radical traps, enabling a truly versatile alkene difunctionalization reaction. Concurrently reported with Leonori and co-workers was Studer and co-workers' studies on the same redox auxiliary (**1.150**)(Figure 27C).[97] Studer focused specifically on a carboamination reaction, rather than the variety of SOMO-philes that Leonori investigated.

1.2.2.3 Mesolytic Cleavage

The discussed redox auxiliaries have been used to produce either heteroatomic radicals or enable the derivitization of carbon centered radicals from various common functional groups. The designed radical fragmentations reveal a reactive radical intermediate. Mesolytic cleavage uniquely accesses ionic intermediates from single electron transfer steps. Advantages to a mesolytic reaction include the generation of ions under neutral conditions, allowing for a wide functional group compatibility while creating a reactive chemical structure.

Knowles and co-workers developed a mesolytic cleavage reaction of TEMPO derived alkoxyamine ethers (**1.152**), for the generation and trapping of carbocations in C–C bond forming reactions.[98] Unique features of this functionality include a weak C–O bond strength estimated at 26 kcal/mol and an oxidation potential near 1 V vs SCE. To achieve mesolytic cleavage, an oxidatively biased Ir(III) photocatalyst was utilized in the presence of a variety of nucleophiles including silyl enol ethers, allyl silanes as alcohols (**1.158**-**1.161**). The alkoxyamine substrate was also general to non-benzylic stabilized carbocations.

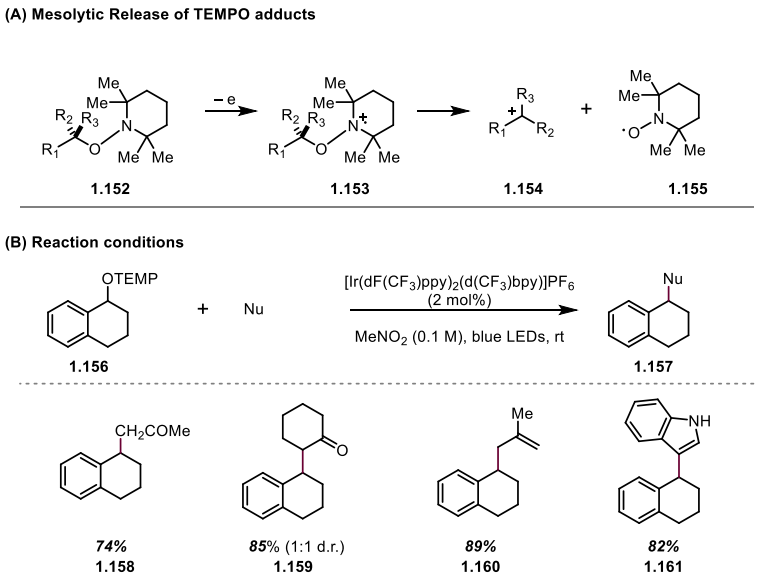

Figure 28: Mesolytic Release of Carbocations from TEMPO adducts

Having established the utility of a mesolytic carbocation generation, Knowles and co-workers applied this strategy to elegantly synthesize polypyrroloindoline dimer natural products.[99] Firstly, an enantioselective synthesis of pyrroloindoline is promoted by light and a chiral phosphate base catalyst upon irradiation. The combination of these catalysts, with TIPS-EBX as an additive, allow for an oxidative cyclization of the tryptophan derivative (**1.162**) for form a hydroxy pyrroloindoline (**1.163**). Furthermore, photocatalysis can be applied in a second step, with mesolytic cleavage of the pyrroloindoline to generate the pyrroloindoline carbocation, which can then be trapped to form **1.164** with an exogenous C_3-indole nucleophile. Impressively, the carbocation intermediate retains the configuration of the stereocenter established in the first step. Overall, this method was useful in the synthesis of (-)-psychotriasine, (-)-chimonanthine and (-)-calycanthidine and exemplified a unique application of visible light photocatalysis in the synthesis of natural products.

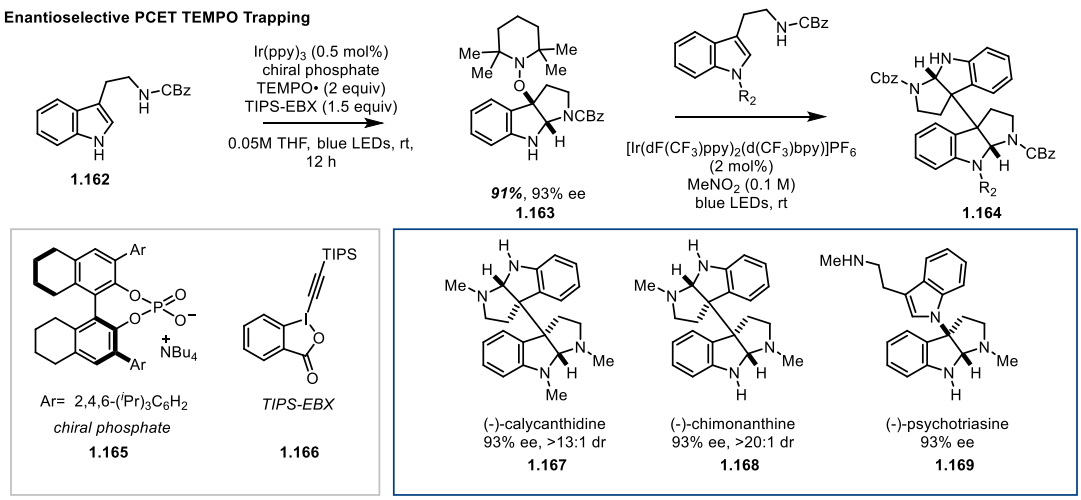

Figure 29: Knowles' Photocatalytic Enantioselective synthesis of polypyrroloindole natural products

1.3 Conclusions:

Visible light photocatalysis has experienced an extraordinary research investment from academia and industry in the development of more efficient, effective and environmentally benign methods to conduct redox chemistry. Many of the design principles investigated by the field's founding authors are still being elaborated and more deeply studied for a general access to carbon and heteroatomic radicals. Activation of covalent redox auxiliaries is one reaction design element that has democratized the utilization of different synthetic functionalities within photoredox catalysis. These auxiliaries are commonly defined through versatile and simplistic synthesis while enabling radical decomposition pathways that result in the generation of benign reaction by-products.

Chapter 2: Rapid Synthesis of $Ir(III)^+$ Polypyridyl Complexes Using Microwave Heating

*Portions of this chapter have been published in Timothy M. Monos, Alexandra Sun, Rory C. McAtee, Corey R. J. Stephenson, *J. Org. Chem.* **2016**, *81*, 6988-6994.

2.1 Introduction

The photophysical properties of Ir(III) based photosensitizers have sustained the attention of synthetic chemists for the development of photoredox catalyzed reactions due to both the high triplet energy and large redox window of these complexes. By comparison, the transition from Ru(II) to Ir(III) catalysts provides an added 12-15 kcal/mol of energy, provided that light of <450 nm is accessible for irradiation. Polypyridyl Ir(III) complex synthesis began with the isolation of *faC*–$Ir(ppy)_3$ by Nonoyama[100] and then Watts[101], showing that cyclometallation first preceded through an Ir–μ intermediate (**2.5)** followed by a challenging final cyclometallation (**2.2**) (Figure 32B). Konno and Sasaki later followed with a demonstration of a microwave irradiation procedure for the synthesis of homoleptic Ir(III) complexes (Figure 32C).[102] While Konno impressively produced *faC*–$Ir(ppy)_3$ in high yields, this required 50-100 equivalents of 2-phenylpyridine in ethylene glycol. At lower ligand equivalents (10-30 equiv), the authors noted that the reaction stopped at the Ir-μ dimer formation. Finally, Davies and co-workers reported the cyclometallation of *m*-pyrazoloarenes to form the Ir-μ dimer with $IrCl_3$ or K_2IrCl_6 in ^{i}PrOH and H_2O (Figure 32B).[103]

Heteroleptic Ir(III) complexes offer a synthetic advantage because the photophysical properties can be orthogonally tuned through ligand diversification. This phenomenon is attributable to the spatial separation of the MLCT state in heteroleptic complexes. As modeled

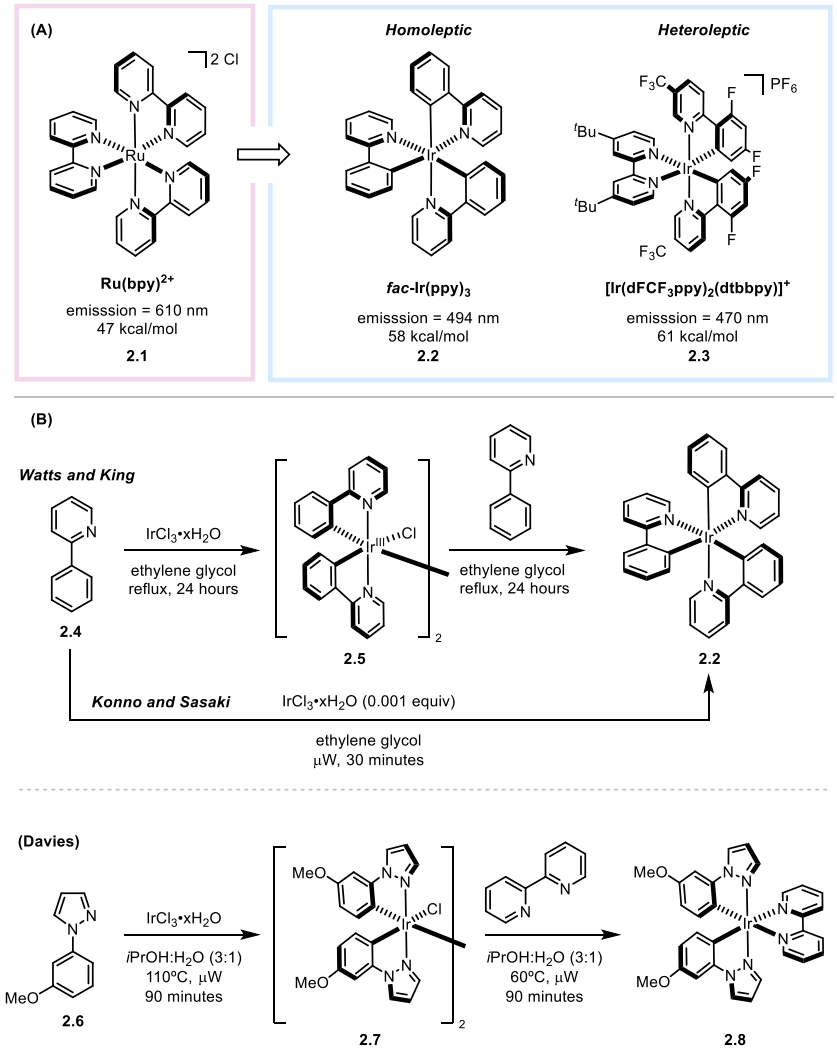

Figure 30: Comparison of Ru(II) to Ir(III) excited state triplet energies and the syntheses of the Ir-μ-dimer complex and monomeric complexes

through DFT calculations, as well as observed in synthetic studies, the ground state LUMO exists primarily on the dative ligand, whereas the metal and cyclometallating ligands constitute the ground state HOMO. This spatial orbital separation in the ground state continues in the MLCT photoexcited state and was first observed by King and Watts in the photoexcitation of $Ir(ppy)_2(bpy)^+$ using time resolved spectroscopy.[101] More practically, Bernhard and Malliaras demonstrated the differential tuning of redox properties through a series of fluorinated

heteroleptic $Ir(III)^{+}$ complexes.[104] The incorporation of fluorine substituents on the cyclometallating ligand increases

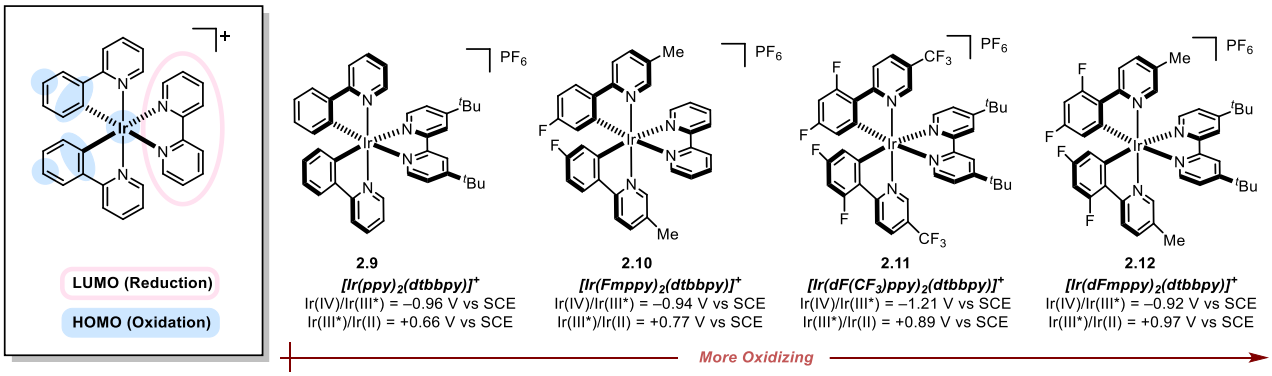

Figure 31: Variance in Ir(III/II) oxidation potential based on cyclometallated ligand fluorination

the oxidation potential of the complex (Ir(IV/III), while minimally effecting the reduction potential (Ir(III/II). Zysmann-Coleman and Henwood have detailed a descriptive account of the effects of ligand structure on photophysics of heteroleptic Ir(III) complexes.[105]

Despite the previous reports by Davies and Konno, most photoredox catalysis reports cited the preparation of $Ir(III)^{+}$ complexes through two separate conduction heating batch reactions. This method is time and energy intensive; more importantly, it precludes library development of $Ir(III)^{+}$ catalysts by ligand diversification. To alleviate the time and energy requirements for photocatalyst synthesis, we adapted Bernhard and Mallarias' method for microwave irradiation to simplify and expedite the preparation of $Ir(III)^{+}$ complexes.

Microwave irradiation is a contemporary tool for a uniform and energy efficient heating of a chemical reaction. By using microwave heating, processing times can be shortened as the reaction solution is evenly heated or superheated under pressure. Organic solvents vary in heating efficiency, a parameter defined by the variables of dielectric loss factor (ε') and dielectric constant (ε''). The dielectric constant of a solvent is defined by the ability of that solvent to mitigate

columbic interactions (F = Colubmic force) between two atoms (p_a and p_b) at a given distance (r) (equation 2.1):

$$F = \frac{p_a p_b}{e'' r^2} \qquad \text{Equation 2.1}$$

The dielectric constant dielectric constant (ε'') of a liquid is constant at a variety of elevated temperatures. The dielectric loss factor (ε') is an intrinsic and aggregate heat storage property of a liquid that decreases at elevated temperature. Nonetheless, polar molecules like ethylene glycol and dimethylsulfoxide exhibit larger ε' values than hexanes or diethyl ether. These two properties are related by a single number δ, where:

$$\tan(\delta) = \frac{e''}{e'} \qquad \text{Equation 2.2}$$

Tabulation of tan(δ) values of a variety of solvents are available in microwave heating reference resources[106], while generally polar solvents such as water, ethylene glycol, acetone, alcohols and dimethyl sulfoxide are sufficiently good starting points for microwave heating optimization.

2.2 Reaction Optimization

To explore the utility of microwave heating in the cyclometallation of 2-phenylpyridine derivatives, we sought to optimize the first cyclometallation process of 2-(2,4-difluorophenyl)-5-trifluoromethyl pyridine (dF(CF_3ppy)$_2$) (Figure 32). Cyclometallation of this substrate provided a challenge given the electron deficient structure of the substrate. Microwave heating a mixture of $IrCl_3$•xH_2O and 2 equiv of 2-(2,4-difluorophenyl)-5-(trifluoromethyl)pyridine resulted in the formation of [(dF(CF_3)ppy)$_2$Ir-μ-Cl]$_2$ (**2.14**) in ***40%*** yield (entry 1). Increasing the stoichiometry of **2.13** to account for the HCl generated in the reaction boosted the yield to ***59%***. Additional experiments to lengthen the time of the reaction or increase the temperature of the reaction did not

produce higher yields of the desired dimer. Comparatively, **2.4** was subjected to the same conditions, resulting in the formation of $[(ppy)_2\text{-Ir-}\mu]_2$ (**2.15**) dimer in ***89%*** yield.

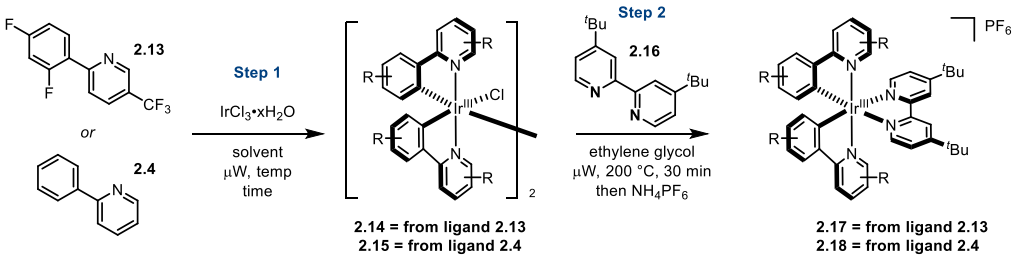

Entry	Ligand	Temperature/Solvent	Ligand (equiv)	Step 1 Time (% Yield)	Step 2 % Yield
1	2.13	200 °C/ethylene glycol	2	1 h (40)	-
2	2.13	200 °C/ethylene glycol	4	1 h (52)	-
3	**2.13**	**200 °C/ethylene glycol**	**8**	**1 h (59)**	**96 (2.17)**
4	2.13	200 °C/ethylene glycol	8	4 h (0)	-
5	2.13	250 °C/triethylene glycol monoethyl ether	8	1 h (0)	-
6	**2.4**	**200 °C/ethylene glycol**	**8**	**1 h (84)**	**98 (2.18)**

Figure 32: Reaction Optimization for $Ir(III)^+$ complex synthesis

Satisfied with the optimization of the first step, dative ligation of the bipyridine ligand was conducted simply by adding the desired bipyridine ligand (2 equiv) to the crude mixture and heating the reaction for another 30 minutes at 200°C. Gratifyingly this produced the desired heteroleptic complex in quantitative yield (**2.17-2.18**).

2.3 Reaction Performance

To demonstrate the utility of this two-step one-pot preparation of $Ir(III)^+$ complexes, a variety of cyclometallating ligands and dative ligands were examined. The conditions were capable of cyclometallating 2-phenylpyridine (**2.4**), 2-(4-fluoro)phenylpyridine and 2-(2,4-difluorophenyl)pyridine (**2.13**), as well as appending para-substituted bipyridines and phenanthroline to the iridium metal center. More importantly, 1.12 grams of $Ir(ppy)_2(dtbbpy)PF_6$ (**2.7**) was synthesized in 5 hours using this method, showcasing the significant decrease in

processing time necessary to obtain these photoactive salts. Notably this process avoids the use of stoichiometric silver or exogenous bases to complete the formation of the heteroleptic complex.

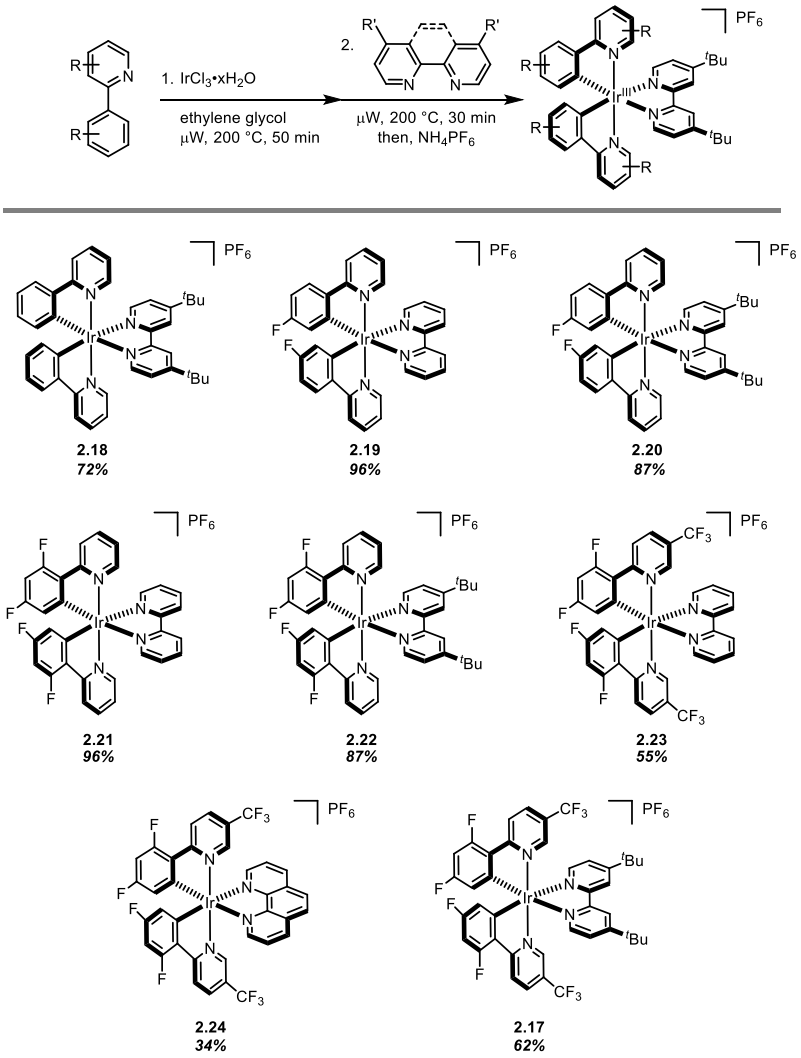

Figure 33: Ir(III)$^+$ reaction scope

2.4 Conclusions

A method for the rapid synthesis of Ir(III)$^+$ polypyridyl complexes is disclosed using microwave heating. These complexes are particularly useful in new reaction development for photoredox catalysis given the high excited state triplet energies and expansive redox couples. This method is ideally suited for library synthesis in which heteroleptic complexes are diversified from a common

Ir-dimer intermediate, and require minimal synthetic processing (work-up, recrystallization, etc.). The conditions extablished can generate $Ir(III)^{+}$ complexes on gram scale.

2.5 Experimental Methods

2.5.1 General Information

All reagents were obtained from commercial suppliers and used without further purification unless otherwise noted. $IrCl_3 \cdot xH_2O$ was purchased from Pressure Chemical, NH_4PF_6 was purchased from Oakwood Products, Inc. and all ligands were obtained from Sigma-Aldrich unless otherwise specified. Microwave heated reactions were carried out in sealed microwave flasks (2-5 mL [CG-4920-01] or 10-20mL [CG-4920-02], Chemglass) and heated by a Biotage Initiator+ microwave synthesizer with a Robot Eight automated sampler. Temperature and pressure was monitored by an infrared sensor on the surface exterior of the vial. Pressure was monitored by a pressure transducer situated at the top of the vial. NMR spectra were obtained on a 700 MHz Varian VNMRS spectrometer and a 500 MHz Varian VNMRS spectrometer. 1H and 13C NMR chemical shifts are reported in ppm relative to the residual acetone (δ 2.09) solvent peak.37 Reactions were monitored by thin layer chromatography (TLC) using silica TLC plates obtained from EMD Millipore; silica gel 60 F254, glass-backed, 250 μm, and were visualized with ultraviolet light.

2.5.2 Microwave Reaction: A Pictorial Guide

Safety Note: Pre-stirring the reaction solution is highly recommended, because the build-up of heterogeneous inorganic material in a microwave reaction can lead to uneven heating of the mixture and risk of explosion. Reactions should never be run without working temperature and pressure monitors on a microwave heating apparatus.

Table 1: Microwave catalyst synthesis, a pictoral guide

<table>
<tr>
<td> 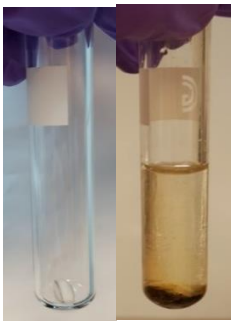

Step 1: Left: Biotage microwave vial (size 2-5 mL) equipped with a magnetic stir bar.

Right: $IrCl_3 \bullet xH_2O$, cyclometalating ligand, and ethylene glycol were added next.</td>
<td> 

Step 2: The sealed reaction vial was pre-stirred for 1 min then heated at 200 ^oC for 50 min at atmospheric pressure in a Biotage Initiator+ microwave synthesizer, as shown above.</td>
</tr>
<tr>
<td> 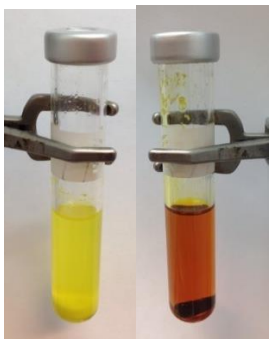

Step 3: Left: After heating for 50 min at 200 ^oC, the reaction mixture appears heterogeneous with visible yellow precipitate. Upon addition of the dative ligand, the vial was resealed and heated to 200 ^oC for 30 min.

Right: After heating for 30 min at 200 ^oC, the reaction mixture appears homogeneous</td>
<td> 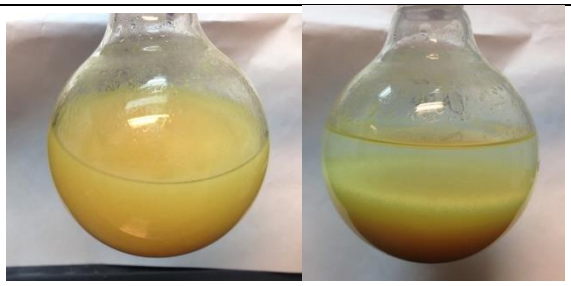

Step 4: Left: The reaction mixture was diluted with DI H_2O and extracted with hexanes. The aqueous portion was collected and heated to 75 ^oC for 15 min to remove remaining organic solvent to give the yellow solution above.

Right: Aqueous ammonium hexafluorophosphate was then added to the mixture, and the whole was cooled in an ice bath. The resulting precipitate was collected and washed with cold DI H_2O and cold diethyl ether. Finally, the precipitate was taken up in acetone, concentrated, and dried in vacuo to yield the title complex.</td>
</tr>
</table>

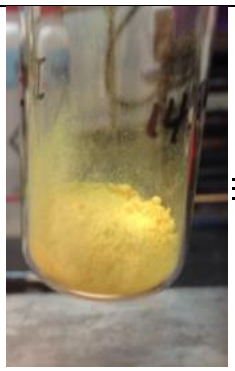

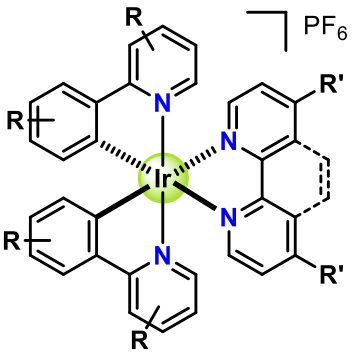

Step 5: Isolated and pure heteroleptic $Ir(C^N)_2(N^N)PF_6$ complex.

2.5.3 Synthetic Procedures

General Procedure for C^N ligand synthesis:

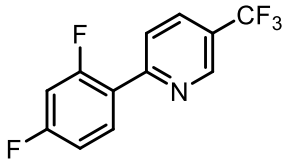

2-(2,4-difluorophenyl)-5-(trifluoromethyl)pyridine (**2.13**).

To a three-necked, 100 mL round bottom flask charged with a magnetic stir bar were added 2-chloro-5-(trifluoromethyl)pyridine (3.1 g, 17.0 mmol, 0.9 equiv), 2,4-difluorophenylboronic acid (3.0 g, 19.0 mmol, 1.0 equiv), 2 M aqueous sodium carbonate (4.03 g, 38.0 mmol, 2.0 equiv), benzene (23 mL), and toluene (17 mL). The mixture was degassed by sparging with N_2 for 15 min. Then $Pd(PPh_3)_4$ (0.505 g, 0.437 mmol) was added to the reaction mixture and degassing was continued for another 15 min. The reaction mixture was heated to reflux for 48 h to generate a yellow solution with yellow precipitate. The progress of the reaction was monitored by TLC (85% ethyl acetate in hexanes). Upon completion of the reaction, the mixture was cooled to room temperature and then extracted with dichloromethane (4 x 20 mL), washed with brine (3 x 20 mL), and dried over Na_2SO_4. Solvent was removed under reduced pressure to give a dark brown oil which solidified at room temperature. The crude product was purified by flash chromatography

using 100% dichloromethane to afford a yellow oil, which crystallized at room temperature. The yellow oil was further dried *in vacuo* to afford the pure ligand in 77% yield (3.81 g, 14.7 mmol) as white crystals. ^{1}H NMR chemical shifts match literature values.[107]

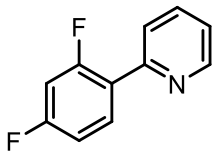

2-(4-fluorophenyl)pyridine.

To a three-necked, 100 mL round bottom flask charged with a magnetic stir bar were added 2-chloropyridine (2.00 g, 17.61 mmol, 1.0 equiv), 4-fluorophenylboronic acid (2.96 g, 21.14 mmol, 1.2 equiv), triphenylphosphine (0.46 g, 1.76 mmol, 0.1 equiv), 2 M aqueous potassium carbonate (6.55 g, 47.39 mmol), and dimethoxyethane (20 mL). The mixture was degassed with N_2 for 15 min. Then 2.5 mol% $Pd(OAc)_2$ (0.1 g, 0.441 mmol) was added to the reaction mixture and degassing was continued for another 15 min. The reaction mixture was heated to reflux for 18 h to generate an orange solution with orange precipitate. The progress of the reaction was monitored by TLC (10% ethyl acetate/hexanes). Upon completion of the reaction, the mixture was cooled to room temperature and then extracted with dichloromethane (4 x 20 mL), washed with brine (3 x 20 mL), and dried over Na_2SO_4. Solvent was removed under reduced pressure, and the crude product was purified by flash chromatography (0-5% ethyl acetate in hexanes) on a 30 g silica column. The pure ligand was obtained in 55% yield (1.68 g, 9.7 mmol) as a white solid. ^{1}H NMR chemical shifts match literature values.[107]

General Procedure A for the Synthesis of Heteroleptic Ir(C^N)(N^N)$_2$ Complexes (100 mg scale):

To a Chemglass microwave vial (size 2-5 mL) equipped with a magnetic stir bar were added $IrCl_3$•xH_2O (50 or 100 mg, 1.0 equiv), cyclometalating ligand (8.0 equiv), and ethylene glycol (5 mL, 32 or 64 μM). The vial was sealed and pre-stirred for 1 min prior to heating under microwave irradiation (200 ^oC, 50 min) at atmospheric pressure.* Upon allowing the mixture to cool to room temperature, the dative ligand was added (1.5 equiv), and the vial was heated under microwave irradiation (200 ^oC, 30 min) at atmospheric pressure. After cooling to room temperature, the reaction mixture was diluted with DI H_2O (25 mL) and extracted with hexanes (3 x 20 mL). The aqueous portion was collected and heated to 75 ^oC for 15 min to remove remaining organic solvent. Aqueous ammonium hexafluorophosphate (2.0 g in 20 mL DI H_2O) was added to the mixture, and the mixture was cooled in an ice bath. The resulting precipitate was collected and washed with cold DI H_2O (10 mL) and cold diethyl ether (10 mL). Finally, the precipitate was taken up in acetone and dried *in vacuo* to afford the desired product.

Procedure for the 500 mg scale synthesis of [Ir(ppy)$_2$(dtbbpy)]PF$_6$ (2.18):

The general procedure A was followed, using $IrCl_3 \cdot H_2O$ (500 mg, 1.6 mmol, 1.0 equiv), 2-phenylpyridine (1.8 μL, 12.6 mmol, 8.0 equiv), and ethylene glycol (15 mL) to obtain a bright yellow solution with yellow solids. **2a** was synthesized using 4,4'-di-*t*-butyl-2,2'-bipyridine (636 mg, 2.36 mmol, 1.5 equiv) to afford a homogeneous orange solution. **2a** was obtained in 78% yield (1.12 g, 1.22 mmol) as a yellow solid after recrystallization with acetone and diethyl ether at low temperatures.

Procedure for the 500 mg scale synthesis of [Ir(dF(CF)3ppy)2(dtbbpy)]PF_6 (2.17):

The general procedure A was followed, using $IrCl_3 \cdot H_2O$ (500 mg, 1.6 mmol), 2-(2,4-difluorophenyl)-5-(trifluoromethyl)pyridine (3.28 g, 12.6 mmol), and ethylene glycol (15 mL). The reaction mixture was sonicated before microwave irradiation to increase homogeneity of the solution. A bright orange solution with green amorphous solids was obtained. **2g** was synthesized using 4,4'-di-*t*-butyl-2,2'-bipyridine (636 mg, 2.36 mmol) to afford an orange solution with green solids. The reaction mixture was diluted with DI H_2O (100 mL) and extracted with hexanes (3 x 75 mL) and ethyl acetate (4 x 75 mL). The ethyl acetate extract was collected, filtered to remove unreacted $IrCl_3$ solids, dried over Na_2SO_4, and concentrated *in vacuo* to afford an orange oil with yellow solids. DI H_2O (75 mL) was combined with the mixture to generate a yellow solution with free-flowing yellow solids. Aqueous ammonium hexafluorophosphate (10.0 g in 100 mL DI H_2O) was then added to the mixture, and the whole was cooled in an ice bath. The resulting yellow precipitate was collected and washed sequentially with cold DI H_2O (4 x 25 mL) and hexanes (4 x 25 mL). Finally, the precipitate was taken up in acetone and dried *in vacuo* to afford a mixture of yellow solids and an orange oil. **2g** was obtained in 50% yield (883 mg, 0.79 mmol) as a light yellow solid after recrystallization with acetone and diethyl ether at low temperatures.

2.5.4 Characterization of Heteroleptic Ir(III)$^{+}$ Complexes:

[Ir(dF(CF)$_3$ppy)$_2$(dtbbpy)]PF$_6$ (2.17):

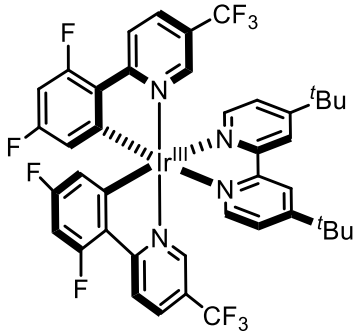

^{1}H-NMR (Acetone-d_6, 700 MHz): δ 8.94 (s, 2H), 8.62 (d, J = 8.9 Hz, 2H), 8.41 (d, J = 8.7 Hz, 2H), 8.19 (d, J = 5.8 Hz, 2H), 7.94 - 7.70 (m, 4H), 6.87 (t, J = 10.3 Hz, 2H), 5.97 (d, J = 7.9 Hz, 2H), 1.43 (s, 18H).**^{13}C–NMR** (Acetone-d_6, 176 MHz): δ 167.83 (s), 165.33 (d, J = 18.6 Hz), 163.85 (d, J = 12.6 Hz), 163.19 (d, J = 12.7 Hz), 161.70 (d, J = 13.2 Hz), 156.00 (s), 155.77 (d, J = 6.9 Hz), 151.09 (s), 145.72 (d, J = 4.7 Hz), 137.18 (s), 126.81 (s), 126.03 (s), 125.23 (d, J = 34.6 Hz), 124.11 - 124.03 (m), 123.90 (d, J = 20.9 Hz), 122.91 (s), 122.67 (s), 121.37 (s), 114.44 (d, J = 17.9 Hz), 99.31 (d, J = 27.1 Hz), 99.09 (s), 99.08 (s), 35.70 (s), 29.45 (s).

[Ir(ppy)$_2$(dtbbpy)]PF$_6$ (2.18):

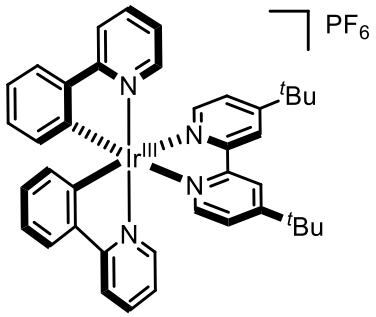

^{1}H-NMR (Acetone-d_6, 700 MHz): δ 8.88 (s, 2H), 8.23 (d, *J* = 8.2 Hz, 2H), 8.03 - 7.92 (m, 3H), 7.88 (d, *J* = 7.6 Hz, 2H), 7.78 (d, *J* = 5.7 Hz, 2H), 7.70 (d, *J* = 5.7 Hz, 2H), 7.12 (t, *J* = 6.5 Hz, 2H), 7.02 (t, *J* = 7.4 Hz, 2H), 6.90 (t, *J* = 7.3 Hz, 2H), 6.33 (d, *J* = 7.5 Hz, 2H), 1.40 (s, 13H).**^{13}C–NMR** (Acetone-d_6, 176 MHz): δ 167.88 (s), 163.97 (s), 155.89 (s), 151.00 (s), 150.18 (s), 149.02 (s), 144.03 (s), 138.55 (s), 131.53 (s), 130.31 (s), 125.48 (s), 124.89 (s), 123.47 (s), 122.32 (s), 121.98 (s), 119.87 (s), 35.51 (s), 29.51 (s).

[Ir(Fppy)$_2$(bpy)]PF$_6$ (2.19):

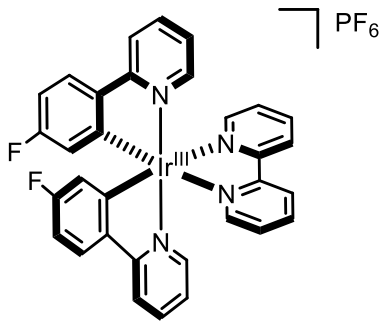

^{1}H-NMR (Acetone-d_6, 500 MHz): δ 8.91 (d, *J* = 8.2 Hz, 2H), 8.37 (td, *J* = 8.0, 1.4 Hz, 2H), 8.28 (d, *J* = 8.2 Hz, 2H), 8.21 (d, *J* = 5.3 Hz, 2H), 8.11 - 7.97 (m, 4H), 7.87 (d, *J* = 5.8 Hz, 2H), 7.81 - 7.73 (m, 2H), 7.22 (t, *J* = 6.6 Hz, 2H), 6.87 (td, *J* = 8.8, 2.5 Hz, 2H), 5.98 (dd, *J* = 9.5, 2.5 Hz, 2H).

^{13}C–NMR (Acetone-d_6, 176 MHz): δ 166.48 (s), 164.40 (s), 162.96 (s), 155.92 (s), 153.51 (d, *J* = 5.8 Hz), 150.78 (s), 149.28 (s), 140.51 (s), 139.91 (s), 139.06 (s), 128.74 (s), 127.22 (d, *J* = 9.3 Hz), 124.97 (s), 123.68 (s), 120.11 (s), 117.40 (d, *J* = 17.8 Hz), 109.70 (s), 109.57 (s).

[Ir(Fppy)$_2$(dtbbpy)]PF$_6$ (2.20):

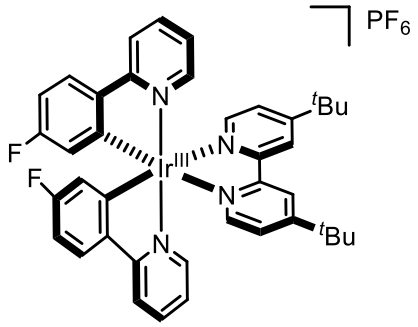

^{1}H-NMR (Acetone-d_6, 700 MHz): δ 8.94 (s, 2H), 8.28 (d, J = 8.2 Hz, 2H), 8.13 - 7.96 (m, 4H), 7.82 (d, J = 5.5 Hz, 2H), 7.77 (dd, J = 5.8, 1.7 Hz, 2H), 7.19 (t, J = 6.2 Hz, 2H), 6.87 (td, J = 8.8, 2.5 Hz, 2H), 5.97 (dd, J = 9.5, 2.5 Hz, 2H), 1.45 (s, 18H). **^{13}C–NMR** (Acetone-d_6, 176 MHz): δ 166.66 (s), 164.46 (s), 164.29 (s), 163.02 (s), 155.81 (s), 154.08 (d, J = 5.6 Hz), 150.37 (s), 149.07 (s), 140.50 (s), 138.99 (s), 127.20 (d, J = 9.3 Hz), 125.66 (s), 123.56 (s), 122.17 (s), 120.11 (s), 117.30 (d, J = 17.7 Hz), 109.57 (s), 109.44 (s), 29.49 (s).

[Ir(dFppy)$_2$(bpy)]PF$_6$ (2.21):

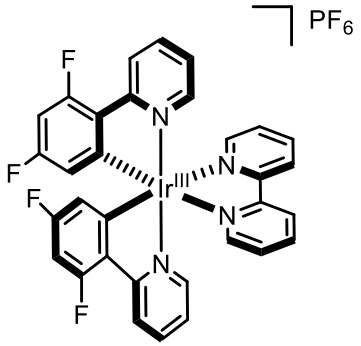

^{1}H-NMR (Acetone-d_6, 700 MHz): δ 8.94 (s, 2H), 8.62 (d, *J* = 8.9 Hz, 2H), 8.41 (d, *J* = 8.7 Hz, 2H), 8.19 (d, *J* = 5.8 Hz, 2H), 7.94 - 7.70 (m, 4H), 6.87 (t, *J* = 10.3 Hz, 2H), 5.97 (d, *J* = 7.9 Hz, 2H), 1.43 (s, 18H). **^{13}C–NMR** (Acetone-d_6, 176 MHz): δ 167.83 (s), 165.33 (d, *J* = 18.6 Hz), 163.85 (d, *J* = 12.6 Hz), 163.19 (d, *J* = 12.7 Hz), 161.70 (d, *J* = 13.2 Hz), 156.00 (s), 155.77 (d, *J* = 6.9 Hz), 151.09 (s), 145.72 (d, *J* = 4.7 Hz), 137.18 (s), 126.81 (s), 126.03 (s), 125.23 (d, *J* = 34.6 Hz), 124.11 - 124.03 (m), 123.90 (d, *J* = 20.9 Hz), 122.91 (s), 122.67 (s), 121.37 (s), 114.44 (d, *J* = 17.9 Hz), 99.31 (d, *J* = 27.1 Hz), 99.09 (s), 99.08 (s), 35.70 (s), 29.45 (s).

[Ir(dFppy)$_2$(dtbbpy)]PF$_6$ (2.22):

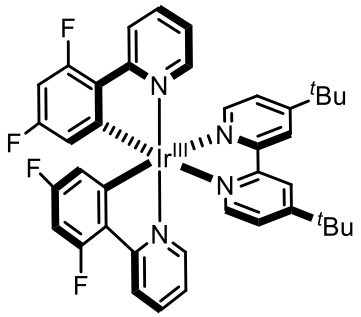

^{1}H-NMR (Acetone-d_6, 500 MHz): δ 8.96 (s, 2H), 8.41 (d, *J* = 8.4 Hz, 2H), 8.09 (dd, *J* = 14.1, 6.8 Hz, 4H), 7.90 (d, *J* = 5.6 Hz, 2H), 7.77 (dd, *J* = 5.8, 1.7 Hz, 2H), 7.24 (t, *J* = 6.7 Hz, 2H), 6.86 – 6.70 (m, 2H), 5.80 (dd, *J* = 8.5, 2.2 Hz, 2H), 1.43 (s, 18H). **^{13}C–NMR** (Acetone-d_6, 176 MHz): δ 164.62 (s), 164.33 (d, *J* = 12.4 Hz), 163.91 (d, *J* = 7.0 Hz), 162.87 (d, *J* = 12.6 Hz), 162.14 (d, *J* = 13.1 Hz), 160.67 (d, *J* = 12.9 Hz), 155.68 (s), 155.25 (d, *J* = 6.4 Hz), 150.44 (s), 149.59 (s), 139.71 (s), 127.89 (s), 125.80 (s), 124.10 (s), 123.61 (d, *J* = 19.9 Hz), 122.44 (s), 113.63 (d, *J* = 15.2 Hz), 98.66 (d, *J* = 27.2 Hz), 98.57 - 98.50 (m), 98.43 (s), 35.59 (s), 29.48 (s).

[Ir(dF(CF)$_3$ppy)$_2$(bpy)]PF$_6$ (2.23):

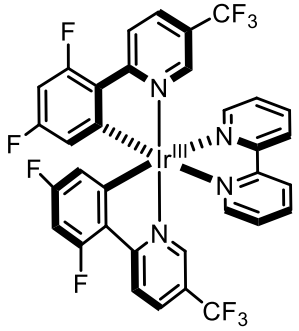

^{1}H-NMR (Acetone-d_6, 700 MHz): δ 8.90 (d, *J* = 8.2 Hz, 2H), 8.62 (d, *J* = 8.9 Hz, 2H), 8.41 (d, *J* = 7.4 Hz, 4H), 8.31 (d, *J* = 5.3 Hz, 2H), 7.98 (s, 2H), 7.87 - 7.73 (m, 2H), 6.87 (t, *J* = 10.9 Hz, 2H), 5.97 (d, *J* = 8.3 Hz, 2H). **^{13}C–NMR** (Acetone-d_6, 176 MHz): δ 167.66 (d, *J* = 6.2 Hz), 165.26 (d, *J* = 12.6 Hz), 163.80 (d, *J* = 12.3 Hz), 163.18 (d, *J* = 12.7 Hz), 161.69 (d, *J* = 13.1 Hz), 155.98 (s), 155.21 (d, *J* = 6.8 Hz), 151.48 (s), 146.20 (d, *J* = 4.4 Hz), 140.71 (s), 137.29 (s), 129.17 (s), 126.87 (s), 125.72 (s), 125.63 - 125.31 (m), 125.31 - 125.22 (m), 125.14 (s), 123.98 (s), 123.90 (d, *J* = 21.0 Hz), 122.90 (s), 121.35 (s), 119.81 (s), 114.46 (d, *J* = 17.9 Hz), 99.51 (s), 99.35 (s), 99.20 (s).

[Ir(dF(CF)$_3$ppy)$_2$(phen)]PF$_6$ (2.24):

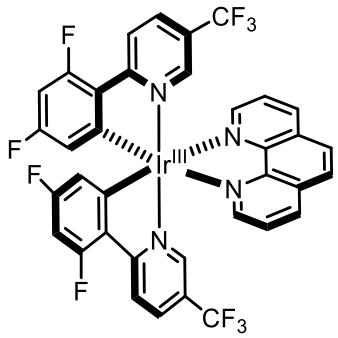

^{1}H-NMR (Acetone-d_6, 500 MHz): δ 9.02 (d, *J* = 8.3 Hz, 2H), 8.69 (d, *J* = 5.1 Hz, 2H), 8.62 (d, *J* = 8.6 Hz, 2H), 8.46 (s, 2H), 8.35 (d, *J* = 8.8 Hz, 2H), 8.16 (dd, *J* = 8.3, 5.1 Hz, 2H), 7.87 (s, 2H), 6.99 - 6.85 (m, 2H), 6.08 (dd, *J* = 8.4, 2.2 Hz, 2H). **^{13}C–NMR** (Acetone-d_6, 176 MHz): δ 167.69 (d, *J* = 6.9 Hz), 165.24 (d, *J* = 12.9 Hz), 163.77 (d, *J* = 12.7 Hz), 163.15 (d, *J* = 13.0 Hz), 161.66 (d, *J* = 13.1 Hz), 154.67 (d, *J* = 7.1 Hz), 152.33 (s), 146.75 (s), 146.46 (d, *J* = 4.6 Hz), 139.72 (s), 137.19 (s), 131.91 (s), 128.63 (s), 127.34 (s), 127.12 (s), 125.33 (s), 125.13 (s), 124.28 (s), 123.76 (d, *J* = 20.9 Hz), 123.69 - 123.55 (m), 122.74 (s), 121.19 (s), 114.71 (d, *J* = 18.0 Hz), 99.58 (s), 99.43 (s), 99.28 (s).

Chapter 3: Visible light mediated reductions of ethers, amines and sulfides

*Portions of this chapter have been published in Timothy M. Monos, Gabriel Magallanes, Leanne J. Sebren, Corey R. J. Stephenson, *J. Photochem. Photobio. A* **2016**, *328*, 240-248. Markus D. Kärkäs, Bryan S. Matsuura, Timothy M. Monos, Gabriel Magallanes, Corey R. J. Stephenson, *Org. Biomol. Chem.* **2016**, *14*, 1853-1914.

3.1 Introduction

3.1.1 The Role of Lignin in Carbon Neutrality

The development of chemical methods for the controlled depolymerization of biomass is critically important to both the global energy balance and sustainable chemical manufacturing. In compliance with the Kyoto protocol, the US DOE has established a goal of 30% liquid petroleum fuel replacement with biofuels and 25% of industrial organic chemicals with biomass by 2025.[108] Future climate focused multi-national agreements, like the Paris Climate Accord, are likely to support the diversification of energy resourcing and the replacement of fossil fuels. Lignocellulosic biomass, plant matter largely excluded from the food supply chain, exemplifies a widely abundant chemical feedstock for petroleum replacement. Lignocellulose is comprised of three major fractions: cellulose (40-60%), hemicellulose (~20%) and lignin (10-30%).[109] Additionally, the energy density of lignin accounts for 40% of the energy content of lignocellulosic biomass.[110] Lignocellulose is multifunctional, providing both sugar derived bulk chemicals, and aromatic fine chemicals; in contrast, biomasses such as cereal grain and oilseeds, which yield single valorized products (ethanol and oil).[111] Finally, the petroleum industry allocates five percent of refining product to chemical manufacture[112]; thus, the technological hurdle lignin valorization must overcome is an attainably small fraction of total fossil fuel replacement.

Technological endeavors for the large-scale processing of lignocellulosic biomass constitute the creation of a biorefinery.[113] The "ideal" biorefinery matches human carbon consumption from transportation, manufacturing and food consumption, with equivalent production of materials, chemicals and fuels from biomass.[114] Simple biorefineries, commonly termed phase I, specialize in a fixed production of one chemical, such as ethanol from grain feedstock (Figure 34) this centers on dry milling but has minimal flexibility to harvest other products from plant matter. Phase II biorefineries produce a larger diversity of products (high fructose corn syrup, corn oil, starch) by using wet in addition to dry milling. Phase III biorefineries, the most advanced and dependent on the fruition of technology development, can handle an array of plant sources and produces a large variety of products using chemical and pyrolytic technologies.[115] The development of full scale Phase III biorefineries is the subject of intense chemical and economic research, with risk analysis suggesting greater product diversity can protect against the energy market volatility.[116, 117]

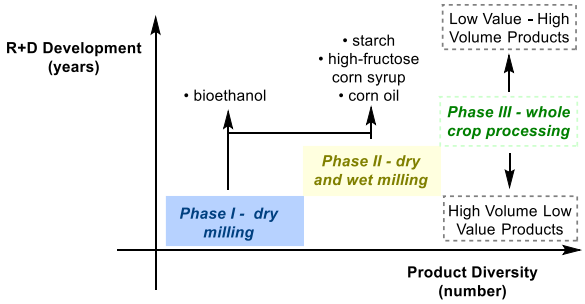

Figure 34: Evolution of the Biorefinery

Lignocellulosic processing currently occurs on 100 million ton/year processing scale for the cellulose isolation and manufacturing of paper products.[118] To separate hemicellulose and lignin from cellulose, three different solvolysis reactions can be employed.[119] The first two, Kraft and Sulfite lignin processing separate the cellulose from the hemicellulose-lignin, and then cleave the

lignin-carbohydrate linkages through either base or acid promoted nucleophilic displacement. These processes are not selective post-carbohydrate removal, thus at the elevated reaction temperatures (70-170°C) further structural rearrangements can occur making the lignin product more recalcitrant (Figure 35).[120,121] Sulfite processing also incorporates sulfur into the lignin structure, which poses complications for heterogeneous catalysis post-pulp processing (Figure 35C).[122] Organic solvolysis (Organosolv), uses organic solvents like ethanol, dioxane and acetone, thus lowering the heating requirements of the reaction and decreasing the harshness of delignification. This process is also characterized by large structural changes to the lignin structure, notably, replacing the benzyliC–sugar ethers with benzyliC–solvent ethers. Despite the challenge of lignin partitioning from cellulose and xylose (hemicellulose), select motifs in the random lignin structure can be identified by correlation NMR, and have been productively targeted for lignin depolymerization efforts (Figure 35B).

The depolymerization of lignin has been a long-standing goal for chemists for nearly one hundred years.[122] Lignin, composed of phenylpropanoid monolingols, is assembled within the plant cell by single electron oxidation enabled random polymerization which results in the synthesis of a variety of polymeric linkages (Figure 35A).[123] Additional chemical complexity ensues from the bonding of lignin to xylose, and other sugars via ether linkages, to form hemicellulose. As stated above, the pulping, or fractionation technology employed to isolate lignin has significant ramification on the operative functional handles of the isolated material. To study the viability of a lignin depolymerization reaction, many model systems of the various linkages have been developed (Figure 35B). These model compounds vary in sophistication, and seldom translate the chemical complexity of the macromolecular environment a catalyst or reagent must decipher for chemoselective C–O or C–C bond cleavage. Regardless, chemistries harnessing the

efficiency of both heterogenous and homogeneous catalysis have been studied towards this end.[119,124,125,126,127]

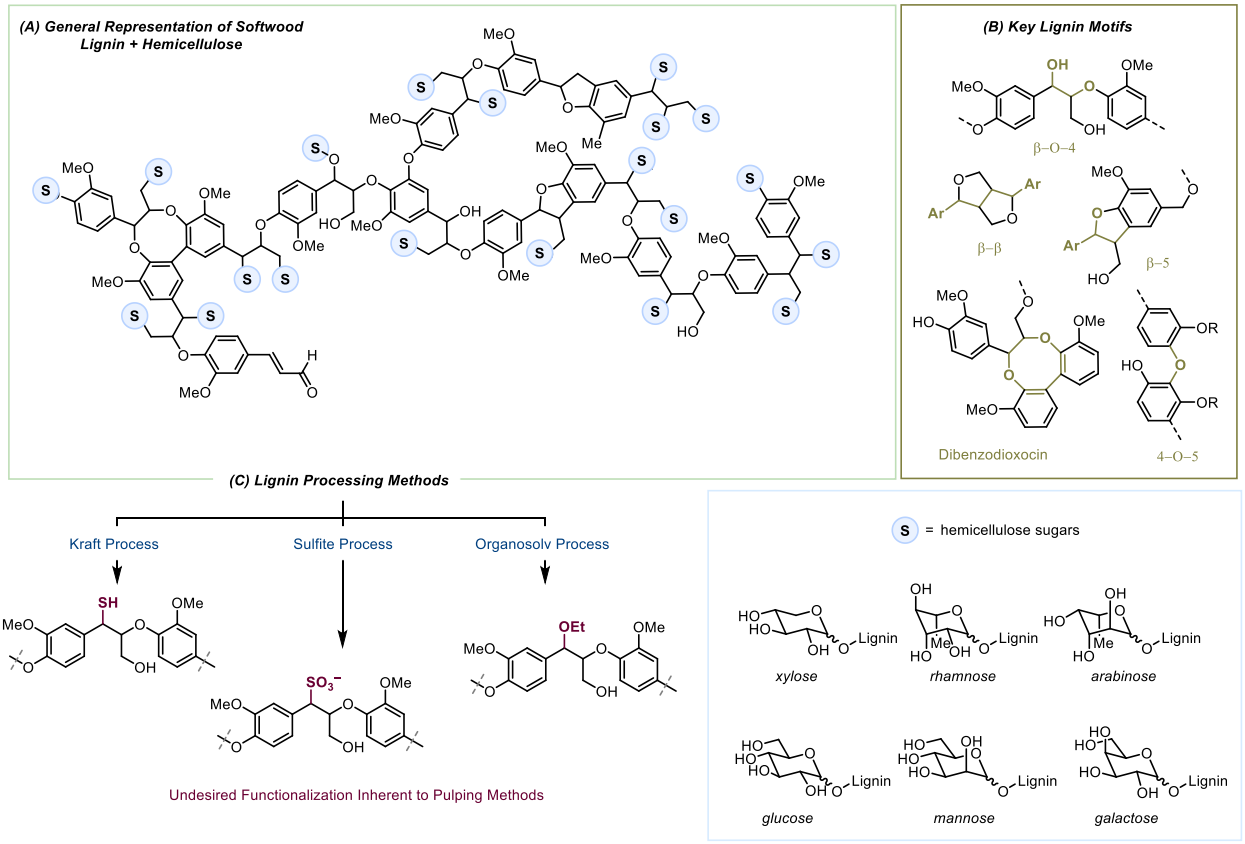

Figure 35: General Representation of Softwood Lignin and Separation Processes from Cellulose and Hemicellulose

3.1.2 Homogeneous Catalysis for Lignin Polymerization

Early lignin depolymerization studies derived inspiration from biochemistry of lignases found in white rot to study the net oxidation of model lignin compounds **3.10-3.13**. Fungi such as *Phanerochaete crystosporium*, employ an Fe(III) porphyrin catalyst, in the presence of hydrogen peroxide, to perform single electron oxidations of the electron rich arenes contained within the lignin polymer.[128,129] This oxidation facilitates the mesolytic fragmentation of the C_α-C_β bond yielding a separated radical and cation fragments which are subsequently trapped by water and H_2O_2 to provide oxygenated products (**3.6-7**). Similarly, the paper bleaching process that removes

the brown color provided by lignin in paper, utilizes a chlorine oxidation process (Figure 36A). This reaction is thought to occur through a similar SET transfer pathway, with aromatic chlorination (**3.5**) and C–C bond cleavage being the major degradation pathways. Early investigations by DiCosimo and Szabo, showcased the ability of Co(II) and Mn(II) catalysts for C_{α}-C_{β} bond cleavage in lignin monomers to occur in the same manner of the Fe(III) porphyrin powered enzymes (Figure 36B). The authors found these conditions to be efficient in the case of compound **3.8**, whereas compounds **3.10-11**, exhibited acid catalyzed degradation faster that oxidative fragmentation. Additionally, this reaction relied upon stoichiometric hydrogen peroxide and elevated temperatures, suggesting safety and scalability in the translation of this reaction to larger scales.

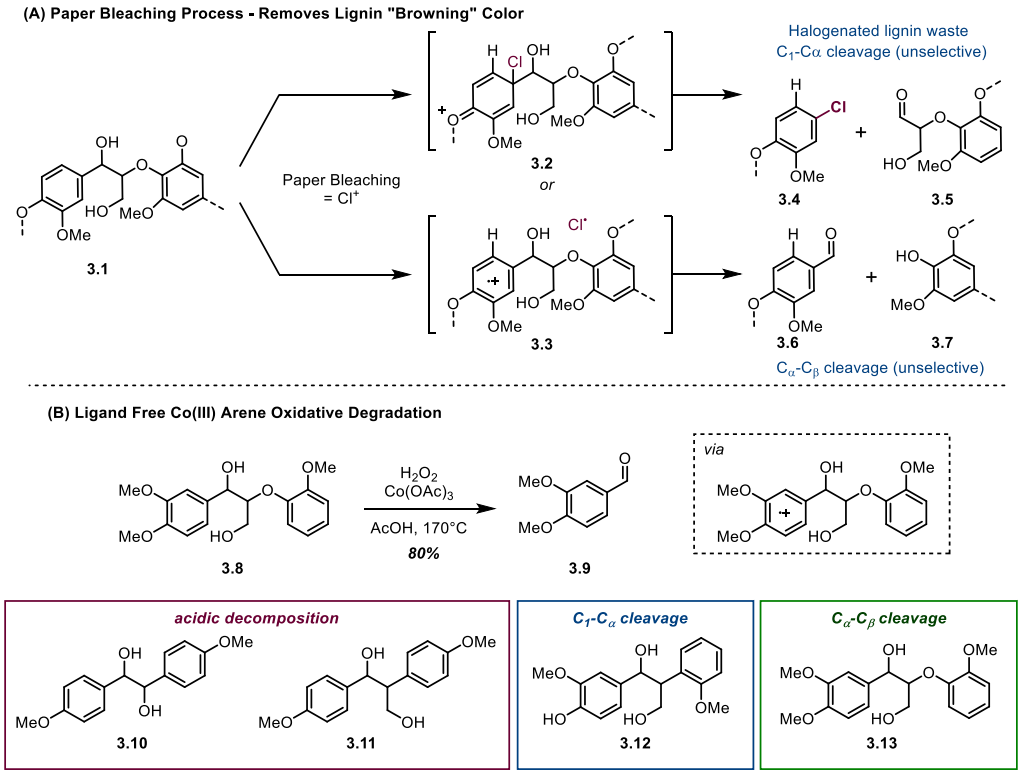

Figure 36: DiCossimo and Szabdo's Arene Oxidation Study of Model Lignans at High Temperature

Many other arene oxidants have been demonstrated for model lignin degradation including copper peroxydisulfate[130], photochemical electron transfer[131], ceric ammonium nitrate (CAN)[132], and anodic electrocatalysis.[133,134] While the mechanistic design of these reactions are identical, an observable difference in reactivity and selectivity was recorded by Mariano and co-workers.[135] Model compounds **3.14-3.17** were synthesized to show both a difference in chemoselectivity between the arene-radical cation mesolytic cleavage of the 1,2-diaryl (β-1) and the β-*O*-4 motifs as well as a kinetic difference between the diastereomers of each motif. Three distinct oxidation methods consisting of 9,10-dicyanoanthracene (DCA) photochemical oxidation, CAN oxidation and lignin peroxidase (LP), were investigated. The authors concluded the photochemical reactions to be the slowest and exhibit the smallest rate differences between diastereomers of each model likely due to back electron transfer after reductive quenching with the photoexcited DCA catalyst. In contrast, the kinetically irreversible oxidation of each substrate with CAN exhibited a 2:1 and a 4:1 difference

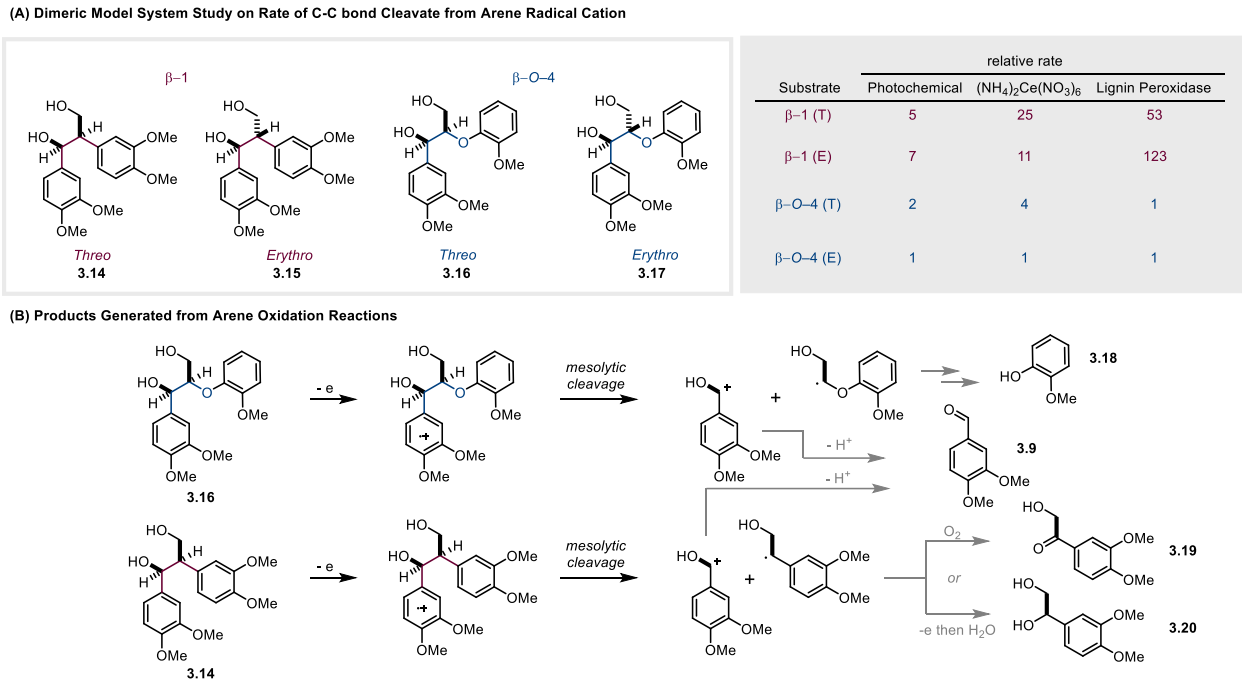

Figure 37: (A) Relative Rates of Radical Cation Fragmentation in Lignin Models Based on Oxidation Method (B) Dimeric Model Lignin Oxidative Degradation Products

in relative rate of mesolytic cleavage for the β-1 and β-*O*-4 models, respectively. Lignin peroxidase exhibited the greatest relative rate difference between the substrates with the oxidation of **3.15** occurring 123 times faster than either **3.14** or **3.16-17**. A year later, Mariano and co-workers realized a similar chemoselectivity using trimeric lignin models containing both the β-1 and β-*O*-4 motifs within one molecule.[136] The mesolytic fragmentation rates in the trimeric models echoed the chemoselectivity of the presented study. Remarkably, with multiple arenes poised for oxidation, equilibration via intramolecular electron transfer between the various arene radical cations resulted in a kinetically selective β-1 C–C fragmentation in the presence of a β–O-4 linkage. Within the highly controlled study of model lignin oxidative decomposition, stereochemical as well as motif composition is critical in realizing both bond cleavage and product formation. The superior reactivity rate exhibited by lignin peroxidase suggests an additional

substrate-enzyme interaction that surpasses the current designs of simple electron transfer reagents. Knowledge of the relative rates of reactivity, while largely supportive of simpler secondary and tertiary aryl ethanols,[137] lends evidence to the genetic design of lignin polymers and highlights another layer of complexity within the field of chemoselective lignin depolymerization.

While a significant focus of lignin C–O degradation has been directed toward the β–O–4 motif, Bozell and co-workers argue phenols are the most prevalent and accessible functional handles in processed lignin material. To leverage this functionality, the authors demonstrated a Co(II) phenol oxidation method by studying a salen ligand (Figure 38, **3.26**) design to enable room temperature reactivity.[138,139] By studying the reactivity of various polymethoxylated phenols towards Co(III)-superoxo complexes, the key ligand effect driving enhanced catalyst reactivity is a Lewis-base auxiliary useful proximal phenol deprotonation.[140,141] This design element is crucial to realizing high reactivity of guaiacyl-like phenols, which exhibit a stronger O-H bond than the syringyl phenol. Overall, the Co(III)-superoxo complex was able to catalyze a phenol O-H abstraction, followed by oxidation of the C_{aryl}-C_{α} bond in high yield at room temperature. These observations also explained the C_{aryl}-C_{α} reactivity of model compound **3.12** (Figure 36B).

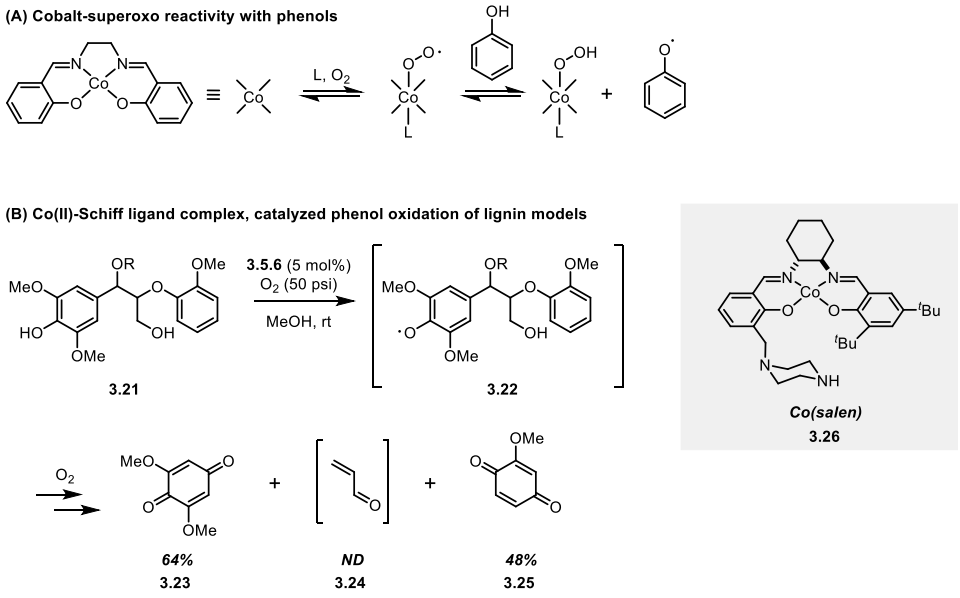

Figure 38: Co(salen) room temperature oxidation of dimeric lignin models to quinones.

Another notable transitional metal catalyst for lignin depolymerization are the vanadium(V) complexes. In contrast to the discussed methods, vanadium catalysis reacts via benzylic H-atom abstraction generating redox neutral, and net oxidative, model lignin fragmentation. The reactivity of V(III-V) redox cycles can be controlled by ligand synthesis and coordination chemistry to toggle between oxidative diol cleavage, phenoxy radical generation and benzylic H-atom abstraction. Toste as well as Hanson, Baker and Silks, discovered and probed the differences between various vanadium complexes. Within the octahedral bis-(8-hydroxyquinoline) oxovanadium complex **3.35**, lignin models possessing free phenols undergo phenol oxidation and liberate quinone and acrolein derivatives, suggesting a mechanism similar to Bozell et. al. (Figure 39A).[142,143] Alternatively, Toste discovered oxovanadium complexes coordinated to a hydroxy-imine ligand form, this complexes to benzylic alcohols, enabling oxidation followed by β–elimination of the γ–hydroxy[144] unit (Figure 39D).[145] Interestingly, oxygen can promote this reactivity, but it is non-essential as phenoxyl radical **3.40** is the critical oxidant for catalytic turnover of the oxovanadium catalyst. One other key parameter in the ligand development of **3.36** was the inclusion of *t*-butyl

groups for steric repulsion of lignin over-coordination and vanadium dimerization. Overall Toste's developed catalyst was later applied to oganosolv lignin isolated from *Miscanthus giganteus*, and showed both the disappearance of the β-*O*-4 motif in correlation NMR studies, as well as a lower average molecular weight by gel permeation chromatography (GPC).[146] Vanillin, syrigic acid, syringaldehyde, 4-hydroxybenzaldehyde, vanillic acid, and 4-hydroxybenzoic acid were observed via GC–MS after the reaction. The application of this Schiff base oxovanadium catalyst to native lignin isolates distinguishes this system for later developments in lignin depolymerization technology development.

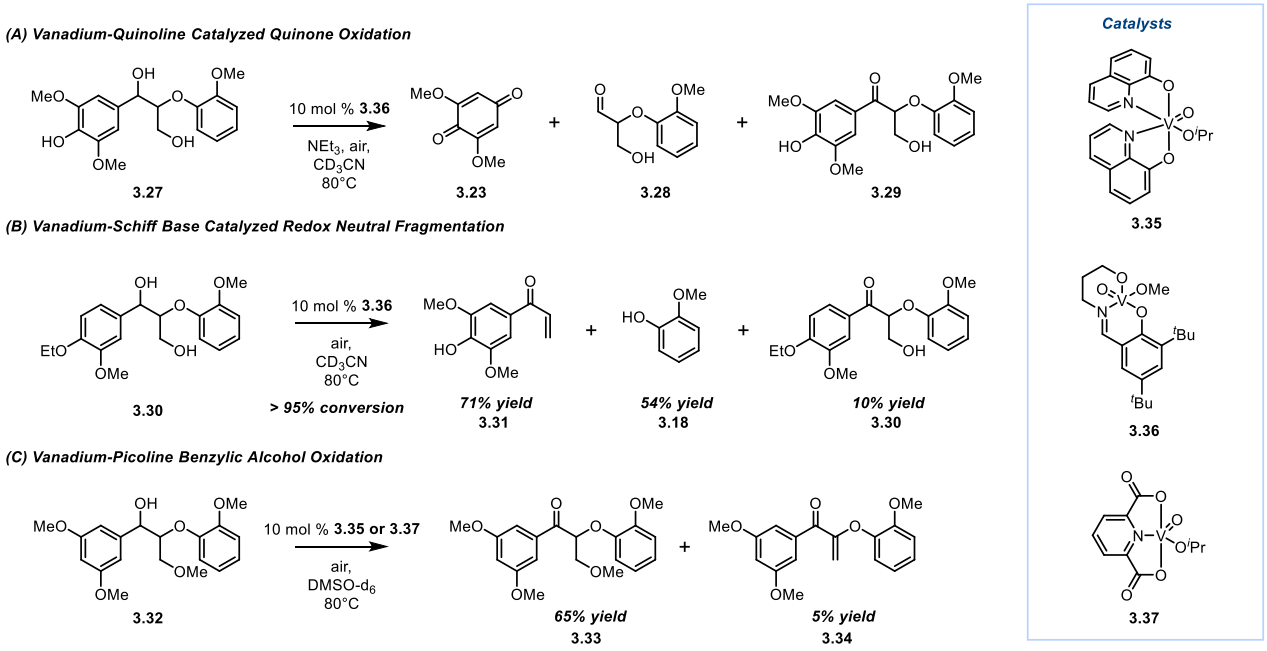

Figure 39: Vanadium Catalysis for Lignin Depolymerization

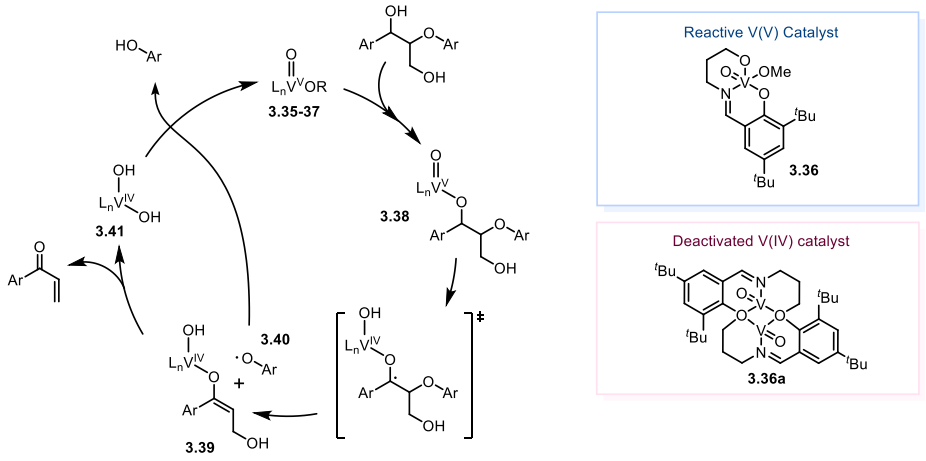

Figure 40: Proposed Mechanism for Vanadium Catalyzed Lignin Depolymerization

In addition to Toste's realization of oxovanadium catalysis for redox neutral lignin depolymerization, transfer hydrogenation and reduction catalysis has been demonstrated to cleave the β–*O*–4 motif. In a seminal study published by Bergman and Ellman, Ru(Ph-Xantphos)(CO) was discovered as uniquely efficient for the conversion of 1-phenyl-2-aryloxyethanols to aryl ketones (Figure 41A-B).[147] This process also exhibited quantitative C–O reduction on a polymeric β–*O*–4 model **3.48**). Unfortunately, as James and co-workers later found the coordination-based reactivity of this complex was not compatible with the γ-hydroxy motif, which preferentially coordinated the metal catalyst (**3.50**) and prevented reactivity (Figure 41C).[148] Other transfer hydrogenation approaches have been investigated by Samec and others, using heterogeneous catalysis as a versatile platform, along with alcohols and formic acid as abundant and environmentally friendly reductants.[149,150]

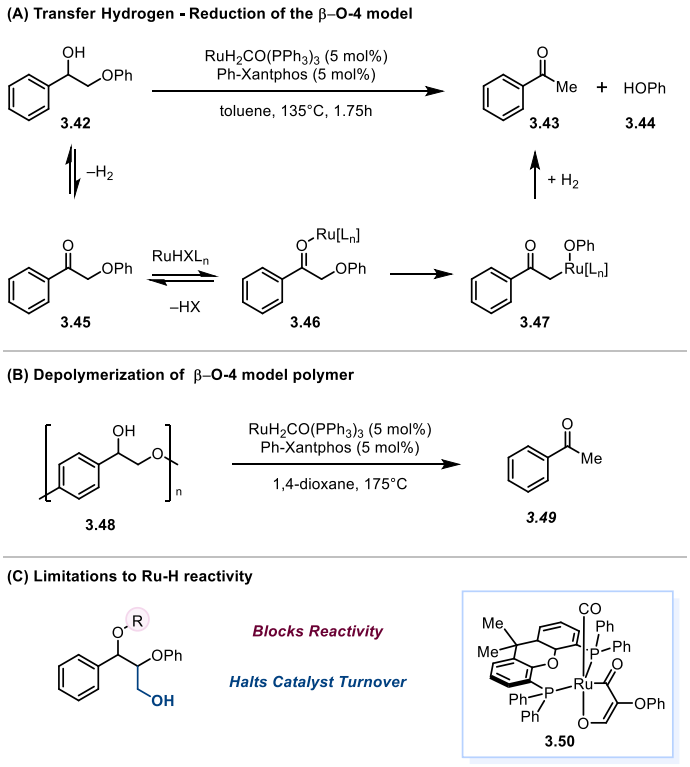

Figure 41: Ruthenium catalyzed transfer hydrogenation redox neutral depolymerization strategy.

One of the most promising homogeneous catalysts for lignin processing has been developed by harnessing the chemoselective oxidation reactivity of oxoammonium salts. Having developed efficient alcohol catalytic oxidations using Cu(I)-nitroxyl catalysis[151], Stahl and co-workers were aware of the reactivity challenges facing a chemoselective lignin oxidation development. Yet, identification of a non-fragmenting oxidation reaction would enable access to hydrolysis or reduction reaction inaccessible in native lignin. Many different stoichiometric and catalytic oxidation reaction have been developed in synthetic chemistry; thus, Stahl and co-workers surveyed three classes of oxidation reaction for reactivity and chemoselectivity on a lignin model substrate containing a benzylic and primary-aliphatic site for reactivity.[152] The key findings in this initial survey established Bobbitt's salt (4-AcNH-TEMPO BF_4, **3.55**, Figure 42)[153,154] as the highest yielding benzylic selective oxidant and the Cu(I) catalytic methods as the lowest yielding

with aliphatiC–primary alcohol selectivity. To harness the reactivity of Bobbitt's salt oxoammonium functionality, the oxoammonium reagent was rendered catalytic by the inclusion of a nitrite-nitrate redox cycle, allowing for oxygen to act as the terminal oxidant (Figure 42B). Gratifyingly this catalytic system translated from model system to the oxidation of Aspen lignin (post cellulitic enzyme processing) (Figure 42C).

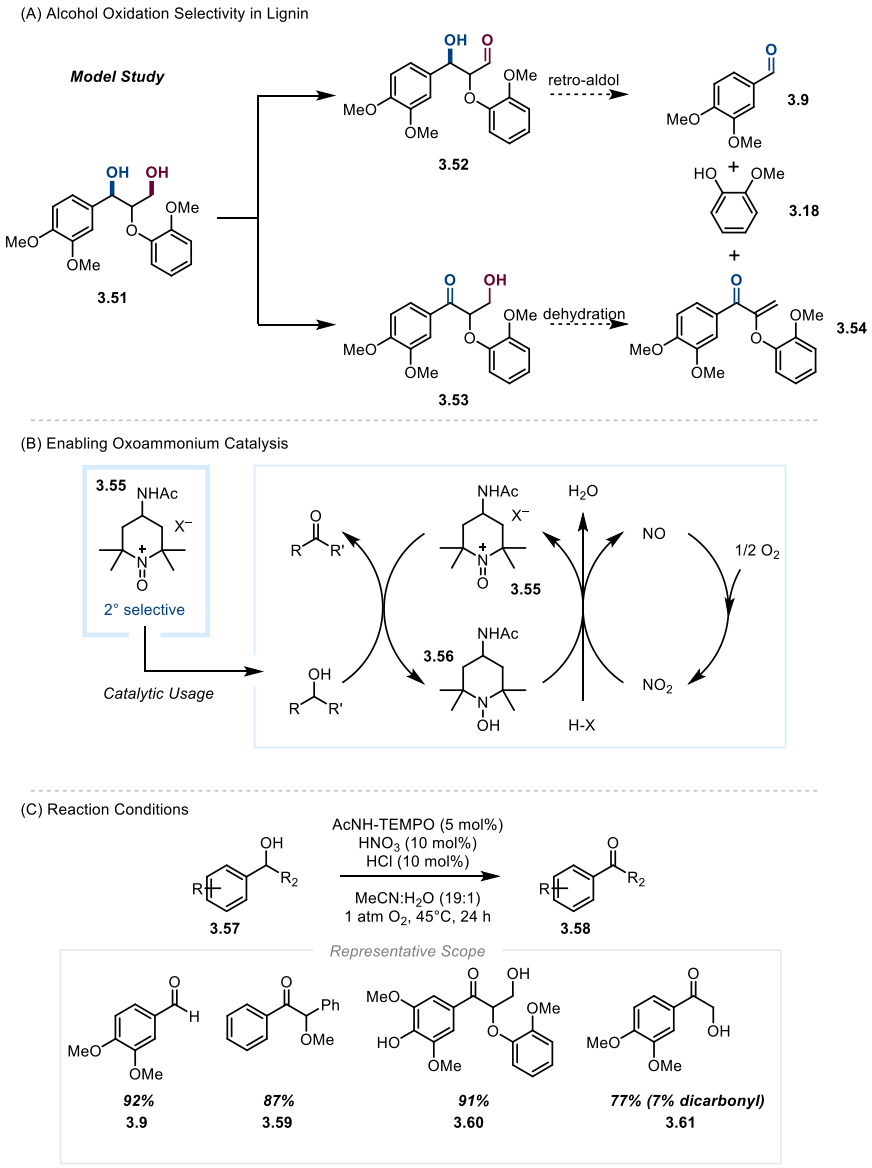

Figure 42: Oxoammonium Catalysis for Benzylic–Secondary Alcohol Selective Oxidation

Preliminary work establishing 4NHAC–TEMPO/NO_3/O_2 catalytic triad for the selective oxidation of the benzylic alcohol functionality in lignin allowed for the exploration of reductive and solvolytic methods to bond cleavage.[155] Interestingly, low valent metal reductions of benzylic ketone **3.62** were ineffective or slower than solvolysis in formic acid-water solution. This keyed Stahl and co-workers into a transition metal-free β–elimination reaction that was followed by solvolysis to create aryl propane dione products (Figure 43). The combination of the catalytic oxidation followed by acid catalyzed solvolysis enabled the conversion of Aspen lignin to 60 wt% lower molecular mass oligomers and isolate syringyl, guaiacyl and coumaryl aldehydes, as well as diones. Most recently, Stahl has partnered with the resources of Ralph, Dumesic and the DOE Great Lakes Bioenergy Research Center to apply this two-step processing method to different lignin sources.[156] Comparably, Aspen lignin was the most compatible with the developed sequence whereas maple and maize based lignins contain larger amounts of ferulate acid motifs which are incompatible with the oxidation method. Aspen lignin processing resulted in fifty percent mass recovery, of which 42% is recovered monomer units (constituting eight different molecules). The metal free and moderate heating required for this process support the further tailoring to species specific lignin to maximize depolymerization yields.

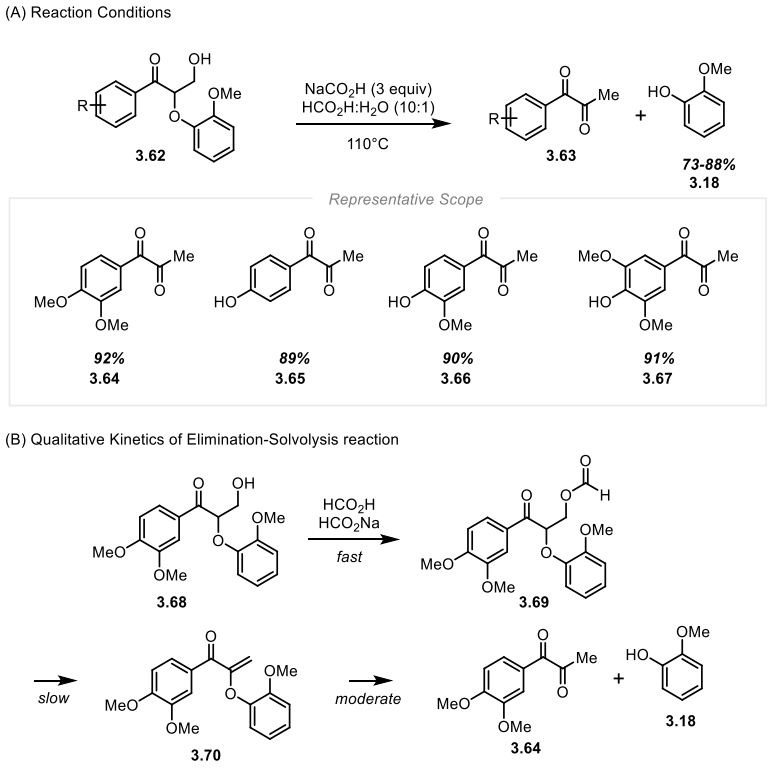

Figure 43: β–Elimination and Solvolysis of Lignin Ketones as Redox Neutral Depolymerization Strategy

The net reduction of aryl ethers is arguably another crucial intersection between catalytic organic synthesis and lignin depolymerization, whereby, investigation of lignin C–O reduction has provided key insights into nickel catalysis and aryl ether utilization as chemical building blocks for target synthesis. The use of phenyl ethers for Kumada cross-coupling was demonstrated by Wenkert and Dankwardt, respectively (Figure 44).[157,158] These methods employed an excess of Grignard reagent and elevated temperatures to enact a low valent Ni redox catalytic cycle to form biaryl products. This process was significantly more effective with naphthalene derived aryl ethers as opposed to benzene.

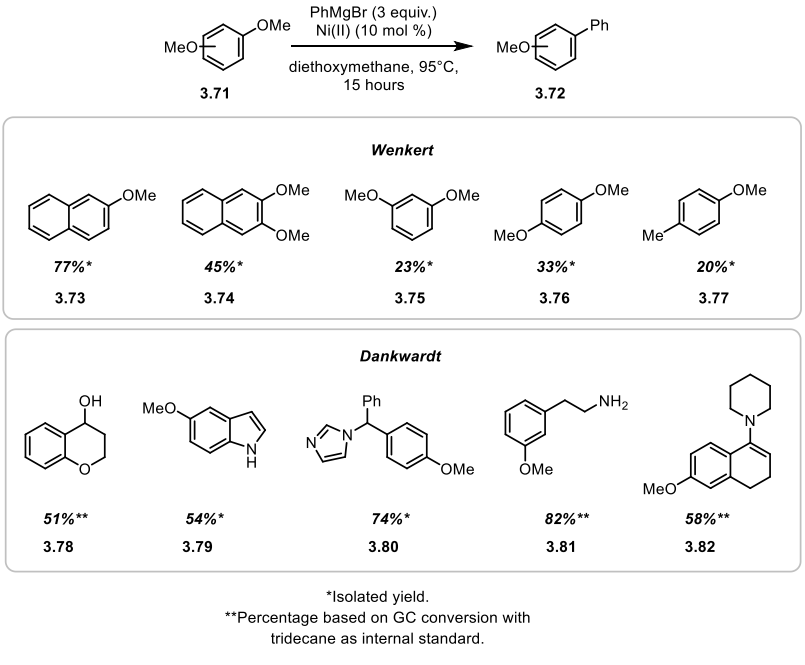

Figure 44: Nickel Catalyzed Kumada Coupling with Methoxy Arenes

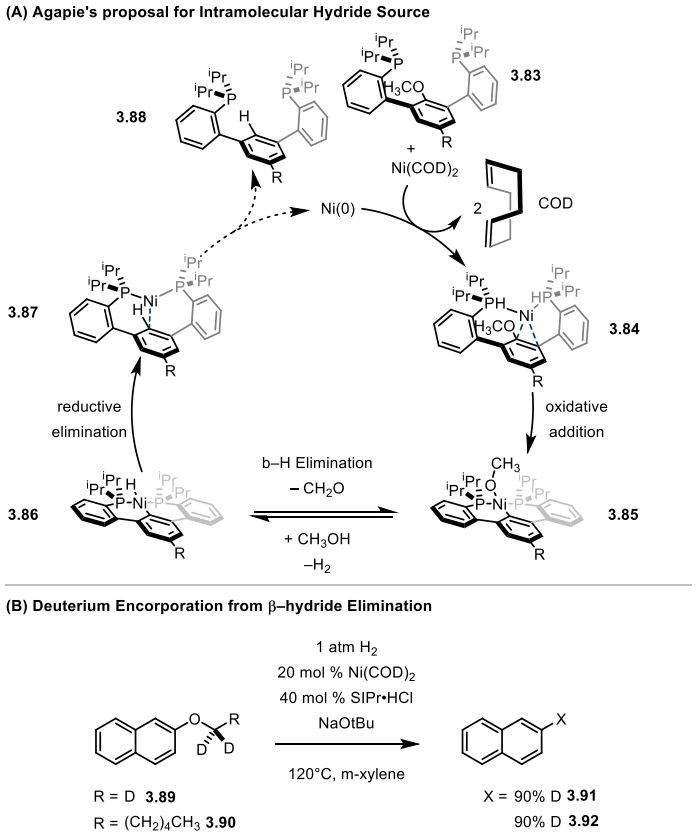

Figure 45: Agapie's Organometallic Model Study of C_{aryl}-O bond insertion

The nickel(0) oxidative addition process was directly studied by Agapie, who utilized an methoxy arene containing 2,6-aryldiphosphine directing groups to promote the key nickel-carbon bond forming process (Figure 45).[159] Through these experiments, an early proposal of β-hydride elimination of the methoxy substituent to provide the key hydride was elucidated with this model system (Figure 45B).

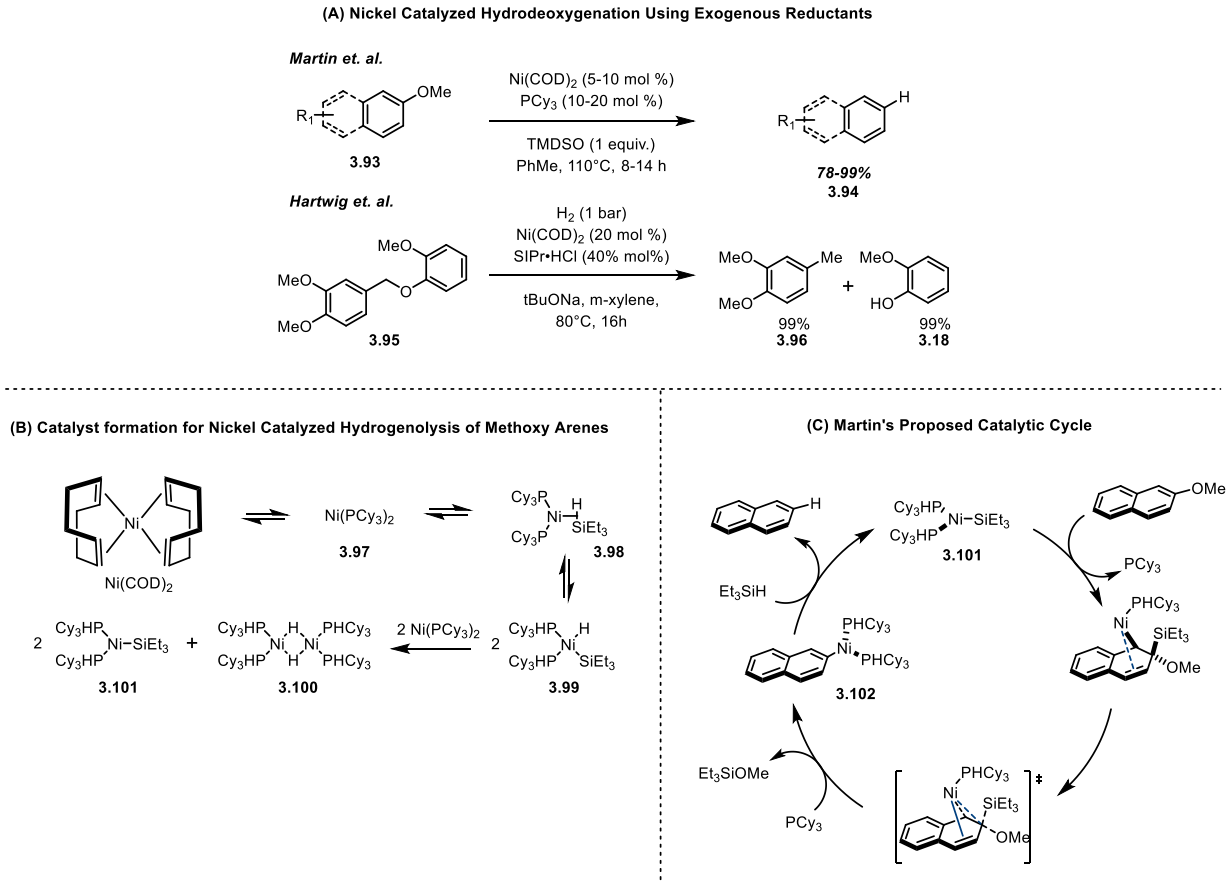

Figure 46: (A) Nickel Catalyzed Hydrodeoxygenation (B) Martin's Mechanistic Proposal for Catalyst Generation (C) Catalysis Mechanism for Ni(0) catalyzed Reductive Deoxygenation of Methoxyarenes

Agapie's results were incongruous with the hydrodeoxygenation chemistry developed by Martin[160,161] and Hartwig[162,163], who found exogenous silane or hydrogen was necessary for reduction and bis-aryl ethers could also participate with nickel in this process (Figure 46A). Martin discovered $Ni(COD)_2$ precatalyst, when stirred in the presence of phosphine ligand and silane

reductant first underwent a ligand displacement and sigma-bond metathesis reaction with silane to be followed by a disproportionation reaction to produce two equivalents of a Ni(0) silane complex (**3.101**) as well as a dimeric Ni(I) hydride complex (**3.100**) (Figure 46B). The Ni(0)-silane complex was proposed as the active catalyst, where formal nickel oxidative addition occurs through a two-step process in which the Ni-Si (**3.100**) bond adds across the enol ether functionality. Then ligation of another phosphine causes alkoxide elimination, followed by silane elimination and 1,2 migration of the nickel to occupy the original position of the oxygen substituent (**3.102**). Finally, σ-bond metathesis replaces the aryl-nickel bond with a hydride and the catalyst turns over (Figure 46C). Recent studies by Hartwig on the Ni(0)-NHC catalyzed hydrodeoxygenation (H_2, not silane) revealed that a neutral Ni-NHC complex is capable of arene coordination, and C–O bond oxidative addition is the rate limiting step.[164] In light of all the information gathered from Ni C–O reductive catalysis, this process exhibits high thermodynamic barriers to accomplish bond cleavage, as well as multiple coordination events between a metal catalyst and substrate. Future work ameliorating the high reaction conditions, and reagent excesses, possibly through the use of electrocatalysis will prove a critical area of development for realizing net reductive valorization of lignin biomass.

3.1.3 Photochemical Reduction of the β–O–4 Lignin Motif.

Visible light mediated redox catalysis offers a unique advantage to the development of biomass processing technology through the mechanistic characteristic of outersphere electron transfer. This mechanistic paradigm stands unique in the field of transition metal catalysis which largely requires the formation of a carbon-metal bond to afford productive reactivity. Additionally, the development of visible light photoredox catalysis promoted a change in stoichiometric oxidants and reductants from toxic metalloid tributyltin hydrides and thermally unstable radical initiators to amines and carboxylic acids that react selectively with photoexcited catalysts.[12,14]

Photochemical reductions of carbon-heteroatom bonds commonly proceed through carbonyl reduction followed by fragmentation. For most visible light photocatalysts, the C–O bond strength, which exhibits a reduction potential of $E_{p/2}$ = –2.23 V vs SCE (**3.103-3.106**),[165] is chemically inert to quenching an excited state Ir(III) or Ir(III)* catalysts[14] (Figure 47). Yet, by targeting an initial reduction, particularly in the presence of a Brønsted or Lewis acid, the thermodynamic barrier for reduction can be lowered to –2.10 vs. SCE.[166,167] This technique was originally demonstrated by Fukuzumi et. al. with the reduction of 2-bromoacetophenones with $Ru(bpy)_3Cl_2$ and $AcrH_2$ (see chapter 1, Figure 11).[168] Further elaboration of the substrate scope of this chemistry was completed by Hasegawa et. al. to aliphatic epoxy ketones (**3.111**) by utilizing a pyrene based photoreductant and UV irradiation (BDMAP, **3.115**, E^{ox*} = –2.4 V vs. SCE).[169] Following these reports, Fensterbank and Ollivier showcased the reductive fragmentation of α–aziridyl aryl ketones (**3.113**) using a similar system to Hasegawa.[170]

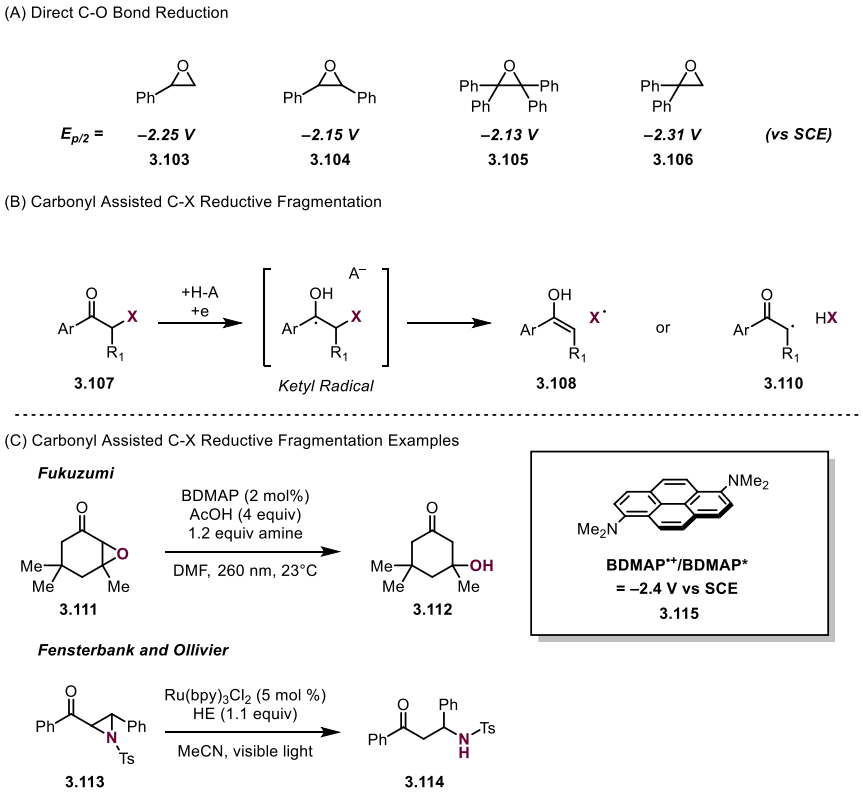

Figure 47: Carbonyl Enabled C–X Bond Reduction

Knowles highlighted the synthetic utility of acid catalysis within α–keto C–X reduction, by utilizing acid catalysts for different photocatalytic ketone reduction reactions (Figure 48). [171,172] In the first instance, this proton-coupled electron transfer catalysis was demonstrated with a ketyl-olefin intramolecular cyclization (**3.116** to **3.117**). Phosphoric acids [$(PhO)_2PO_2H$] in combination with either $Ir(ppy)_3$ or $Ru(bpy)_3^{2+}$ were competent in ketone reduction, with the necessary H-atom provided by 2-phenyl-dihydrobenzothaizoline (BT, **3.118**). Knowles and co-workers further demonstrated the intimacy of the acid catalyst in carbonyl reduction by enabling an enantioselective aza-pinacol cyclization (**3.119** to **3.120**).

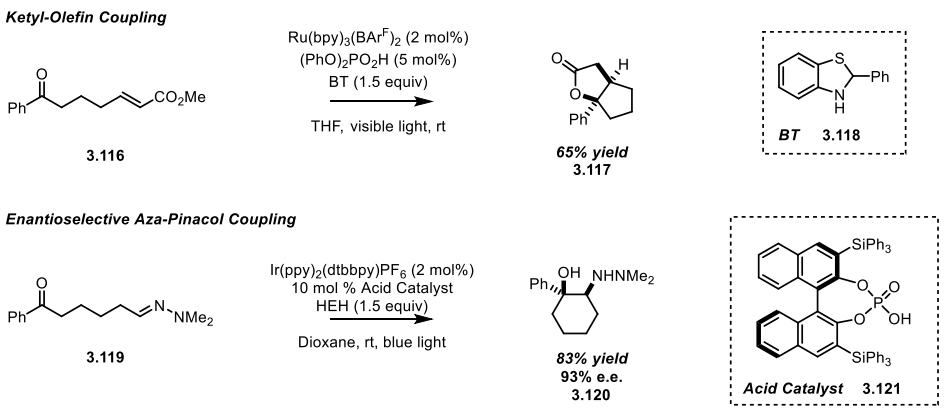

Figure 48: Proton Coupled Electron Transfer Catalyzed Ketyl Radical Transformations

Realizing the ubiquity of the 1,2-ethandiol functionality in lignin chemistry, prior work in this lab was directed to utilizing photoredox catalysis for demonstrating the C–O bond reduction of the β–*O*–4 motif. Mariano's oxidative photochemical electron transfer chemistry[135] suggested a separate strategy targeting a benzylic selective alcohol oxidation for the exploration of photocatalytic carbonyl reduction chemistry would be unique and valuable. DFT calculations conducted by Beckham and co-workers supported the viability of a ketone assisted reductive fragmentation approach by indicating a 13 kcal/mol difference in the C–O bond strengths between β–*O*-4 alcohol and β–*O*-4 ketone (Figure 49A).[173]

To accomplish the initial oxidation Bobbitt's salt,[153] was chosen for a few advantageous properties. The reduction of Bobbitt's salt is a colorimetric reaction, making qualitative analysis of reaction progress trivial. More importantly, in comparison to simple alcohols and model ketone substrates, hydroxylamine **3.56** adheres to silica, allowing for a simple separation of reagent and product following the reaction. Lastly, Bobbitt's salt can be stoichiometrically re-oxidized from **3.125** to **3.55** by using commercial bleach (Figure 49B). Gratifyingly, this reagent reacts with near

quantitative yields of benzylic oxidation to provide the key aryl ketone intermediates for the reduction step (Figure 50).

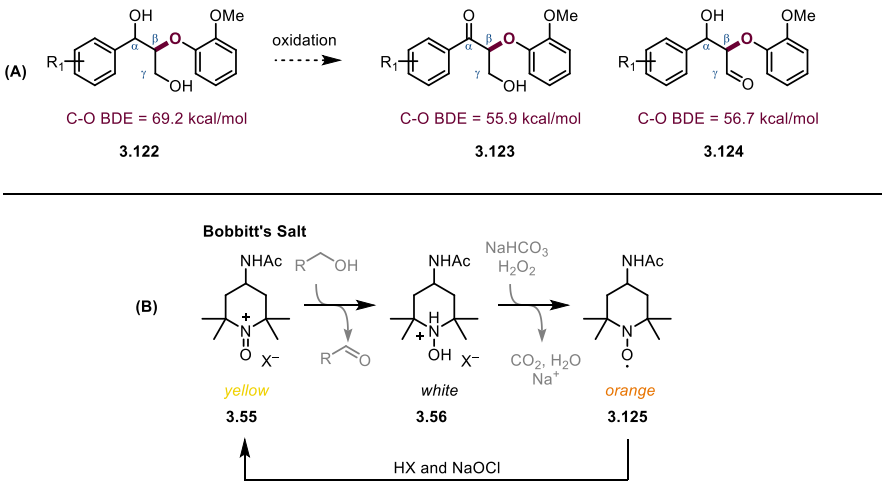

Figure 49: (A) C–O bond weakening upon proximal alcohol oxidation (B) Stoichiometric redox cycling of Bobbitt's Salt

After stoichiometric oxidation, photochemical conditions using a slight excess of DIPEA and formic acid, in addition to an $Ir(III)^{+}$ catalyst were sufficient for reductive fragmentation of the oxidized model lignins (Figure 50).[174] For this general protocol, a strong reductant (Ir(III/II) = -1.65 V vs. SCE) was needed to overcome the activation barrier to reducing electron rich aryl ketones. To demonstrate the scalability of this sequence, batch-to-flow experiments were conducted to process the oxidation step in batch followed by flow processing to efficient photocatalysis. Furthermore, reductive cleavage of **3.135** was demonstrated in the presence of lignosulfonate, a dark brown lignin solid, to demonstrate that photocatalysis is still possible within a complex mixture of photoabsorbing compounds.

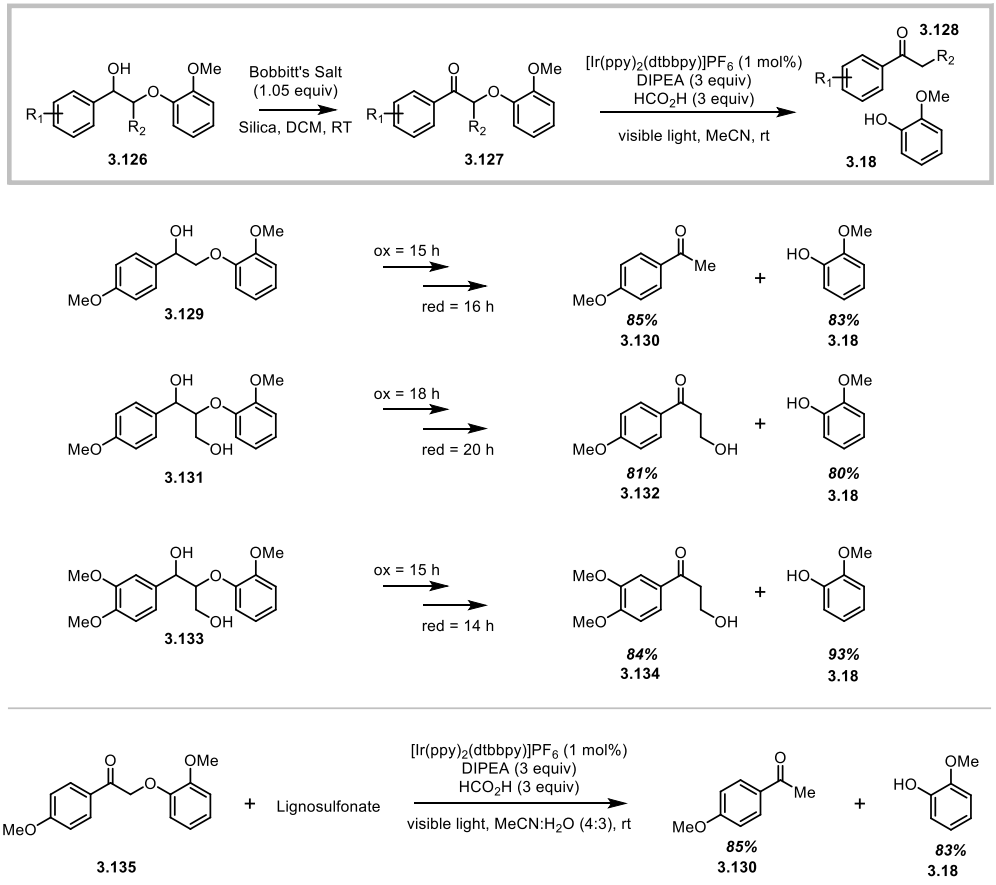

Figure 50: Two step, redox neutral β–O–4 cleavage of lignin model systems (batch processing)

3.2 Reaction Optimization

After the publication of our group's first lignin depolymerization technique,[174] we questioned two aspects about this transformation:

(1) Could the super-stoichiometric excess of terminal reductants (^{i}PrNEt$_2$ – HCO_2H) be minimized?

(2) Is this process general to reduction of unstrained C–N and C–S bonds?

To address the reagent stoichiometry challenge, we hypothesized that the necessary electron and H_2 for this transformation could come from simple alcohol solvents, such as ethanol. To enable

H-atom abstraction from ethanol, a catalytic cycle employing an oxidative quenching event between the ketone substrate and the photocatalyst, rather than a reductive quenching event

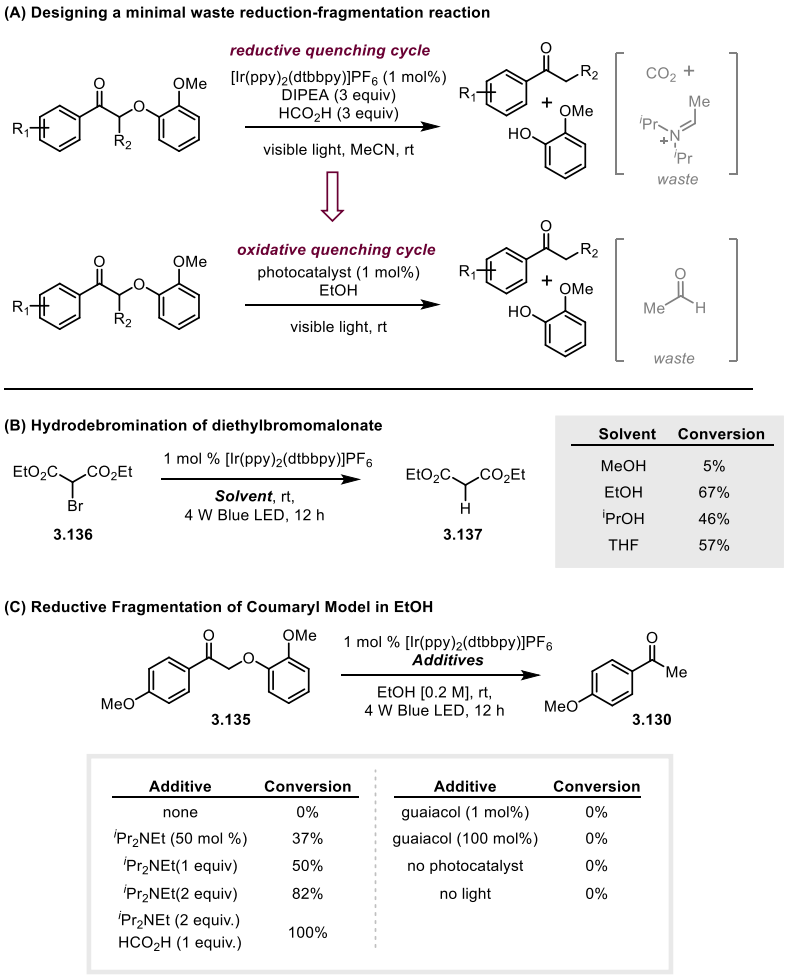

Figure 51: Testing a minimal waste reductive fragmentation reaction

between amine and photocatalyst, would be necessary to identify (Figure 51A). To test this hypothesis, reductive debromination of diethylmalonate (**3.136**) was investigated in methanol, ethanol, isopropyl alcohol and tetrahydrofuran (Figure 51B). The latter three solvents were capable of bromomalonate reduction by H-atom donation (45-67% conversion of bromomalonate). However, this concept did not extend to lignin model system **3.135**, as conducting the reaction without terminal reductants did not process any of the starting material (Figure 51C). Separately,

guaiacol was also not found to be an acid catalyst for this reaction. The conversion of substrate **3.135** trended with the stoichiometry of Hünig's base ($^{i}Pr_2NEt$), while the addition of formic acid enabled full conversion of the starting material. While the original hypothesis of ethanol H-atom donation was not realized, lower equivalents of the terminal reductants were identified.

3.3 Reaction Performance

The developed reaction conditions in ethanol solvent were applied to a panel of aryl ketone substrates to investigate the scope (Figure 52). Overall, slightly diminished yields for the ketone fragment were observed in comparison to the first-generation conditions. Aryl ketones **3.138-3.140** occurred with increasing reaction times to accommodate the kinetic resistance to fragmentation via back electron transfer. The highest yielding substrate (**3.141**) lacked the γ–hydroxy functionality, whereas substrate **3.142** failed to convert, as equilibration to the acetal in ethanol masks the acceptor functionality.

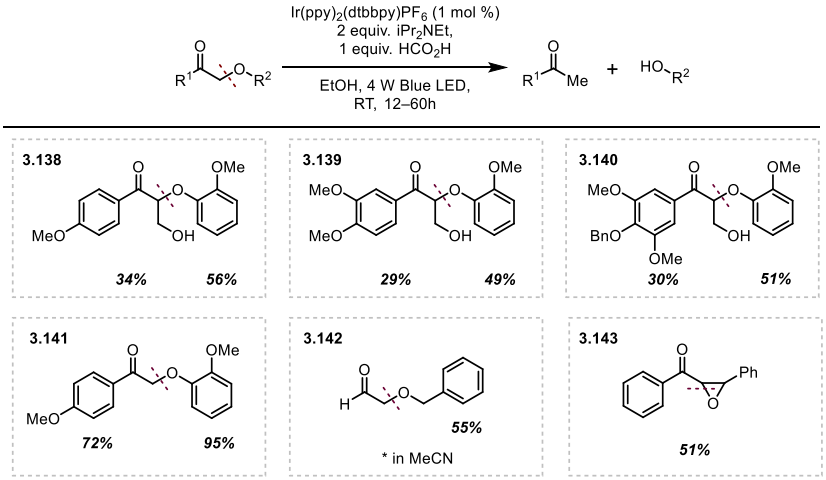

Figure 52: Reductive Fragmentation of α–keto ethers

To address the second aim of this project, α–keto amines and sulfides were investigated as substrates for unstrained C–N and C–S reductive fragmentation (Figure 53). Sulfonamide (**3.145**) and methylaniline (**3.146**) substrates reacted quickly whereas unprotected aniline (**3.144**),

fragmented in high yield after an initial induction period. C–S reductive fragmentation was general across a wide range of substituted aryl ketones, with the highest yield of fragmentation attributable to a naphthyl aryl ketone (**3.152**). Electron deficient arenes (**3.148**) marginally outperformed electron rich (**3.150**) acetophenone-based substrates. The sulfur fragment was never isolated as the free mercaptan as participation in the catalytic cycle or off cycle oxidation occurred to generate the disulfide species.

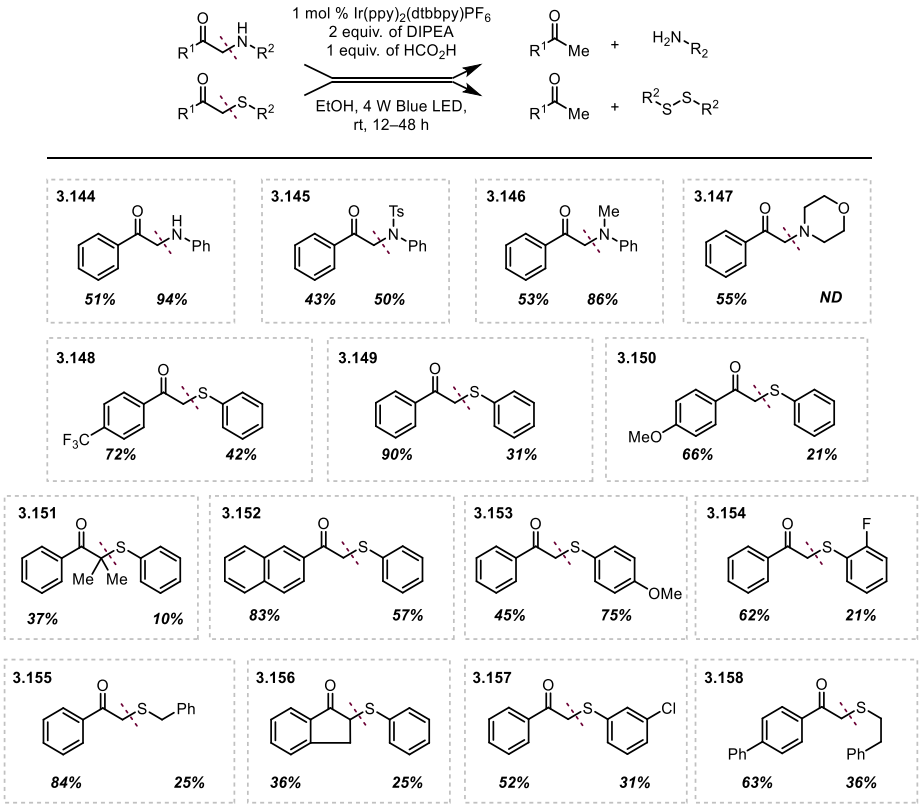

Figure 53: Reductive Fragmentation of α-keto amines and sulfides

In the absence of C–X fragmentation, radical-radical pinacol coupling was observed (**3.159-66**) (Figure 54). This reactivity was consistent with leaving groups exhibiting high pK_a values – ethers, hydroxide and amides. The observed yields of these processes were highly variable and sometimes solvent dependent. No further exploration into the formation of the homo-pinacol products was

undertaken, as Reuping et. al. published a report for this process during our development of this chemistry.[175]

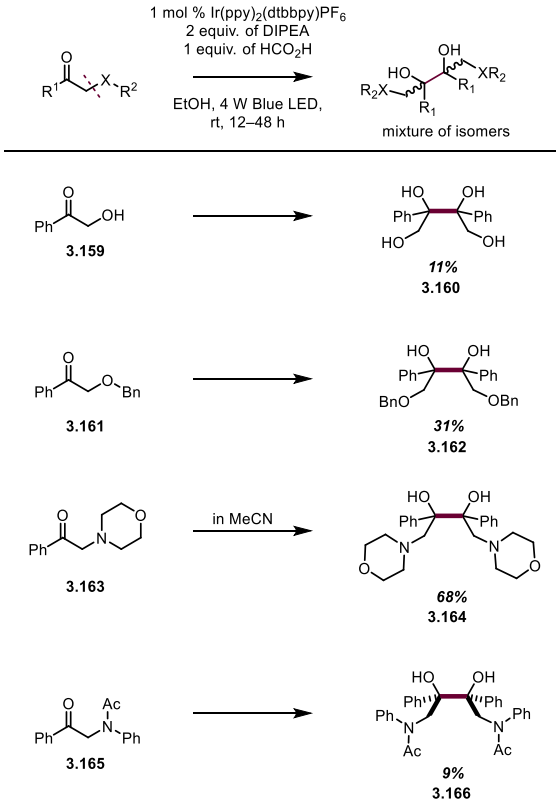

Figure 54: Observed Ketyl Radical Pinacol Coupling in the absence of fragmentation

3.4 Conclusions

Homogeneous transition metal catalysis has contributed notable, detailed investigations on lignin depolymerization strategies that span each of the three different redox economies (oxidative, reductive and neutral). Each of these approaches aims to liberate homologous monomeric species from lignin to usage as building block molecules in the fine chemicals and pharmaceutical research sectors; a challenging but attainable replacement of refined petroleum feedstock sources. While net oxidative and reductive approaches necessitate addressing the challenge of employing highly abundant reagents (oxygen and hydrogen), the redox neutral strategy can ideally shuttle hydrogen and oxygen in order to afford small oligomers and monomeric products. Each approach to lignin

valorization holds promise in producing value-added products. Since the publication of our second-generation reduction conditions,[176] group members have continued to pursue the notable goal of redox-neutral lignin depolymerization. Towards this end, Bosque et. al. have identified a competent catalyst for the catalytic electrochemical oxidation of lignin model systems as well as pine-wood derived organosolv lignin.[177] In addition, Kärkäs et. al. has demonstrated a photochemical Pd(II)-persulfate oxidation of lignin model substrates.[178] These methods, along with the distinguished examples discussed suggest the development of a robust lignin depolymerization processing method will be championed in the near future.

3.5 Experimental Methods

3.5.1 General Information

All chemicals were used as received. Reactions were monitored by TLC and visualized with a dual short wave/long wave UV lamp. Column flash chromatography was performed using 230-400 mesh silica gel or via automated column chromatography. Preparative TLC purifications were run on silica plates of 1000 μm thickness. NMR spectra were recorded on Varian MR400, Varian Inova 500, Varian Vnmrs 500, or Varian Vnmrs 700 spectrometers. Chemical shifts for ^{1}HNMR were reported as δ, parts per million, relative to the signal of CHCl3 at 7.27 ppm. Chemical shifts for ^{13}CNMR were reported as δ, parts per million, relative to the center line signal of the CDCl3 triplet at 77.16 ppm. Chemical shifts for ^{19}FNMR were reported as δ, parts per million, relative to the signal of a trifluorotoluene internal standard at –63.72 ppm. The abbreviations s, br. s, d, dd, br. d, ddd, t, q, br. q, qi, m, and br. m stand for the resonance multiplicity singlet, broad singlet, doublet, doublet of doublets, broad doublet, doublet of doublet of doublets, triplet, quartet, broad quartet, quintet, multiplet and broad multiplet, respectively. IR spectra were recorded on a Perkin-Elmer Spectrum BX FT-IR spectrometer fitted with an ATR accessory. Mass Spectra were

recorded at the Mass Spectrometry Facility at the Department of Chemistry of the University of Michigan in Ann Arbor, MI on an Agilent Q-TOF HPCL-MS with ESI high resolution mass spectrometer. Gas Chromatography yields were run on a Shimadzu GC–MS QP2010 SE with an Rx1 5sil MS column. Yields were calculated based on linear calibration curve of 4-methoxyacetophenone. Electrochemical data was collected on a CHI600E potentiostat with the accompanying CH Instruments software. LED lights and the requisite power box and cables were purchased from Creative Lighting Solutions (http://www.creativelightings.com) with the following item codes: CL-FRS5050-12WP-12V (4.4W blue LED light strip), CL-FRS5050WPDD-5M- 12V-BL (72 W LED strip), CL-PS94670-25W (25 W power supply), CL-PS16020-150W (150 W power supply), CL-PC6FT-PCW (power cord), CL-TERMBL-5P (terminal block).

Unless stated otherwise, all reactions were run on a 1.0 mmol scale in a 2 or 4 dram vial equipped with stir bar and cap. One 4w LED strip was wrapped in a circle around the reaction with the reaction about 3-4 inches from the light source. At this distance the temperature of the reactions did not exceed 35 ˚C.

3.5.1.1 Preparation of Starting Materials

Coumaryl Model System (3.138)

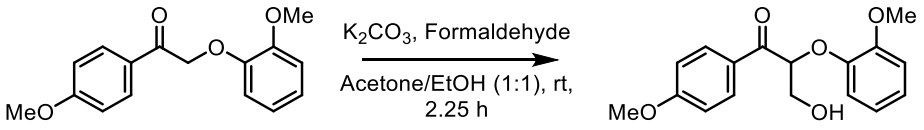

3.138 was synthesized using the following literature procedure.[179] A round bottom was charged with potassium carbonate (1.33 g, 9.70 mmol, 1.2 eq.), 2-(2-methoxyphenoxy)-1-(4-methoxyphenyl)ethan-1-one (2.20 g, 8.1 mmol), and formaldehyde (37 % $wt_{(aq)}$, 363 mg, 12 mmol,

1.5 eq.), in a solution of acetone and ethanol (12 mL, 1:1). Reaction was stopped after 2 hours and 15 minutes and passed through a celite plug and washed with acetone. The mixture was concentrated to an oil and purified using SiO_2 chromotography (R_f = 0.4 in 4:6 EtOAc:Hex). The product's spectra corresponded to previous reports.[180]

^{1}H NMR (400 MHz, $CDCl_3$) δ 8.08 (d, J = 8.9 Hz, 2H), 7.04 – 6.96 (m, 1H), 6.96 – 6.87 (m, 4H), 6.82 (td, J = 8.0, 1.3 Hz, 1H), 5.39 (t, J = 5.3 Hz, 1H), 4.06 (d, J = 5.3 Hz, 2H), 3.87 (s, 3H), 3.85 (s, 3H), 3.00 (bs, 1H).

Coniferyl Model System (3.139)

The coniferyl model system was synthesized based on literature precedent.[180,181] Spectral data was consistent with previous preparations.

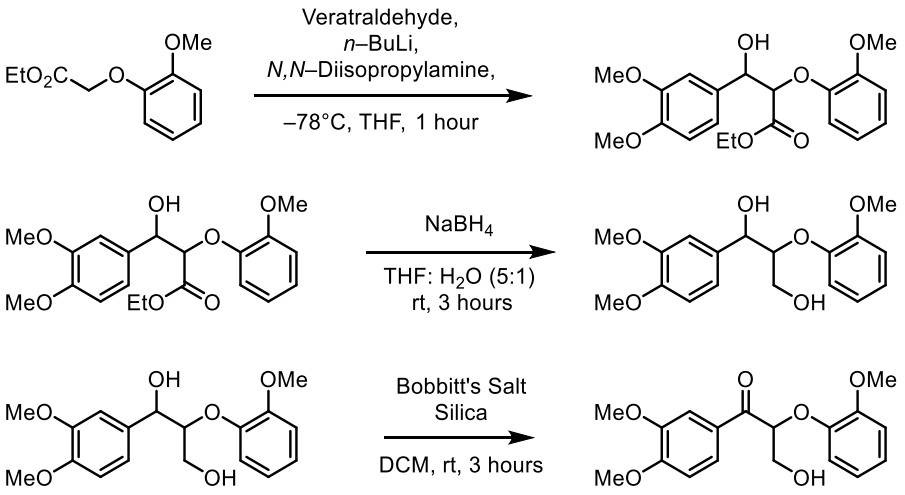

Step 1: A solution of β–hydroxester[4] (38.5 mmol, 8.0 g) in THF (38 mL) was cannulated at –78 °C to a solution of LDA (41.86 mmol, 5.87 mL, 1.1 eq.) in THF (60 mL) and stirred for 30 minutes at this temperature. At this time, a solution of 3,4-dimethoxybenzaldehyde (38.05 mmol, 6.32 g, 1 eq.) was cannulated at –78 °C into this reaction. The reaction was stirred at –78 °C for 1 hour and then warmed to room temperature. After this time, the reaction was quenched with saturated

ammonium chloride and extracted with ethyl acetate. The organic portions were combined, dried and concentrated *in vacuo*. The mixture was purified by column chromatography (40% EtOAc in Hexanes to afford) ethyl 3-(3,4-dimethoxyphenyl)-3-hydroxy-2-(2-methoxyphenoxy)propanoate in (12.4 g, 86% yield, mixture of diastereomers).

Step 2: THF and water were added in a 5:1 (3.75 mL:1.25 mL) ratio to pure ethyl 3-(3,4-dimethoxyphenyl)-3-hydroxy-2-(2-methoxyphenoxy)propanoate (8.57 mmol, 3.22 g) to afford a concentrated solution. To this solution, sodium borohydride (42.85 mmol, 1.62 g, 5 equiv.) was added portion wise at 0 °C. This reaction was stirred and monitored by TLC. Upon completion, the reaction was quenched with saturated ammonium chloride and extracted with ethyl acetate. The organic layer was combined, dried and concentrated *in vacuo*. The reaction yielded 1-(3,4-dimethoxyphenyl)-2-(2-methoxyphenoxy)propane-1,3-diol in 83 % yield (2.86 g), and no further purification was used.

^{1}H NMR (400 MHz, $CDCl_3$) δ 7.14 (dd, J = 7.9, 1.5 Hz, 1H, minor diastereomer), 7.11-7.05 (m, 1H, major diastereomer, 1H minor diastereomer, overlap), 7.01-6.89 (m, 5H, major diastereomer, 2H, minor diastereomer, overlap), 6.87-6.83 (m, 1H, major diastereomer, 1H, minor diastereomer, overlap), 4.99 (d, J = 4.7 Hz, 1H, minor diastereomer), 4.98 (t, J = 4.7 Hz, 1H, major diastereomer), 4.16 (ddd, J = 6.0, 4.7, 3.4 Hz, 1H, major diastereomer), 4.04 (m, 1H, minor diastereomer), 3.95-3.89 (m, 1H, major diastereomer), 3.92 (s, 3H, minor diastereomer), 3.88 (s, 3H, major diastereomer, 3H, minor diastereomer), 3.88 (s, 3H, major diastereomer, 3H minor diastereomer), 3.69 (m, 1H, minor diastereomer) 3.66 (m, 1H, major diastereomer), 3.63 (m, 1H minor diastereomer), 3.48 (dd, J = 12.5, 3.9 Hz, 1H, minor diastereomer), 2.96 (bs, 2H).

Step 3: 1-(3,4-dimethoxyphenyl)-2-(2-methoxyphenoxy)propane-1,3-diol (3.59 mmol, 1.20 g) was diluted in DCM to 10 mL. To this rapidly stirring solution, a freshly ground mixture of

Bobbitt's Salt (4-(Acetylamino)-2,2,6,6-tetramethyl-1-oxo-piperidinium tetrafluoroborate) and silica (1:1 with weight of starting alcohol), in one portion to the reaction. Care needs to be taken to run this reaction very dilute, as congealing of the silica gel and Bobbitt's salt will happen. The reaction was stirred for 3 hours, filtered, washed with DCM and concentrated *in vacuo*. The crude mixture was purified on silica to afford the product (1.2 g, 84% yield).

^{1}H NMR (400 MHz, $CDCl_3$) δ 7.76 (dd, *J* = 8.5, 1.9 Hz, 1H), 7.63 (d, *J* = 1.8 Hz, 1H), 7.02 (td, *J* = 8.2, 1.6 Hz, 1H), 6.95 – 6.91 (m, 2H), 6.90 (d, *J* = 8.3 Hz, 1H), 6.84 (td, *J* = 8.0, 1.4 Hz, 1H), 5.41 (t, *J* = 5.3 Hz, 1H), 4.08 (d, *J* = 5.3 Hz, 2H).

Benzylsinapyl Model System (3.140)

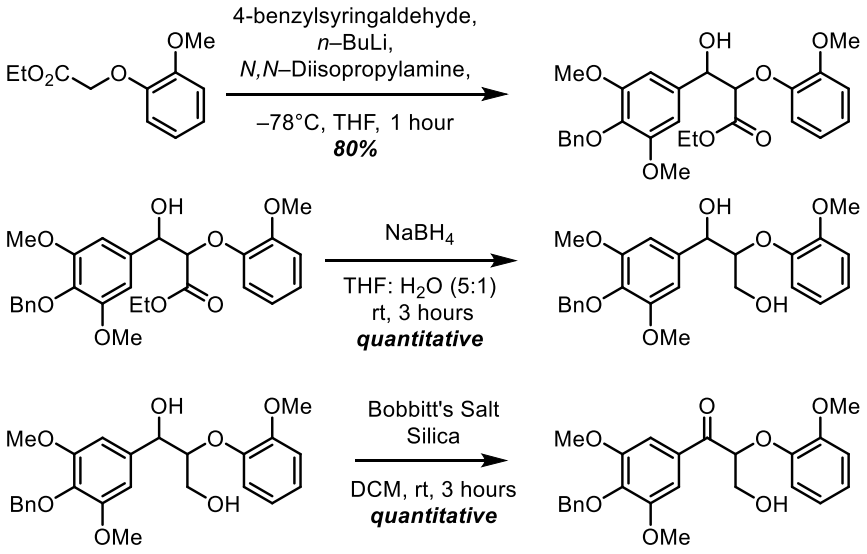

The sinapyl model system was synthesized based on literature precedent.[180,181] Spectral data was consistent with previous preparations. Exactly the same steps were taken for the synthesis of the **3.18.3** as **3.18.2**.

Step 1: ^{1}H NMR (500 MHz, $CDCl_3$) δ 7.13 – 6.97 (m, 4H), 6.97 – 6.81 (m, 7H), 5.16 (d, J = 4.9 Hz, 1H), 5.07 (minor isomer, d, J= 7.22, 1H), 4.75 (d, J = 5.0 Hz, 1H), 4.49 (minor isomer, d, J = 7.2 Hz, 1H), 3.90 (s, 3H), 3.89 (m, 9H), 1.17 (t, J = 7.1 Hz, 3H).

Step 2: ^{1}H NMR (400 MHz, $CDCl_3$) δ 7.48 (d, *J* = 8.2 Hz, 1H, major diastereomer), 7.48 (d,*J*=8.2 Hz, 1H, minor diasteromer), 7.35 (m, 1H, major diastereomer), 7.35 (m, 1H, minor diasteromer), 7.31 – 7.28 (m, 1H, major diasteriomer), 7.31 – 7.28 (m, 1H, minor diasteriomer), 5.02 (d, *J* = 14.4 Hz, 2H, major diastereomer), 4.97 (d, *J* = 4.5 Hz, 2H, minor diastereomer), 4.17 (m, 1H, major diasteromer), 4.02 (m, 1H, minor diasteromer), 3.91 (s, 3H, major diasteromer), 3.83 (s, 6H, minor diasteromer), 3.81 (s, 6H, major diasteromer), 3.66 (dt, *J* = 7.5, 4.0 Hz, 1H), 3.52 (dd, *J* = 12.5, 3.7 Hz, 1H).

3.18.3 ^{1}H NMR (400 MHz, $CDCl_3$) δ 7.38 (d, J = 7.3 Hz, 1H), 7.23 (dd, J = 12.2, 7.3 Hz, 1H), 6.88 (d, J = 7.7 Hz, 1H), 6.80 (d, J = 8.0 Hz, 1H), 6.74 (d, J = 7.4 Hz, 1H), 5.32 (t, J = 5.1 Hz, 1H), 5.03 (s, 1H), 4.03 (d, J = 5.0 Hz, 1H), 3.74 (s, 3H), 3.72 (s, 2H).

2-(2-methoxyphenoxy)-1-(4-methoxyphenyl)ethan-1-one (3.141)

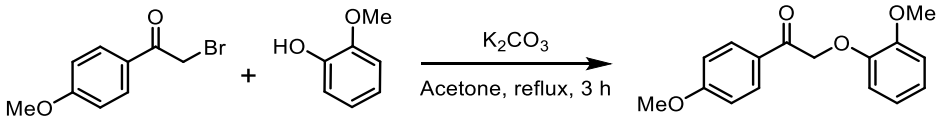

was prepared according to literature procedures.[180,182] A suspension of 2-bromo-1-(4 methoxyphenyl)ethanone (60 mmol, 13.7 g) was added to a mixture of K_2CO_3 (88.8 mmol, 12.2 g, 1.48 eq.) in acetone. To this mixture, guaiacol (73.8 mmol, 9.1 g, 1.23 eq.) was added. The reaction was equipped with a water condenser and heated to reflux for 3 hours. After this time, the reaction was cooled, filtered and concentrated *in vacuo*. The product was crystallized in hot

methanol to afford white crystals (13.7 g, 84%). Spectral data agreed with previous characterization data.

^{1}H NMR (400 MHz, $CDCl_3$) δ 8.03 (d, J = 8.8 Hz, 1H), 7.05 – 6.90 (m, 2H), 6.86 (d, J = 3.4 Hz, 1H), 5.29 (s, 1H), 3.89 (d, J = 3.5 Hz, 3H). ^{13}C NMR (176 MHz, $CDCl_3$) δ ppm 55.49, 55.91, 71.99, 76.81, 76.99, 77.17, 109.99, 112.15, 113.92, 114.70, 120.77, 122.30, 127.71, 130.50, 147.61, 149.72, 163.92, 193.12 IR (neat) 2900.6, 2844.6, 2000.3, 1922.3, 1691.2, 1601.7, 1572.4, 1503.8, 1458.1, 1420.9, 1360.9, 1334.3, 1246.7, 1213.1, 1172.2, 1187.1, 1129.3, 1109.4, 1083.7, 1054.7, 1014.1, 963.6, 918.1, 830.7, 810.4, 749.8, 637.8, 616.7 HRMS (ESI) *m/z* 273.1121 $[M+H]^+$

2-(benzyloxy)-1-phenylethan-1-one (3.146)

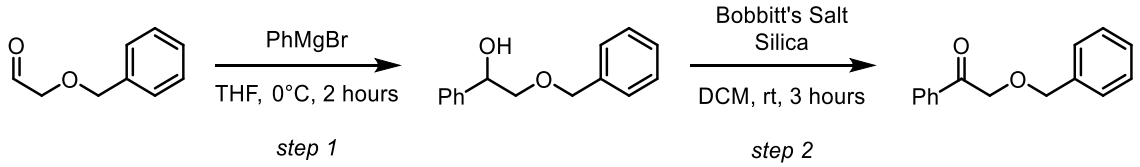

Step 1: To a solution of benzyloxyacetaldehyde (10.0 mmol, 1.40 mL) in THF (40 mL) at 0 °C, phenyl magnesium bromide (2.8 M in hexanes, 3.93 mL) was added dropwise. The reaction was allowed to warm to room temperature and stir for 2 hours. After this time, the reaction was quenched with saturated ammonium chloride. The reaction mixture was separated, and the aqueous layer was extracted with ether. Organic layer was combined and washed with brine, dried over sodium sulfate and concentrated *in vacuo*. The product, 2-(benzyloxy)-1-phenylethan-1-ol, was afforded in 82% and taken on to the next step without purification.

Step 2: 2-(benzyloxy)-1-phenylethan-1-ol (73.88 mmol, 1800 mg) was diluted into solution with DCM (80 mL). To this solution, an freshly ground mixture of Bobbitt's salt (4-(Acetylamino)-2,2,6,6-tetramethyl-1-oxo-piperidinium tetrafluoroborate) and silica (1:1 wt. with starting

alcohol)) were added and the reaction was stirred for 3 hours. After this time, the reaction was filtered and washed with 3 portions of 20 mL of DCM. The resultant liquor was concentrated *in vacuo* and purified on silica to yield the product (80%). Spectra data was consistent with those reported in the literature.[180]

^{1}H NMR (500 MHz, $CDCl_3$) δ 7.94 (d, J = 7.7 Hz, 8H), 7.59 (t, J = 7.4 Hz, 4H), 7.47 (t, J = 7.7 Hz, 8H), 7.43 – 7.29 (m, 19H), 4.78 (s, 9H), 4.72 (s, 9H).

3.5.1.2 Phenylethanone Amines

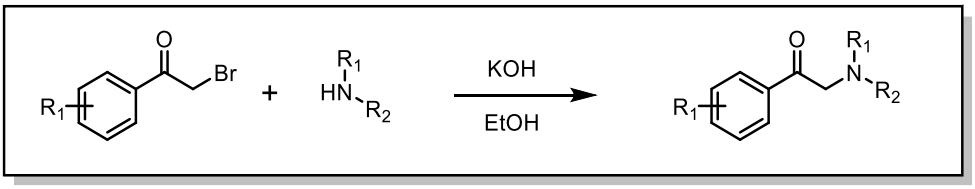

2-bromoacetophenone (2.0 g, 10.05 mmol) and ethanol (50 mL, 0.2 M in starting material) were added to a dry round bottom flask equipped with a magnetic stir bar. Aniline (1.83 mL, 20.10 mmol, 2 eq.) was added drop-wise, as a white precipitant formed immediately upon addition. This was allowed to stir for 3 hours, upon which the solution was filtered, concentrated *in vacuo*, and recrystallized using ethanol.

1-phenyl-2-(phenylamino)ethan-1-one (3.144)

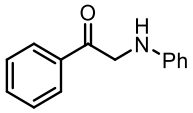

- ^{1}H NMR (400 MHz, CDCl3) δ 8.03 (d, J = 7.3 Hz, 2H), 7.65 (t, J = 7.4 Hz, 1H), 7.53 (t, J = 7.7 Hz, 2H), 7.31 – 7.22 (m, 3H), 6.81 (t, J = 7.6 Hz, 3H), 4.67 (s, 2H). ^{13}C NMR (176 MHz, CDCl3) δ 194.98, 146.95, 134.89, 133.86, 129.37, 128.88, 127.75, 117.94, 113.13, 50.41. IR (neat) 3410.9, 1686.3, 1601.9, 1508.4, 1444.8, 1356.9, 1321.6, 1261.8, 1219.9, 1178.8, 1147.7, 984,864.4, 743.6, 684.2, 663.5. HRMS (m/z) – 212.1070 [M+H]+. Rf (7:3 Hexanes:EtOAc) = 0.64

4-methy-N-(2-oxo-2-phenylethyl)-N-phenylbenzenesulfonamide (3.145)

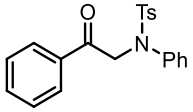

- ^{1}H NMR (700 MHz, CDCl3) δ 7.95 (dd, J = 8.2, 1.1 Hz, 2H), 7.60 (d, J = 7.4 Hz, 1H), 7.59 – 7.55 (m, 2H), 7.47 (t, J = 7.8 Hz, 2H), 7.32 – 7.23 (m, 5H (2+3), overlap with CHCl3), 7.18 – 7.14

(m, 2H), 5.05 (s, 2H), 2.44 (s, 3H). ^{13}C NMR (176 MHz, CDCl3) δ 193.87, 143.86, 139.74, 135.61, 135.06, 133.78, 129.53, 129.22, 128.86, 128.85, 128.39, 128.16, 77.34, , 76.98, 57.78, 21.75. IR (neat): 3061.9, 2917.1, 1707.2, 1595.3, 1491.8, 1447.4, 1335.1, 1364.6, 1305.8, 1291.6, 1212.6, 1184.4, 1103.8, 1089.9, 1029.7, 1011.6, 1000.4, 980.1, 881.8, 935.3, 912.4, 809.2, 768.2, 755.0, 768.2, 729.9, 667.0, 692.9 HRMS (m/z) = 366.1158 [M+H].

2-(methyl(phenyl)amino)-1-phenylethan-1-one (3.146)

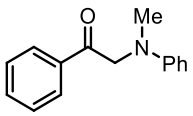

^{1}H NMR (700 MHz, $CDCl_3$) δ 8.00 (d, *J* = 7.3 Hz, 2H), 7.62 (t, *J* = 7.3 Hz, 1H), 7.51 (t, *J* = 7.8 Hz, 2H), 7.22 (dd, *J* = 8.4, 7.4 Hz, 2H), 6.74 (t, *J* = 7.3 Hz, 1H), 6.69 (d, *J* = 8.6 Hz, 2H), 4.79 (s, 2H), 3.12 (s, 3H). ^{13}C NMR (176 MHz, $CDCl_3$) δ 195.64 (s), 135.78 (s), 133.45 (s), 128.62 (s), 128.05 (s), 66.66 (s), 53.71 (s). Previously synthesized by Zhao and co-workers.[183]

2-morpholino-1-phenylethan-1-one (3.147)

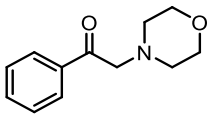

^{1}H NMR (400 MHz, CDCl3) δ 8.01 (d, J = 7.2 Hz, 1H), 7.59 (t, J = 7.4 Hz, 1H), 7.47 (t, J = 7.6 Hz, 1H), 3.83 (s, 1H), 3.81 – 3.74 (m, 2H), 2.69 – 2.58 (m, 2H). This material was prepared, isolated as an off white solid, and then immediately used, as this product decomposed in the presence of air to a dark orange solid. Previously characterized by Hasegawa and coworkers.[184]

3.5.1.3 Phenylethanone Sulfides

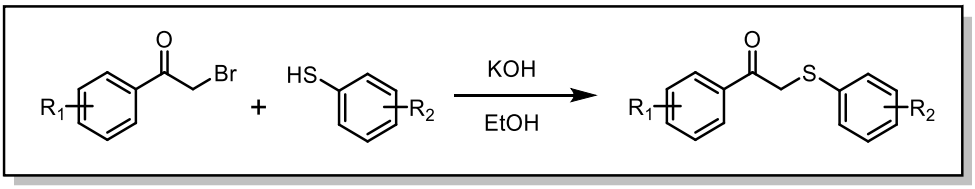

Prepare a solution of thiol and base ethanol solution, 0.2 M with respect to the thiol. Allow for equilibration and cooling for 30 minutes. Separately, prepare a solution of 2-bromoacetophenone in ethanol, and add slowly to the reaction. Allow appropriate time for reaction. Quench the reaction with an equimolar amount of acid, and then precipitate the product by adding a large excess of water. Crude crystals can be recrystallized in MeOH-H_2O.

1-phenyl-2-(phenylthio)ethan-1-one (3.149)

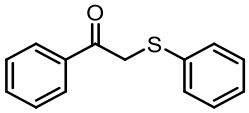

^{1}H NMR (700 MHz, $CDCl_3$) δ 7.96 (dd, J = 8.4, 1.2 Hz, 2H), 7.96 (dd, J = 8.4, 1.2 Hz, 2H), 7.60 (ddt, J = 8.6, 7.2, 1.2 Hz, 1H), 7.48 (dd, J = 8.1, 7.4 Hz, 2H), 7.42 –7.38 (m, 2H), 7.32 – 7.28 (m, 2H), 7.26 – 7.21 (m, 1H), 4.29 (s, 2H). ^{13}C NMR (176 MHz, $CDCl_3$) δ 133.47, 130.52, 129.05, 128.67, 128.67, 127.11, 41.2. IR (neat) 3074.1, 1668.8, 1596, 1578.4, 1479.2, 1444.9, 1416.1, 1273.2, 1185.8, 1133.9, 1072.5, 1011.2, 941.7, 898, 804.3, 740.5, 722, 66.6, 648.1, 614.1. HRMS (m/z) = 229.0682 $[M+H]^+$. R_f (EtOAc/Hexanes (1:5)) = 0.50

1-(4-methoxyphenyl)-2-(phenylthio)ethan-1-one (3.150)

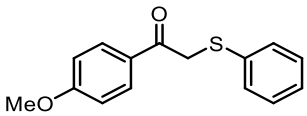

^{1}H NMR (500 MHz, $CDCl_3$) δ 7.98 – 7.91 (m, 2H), 7.43 – 7.37 (m, 2H), 7.32 – 7.27 (m, 2H), 7.25 – 7.20 (m, 1H), 6.97 – 6.92 (m, 2H), 4.25 (s, 2H), 3.89 (s, 3H). ^{13}C NMR (176 MHz, $CDCl_3$) δ 192.68, 163.76, 135.03, 131.02, 130.34, 129.00, 128.37, 126.94, 113.83, 55.49, 40.95. IR (neat) 1658.2, 1601.4, 1572, 1508.6, 1480.4, 1420.3, 1436.7, 1395.9, 1310.5, 1262.6, 1199.9, 1173.8, 1023.7, 991.6, 817.8, 734.3, 690, 633.1. HRMS (m/z) 259.0682 $[M+H]^+$ R_f (EtOAc/Hexanes 1:5) 0.55.

2-((4-methoxyphenyl)thio)-1-phenylethan-1-one (3.153)

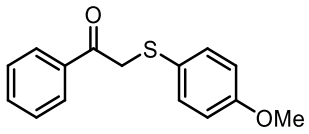

^{1}H NMR (500 MHz, $CDCl_3$) δ 7.93 (d, J = 7.8 Hz, 2H), 7.57 (d, J = 7.3 Hz, 1H), 7.47 (t, J = 7.6 Hz, 2H), 7.37 (d, J = 8.6 Hz, 2H), 6.83 (d, J = 8.6 Hz, 2H), 4.14 (s, 2H), 3.80 (s, 3H). ^{13}C NMR (176 MHz, CDCl3) δ 194.29 (s), 159.73 (s), 135.45 (s), 134.65 (s), 133.29 (s), 132.64 (s), 130.48 (s), 128.94 (s), 128.65 (d, J = 18.3 Hz), 126.30 (s), 124.52 (s), 114.82 (s), 114.63 (d, J = 18.7 Hz), 77.18 (s), 76.99 (s), 76.81 (s), 55.29 (s), 42.79 (s). IR (neat) 2937.2, 2835.3, 1674.0, 1591.1, 1492.3, 1461.7, 1447.4, 1406.0, 1274.1, 1242.8, 1196.2, 1172.8, 1133.5, 1104.0, 1075.9, 1027.9, 1014.0, 1075.9, 1027.9, 1014.0, 825.8, 798.3, 748.4, 723.8, 686.9. HRMS (m/z): 259.0788 $[M+H]^+$.

2-(phenylthio)-1-(4-(trifluoromethyl)phenyl)ethan-1-one (3.148)

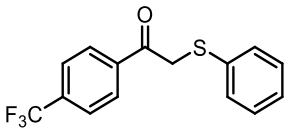

^{1}H NMR (700 MHz, CDCl3) δ 8.04 (d, J = 8.1 Hz, 15H), 7.74 (d, J = 8.1 Hz, 15H), 7.41 – 7.36 (m, 14H), 7.30 (ddd, J = 6.6, 2.4, 0.8 Hz, 14H), 7.28 (t, J = 1.3 Hz, 3H), 7.27 – 7.25 (m, 4H), 4.26

(s, 16H). ^{13}C NMR (176 MHz, CDCl3) δ 193.18 (s), 138.21(s), 135.08(s), δ 134.80 (q, J = 32.8 Hz), 134.70 (s), 134.52 (s), 134.10 (s), 131.18 (s), 129.35 (s), 129.21 (s), 125.98 (s), 125.88 (q, J = 3.7 Hz), 123.65 (q, J = 272.7 Hz), 121.33 (s), 41.42 (s). ^{19}F NMR (471 MHz, CDCl3) ppm = –64.17 (s, 3 F). IR (neat) 2896.7, 1679.3, 1580.0, 1511.7, 1482.4, 1438.6, 1409.9, 1393.0, 1326.1, 1311.2, 1311.2, 1285.7, 1195.7, 1162.8, 1111.1, 1065.1, 1026.9, 1015.1, 992.4, 964.0, 900.1, 854.4, 839.0, 825.5, 739.9, 701.1, 689.8. HRMS (m/z) = 297.055 $[M+H]^+$. R_f (9:1 Hexanes:EtOAc) = 0.36 (stains light green in vanillin)

1-(naphthalen-2-yl)-2-(phenylthio)ethan-1-one (3.152)

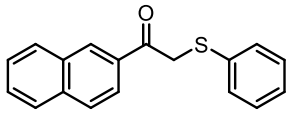

^{1}H NMR (700 MHz, $CDCl_3$) δ 8.44 (s, 1H), 8.02 (dd, J = 8.6, 1.6 Hz, 1H), 7.96 – 7.86 (m, 3H), 7.63 (t, J = 7.4 Hz, 1H), 7.57 (t, J = 7.5 Hz, 1H), 7.43 (d, J = 7.5 Hz, 2H), 7.30 (t, J = 7.5 Hz, 2H), 7.25 (t, J = 7.3 Hz, 1H), 4.41 (s, 2H). ^{13}C NMR (176 MHz, CDCl3) δ 194.20, 135.86, 134.95, 132.85, 132.56, 130.87, 130.73, 129.79, 129.25, 128.88, 128.73, 127.94, 127.35, 127.02, 124.36, 41.53. IR (neat) 3073.2, 3048.4, 2952.3, 2898.7, 2898.7, 1676.0, 1622.7, 1581.6, 1505.9, 1478.8, 1466.1, 1436.0, 1389.7, 1355.9. 1293.9, 1271.1, 1244.5, 1164.5, 1124.3, 1093.9, 1070.5, 1024.1, 1024.1, 984.5, 972, 944.7, 925.8, 890.3, 864.5, 810.1, 767.9, 748.6, 727.7, 685.7. HRMS (m/z): 301.0658 $[M+Na^+]$. R_f (9:1 Hexanes:EtOAc) = 0.32

2-((3-chlorophenyl)thio)-1-phenylethan-1-one (3.157)

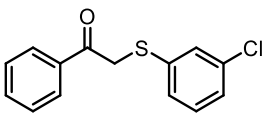

^{1}H NMR (700 MHz, $CDCl_3$) δ 7.96 (dd, J = 8.4, 1.2 Hz, 1H), 7.61 (ddd, J = 2.4, 1.8, 1.2 Hz, 1H), 7.52 – 7.47 (m, 1H), 7.38 (t, J = 1.6 Hz, 1H), 7.27 (m, 1 H) overlap with chloroform, 7.22 (t, J = 7.5 Hz, 1H), 7.21 – 7.19 (m, 1H), 4.32 (s, 1H). ^{13}C NMR (126 MHz, $CDCl_3$) δ 193.72, 137.10, 135.41, 133.82, 130.21, 129.80, 128.92, 128.80, 128.16, 127.24, 41.02. IR (neat) 3052.3, 2943.0, 2913.8, 1686.2, 1593.2, 1573.4, 1561.6, 1561.6, 1464.3, 1445.8, 1404.1, 1382.3, 1382.3, 1322.5, 1308.1, 1288.9, 1196.9, 1180.2, 1116.2, 1086.1, 1086.1, 1077.5, 1026.0, 999.3, 980.0, 884.0, 884, 871.3, 775.7, 765.0, 751.5, 687.0, 680.2. HRMS (m/z): 263.0292 [$M+H^+$]. R_f (9:1 Hexanes:EtOAc) = 0.33

((2-fluorophenyl)thio)-1-phenylethan-1-one (3.154)

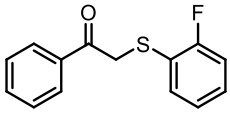

^{1}H NMR (700 MHz, $CDCl_3$) 7.96 (dd, J = 8.4, 1.2 Hz, 1H), 7.61 (tt, J = 7.41, 1.21 Hz, 1H), 7.51 – 7.48 (m, 1H), 7.38 (t, J = 1.6 Hz, 1H), 7.27(dt, J = 7.48,1.57 Hz, 1H overlap with CDCl3), 7.22 (t, J = 7.5 Hz, 1H), 7.21 – 7.19 (m, 1H) , 4.32 (s, 2H). ^{13}C NMR (126 MHz, CDCl3) δ 193.98 (s) 162.17 (d, J = 246.5 Hz), 135.52 (s), 134.05 (s), 134.04 (s), 133.65 (s), 129.96 (d, J = 8.0 Hz), 128.80 (d, J = 9.5 Hz), 124.74 (d, J = 3.8 Hz), 121.33 (d, J = 17.6 Hz), 116.02 (d, J = 22.5 Hz), 40.51 (s). ^{19}F NMR (471 MHz, CDCl3) δ -109.06 (ddd, J = 9.4, 7.5, 5.5 Hz). IR (neat) 3070.3, 2947.6, 2911.4, 1679.9, 1593.5, 1578.8, 1565.6, 1465.8, 1445.9, 1397.5, 1317.6, 1284.4, 1261.9, 1220.1, 1191.4, 1180.6, 1160.0, 1123.1, 1070.2, 1031.3, 999.4, 983.7, 927.8, 888.2, 852.9, 826.9, 806.3, 806.3, 743.3, 687.4, 678.4. HRMS (m/z) = 269.0407 [M+ Na^+]. R_f (9:1 Hexanes:EtOAc) = 0.40

2-methyl-1-phenyl-2-(phenylthio)propan-1-one (3.151)

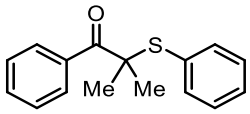

^{1}H NMR (700 MHz, CDCl3) δ 8.25 (d, J = 8.4 Hz, 2H), 7.54 (td, J = 7.7, 1.0 Hz, 1H), 7.46 (t, J = 7.7 Hz, 2H), 7.38 – 7.32 (m, 3H), 7.32 – 7.24 (m, 2H, overlap with CHCl3), 1.57 (s, 6H). ^{13}C NMR (176 MHz, CDCl3) δ 201.20 (s), 137.90 (s), 137.16 (s), 132.49 (s), 131.78 (s), 130.48 (s), 130.16 (s), 129.59 (s), 128.84 (s), 55.67 (s), 27.59 (s). IR (neat) : 3060.3, 2967.4, 2928.0, 1665.8, 1595.6, 1574.2, 1473.5, 1460.9, 1438.7, 1383.5, 1364.5, 1304.0, 1259.7, 1157.3, 1118.8, 1088.3, 1068.0, 1024.9, 1002.0, 975.5, 881.6, 792.4, 750.0, 732.1, 702.2. HRMS (m/z) = 257.0994 [M+H+] Rf (9.5:0.5 Hexanes:EtOAc) = 0.42

2-(phenylthio)-2,3-dihydro-1H-inden-1-one (3.156)

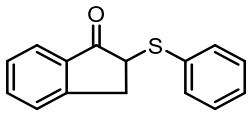

^{1}H NMR (700 MHz, $CDCl_3$) δ 3.13 (dd, J=17.54, 3.75 Hz, 8 H) 3.63 (dd, J=17.71, 7.66 Hz, 9 H) 4.08 (dd, J=7.83, 3.75 Hz, 8 H) 7.21 - 7.30 (m, 29 H) 7.34 - 7.42 (m, 15 H) 7.44 - 7.52 (m, 15 H) 7.54 - 7.67 (m, 9 H) 7.78 (d, J=7.66 Hz, 7 H). ^{13}C NMR (176 MHz, CDCl3) δ ppm 34.79, 50.34, 124.58, 126.29, 127.12, 127.46, 127.67, 127.84, 128.95, 132.30, 133.28, 135.26, 135.43, 152.06, 202.23. IR (neat) 3058.7, 2906.7, 1763.5, 1721.7, 1602.1, 1580.3, 1602.1, 1580.3, 1481.7, 1470.7, 1437.9, 1419.7, 1325.4, 1299.4, 1273.8, 1205.8, 1185.6, 1173.6, 1146.0, 1087.8, 1020.8, 1008.1, 957.1, 892.4, 849.7, 792.9, 780.4, 740.6, 729.8, 711.0, 689.5. HRMS (m/z) = 241.0682 [$M+H^+$] R_f (9:1 Hexanes:EtOAc)= 0.46

2-(benzylthio)-1-phenylethan-1-one (3.155)

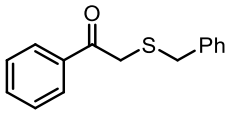

^{1}H NMR (500 MHz, CDCl3) δ 3.67 (s, 2 H) 3.76 (s, 2 H) 7.17 - 7.28 (m, 2 H) 7.32 (t, J=7.46 Hz, 2 H) 7.34 - 7.38 (m, 2 H) 7.43 - 7.49 (m, 2 H) 7.52 - 7.60 (m, 1 H) 7.93 (d, J=8.07 Hz, 2 H) ^{13}C NMR (176 MHz, CDCl3): δ 194.40, 137.26, 135.36, 133.32, 129.26, 128.68, 128.64, 128.52, 127.22, 36.06, 35.82. IR (neat): 1670.2, 1595.7, 1449.8, 1394.7, 1292.3, 1197.4, 998.8, 751.1, 685.3, 638.4, 552.6, 536.0, 526.3, 497.6, 480.1, 447.3, 417.9, 412.5. HRMS (m/z) = 265.0658 [M+Na^{+}].

1-([1,1'-biphenyl]-4-yl)-2-(phenethylthio)ethan-1-one (3.158)

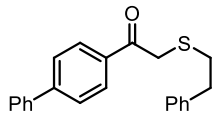

^{1}H NMR (700 MHz, $CDCl_3$) δ δ 8.06 (d, J = 8.4 Hz, 2H), 7.70 (d, J = 8.4 Hz, 2H), 7.64 (dd, J = 8.2, 1.1 Hz, 2H), 7.49 (t, J = 7.7 Hz, 2H), 7.42 (t, J = 7.4 Hz, 1H), 7.30 (dd, J = 9.5, 5.7 Hz, 2H), 7.22 (dd, J = 7.2, 5.3 Hz, 3H), 3.84 (s, 2H), 2.93 (dd, J = 8.9, 6.4 Hz, 2H), 2.89 – 2.83 (m, 2H). ^{13}C NMR (176 MHz, CDCl3) δ 194.16, 146.22, 140.22, 139.95, 133.96, 129.55, 129.12, 128.73, 128.63, 128.45, 127.48, 127.43, 126.57, 37.20, 35.72, 33.79. IR (neat): 2914.2, 2139.9, 2183.1, 2172.7, 2066.2, 1977.0, 2017.31971.9, 1955.0, 1660.3, 1599.9, 1560.5, 1485.1, 1452.8, 1419.8, 1310.9, 1288.9, 1270.1, 1204.5, 1139.5, 1159.9, 1072.8, 1034.3, 1002.6, 927.7 855.8, 845.8, 714.5, 698.5, 988.2, 647.5, 633.9, 609.3, 615.0, 620.1, 604.0 HRMS (m/z) = 333.1308 [M+H^{+}]. R_f (9:1 Hexanes:EtOAc): 0.55 (brown in anisaldehdye stain).

3.3.2 General Reaction Procedure: Photoredox Reductive Fragmentation

Phenyl ketone (0.50 mmol – 1.0 mmol) was added to a round bottom or 4 dram vial with $^{i}Pr_2NEt$ (2 equiv.), HCO_2H (1 equiv.) and photocatalyst [$Ir(ppy)_2$(dtbbpy)PF6] (1 mol %). These reactants were diluted in EtOH (5 mL, 0.20 M in starting material), and irradiated by 1x4W Blue LED strip until reaction completion (6-96 hours). At this point the ethanol was removed *in vacuo*, and the resulting oil was diluted in water and extracted with ethyl acetate. The organic portion was washed with 4 N HCl(aq), saturated sodium bicarbonate solution, brine and finally dried with sodium sulfate, after which it was concentrated to an oil. If the starting material contained acetophenone as the phenacyl fragment, 1 eq. of PhTMS was added to the oil and the mixture was diluted in $CDCl_3$. This was analyzed via ^{1}H NMR to obtain an accurate acetophenone yield. If the starting material yields an acetophenone derivative heavier than acetophenone, then the PhTMS standardization step was omitted. After which the crude reaction was purified by silica chromatography to afford the fragmentation products.

Reduction of 3.138

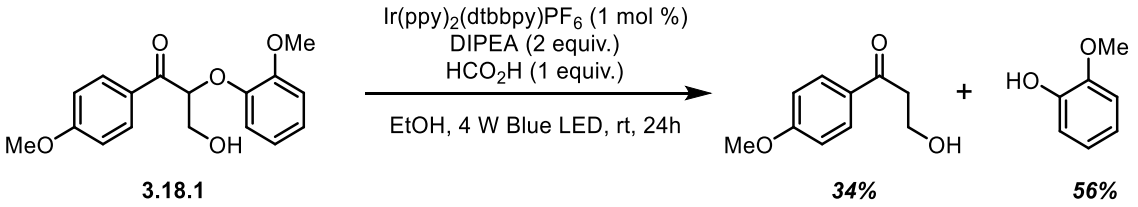

To an oven dried 1 dram vial, 3-hydroxy-2-(2-methoxyphenoxy)-1-(4-methoxyphenyl)propan-1-one (75 mg, 0.25 mmol), $Ir(ppy)_2(dtbbpy)PF_6$ (2.27 mg, 2.5 µmol) and DIPEA (0.040 mL, 0.25 mmol) were added. The vial was capped and irradiated by 1x4W Blue LED for 24 hours. After this time, the solvent was removed *in vacuo* and purified via SiO_2 chromatography (6:2:1:1 Hexanes, DCM, Acetone, Methanol). This afforded 9.6 mg (56%) of guaiacol and 10.6 mg (34%) of 3-hydroxy-1-(4-methoxyphenyl)propan-1-one. The spectra were consistent with previous reports.[180]

3-hydroxy-1-(4-methoxyphenyl)propan-1-one: ^{1}H NMR (400 MHz, $CDCl_3$) δ 7.99 – 7.86 (m, 1H), 7.02 – 6.80 (m, 1H), 4.00 (d, J = 4.6 Hz, 1H), 3.85 (d, J = 7.7 Hz, 2H), 3.16 (t, J = 5.3 Hz, 1H), 2.75 (s, 1H).

Reduction of 3.139

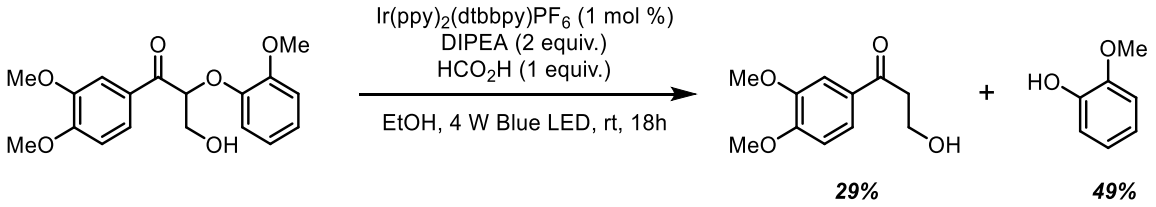

To an oven dried 1 dram vial, 3-hydroxy-2-(2-methoxyphenoxy)-1-(4-methoxyphenyl)propan-1-one (50 mg, 0.15 mmol), $Ir(ppy)_2(dtbbpy)PF_6$ (1.37 mg, 1.5 μmol) and DIPEA (52 μL, 0.30 mmol) were added. The vial was capped and irradiated by 1x4W Blue LED for 48 hours. The reaction was worked up by diluting in water and separating with ethyl acetate. The combined organic layer was washed with brine and dried over Na_2SO_4. Crude product was concentrated *in vacuo* to a yellow oil. Products were obtained by SiO_2 column purification using a 6:2:1:1 mixture of Hexanes, DCM, Acetone, Methanol, respectively. This afforded 9.14 mg (29%) of 1-(3,4-dimethoxyphenyl)-3-hydroxy-propan-1-one and 9.00 mg of guaiacol (48%). The spectra of the products was consistent with previous reports.[1]

1-(3,4-dimethoxyphenyl)-3-hydroxy-propan-1-one: ^1H NMR (500 MHz, $cdcl_3$) δ 7.60 (dd, *J* = 8.4, 2.0 Hz, 1H), 7.54 (d, *J* = 1.9 Hz, 1H), 6.91 (d, *J* = 8.4 Hz, 1H), 4.03 (t, *J* = 5.3 Hz, 2H), 3.96 (s, 3H), 3.95 (s, 3H), 3.21 (t, *J* = 5.3 Hz, 2H).

Reduction of 3.140

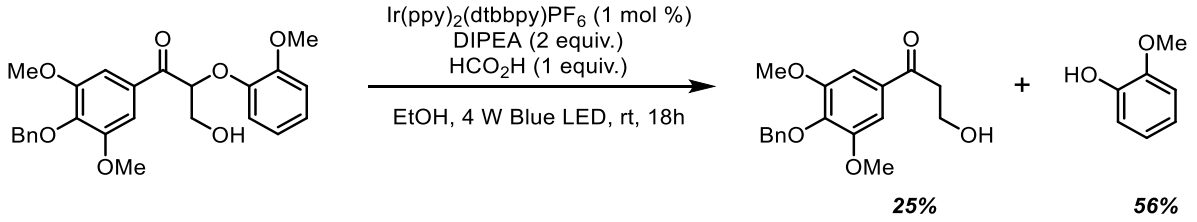

To an oven dried 1 mL vial, 1-(4-(benzyloxy)-3,5-dimethoxyphenyl)-3-hydroxy-2-(2-methoxyphenoxy)propan-1-one (28 mg, 0.06 mmol), $Ir(ppy)_2(dtbbpy)PF_6$ (0.58 mg, 0.6 µmol) and DIPEA (23 µL, 0.13 mmol) and formic acid (3 µL, 0.06 mmol) were added. The vial was capped and irradiated by 1x4W Blue LED for 60 hours. The reaction was worked up by diluting in 5% citric acid aqueous solution and separating with ethyl acetate. The combined organic layer was washed with brine and dried over $MgSO_4$. Crude product was concentrated *in vacuo* to a yellow oil. Products were obtained by SiO_2 column purification using a 3:7 Hexanes:Ethyl Acetate mixture. This afforded 5.0 mg (24.75%) of 1-(4-(benzyloxy)-3,5-dimethoxyphenyl)-3-hydroxypropan-1-one and 4.10 mg (52%) of guaiacol.

1-(4-(benzyloxy)-3,5-dimethoxyphenyl)-3-hydroxypropan-1-one: ^1H NMR (500 MHz, $CDCl_3$): δ 7.47 (d, J = 7.2 Hz, 2H), 7.36-7.29 (m, 3H), 7.21 (s, 2H), 5.12 (s, 2H), 4.04 (t, J=5.3 Hz, 2H), 3.89 (s, 6H), 3.21 (t, J=5.3 Hz, 2H). ^{13}C NMR (126 MHz, $CDCl_3$) = 199.45, 153.62, 141.98, 137.40, 132.21, 128.57, 128.37, 128.22, 105.75, 75.18, 58.38, 56.47. IR (neat) 2929.3, 1675.1, 1585.9, 1455.0, 1413.9, 1320.5, 1157.6, 1126.7, 700.9HRMS (m/z) = 317.1381 $[M+1]^+$ R_f: 0.21 (7:3 EtOAc:Hexanes)

Reduction of 3.141

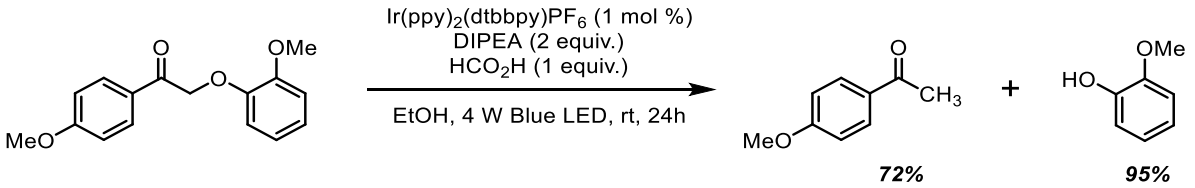

Following General Procedure A, this reaction yielded 127 mg of 4-methoxyacteophenone (72%) and 106 mg guaiacol (95%) after column purification (8:2 Hexanes:EtOAc). Spectra of products corresponded to previous reports.[180]

4-methoxyacetophenone ^{1}H NMR (500 MHz, $CDCl_3$) δ 7.95 (d, *J* = 8.3 Hz, 1H), 6.95 (d, *J* = 8.4 Hz, 1H), 3.88 (d, *J* = 0.5 Hz, 2H), 2.57 (d, *J* = 0.7 Hz, 2H). R_f (7:3 Hexanes:EtOAc): 0.40

Guaiacol (4) ^{1}H NMR (500 MHz, $CDCl_3$) δ 6.96 – 6.92 (m, 1H), 6.91 – 6.84 (m, 3H), 5.61 (s, 1H), 3.91 (s, 3H). R_f (6:4 Hexanes:Ethyl Acetate) = 0.7 (stains purple in anisaldehdye).

Reduction of 3.142

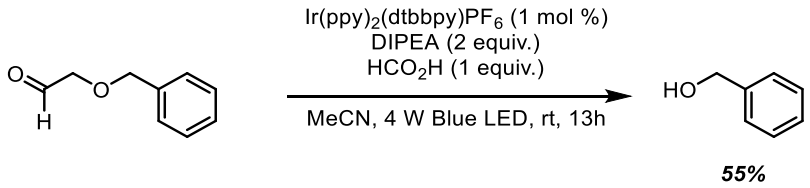

To a flame dried, 24 mL round bottom flask with stir bar, starting material (**3.18.5**) (1.00 mmol, 150 mg) and photocatalyst ($Ir(ppy)_2(dtbbpy)PF_6$) (9.14 mg, 0.01 mmol, 0.01 eq.) were added. The reaction was diluted in 5 mL of MeCN and DIPEA (0.350 mL, 2.00 mmol) and HCO_2H (0.040 mL, 1.00 mmol) were added. The reaction was capped and irradiated with 1x4W Blue LED for 13 hours. At this time, the reaction was deemed complete by TLC, and was worked up by removing the solvent *in vacuo*. The resultant oil was diluted in water, and separated with ethyl acetate. The organic layer was washed with 4 N HCl aliquots as well as brine. The organic fraction was dried over Na_2SO_4 and concentrated *in vacuo*. Purification by SiO_2 chromatography yielded 30 mg of benzyl alcohol (55% yield). Spectra of product corresponded with previous reports.[185]

Benzyl Alcohol: ^1H NMR (500 MHz, $CDCl_3$) δ 7.41 – 7.28 (m, 5H), 4.71 (s, 2H).

Reduction of 3.143

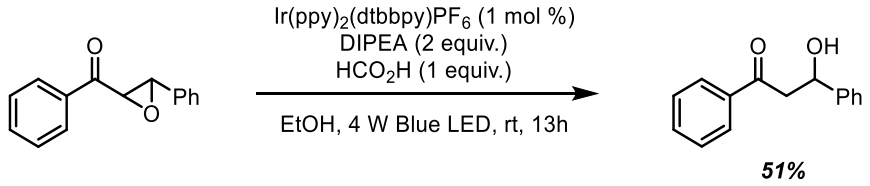

Following General Procedure A, this reaction yielded 115 mg of 3-hydroxy-1,3-diphenyl-propan-1-one (**3.18.6**) (51%) after column purification (9:1 Hexanes:EtOAc). Spectra of product corresponded with previous reports.[13]

3-hydroxy-1,3-diphenyl-propan-1-one: ^{1}H NMR (400 MHz, $CDCl_3$) δ 7.97 (d, J = 7.3 Hz, 2H), 7.60 (t, J = 7.3 Hz, 1H), 7.51 – 7.42 (m, 4H), 7.40 (t, J = 7.5 Hz, 2H), 7.32 (t, J = 7.2 Hz, 1H), 5.37 (t, J = 5.9 Hz, 1H), 3.58 (s, 1H), 3.39 (d, J = 6.0 Hz, 2H).

Pinacol coupling of 3.159

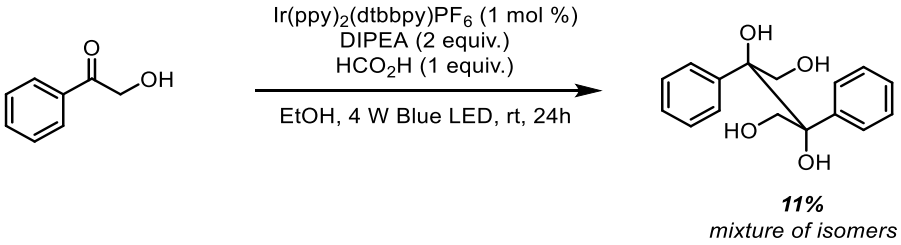

11%
mixture of isomers

Following General Procedure A, the reaction was stopped after 24 hours and worked up by diluting in water and extracting with ethyl acetate. The organic layer was combined and extracted with brine to yield a yellow oil. The crude mixture was separated on silica to yield 32.4 mg (11%) yield as a mixture of isomers).

3.160 ^{1}H NMR (500 MHz, $CDCl_3$) (1.4:1 racemic:meso) δ 7.38 – 7.28 (m, 3H), 7.26 – 7.16 (m, 3H), 6.99 (bs 1H), 6.98 (bs, 1H), 4.22 (d, J = 11.7 Hz, 1H), 3.98 (dd, J = 28.3, 11.8 Hz, 2 H), 3.52 (d, J = 11.8 Hz, 1H). ^{13}C NMR (126 MHz, $CDCl_3$) δ 140.53, 139.45, 128.03, 127.82, 127.71, 127.62, 127.23, 127.10, 80.25, 79.55, 66.47, 66.32. IR (neat*)*: 3379.4, 2946.3, 2246.0, 1956.1, 1601.2, 1492.5, 1446.3, 1384.2, 1184.8, 1119.3, 1066.0, 1051.7, 953.3, 906.8, 841.5, 761.8, 729.1, 702.4, 645.0, 620.8, 611.2. HRMS (*m/z*) = 292.2268

Pinacol coupling of 3.161

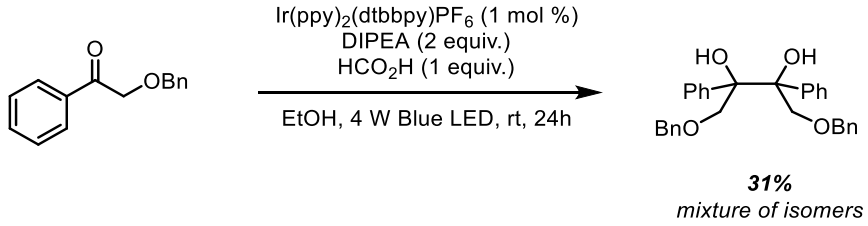

31%
mixture of isomers

Following General Procedure A, this reaction yielded a solid pinacol isomer (6.6 mg, 21%) which was filtered from the reaction solution and dried before analysis. The remainder of the reaction was worked up by washing with water and extracting 3 times with ethyl acetate. The combined organic layer was washed with brine and then concentrated and purified on silica to yield another isomer (3.1 mg, 10%).

3.162: ^{1}H NMR (500 MHz, $CDCl_3$) (solid) δ 7.35 – 7.28 (m, 3H), 7.26 – 7.18 (m, 5H), 7.17 – 7.12 (m, 2H), 4.42 (q, J = 11.9 Hz, 2H), 4.05 (d, J = 9.7 Hz, 1H), 3.89 (s, 1H), 3.77 (t, J = 12.6 Hz, 1H). ^{13}C NMR (176 MHz, $CDCl_3$) (solid) δ 141.27, 137.77, 128.48, 127.97, 127.88, 127.38, 127.18, 127.03, 79.30, 74.71, 73.77. HRMS (*m/z*)(solid) = 477.2036 [M+Na^+] IR (neat) (solid pinacol) = 3548.0, 1495.1, 1446.3, 1403.8, 1359.9, 1301.6, 1252.2, 1208.2, 1127.6, 1101.4, 1066.4, 1048.8, 1034.2, 914.6, 818.6, 738.5, 703.1, 616.3, 600.2, 582.1, 558.8, 545.1, 536.3, 528.8, 512.9, 505.8, 501.9, 487.1, 480.3, 46739, 452.7, 445.7

3.162: ^{1}H NMR (700 MHz, $CDCl_3$) (oil) δ 7.33 – 7.27 (m, 3H), 7.18 (m, 5H), 7.11 (m, 2H), 4.50 (q, J = 12.0 Hz, 2H), 4.14 (s, 1H), 4.07 (d, J = 9.8 Hz, 1H), 3.69 (d, J = 9.8 Hz, 1H). ^{13}C NMR (176 MHz, $CDCl_3$) (oil) δ 140.71, 137.76, 128.52, 127.92, 127.90, 127.32, 127.25, 79.74, 74.06, 73.94 HRMS (*m/z*)(oil) = 477.02035

Reduction of 3.144

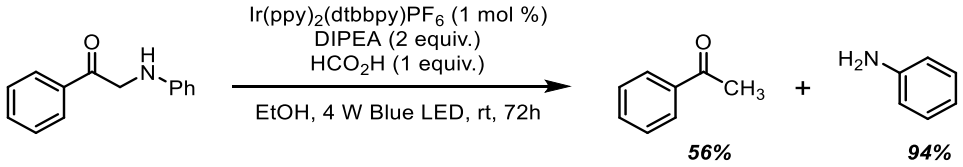

Following General Procedure A, this reaction was analyzed by ^{1}H NMR to yield 56% acetophenone and 94% aniline.

Acetophenone ^{1}H NMR: (500 MHz, $CDCl_3$) δ 7.97 (d, *J* = 7.7 Hz, 1H), 7.58 (t, *J* = 7.4 Hz, 1H), 7.48 (t, *J* = 7.7 Hz, 1H), 2.62 (s, 3H). R_f (9:1 Hexanes:EtOAc): 0.50 (orange in anisaldehyde stain).

Aniline: ^{1}H NMR: (400 MHz, $CDCl_3$) δ 7.16 (m, 2H), 6.67 (m, 3H)

Reduction of 3.145

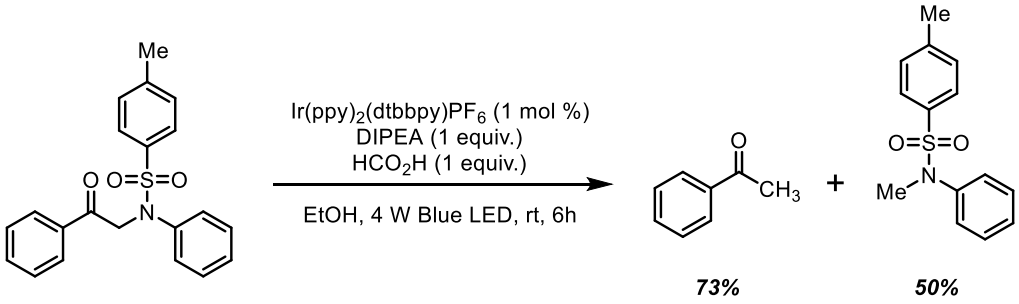

Following General Procedure A, this reaction was analyzed by ^{1}H NMR to yield 73% acetophenone. Column purification afforded a 50% yield of *N*-tosyl aniline. Spectra of products corresponded to those in the literature.[186]

Acetophenone ^{1}H NMR: (500 MHz, $CDCl_3$) δ 7.97 (d, *J* = 7.7 Hz, 1H), 7.58 (t, *J* = 7.4 Hz, 1H), 7.48 (t, *J* = 7.7 Hz, 1H), 2.62 (s, 3H). R_f (9:1 Hexanes:EtOAc): 0.50 (orange in anisaldehyde stain)

4-methyl-*N*-phenylbenzenesulfonamide ^{1}H NMR: (500 MHz, $cdcl_3$) δ 7.70-7.69 (m, 2H), 7.27-7.22 (m, 3H), 7.09-7.12 (m, 4H), 2.38 (s, 3H).

Reduction of 3.146

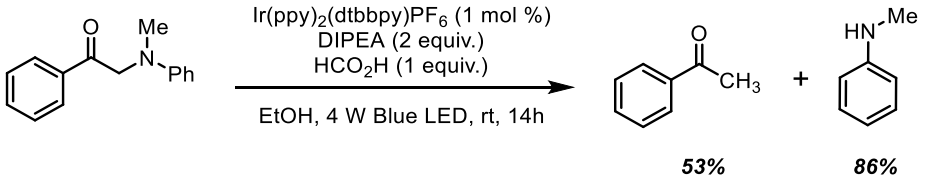

Following General Procedure A, this reaction was analyzed by ^{1}H NMR to yield 53% acetophenone and 86% *N*-methyl aniline.

Acetophenone ^{1}H NMR: (500 MHz, $CDCl_3$) δ 7.97 (d, *J* = 7.7 Hz, 1H), 7.58 (t, *J* = 7.4 Hz, 1H), 7.48 (t, *J* = 7.7 Hz, 1H), 2.62 (s, 3H). R_f (9:1 Hexanes:EtOAc): 0.50 (orange in anisaldehyde stain)

***N*-methylaniline** ^{1}H NMR: (500 MHz, $cdcl_3$) δ 7.21 (t, *J* = 7.4 Hz, 1H), 6.727(t, J = 7.5, 1H) 6.64 (d, *J* = 8.5, 2H), 2.85 (s, 3H).

Reduction and Pinacol Coupling of 3.147

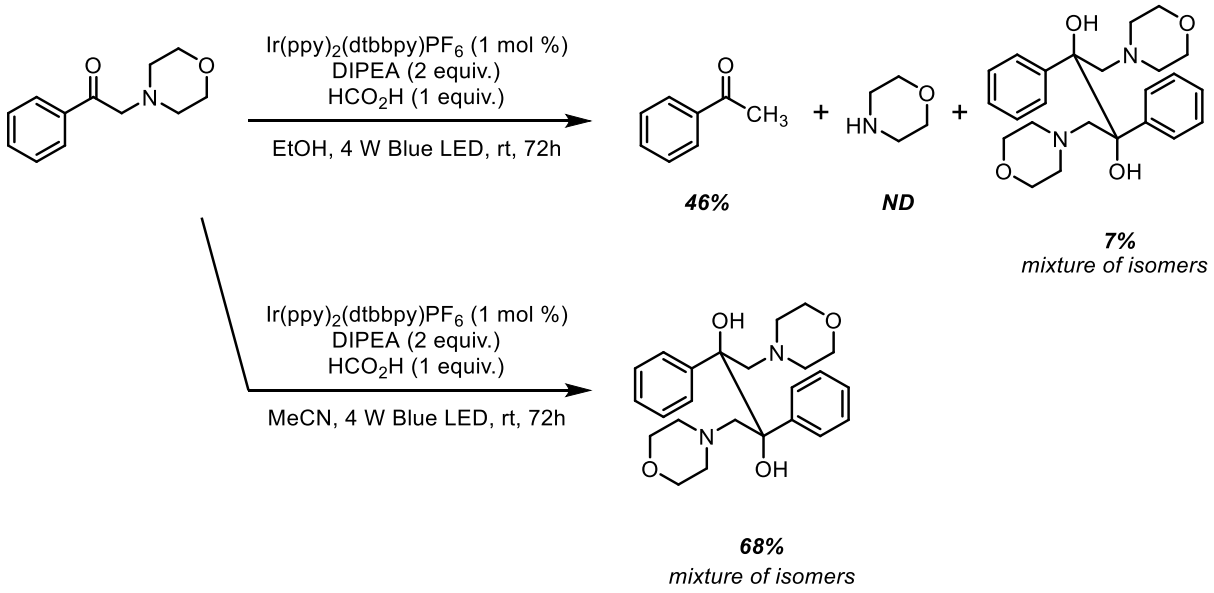

Following General Procedure A, this reaction was analyzed by ^{1}H NMR to yield 46% acetophenone. The morpholine is lost in the workup, however, the pinacol dimer is isolable in a filtration step prior to the organic work up. When dried this accounted for a 7% yield. Separately, if the reaction was run in MeCN, with the same additives, after 4 hours a white solid was isolated as a mixture of pinacol dimer isomers in 68% yield. From the solid, the meso isomer was recrystallized in ethanol and characterized.

3.164, meso isomer ^{1}H NMR (500 MHz, $CDCl_3$) δ 7.72 (d, J = 7.4 Hz, 2H), 7.30 (t, J = 7.7 Hz, 2H), 7.22 (t, J = 7.2 Hz, 1H), 4.98 (s, 1H), 3.37 (t, J = 4.5 Hz, 4H), 2.94 (d, J = 13.3 Hz, 1H), 2.63 (d, J = 13.3 Hz, 1H), 2.05 (m, 2H), 1.85 (m, 2H). ^{13}C NMR (126 MHz, $CDCl_3$) (meso) δ 145.53, 128.10, 127.17, 126.57, 75.91, 66.95, 64.26, 54.25.HRMS (*m/z*) = 413.2435 [$M+H^+$]

3.164, IR (neat) (mixture of isomers**)**: 2956.1, 2814.5, 1596.4, 1442.5, 1382.1, 1298.1, 1249.8, 1115.6, 1063.9, 1035.5, 1001.5, 958.0, 940.6, 920.5, 864.5, 800.1, 766.2, 702.5, 740.7, 572.2, 551.9, 544.1, 470.6, 464.2, 451.0

Pinacol Coupling of 3.165

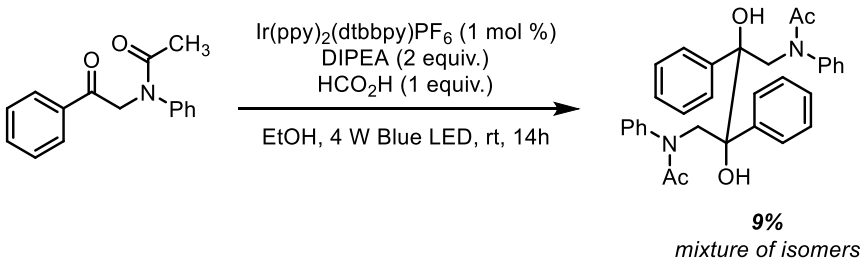

Following General Procedure A, this reaction yielded the following pinacol dimer which was isolated by filtration from the ethanol reaction solution in 27 mg (9% yield, mixture of isomers 2:1, racemic:meso).

3.166 ^{1}H NMR (700 MHz, $(CD_3)_2SO$) [meso:racemic (1:2)] δ 7.22 (t, *J* = 7.1 Hz, 2H), 7.19 (t, *J* = 7.0 Hz, 2H), 7.17 – 7.13 (m, 2H), 6.88 (t, *J* = 7.1 Hz, 1H), 6.60 (s, 1H), 6.43 (s, 2H), 4.95 (d, *J* = 14.5 Hz, 1H), 4.39 – 4.30 (m, 1H), 3.95 (d, *J* = 14.6 Hz, 2H), 3.82 (d, *J* = 14.6 Hz, 2H), 1.59 (s, 3H), 1.46 (s, 6H). ^{13}C NMR (126 MHz, $(CD_3)_2SO$) δ 185.51, 185.34, 174.61, 174.36, 174.31, 144.71, 142.07, 141.67, 129.26, 127.90, 127.75, 127.62, 127.37, 127.00, 126.55, 126.21, 87.38, 82.15, 81.14, 58.31, 58.10, 22.98, 22.75. HRMS (*m/z*) = 509.2435 [M+H$^+$] IR (neat): 3224.1 (broad OH), 3054.6, 1624.9, 1591.9, 1494.4, 1443.5, 1397.8, 1354.1, 1298.4, 1241.3, 1176.1, 1116.6,1068.4, 1019.7, 784.0, 741.2, 884.0, 843.8, 765.9, 746.8, 726.1, 695.8, 635.5, 623.9, 608.7, 558.9, 551.9, 526.6, 502.4, 491.2, 484.4, 477.9, 467.4, 449.3, 436.4, 421.3, 411.3

Reduction of 3.148

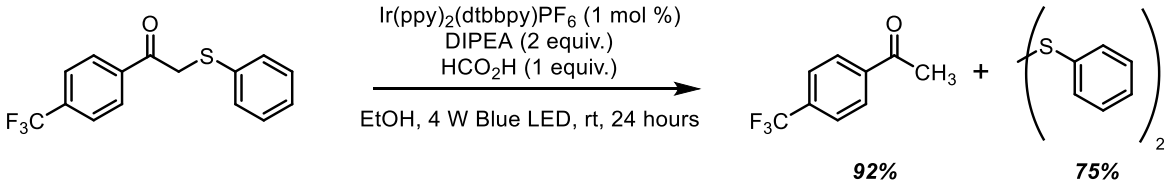

Following General Procedure A, this reaction was analyzed by ^{1}H NMR to yield 72% acetophenone. Products were isolated via SiO_2 chromatography (9:1 Hexanes:EtOAc) to afford dibenzyl disulfide (45.6 mg, 42% yield, white solid). Spectral data of fragmentation products agreed with previous reports.[187,188]

4-trifluoromethyl acetophenone: ^{1}H NMR: ^{1}H NMR (700 MHz, cdcl$_3$) δ 8.07 (d, *J* = 8.4 Hz, 1H), 7.75 (d, *J* = 8.4 Hz, 1H), 2.66 (s, 2H). R_f (9:1 Hexanes:EtOAc) = 0.23, stains brick red in vanillin

Diphenyl Disulfide: ^{1}H NMR (400 MHz, $CDCl_3$) δ 7.51 (d, *J* = 7.7 Hz, 4H), 7.32 (t, *J* = 7.5 Hz, 4H), 7.24 (t, *J* = 7.3 Hz, 2H). ^{13}C NMR (100 MHz, $CDCl_3$) δ 136.98 (s), 129.03 (s), 127.46 (s), 127.11(s). R_f (9:1 Hexanes:Ethyl Acetate) – 0.70

Reduction of 3.149

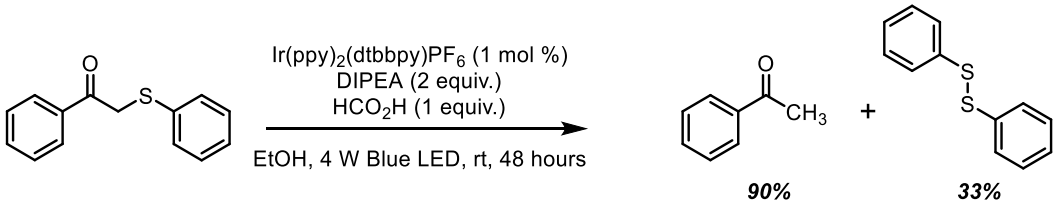

Following General Procedure A, this reaction was analyzed by ^{1}H NMR to yield 90% acetophenone. Diphenyl disulfide was isolated via SiO_2 chromatography to obtain a white solid (33.90 mg, 31%) (9:1 Hexanes:EtOAc). Spectral data of fragmentation products agreed with previous reports.[187,188]

Acetophenone ^{1}H NMR: (500 MHz, cdcl$_3$) δ 7.97 (d, *J* = 7.7 Hz, 1H), 7.58 (t, *J* = 7.4 Hz, 1H), 7.48 (t, *J* = 7.7 Hz, 1H), 2.62 (s, 3H). R_f (9:1 Hexanes:EtOAc): 0.50 (orange in anisaldehyde stain).

Diphenyl Disulfide ^{1}H NMR (400 MHz, $CDCl_3$) δ 7.51 (d, *J* = 7.7 Hz, 4H), 7.32 (t, *J* = 7.5 Hz, 4H), 7.24 (t, *J* = 7.3 Hz, 2H). ^{13}C NMR (100 MHz, $CDCl_3$) δ 136.98 (s), 129.03 (s), 127.46 (s), 127.11 (s). R_f (9:1 Hexanes:Ethyl Acetate) – 0.70

Reduction of 3.150

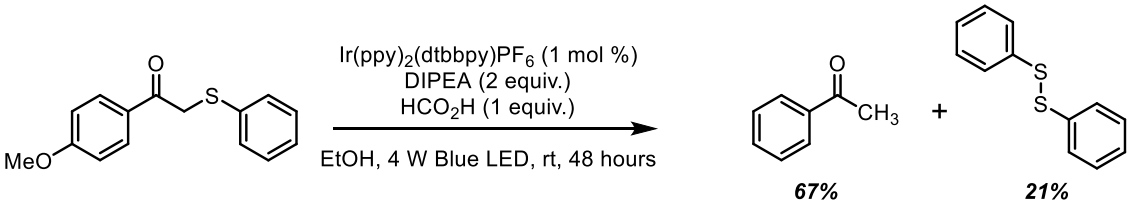

Following General Procedure A, products were isolated via SiO_2 chromatography (9:1 Hexanes:EtOAc) to yield 4-methoxyacetophenone (101.7 mg, 67% yield, white solid), and diphenyl disulfide (23.7 mg, 21% yield, white solid). Spectral data of fragmentation products agreed with previous reports. [187,188]

4-Methoxyacetophenone: ^{1}H NMR: δ 7.95 (d, J = 8.3 Hz, 1H), 6.95 (d, J = 8.4 Hz, 1H), 3.88 (d, J = 0.5 Hz, 2H), 2.57 (d, J = 0.7 Hz, 2H). R_f (7:3 Hexanes:EtOAc): 0.40

Diphenyl Disulfide: ^{1}H NMR (400 MHz, $CDCl_3$) δ 7.51 (d, *J* = 7.7 Hz, 4H), 7.32 (t, *J* = 7.5 Hz, 4H), 7.24 (t, *J* = 7.3 Hz, 2H). ^{13}C NMR (100 MHz, $CDCl_3$) δ 136.98 (s), 129.03 (s), 127.46 (s), 127.11 (s). R_f (9:1 Hexanes:Ethyl Acetate) – 0.70

Reduction of 3.151

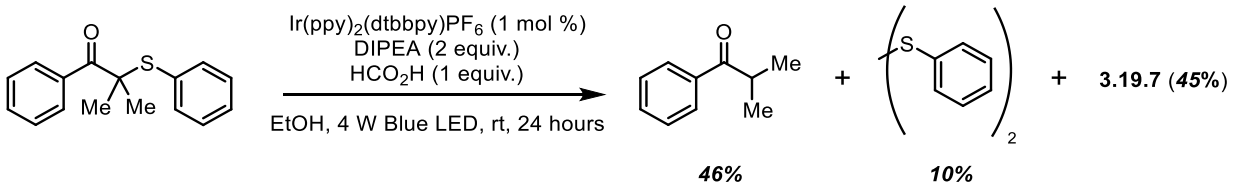

Following General Procedure A, products were isolated via SiO_2 chromatography (9:1 Hexanes:EtOAc) to afford 2-methyl-1-phenyl-propan-1-one (67.9 mg, 46%), diphenyl disulfide (22.1 mg, 10% yield, white solid). Because the reaction was not run to completion, 114.3 mg of starting material was recovered (45%). Spectral data of fragmentation products agreed with previous reports.[188,189]

2-methyl-1-phenylpropan-1-one: ^{1}H NMR (400 MHz, $CDCl_3$) δ 7.97 (d, *J* = 7.2 Hz, 1H), 7.57 (t, *J* = 7.3 Hz, 1H), 7.48 (t, *J* = 7.5 Hz, 1H), 3.70 – 3.42 (m, 1H), 1.24 (s, 3H), 1.24 (s, 2H), 1.22 (s, 2H). R_f (9:1 Hexanes:Ethyl Acetate): 0.48

Diphenyl Disulfide: ^{1}H NMR (400 MHz, $CDCl_3$) δ 7.51 (d, *J* = 7.7 Hz, 4H), 7.32 (t, *J* = 7.5 Hz, 4H), 7.24 (t, *J* = 7.3 Hz, 2H). ^{13}C NMR (100 MHz, $CDCl_3$) δ 136.98 (s), 129.03 (s), 127.46 (s), 127.11 (s). R_f (9:1 Hexanes:Ethyl Acetate) – 0.70

Reduction of 3.152

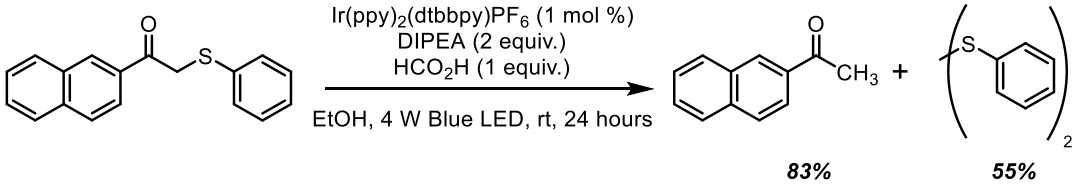

Following General Procedure A, products were isolated via SiO_2 chromatography (9:1 Hexanes:EtOAc) to afford dibenzyl disulfide (60.7 mg, 55% yield, white solid), and 2-napthylacteophenone (140 mg, 83% yield). Spectral data of fragmentation products agreed with previous reports. [187,188]

2-Napthylacetophenone: ^{1}H NMR: (400 MHz, $CDCl_3$) δ 8.49 (s, 1H), 8.05 (dd, J = 8.6, 1.7 Hz, 1H), 7.99 (d, J = 8.0 Hz, 1H), 7.95 – 7.86 (m, 2H), 7.65 – 7.60 (m, 1H), 7.60 – 7.54 (m, 1H), 2.75 (s, 3H). R_f (9:1 Hexanes:EtOAc) = 0.35, stains red in anisaldehdye

Diphenyl Disulfide: ^{1}H NMR (400 MHz, $CDCl_3$) δ 7.51 (d, *J* = 7.7 Hz, 4H), 7.32 (t, *J* = 7.5 Hz, 4H), 7.24 (t, *J* = 7.3 Hz, 2H). ^{13}C NMR (100 MHz, $CDCl_3$) δ 136.98 (s), 129.03 (s), 127.46 (s), 127.11 (s). R_f (9:1 Hexanes:Ethyl Acetate) – 0.70

Reduction of 3.153

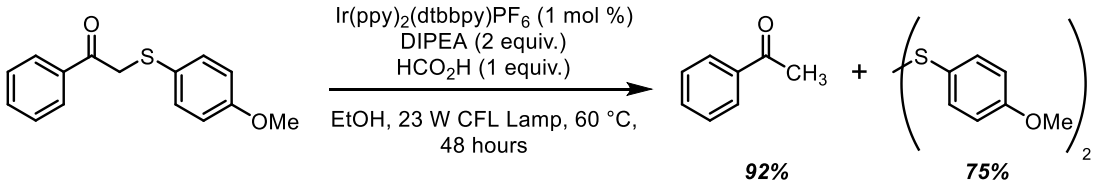

Following General Procedure A, the reaction temperature was modified to 60 °C. The reaction was set up in a round bottom that was heated by a translucent oil bath in which a 23 W CFL light irradiated the reaction. This reaction was analyzed by ^{1}H NMR to yield 92% acetophenone. Products were isolated via SiO_2 chromatography (9:1 Hexanes:EtOAc) to yield acetophenone (101.7 mg, 67% yield, white solid), and (4-OMe)diphenyl disulfide (7.5 mg, 5% yield, white solid). Spectral data of fragmentation products agreed with previous reports.[187,188]

Acetophenone ^{1}H NMR**:** (500 MHz, cdcl$_3$) δ 7.97 (d, *J* = 7.7 Hz, 1H), 7.58 (t, *J* = 7.4 Hz, 1H), 7.48 (t, *J* = 7.7 Hz, 1H), 2.62 (s, 3H). R_f (9:1 Hexanes:EtOAc): 0.50 (orange in anisaldehyde stain)

(4-methoxy)diphenyl disulfide: ^{1}H NMR (700 MHz, $CDCl_3$) δ 7.48 – 7.38 (m, 4H), 6.87 – 6.81 (m, 4H), 3.81 (s, 4H). R_f (9:1 Hexanes:EtOAc): 0.68

Reduction of 3.154

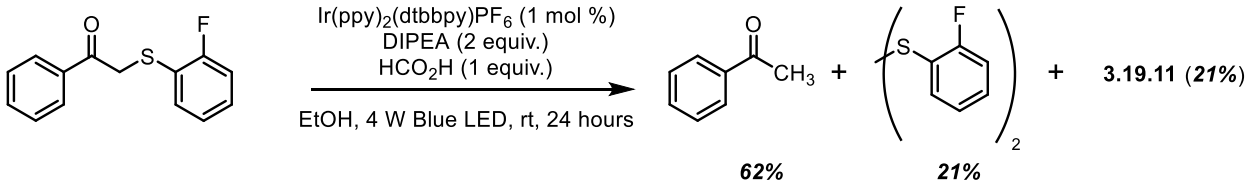

Following General Procedure A, this reaction was analyzed by ^{1}H NMR to yield 62% acetophenone. Products were isolated via SiO_2 chromatography (9:1 Hexanes:EtOAc) to afford (2-fluoro)dibenzyl disulfide (18.8 mg, 15% yield, white solid). Because the reaction was not run to completion, 52 mg of starting material was recovered (21%). This reaction goes to full completion when run in MeCN at 60 °C (97% Acetophenone, 21% (2-fluoro)diphenyl disulfide) Spectral data of fragmentation products agreed with previous reports.[180,182]

Acetophenone ^{1}H NMR: (500 MHz, cdcl$_3$) δ 7.97 (d, *J* = 7.7 Hz, 1H), 7.58 (t, *J* = 7.4 Hz, 1H), 7.48 (t, *J* = 7.7 Hz, 1H), 2.62 (s, 3H). R_f (9:1 Hexanes:EtOAc): 0.50 (orange in anisaldehyde stain)

(2-Fluoro)Diphenyl Disulfide: ^{1}H NMR: (500 MHz, $CDCl_3$) δ 7.60 (td, *J* = 7.7, 1.6 Hz, 1H), 7.30 – 7.25 (m, 2H), 7.13 (td, *J* = 7.6, 1.1 Hz, 1H), 7.10 – 7.04 (m, 1H). ^{13}C NMR (176 MHz, $CDCl_3$) δ 161.41, 160.00, 131.39, 129.92, 129.88, 124.91, 124.89, 123.79, 123.69, 116.01, 115.89. R_f (9:1 Hexanes:EtOAc) = 0.53

Reduction of 3.155

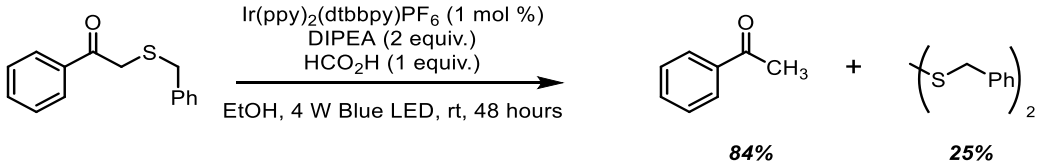

Following General Procedure A, this reaction was analyzed by ^{1}H NMR to yield 84% acetophenone. Products were isolated via SiO_2 chromatography (9:1 Hexanes:EtOAc) to afford dibenzyl disulfide (62 mg, 25% yield, white solid). Spectral data of fragmentation products agreed with previous reports.[187,188]

Acetophenone: ^{1}H NMR: (500 MHz, cdcl$_3$) δ 7.97 (d, *J* = 7.7 Hz, 1H), 7.58 (t, *J* = 7.4 Hz, 1H), 7.48 (t, *J* = 7.7 Hz, 1H), 2.62 (s, 3H). R_f (9:1 Hexanes:Ethyl Acetate) = 0.42 (stains yellow in anisaldheyde).

Dibenzyl Disulfide ^{1}H NMR: (500 MHz, $CDCl_3$) δ 7.33 (t, *J* = 7.2 Hz, 2H), 7.29 (d, *J* = 7.1 Hz, 1H), 7.26 – 7.22 (m, 2H), 3.61 (s, 2H). R_f (9:1 Hexanes:Ethyl Acetate) – 0.65

Reduction of 3.156

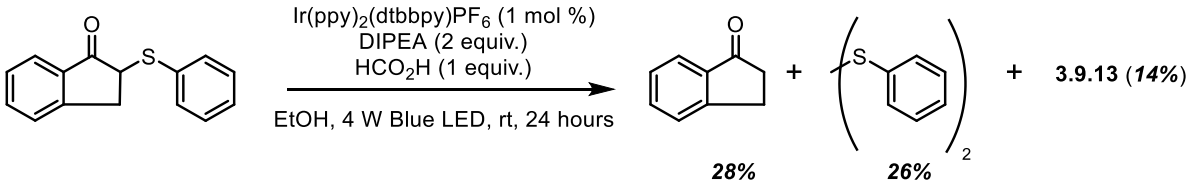

Following General Procedure A, products were isolated via SiO_2 chromatography (9:1 Hexanes:EtOAc) to afford diphenyl disulfide (22.1 mg, 10% yield, white solid). 2-methyl-1-phenyl-propan-1-one (13.67 mg, 14%), and 37.13 mg (28.1%) of 1-Indanone were isolated as an inseparable mixture (1:1.3). Spectral data of fragmentation products agreed with previous reports.[180]

Indanone: ^{1}H NMR (700 MHz, $CDCl_3$) δ 7.78 (d, *J* = 7.6 Hz, 1H), 7.60 (t, *J* = 7.4 Hz, 1H), 7.50 (dd, J = 8.1, 7.3 Hz, 2H), 7.39 (dd, J = 14.6, 7.2 Hz, 2H), 3.19 – 3.15 (m, 2H), 2.74 – 2.68 (m, 2H). R_f (9:1 Hexanes:EtOAc)= 0.46 (co-elute with starting material)

Diphenyl Disulfide ^{1}H NMR (400 MHz, $CDCl_3$) δ 7.51 (d, *J* = 7.7 Hz, 4H), 7.32 (t, *J* = 7.5 Hz, 4H), 7.24 (t, *J* = 7.3 Hz, 2H). ^{13}C NMR (100 MHz, $CDCl_3$) δ 136.98 (s), 129.03 (s), 127.46 (s), 127.11 (s) R_f (9:1 Hexanes:Ethyl Acetate) – 0.70

Reduction of 3.157

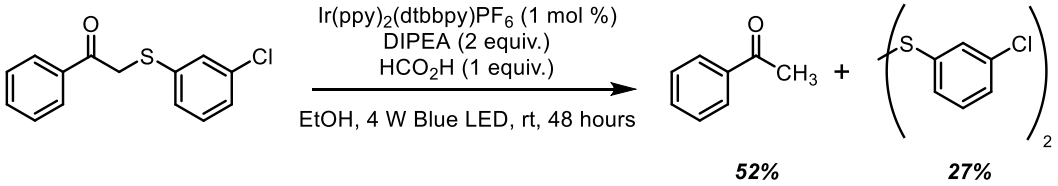

Following General Procedure A, products were isolated via SiO_2 chromatography (9:1 Hexanes:EtOAc) to afford dibenzyl disulfide (60.7 mg, 55% yield, white solid), and 2-napthylacteophenone (140 mg, 83% yield). Spectral data of fragmentation products agreed with previous reports. [187,188]

2-Napthylacetophenone ^{1}H NMR: (400 MHz, $CDCl_3$) δ 8.49 (s, 1H), 8.05 (dd, J = 8.6, 1.7 Hz, 1H), 7.99 (d, J = 8.0 Hz, 1H), 7.95 – 7.86 (m, 2H), 7.65 – 7.60 (m, 1H), 7.60 – 7.54 (m, 1H), 2.75 (s, 3H). R_f (9:1 Hexanes:EtOAc) = 0.35, stains red in anisaldehdye

Diphenyl Disulfide ^{1}H NMR (400 MHz, $CDCl_3$) δ 7.51 (d, *J* = 7.7 Hz, 4H), 7.32 (t, *J* = 7.5 Hz, 4H), 7.24 (t, *J* = 7.3 Hz, 2H). ^{13}C NMR (100 MHz, $CDCl_3$) δ 136.98 (s), 129.03 (s), 127.46 (s), 127.11 (s). R_f (9:1 Hexanes:Ethyl Acetate) – 0.70

Reduction of 3.158

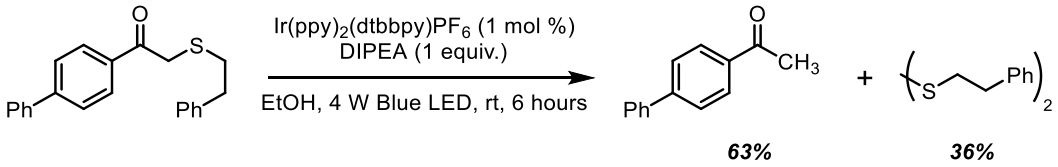

3.158 (332.46 mg, 1.0 mmol) was added to a 4 dram vial with DIPEA (1 equiv.), and photocatalyst [$Ir(ppy)_2(dtbbpy)PF_6$] (1 mol %). These reactants were diluted in EtOH (5 mL, 0.20 M in starting material), and irradiated by 1x4W Blue LED strip until reaction completion (6 hours). At this point the ethanol was removed *in vacuo*, and the resulting oil was diluted in water and extracted with ethyl acetate. The organic portion was washed with 4 N $HCl_{(aq)}$ and dried with Na_2SO_4, after which it was concentrated to an oil. The crude reaction was purified by SiO_2 chromatography to afford the fragmentation products, which agreed with previously reported characterization.[190]

4-phenylacetophenone ^{1}H NMR: (400 MHz, $CDCl_3$) δ 8.05 (d, J = 8.5 Hz, 1H), 7.70 (d, J = 8.5 Hz, 1H), 7.67 – 7.62 (m, 1H), 7.49 (t, J = 7.4 Hz, 1H), 7.42 (t, J = 7.3 Hz, 1H), 2.66 (s, 2H). R_f (9:1 Hexanes:EtOAc): 0.50 (orange in anisaldehyde stain)

Phenylethyl disulfide: ^{1}H NMR (700 MHz, $CDCl_3$) δ 7.30 (t, J = 7.6 Hz, 4H), 7.21 (m, 6H), 3.01 – 2.96 (m, 4H), 2.94 (dt, J = 7.3, 2.6 Hz, 4H). ^{13}C NMR (176 MHz, $CDCl_3$) δ 140.16, 128.76, 128.66, 126.55, 40.34, 35.87. HRMS (*m/z*) = 274.0847 R_f (9:1 Hexanes:EtOAc): 0.72 (light yellow in anisaldehdye stain).

Chapter 4: Arylsulfonyl Acetamides as Bifunctional Reagents for Alkene Aminoarylation

4.1 Introduction: Alkene Aminoarylation Methodologies

4.1.1 Significance

Alkenes are fundamental functionalities in synthetic organic chemistry. The prevalence of alkenes in the synthesis of polymers and natural products is a testament to the versatility of synthetic operations used to elaborate this simple motif. Alkenes participate in all of the mechanistically distinct classes of reactions like nucleophilic substitution, pericyclic reactions, and radical reactions. Despite the breadth of history contained within alkene functionalization, contemporary catalytic reaction designs continue to evaluate alkenes for demonstrating solutions to enantioselective, diastereoselective, and regioselective reactions with the promise of discovering more efficient or versatile methods for chemical synthesis.[191,192,193]

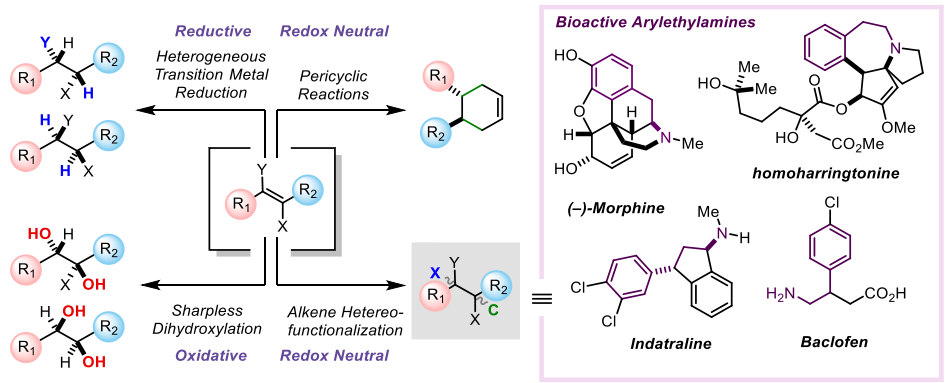

Figure 55: Alkene Difunctionalization and Bioactive Arylethylamines

The diversity of catalytic alkene functionalization reactions can be divided by the identities of the new bonds created during a reaction. As such, reductive (H,H), redox neutral (C,C) or oxidative functionalizations (X, X or C, X where X = O, N, S) are possible with the selection of appropriate

reagent and catalyst combinations. Traditional heterogeneous transition metal catalyzed reductions and oxidation of alkenes simply provide stereodefined alkanes and diols. Alkene functionalization reactions involving the generation of a C–C bond as well as a C–X bond constitute a unique field for chemical discovery. In these three component couplings, catalysts must chemically distinguish the alkene from both of the heteroatomic or carbonic reagents, as well as the regiochemistry of the alkene (Figure 55).

Aminoarylation, a subset of alkene carboamination reactivity, is an advantageous transformation that provides direct access to the highly biologically active phenethylamine pharmacaphore and nitrogen heterocycles.[194] A wide variety of solutions to aminoarylation have been developed utilizing late transition metals such as palladium, copper, nickel, and rhodium, as well as Meerwein arylation chemistry and visible light redox catalysis. The reported chemistries can be evaluated by several design factors such as catalytic metal identity, ligand structure and availability, chemoselectivity as measured by reaction temperature, the presence or absence of terminal oxidants and reductants, and mechanistic understanding for rational stereochemical design and utilization of reactivity.

4.1.2 Transition metal Catalyzed Aminoarylation

Prior to 2004, palladium complexes involving the coordination of an amine nucleophile and aryl electrophile were relegated to arene amination reactivity.[195,196,197] Ney and Wolfe expanded this focus of reactivity by intercepting arylpallado-amides with alkenes to provide a general and catalytic methodology for alkene aminoarylation (Figure 56).[198] Remarkably, aminoarylation of *N*-phenyl-4-pentenylamine (**4.1**) with [$Pd_2(dba)_3$] (1 mol %) and a bidentate phosphine ligand (1,4-bis(diphenylphosphino)butane, dppb) provided the desired product (**4.3**) in a 94% yield, with a minimal amount of regioisomer **4.4**. This process was general for a variety of bromoarene

electrophiles, showcasing a combinatorial synthesis of 2-arylpyrrolidines. Substrate **4.5**, containing an internal olefin, was indicative of the complexity of mechanistic operations occurring in solution. Reacting **4.5** with [$Pd_2(dba)_3$] (1 mol %), monodentate P(*o*-tolyl)$_3$, and bromonaphthalene, a mixture of *N*-arylation, regioisomeric aminoarylations, and Heck amination was observed (Figure 56B). The authors utilized this substrate to draw early conclusions about the reaction mechanism; a *syn*-aminopalladation of Pd-amide complex **4.10** generates Pd-C intermediate **4.11**, which can either reductively eliminate or β-hydride eliminate and isomerize to provide both **4.9** and **4.8**, respectively.[199] Overall, this reaction was a crucial demonstration of palladium catalyzed and diastereoselective aminoarylation reactivity, proving palladium amide intermediates are capable of more than arene amination.

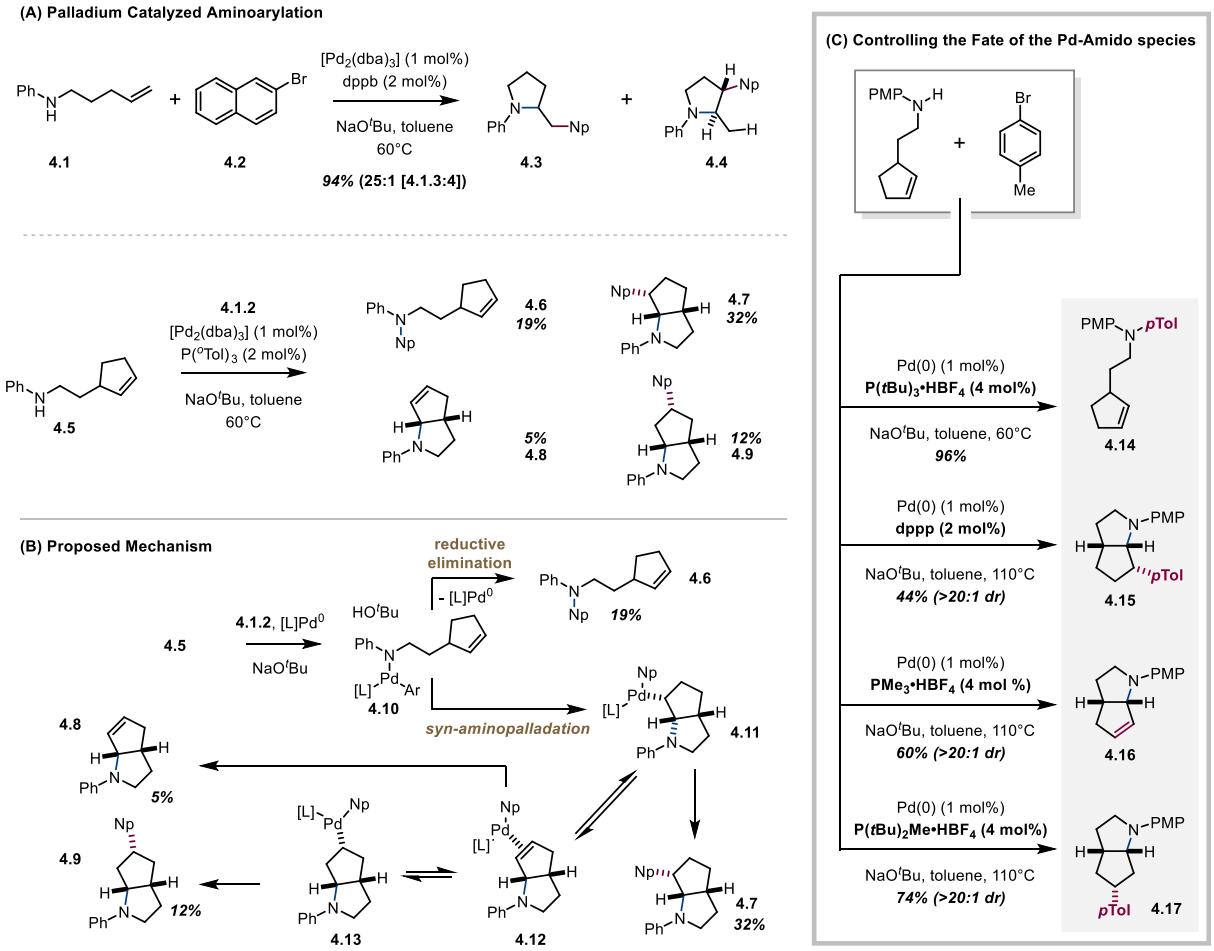

Figure 56: Palladium(0) Catalyzed Intramolecular Aminoarylation

With the proof-of-concept established for a palladium catalyzed aminoarylation reaction, Wolfe and co-workers investigated reaction conditions enabling the use of more general nitrogenous substrates. In one instance, the authors found both amine arylation and alkene aminoarylation were feasible in a single step in high yield.[200,201] Another valuable modification to the original protocol was changing the base from *tert*-butoxide anion to carbonate anion in order for amides and carbamates to participate in the reaction.[202] The elevated reaction temperatures employed caused decomposition of carbamate substrates to isocyanates in the presence of strong base. Moreover, further exploration of ligand stereoelectronic influence on the palladium center modulated relative rates of *N*-arylation, aminoarylation, and Heck-amination to yield specific protocols to access each

reaction pathway (Figure 56C). Fortunately, these different reaction pathways are discernable within the structural variance of the phosphine ligand class.[203,204] Research efforts have culminated in an enantioselective aminoarylation reaction in which monodentate phosphoramidite ligand (*R*)-Siphos-PE induces an enantiomeric selectivity upwards of 92%. To demonstrate the utility of this enantioselective method, (–)-tylophorine (**4.20**) was synthesized in 88% ee (Figure 57).[205]

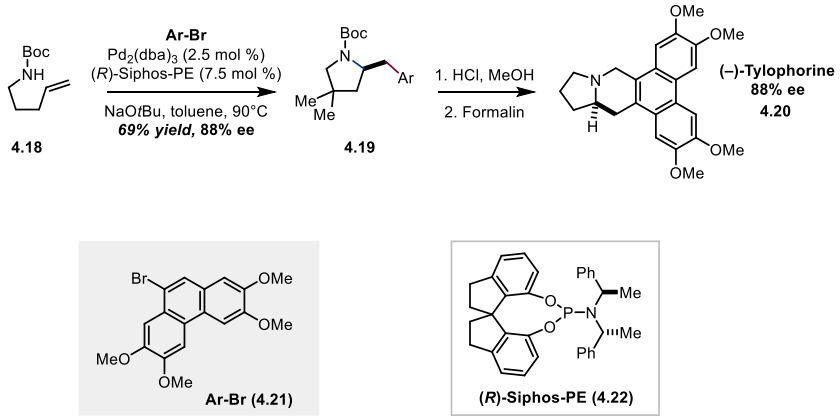

Figure 57: Synthesis of (–)-Tylophorine using Pd(0) catalyzed alkene aminarylation as stereo-defining step

While *syn*-aminopalladation was the initial mechanistic step observed in the early aminoarylation chemistry developed by Wolfe and co-workers, further exploration revealed reaction conditions that promote an *anti*-aminopalladation across alkenes (Figure 58A).[206] Studying the aminoarylation reaction for the synthesis of cyclic ureas (**4.23**, **4.25**), oxidative addition with aryl triflates, in combination with solvents and ligands that implicate a more electron deficient palladium center, the *anti*-aminopalladation product was observed (Figure 58A). Importantly, the stereoselectivity could be reversed based on the choice of an electron-rich or an electron-poor metal center. Oxidative addition to aryl bromides along with **4.30** in toluene as the solvent proved effective for *syn*-aminopalladation (Figure 58B). Wolfe, White, and Hutt later developed an *anti*-aminopalladation reaction for the synthesis of enantiopure aminoindanes (Figure 58D).[207] Interestingly, substrate design in this reaction decoupled the amine and alkene

reactants, to afford an electron poor metal center coordinated to the alkene after oxidative addition. Intermolecular nucleophilic attack of amine (**4.34**) on a cationic palladium(II)(aryl)(olefin) that leads to an alkyl-Pd(Ar) complex which regenerates the palladium catalyst through reductive elimination. PHOX ligands **4.38** were found to control the enantioselectivity of this process to an impressive 99:1 ee presumably via the steric interaction between the *tert*-butyl group and the alkene. Other works relying on aryl triflates for aminoarylation have similarly produced *anti*-aminopalladation aminoarylation products. *Anti*-aminopalladation can also occur from intramolecular amine addition to a Pd(II)-alkene complex lacking a Pd-aryl substituent. In this sense, Michael and co-workers found a catalytic methodology beginning with this *anti*-aminopalladation step, followed by an oxidation of Pd(II) to Pd(IV) by NFBS that terminated with an arene C–H activation and reductive elimination (Figure 58E).[208]

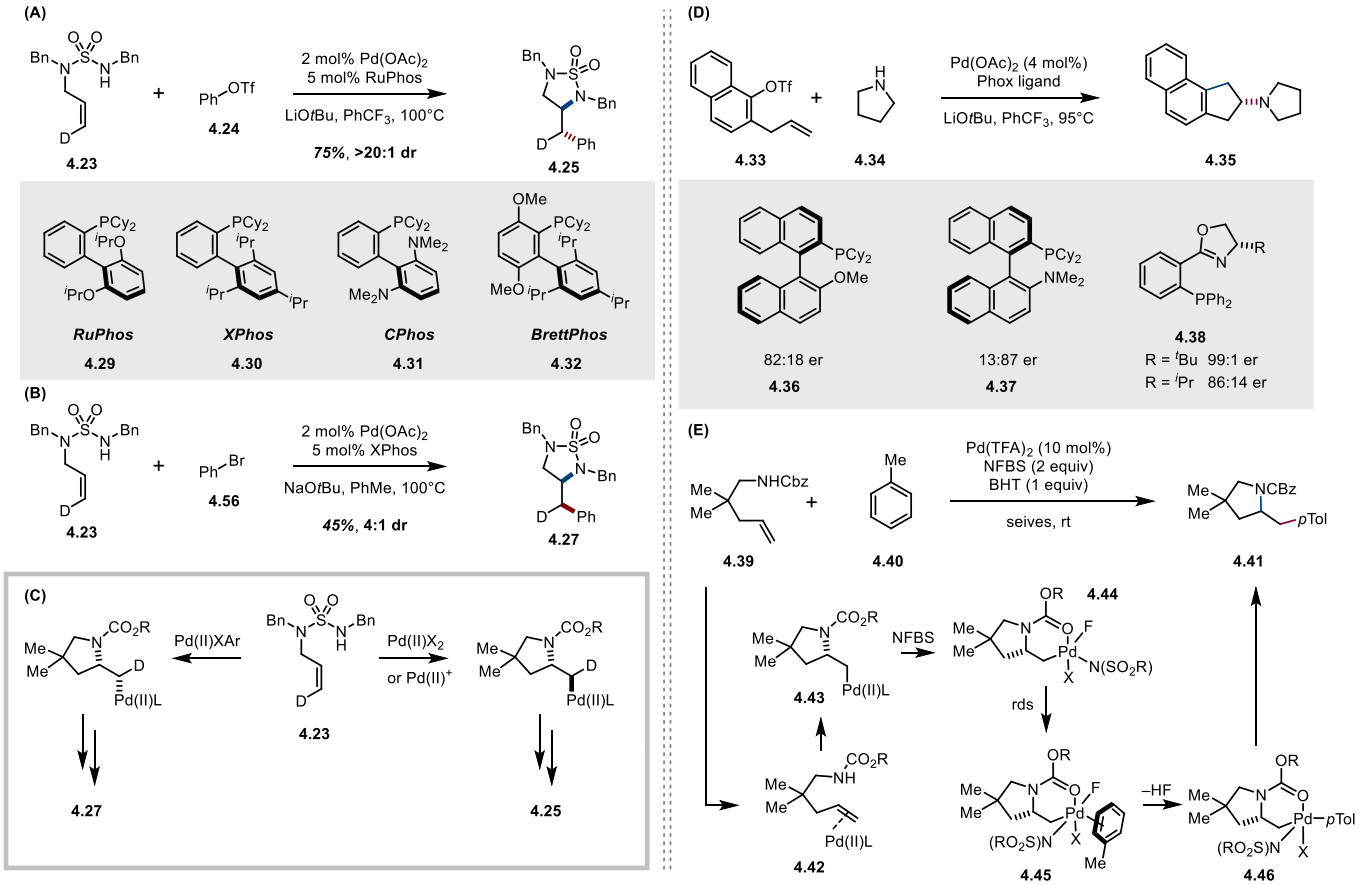

Figure 58: Antiaminopalladation Reactivity with Pd(0-II) and Pd(II-IV) catalysis

Directed aminoarylation of alkenes using Pd and Ni has been reported by Engle and co-workers, wherein an 8-amidoquinoline directing group enables intermolecular incorporation of *N*-nucleophiles and aryl electrophiles.[209] The 8-amidoquinoline, originally disclosed by Dauglis,[210] as the superior directing group for Pd(IV) arene C–H activation, enables both Pd and Ni to mediate alkene difunctionalization in Engle's reaction design. Engle's reaction conditions harness Pd(II-IV) catalysis and are characterized by high reaction temperatures (100 °C) and a low diastereoselectivity compared to Pd(0)-phosphine catalysis. A wide variety of amide nucleophiles and aryl electrophiles are compatable in these conditions and enable direct access to aminoarylation products reminiscent of molecules like Baclofen (Figure 55). Data supporting a mechanistic hypothesis of a rate determining reductive elimination explains the relative rate

difference in reactivity between different aryl electrophiles (**4.51-4.60**) as well as a lack of diastereoselective control. Alkene difunctionalization reactivity has additionally been explored for bis-carbofunctionalization and hetero-hydrofunctionalization using Pd(II) and Ni(0) catalysis.[211,212,213,214]

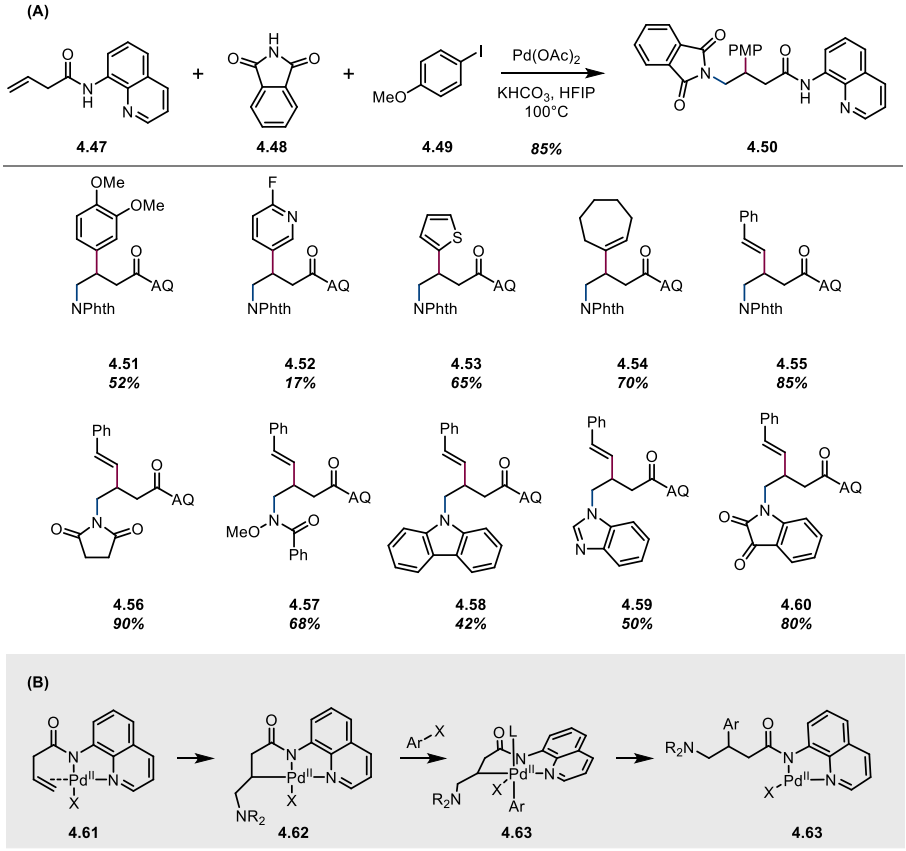

Figure 59: Amidoquinoline directed alkene aminoarylation (A) Reaction Conditions and Representative Scope (B) Mechanism Hypothesis

Aminoarylation for the synthesis of indolines was realized by Jamison and Tasker, keenly employing photoredox-nickel dual catalysis to surmount the challenge of Ni(II)-amido reductive elimination.[215] Recent developments in cross-coupling catalysis have ameliorated the thermodynamic barriers for oxidative addition and reductive elimination by using radicals

generated using photoredox catalysis.[216] Radicals force transition metal intermediates, particularly Ni, to operate in odd electron manifolds such as Ni(I) and Ni(III), in contrast to the canonical cycles of Ni(0-II) that are often postulated in accordance with Pd(0-II) catalysis. Using this rationale, Jamison and Tasker hypothesized that Ru^{2+} photocatalysis could enable a Ni(II)-amido oxidation to a Ni(III)-amido species that would drive reductive elimination and create an indoline from *o*-haloanilides and terminal alkenes. The success of this process surmounts issues raised by Larock in the synthesis of indoles, including reductive elimination and undesired β–hydride elimination often encountered in Pd catalysis.[217] This process impressively functionalizes electronically unactivated terminal alkenes in an intermolecular fashion, yet lacks the stereocontrol of Pd-phosphine catalyzed processes.

While radical reactivity can enhance Ni catalysis for aminoarylation, copper catalyzed processes likely require the formation of radical intermediates. Oxidative carboamination studied

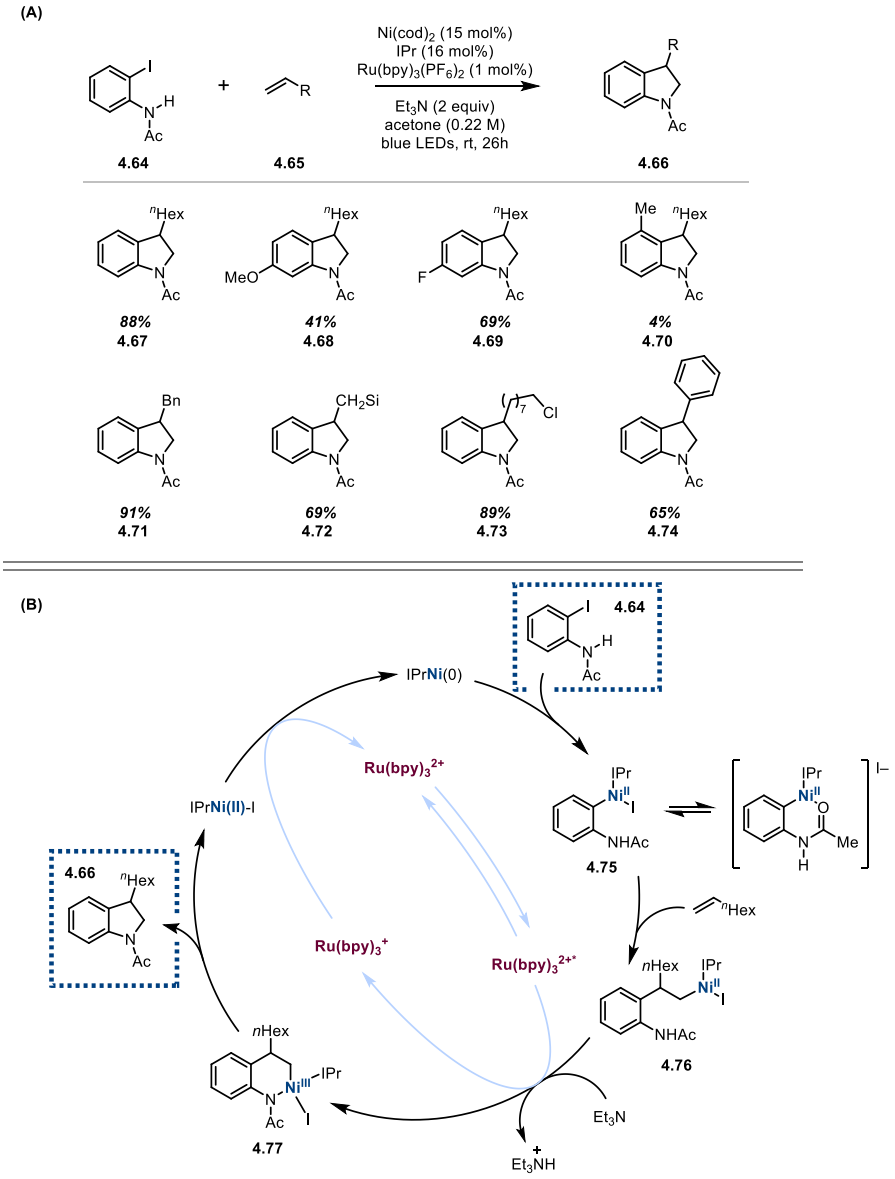

Figure 60: Ni(0)-Ru(II) dual catalysis for indoline synthesis

by Chemler and co-workers has championed the use of this inexpensive metal along with oxygen or manganese dioxide as a terminal reductant to difunctionalized alkenes in an intramolecular design similar to Wolfe (Figure 61).[218,219] Radical trapping experiments reveal that after *syn*-aminocupration, TEMPO adducts form with the Cu-alkyl bond (Figure 61B).[220] While this reaction design is most useful for oxidative difunctionalization of alkenes (Figure 61D), intramolecular oxidative cyclization into the benzenesulfonamide functionality is an efficient process (Figure

61C). Furthermore, copper catalysis is amenable to enantioselective transformation with the use of stereodefined bis-oxazoline ligands.

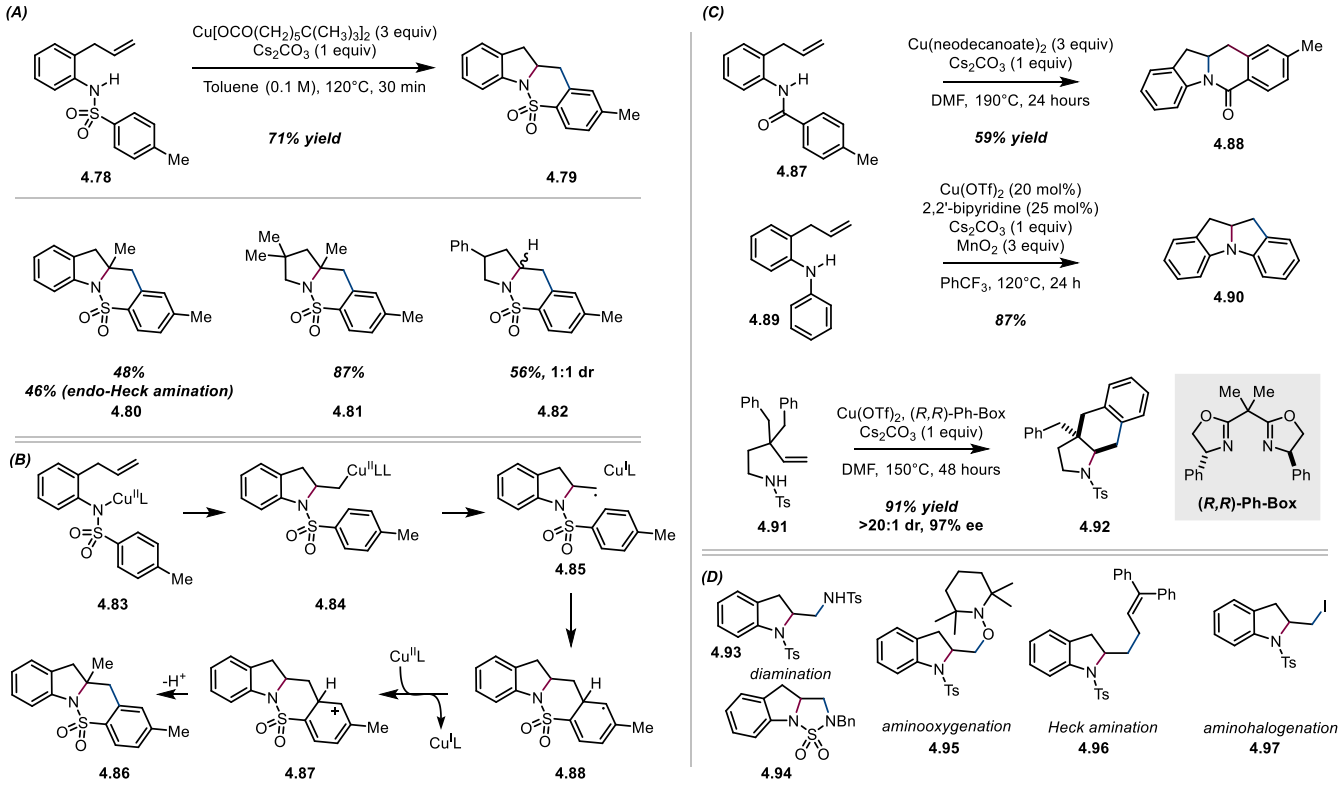

Figure 61: Copper Catalyzed Aminoarylation

A separate demonstration of an enantioselective copper catalyzed aminoarylation was developed by Liu and co-workers (Figure 62A).[221] The key redox design in this reaction was the use of *N*-fluoro-*N*-alkylsulfonamides as both the copper oxidant and nitrogen nucleophile, followed by arylation with a boronic acid derivative (Figure 62B). Notably, this reaction performs aminoarylation with only one excess equivalent of amine nucleophile and aryl electrophile to the targeted styrene derivative. Substrate scope demonstration of only aryl alkenes suggests the allylic functionality is not compatible with the developed conditions. A mechanistic experiment showcased the proclivity of the amidocuprate intermediate to react intramolecularly faster with a

terminal aliphatic olefin than with an exogenous aryl alkene, albeit in low yield forming a variety of products (Figure 62).

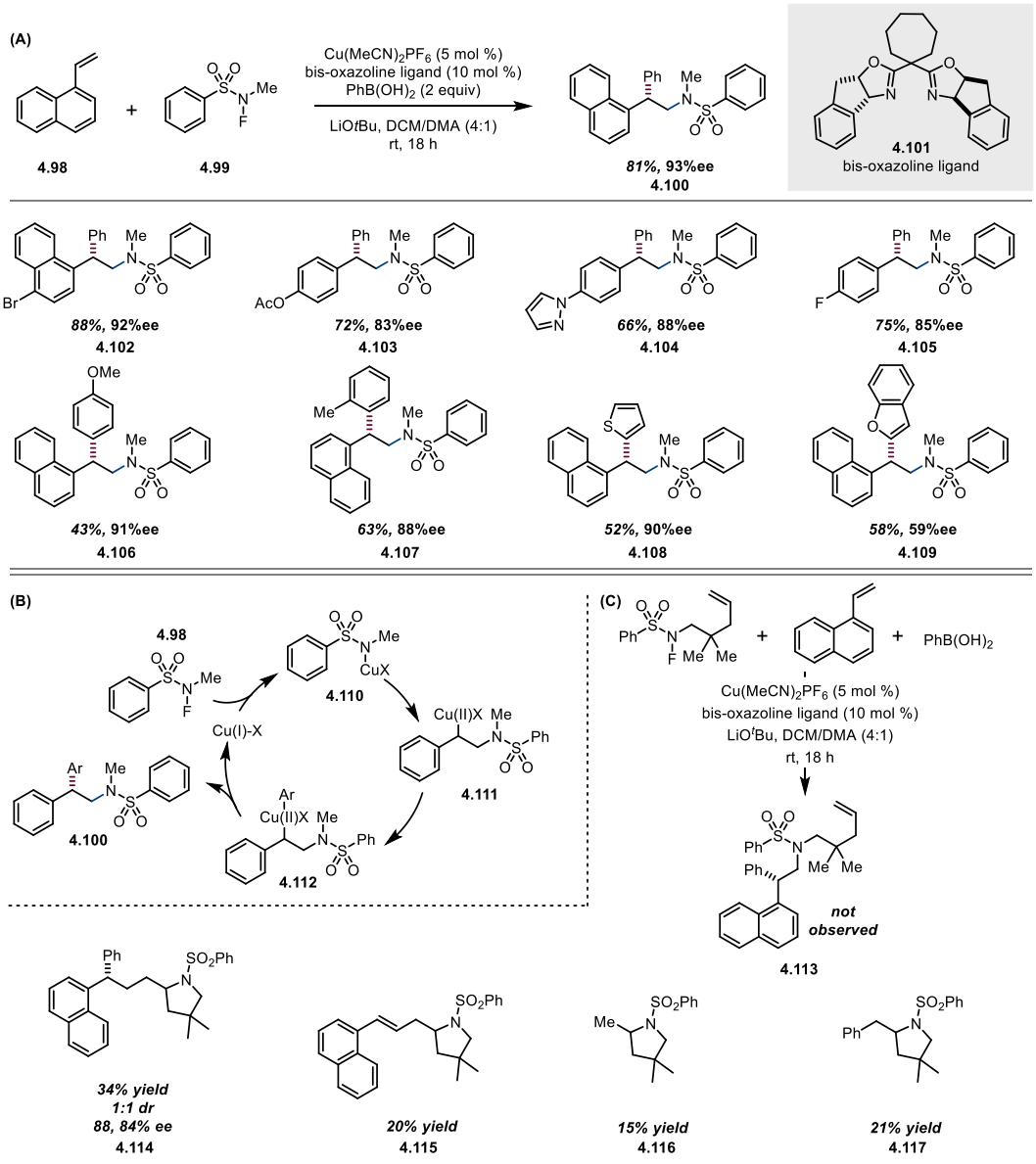

Figure 62: Enantioselective Copper Catalyzed Aminoarylation Reaction

Toste and co-worker found a method for aminoarylation that mitigates the heating requirements of Pd, Ni, and Cu catalyzed reaction using gold catalysis and a fluorine oxidant (Figure 63). [222] Gold is mechanistically distinct from Pd and Ni, as it preferentially coordinates π-systems to enable nucleophilic attack rather than heteroatom coordination followed by alkene insertion.

Hydroamination reactivity in this sense precedes aminoarylation chemistry for a number of activated and unactivated alkene substrates.[223,224] Yet, aminoarylation using amido-alkenes (**4.118**) and boronic acids (**4.119**) presented a perplexing dichotomy of mechanistic scenarios which rationalize aminoarylation.[225] Some were quick to postulate gold mediated aminoarylation is directly analogous to Pd and Ni, [226] while Toste favored a bimolecular reductive elimination (Figure 63B). Following the preliminary publication of this aminoarylation,[222] Toste and co-workers intensely studied the mechanism of reactivity to find that a bimetallic gold complex is responsible for the key arylation step of the designed reaction (**4.122**). Overall, the aminoauration process proceeds *anti*, similarly to electrophilic $Pd(II)^{+}OTf^{-}$ complexes, and Selectfluor oxidizes gold to promote the arylation step. Interestingly, a follow up study found that intramolecular aminoarylation is significantly outcompeted by intermolecular oxyarylation (Figure 63C).[227] This chemistry demonstrates the importance of mechanistic investigation and showcases the principle of multiple reaction designs within a similar substrate class for a given transformation.

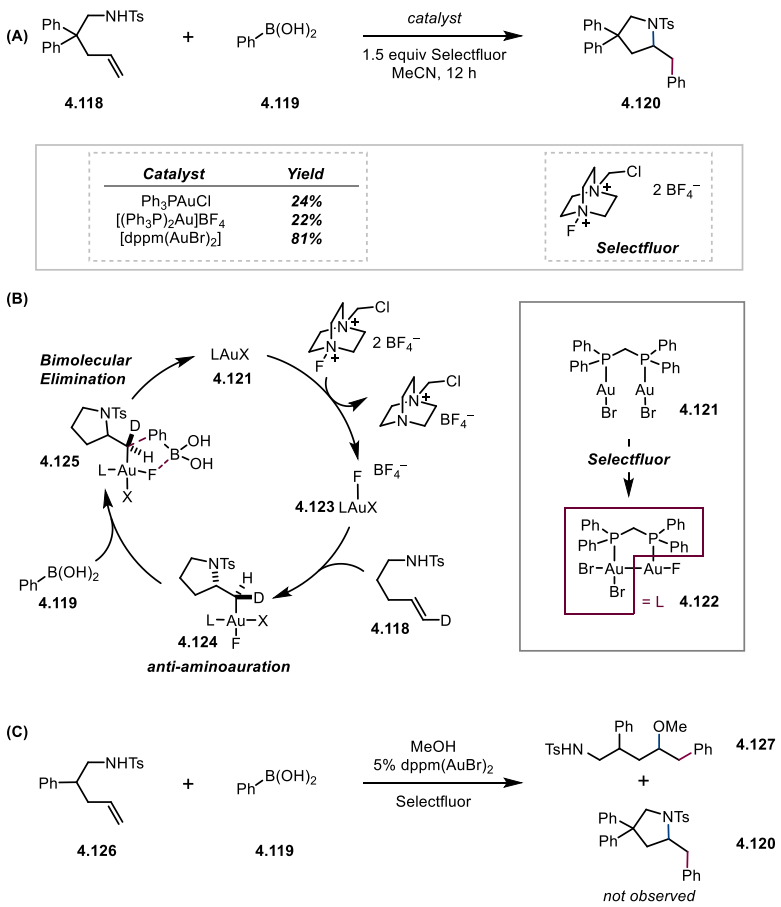

Figure 63: Bimetallic Gold Catalyzed Aminoarylation

While radical intermediates were eluded to in the instance of copper (II) catalyzed oxidative aminoarylation chemistry, Meerwein arylation for the difunctionalization of alkenes relies specifically on the generation of arene and affords products in high yields. A variety of different functionalities can arise from Meerwein alkene arylation because the resultant radical can either be oxidized and trapped by nucleophiles, such as acetonitrile to provide aminoarylation products, oxidized and deprotonated to form a new alkene bond, or trapped with a radical traps such as Selectfluor, TEMPO, peroxide or another alkene.[228] Functional groups such as diazonium, aryliodonium, ammonium and boronate provide access arene σ radicals through favorable reduction or oxidation processes (Figure 64). Mechanistic proposals accounting for reactivity acknowledge both catalytic and propagative reactions, depending on the lability of the arene sigma

radical precursor. Meerwein arylation is most effective for electronically activated alkenes such as acrylonitrile and styrene, as the rate of radical addition is an order of magnitude faster than for aliphatic olefins (10^8 $M^{-1}s^{-1-}$ vs 10^7 $M^{-1}s^{-1}$). Rate of aryl radical addition to unactivated olefins is competitive with H-atom abstraction from allylic positions, or solvent, if improperly chosen.

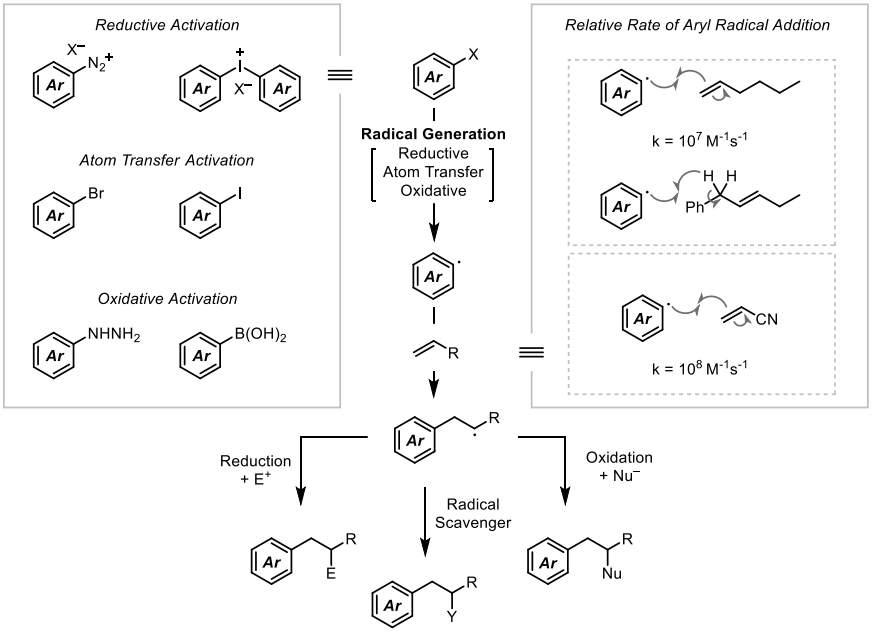

Figure 64: Meerwein Alkene Arylation Reaction Design

Examples of Meerwein-based aminoarylation operate efficiently with visible light photocatalysis, as oxidative quenching from a photoexcited complex with an arene diazonium cation or diaryliodonium salt is a fast and favorable process (Figure 65).[229] Aminoarylation is completed after arene radical addition, oxidation of the subsequent carbon centered radical followed by Ritter trapping and hydrolysis. More complex reaction designs enabling cation trapping with amine nucleophiles were realized by Glorius and co-workers with a dual photoredox gold catalyzed aminoarylation reaction (Figure 66).[230] The authors propose this reaction proceeds through an Au(I-III) redox cycle in which single electron oxidation of an Au(I) species first occurs through a ligation of the aryl radical to the metal center, followed by a redox event between the

aryl-Au(II) species and Ru(III) catalyst. Gold activation of the alkene system directs a *trans*-aminoauration followed by stereoretentive reductive elimination from the Au(III) intermediate is proposed by the authors. Alternatively, this can be explained through Meerwein arylation chemistry. Regardless, the process affords amino and hydroxyarylated products in high yields at room temperature, a remarkable achievement for alkene difunctionalization.

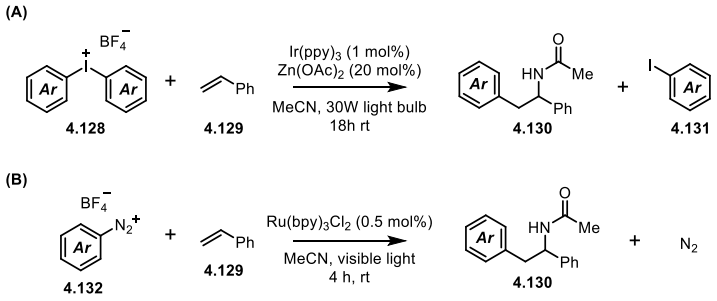

Figure 65: Photoredox Catalyzed Meerwein Aminoarylation

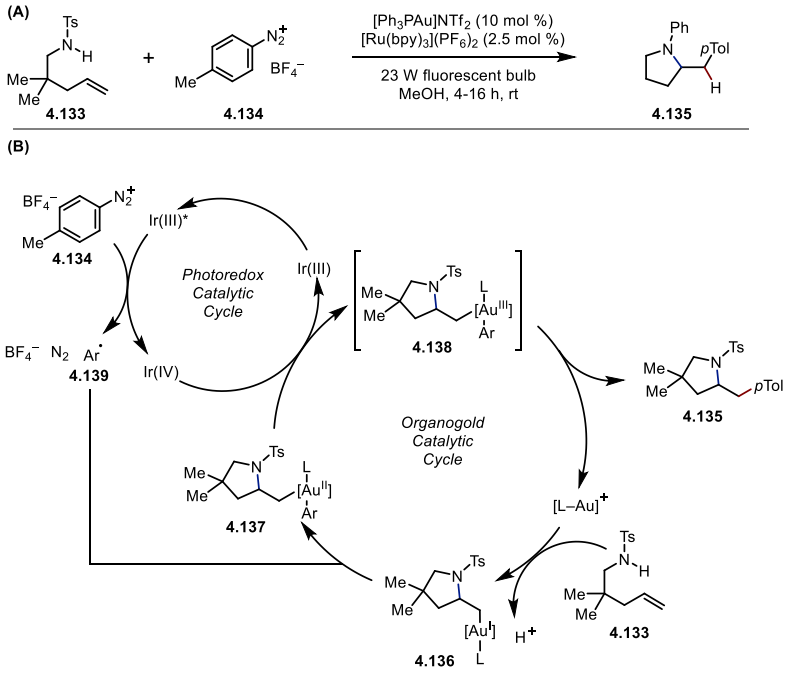

Figure 66: Dual Gold-Photoredox Catalyzed Meerwein Aminoarylation

4.2.3 Visible Light Photoredox Catalyzed Hydro- and Carboamination Reactions

Improvements in the design of carboamination reactions using visible light catalysis have resulted in the redox activation of either the nitrogen nucleophile or alkene, as opposed to the aryl reactant.[231] In multiple instances, Knowles and co-workers have realized the addition of open shell nitrogen nucleophiles – ammonium radicals and amidyl radicals – to alkenes (Figure 67). While nitrogen centered radicals were known to be synthetically advantageous for providing C–N bonds in direct, single operation, the literature was largely populated with thermally unstable amidyl radical precurors (*N*-chloroamines) or elaborate fragmentable redox-auxiliaries (for more see chapter 1).[232] Conversely, catalytic single electron oxidation and proton-coupled electron transfer steps, as realized by Knowles, allowed for native substrates, amines and amides alike, to become activated and chemoselectively react with alkenes in both intra- and intermolecular fashions. The simplicity of this reactivity was first realized for the synthesis of 2-aryl piperidines and pyrrolidines (Figure 67A). Hammett analysis suggests the rate limiting step of this transformation lies in the ammonium radical addition to the π-system. Additionally, deuterium labeling studies suggest the hydrogen atom is incorporated into the product through a reduction and protonation of **4.144** by solvent.

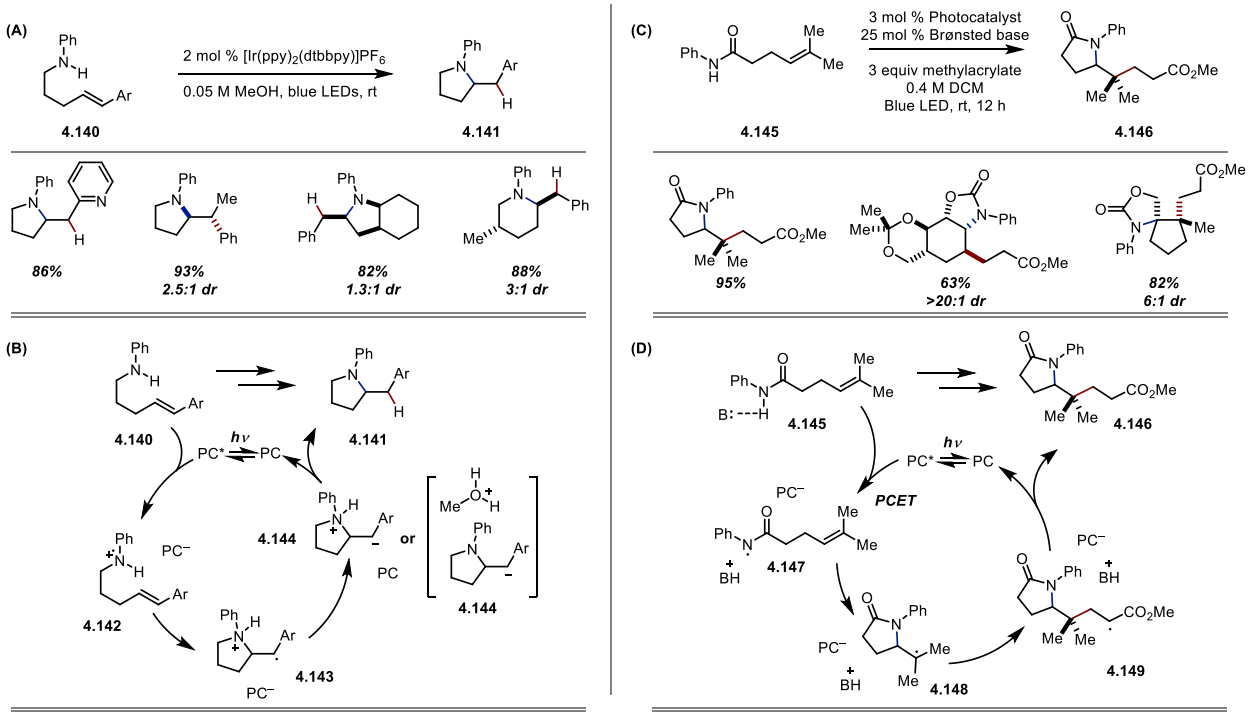

Figure 67: Alkene Hydroamination and Carboamiation using redox activation of nitrogenous functional groups

Having proven the efficacy and simplicity of photoredox catalyzed nitrogen centered radical reactivity, Knowles and co-workers developed a proton-coupled electron transfer methodology for the activation of amides for alkene carboamidation and hydroamidation. This catalyst system focused on an oxidizing photocatalyst in combination with a weak base to enact a weak acid-base reaction between the acid catalyst and amide substrate, followed by an oxidation event caused by a photoexcited catalyst.[233] The success of this approach hinged on the matching amide N-H BDE with the bond dissociation free energy (BDFE) the catalyst system was capable of activating. An optimized match was found with organic soluble phosophate base along with heteroleptic $Ir(III)^{+}$ photocatalyst calculated for a 97 kcal/mol BDFE activation energy. Paring an intramolecularly tethered alkene, along with an acrylate radical trap, carboamidation of a variety of substrates occurred in high yields.[234] The same PCET design also works for hydroamidiation, whereby the acrylate trap can be replaced with a thiophenol catalyst to terminate the radical cyclization with an

H-atom.[235] Knowles has additionally developed hydroamination and carboamination of alkenes with aliphatic amines and sulfonamides.[236,237]

At the same time Knowles was developing the synthetic applications of PCET catalysis, Nicewicz and coworkers found an efficient catalyst system for alkene hydro and carboamination relying on alkene oxidation as the key reactive intermediate (Figure 68).[238] To accomplish this, various *N*-alkyl and aryl acridinium photocatalysts were investigated. *N*-alkyl and aryl acridinums exhibit visible light sensitivity and are potent oxidants when photoactivated ($E_{p/2}$ = 1.45 V (T_1), 2.08 (S_1)).[239,240] These molecules in combination with an H-atom transfer catalyst, simply realized as thiophenol and the derivatives thereof, are efficient catalysts for alkene difunctionalization.[241] Notably this generates *anti*-Markonikov products in direct contrast to the Meerwein-based aminoarylation reactivity. The mechanistic understanding of this reactivity begins with a reductive quenching event between a photoexcited acridinium catalyst and alkene substrate. This generates an alkene radical cation which is poised for nucleophilic attack. Functionalization with either a nitrogen or oxygen-based nucleophile followed by radical trapping through H-atom transfer affords the targeted product. Dual catalyst turnover occurs through thiyl reduction from the reduced acridinium.[242]

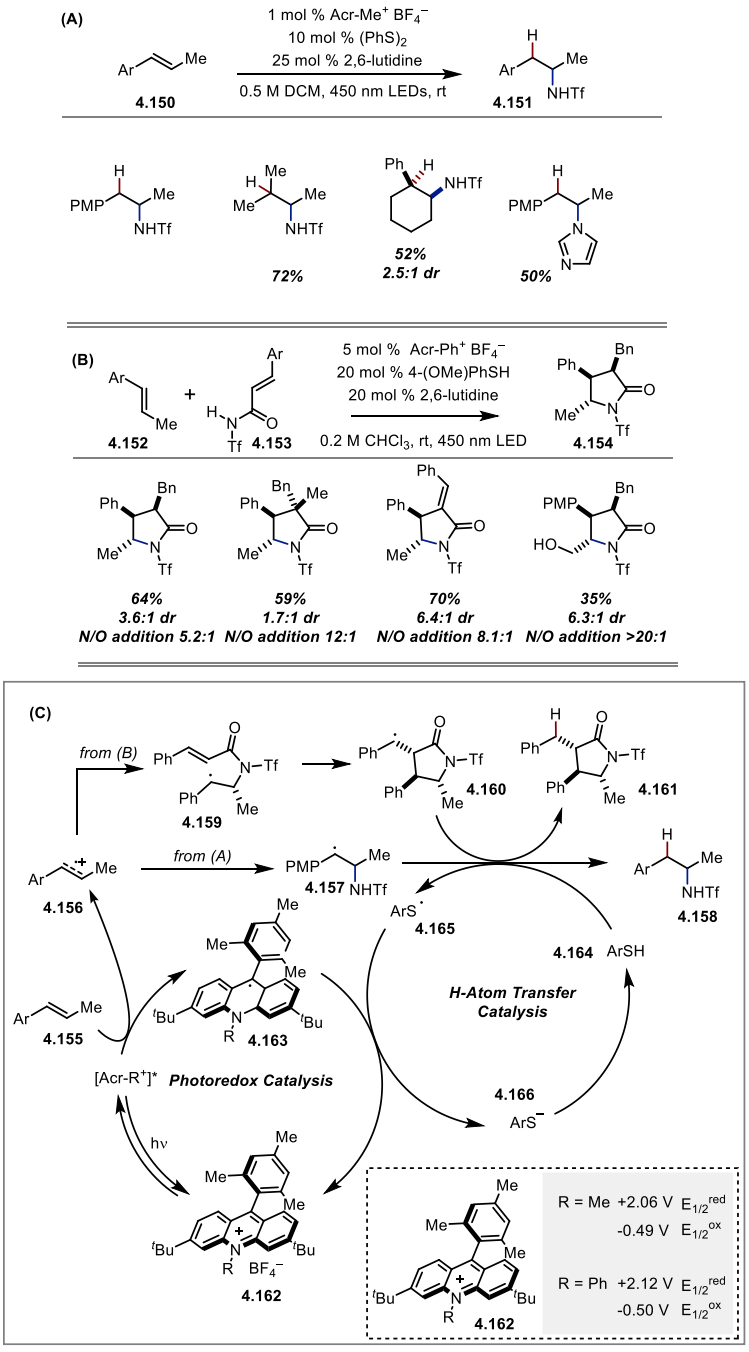

Figure 68: Acridinium Photocataylsis for alkene amination

4.14.2.4 Photochemical Smiles Rearrangement: Sulfonamides for Aminoarylation Reactivity

The dearth of carboamination and aminoarylation literature reveals the majority of reaction designs rely upon the tethering of two of the three aminoarylation reactants together to bias the

formation of this three-component coupling. This largely results in the aminoarylation of pentenamines and hexemamines to form pyrrolidine and piperidine derivatives. A notable exception to this reaction design was realized by Rovis and co-workers, wherein *N*-enoxyphthalimdes (tethered N and C synthons) were transposed across alkenes using Rh(I-III) catalysis in a diastereoselective manner.[243] While this approach can leverage the incorporation of a variety of arenes through transition metal catalyzed arylation, it limits the scope of alkenes for functionalization. Conversely, Meerwein-based aminoarylation methods lack stereocontrol, and solely provide Markovnikov regioselectivity.

Inspiration to bridge the gap between stereoselective transition metal catalyzed aminoarylation and visible light photocatalysis was provided through our lab's work proving a photochemical Smiles rearrangement.[244,245] The Smiles rearrangement is an intramolecular nucleophilic aromatic substitution reaction that is controlled by the relative acidity between the two interchangeable heteroatomic nucleophiles (Figure 70).[246] Truce expanded Smiles' original reactivity by showcasing the possibility of carbon nucleophiles for this rearrangement.[247] Yet, Pennell and Motherwell are often cited as key contributors for the demonstration of radical reactivity for a Smiles-Truce rearrangement.[248] This was critically acclaimed and expanded upon by many others, as it affords a simple and reliable method for arene functionalization reactivity without the complexity of transition metal catalysis.[249,250] The Smiles rearrangement is most commonly conducted in net reducing conditions, while more general examples of radical mediate intramolecular aryl transposition are noted in redox neutral[251,252,253,254,255,256,257] and net-oxidative conditions[258]. Sulfonate esters largely identify a Smiles rearrangement; however, this rearrangement is not limited to this functionality.[259,260]

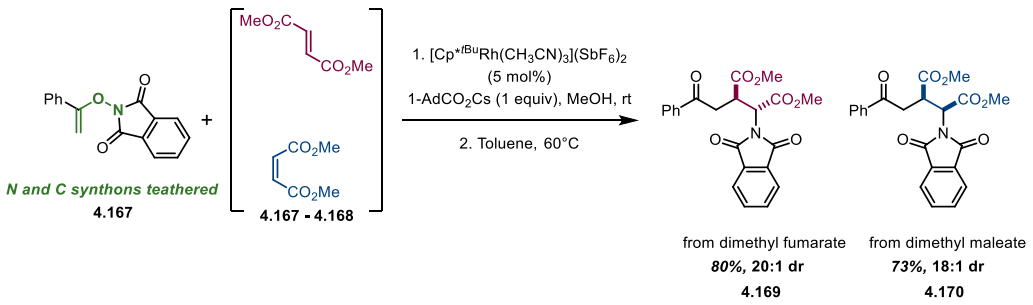

Figure 69: Intermolecular carboamination using teathered N-C synthons

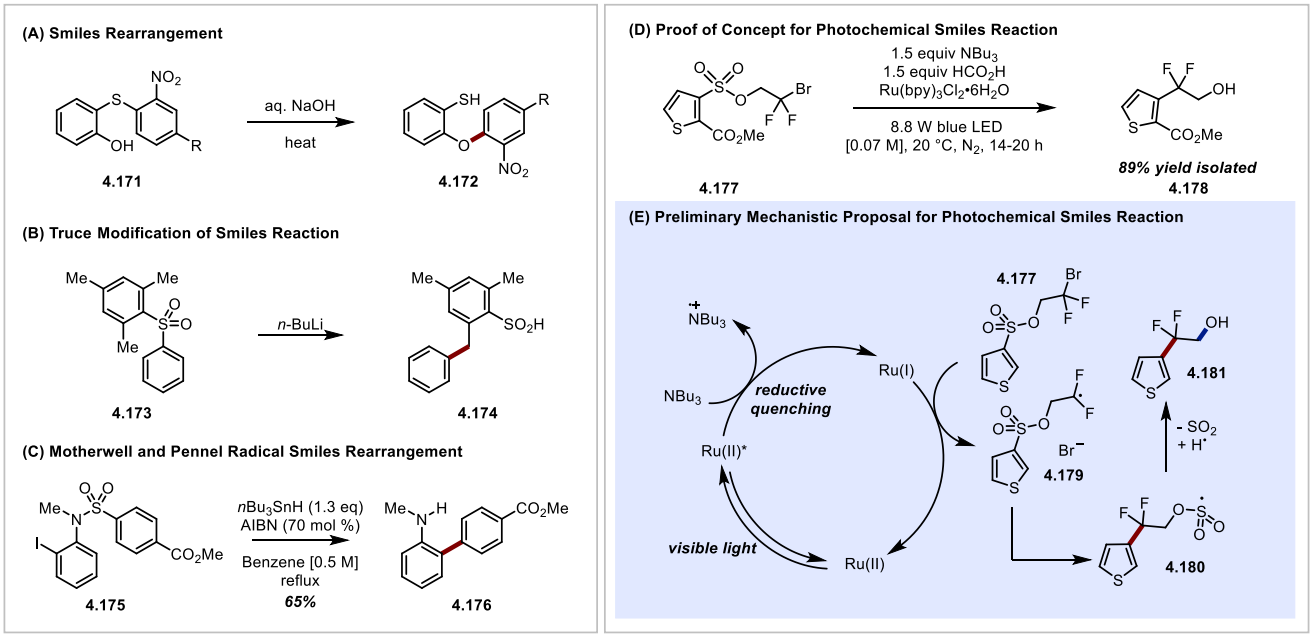

Figure 70: Key Developments in the Smiles Rearrangement

Given the variety of radical based Smiles examples, and the reliability of fragment-based coupling methods being popularized in photoredox catalysis, Douglas et. al. hypothesized a Smiles-Truce rearrangement of difluorobromoethylsulfonate arenes would generate aryldifluoroethanols in high yield (Figure 70D,E). [244, 261] Additional synthetic impetus was provided by Eli Lilly, who was in search of a more efficient methods for the synthesis of ORL-1 antagonist lead.[262] Gratifyingly, using a slight excess of tributylamine and formic acid and Ru(II) photocatalysis, **4.182** was isolated in nearly quantitative yield. Moreover, this process was general to a variety of arenes and heteroarenes. The highest yields were found with five-membered

heterocycles and naphthalene based arenes as radical addition to these π-systems is enthalpically lower than that of a benzene or pyridine system (Figure 71).

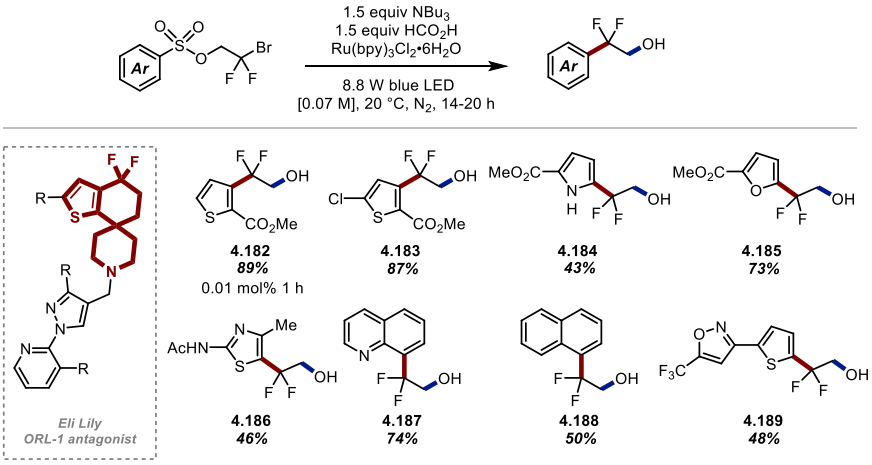

Figure 71: Representative Scope of Photochemical Smiles Rearrangement

Further exploration of the mechanism of reactivity, through scale up efforts towards **4.16.19**, illustrated a more complex mechanistic picture than originally hypothesized in the first report. Off target intermediates **4.190-4.191** were identified and found to minimally contribute to starting material consumption (<20% yield). These byproducts likely arose from the modification of reaction concentration (0.07 M – 0.25 M), as 0.01 M expended too much solvent during early scale-up efforts. An initial exotherm within the first 10 minutes of the reaction was found to occur for substrate **4.177**. Overall, this lead to the realization that the Smiles rearrangement of **4.177** could occur thermally, as both the difluorobromo group and the thiophene were sufficiently activated for homolysis and then radical aryl functionalization. Thermal reactivity was less efficient in the case of napthylsulfonate ester **4.192c**, and completely absent in quinoline and styrenyl substrates **4.192n** and **4.193**. These findings led Douglas to adapt a photochemical reactor for the processing of **4.177** on 100 gram scale that required a 300W white LED light, and not a blue light source to target Ru(II) photocatalysis (Figure 72). The result of these two investigations

fostered an interest in the synthetic utility of sulfonate ester derivatives as aryl transfer synthesis and spurred further development of photoredox catalyzed chemistry.

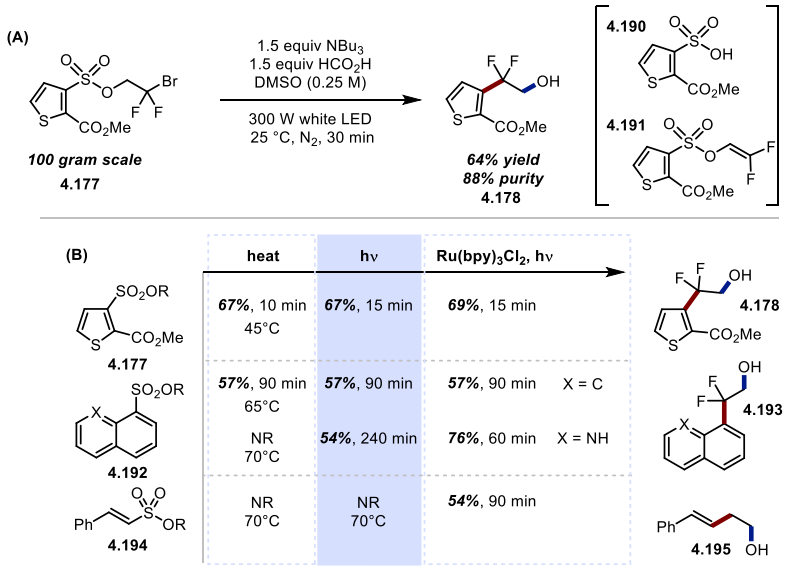

Figure 72: (A) 100 Gram Scale Reaction Conditions for the Synthesis of 4.17.2 (B) Comparing activation methods for Smiles rearrangement using heat and photochemical conditions from (A)

4.2 Aminoarylation Reaction Design and Evaluation:

Fascinated by aryl transfer using sulfonate esters, as well as the synthetic inefficiency of the ubiquitous "Smiles synthon" (Figure 73A), we questioned whether a redox neutral approach, as opposed to net reductive, could enable an *in-situ* Smiles-Truce rearrangement. This would allow for a simplification of the "Smiles synthon" to alkene and sulfonamide derived starting materials. Mechanistically, we hypothesized that a reductive quenching of a sufficiently oxidizing photocatalyst could provide either a sulfonamidyl radical, akin to Knowles, or an alkene radical cation, similarly to Nicewicz. [233,241] Either radical intermediate would find the corresponding counterpart, and form the key carbon-centered radical **4.242**. From here, aryl transfer followed by SO_2 extrusion and H-atom transfer would provide the desired aminoarylation product (**4.241**).

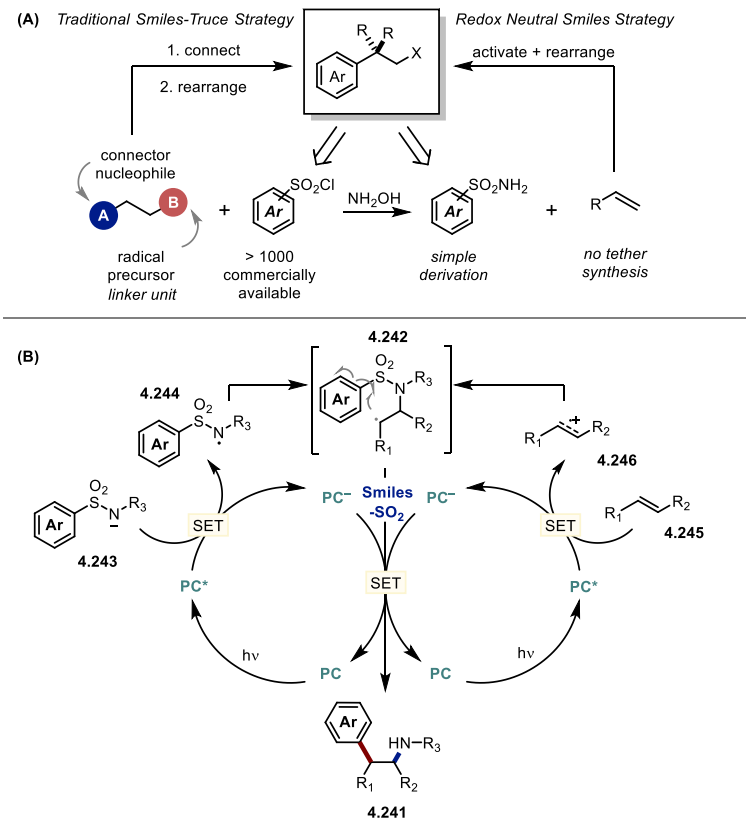

Figure 73: Redox Neutral Aminoarylation (A) Impetus and (B) Hypothesis

Reaction optimization began with a solvent screen and excess loading of the nucleophile and base to promote intermolecular trapping (Figure 74, entry 3). Interestingly, no aminoarylation reactivity was observed in solvents less polar than MeCN; DMF at 0.1 M was found to ideally produce the desired product. In MeCN, aminoarylation was out competed by 4+2 dimerization of the vinyl anisole (Figure 74, entry 2).[263] Further experiments revealed excess nucleophile did not promote more product formation, supporting the presumption that the highest concentration of active aminoarylation intermediate is less than or equal to the amount of photocatalyst. Testing various weak acetate and phosphate bases demonstrated regulatory role of the base for this reaction; stronger bases such as pyridine or *tert*-butoxide decomposed the catalyst likely through ligand substitution (Figure 74, entry 5-8) (Figure S4.6). Exogenous H-atom donor additives targeted for quenching the amidyl radical formed in solution were not found to improve the

reaction yield (Figure 74, entries 11-12). Finally, the structure-reactivity relationship between the amide functionality and aminoarylation were optimized for the smallest and most acidic among a group of amides and carbonates (Figure 75, **4.201-4.204**).

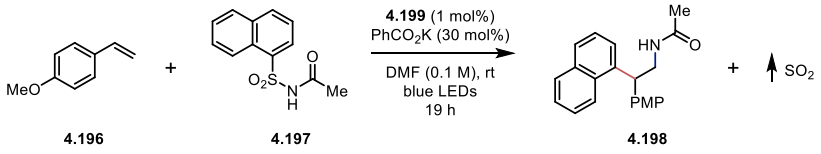

4.196 **4.197** **4.198**

Entry	Deviation from above	Yield
1	none	*41%*
2	MeCN as solvent	*<5%*
3	3 equiv of xx; 3 equiv of KOAc	*46 %*
4	1-naphthylsulfonamide instead of xx	*0 %*
5	KOAc as base	*38%*
6	K_3PO_4 as base	*41%*
7	CF_3CO_2K	*<5%*
8	pyridine as base	*<5%*
9	**4.19.5** instead of **4.19.4**	*0%*
10	10 euqiv of ^{i}PrOH added	*34%*
11	0.60 equiv of 1,4-cyclohexaidene added	*30%*
12	exclusion of light or photocatalyst	*0%*

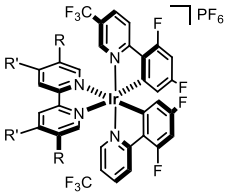

R = CF_3, R' = H: [Ir(dF(CF_3)ppy)$_2$(5,5'd(CF_3)bpy)](PF_6) **(4.199)**

R = H, R' = ^{t}Bu: [Ir(dF[CF_3]ppy)$_2$(dtbbpy)](PF_6) **(4.200)**

Figure 74: Reaction Optimization Experiments for Photocatalytic Aminoarylation

Aminoarylation reaction yield increased when the alkene coupling partner was modified from vinyl anisole to *trans*-anethole (Figure 75). This allowed us to demonstrate a scope of aminoarylation of a variety of arenes and heteroarenes in good to excellent yield (**4.205-4.222**). Concomitant in this scope investigation was the realization of aminoarylation products in excellent diastereoselectivity. To support this hypothesis, crystal structure analysis of products **4.213** and **4.214** confirmed the *syn*-facial arrangement of the amide and aryl groups, as well as the *anti*-facial arrangement of the alkene substituents in the alkane product.

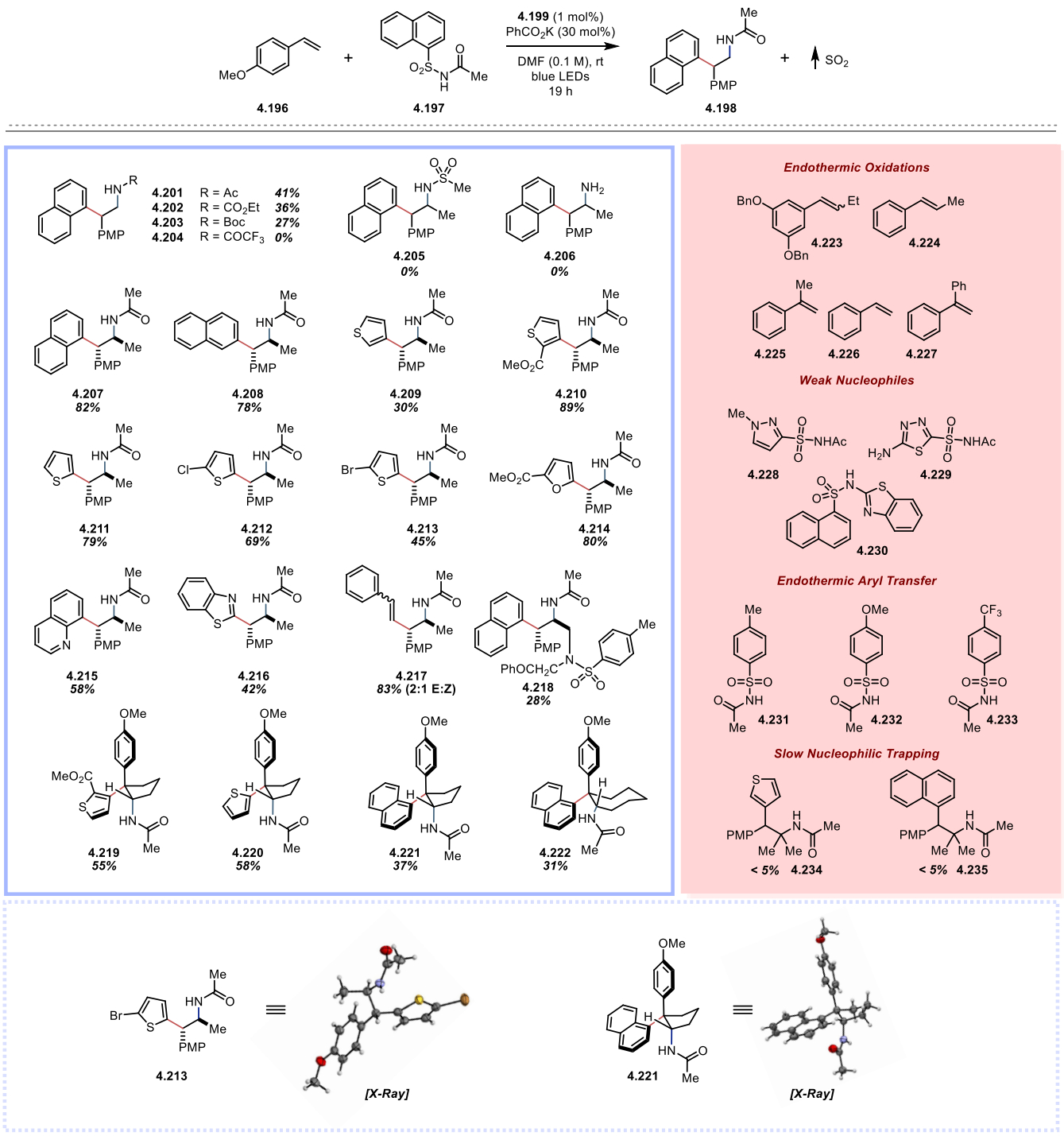

Figure 75: Aminoarylation Substrate Scope (blue) and limitations (red)

Intrigued by the observed diastereoselectivity of the reaction, we investigated the impact of alkene configuration on the reaction outcome. We hypothesized that both *E* and *Z* alkenes would convert to the same aminoarylation product through bond rotation in benzylic radical **4.242** (Figure 73B). Indeed, this result was initially supported by the transformation of *Z*-anethole to **4.207** in 72% yield, a very similar isolation as compared to the aminoarylation of *E*-anethole (Figure 76). Delving deeper into mechanistic studies, a systematic evaluation of the different processes at play were investigated. Firstly, excited state $Ir(III)^+$ photocatalyst quenching was observed between both anethole isomers, but not with the neutral sulfonamide. Interstingly, the *Z*-anethole interacted with the photoexcited $Ir(III)^+$ catalyst half as fast as *E*-anethole, as demonstrated in the values of the slope obtained in a Stern-Volmer quenching study. If left unreacted, $Ir(dF(CF_3)ppy)_2(5,5'd(CF_3)bpy)PF_6$ will isomerize a mixture of anethole isomers to a photostationary state of 1.5:1 *Z*:*E* anethole isomers due to the quenching rate difference (see section 4.4.2.3.4). Photoisomerization of *E*-anethole to *Z*-anthole is a slower process than the reverse, as the steric interaction between the *para*-methoxyphenyl and methyl substituents on the alkene are less pronounced (Figure 78). Secondly, initial rate quantification of alkene isomer consumption, sulfonamide consumption and product formation are all similar in magnitude and much slower than the excited state quenching process (Table 2). Having obtained these rates, along with the rate of photoisomerization, the data suggests the fastest process is alkene isomerization, followed by nucleophilic trapping and and product formation; this leads one to conclude that this process is diastereoconvergent due to a fast alkene isomerization followed by a favorable nucleophilic trapping and Smiles-Truce rearrangement.

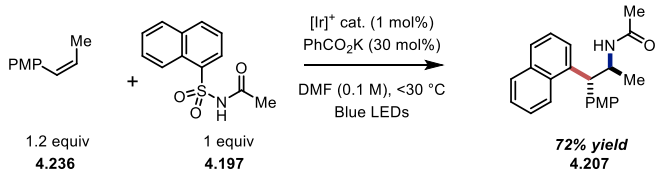

Figure 76: Initial observation of diastereoconvergence by aminoarylation of *Z*-anethoole

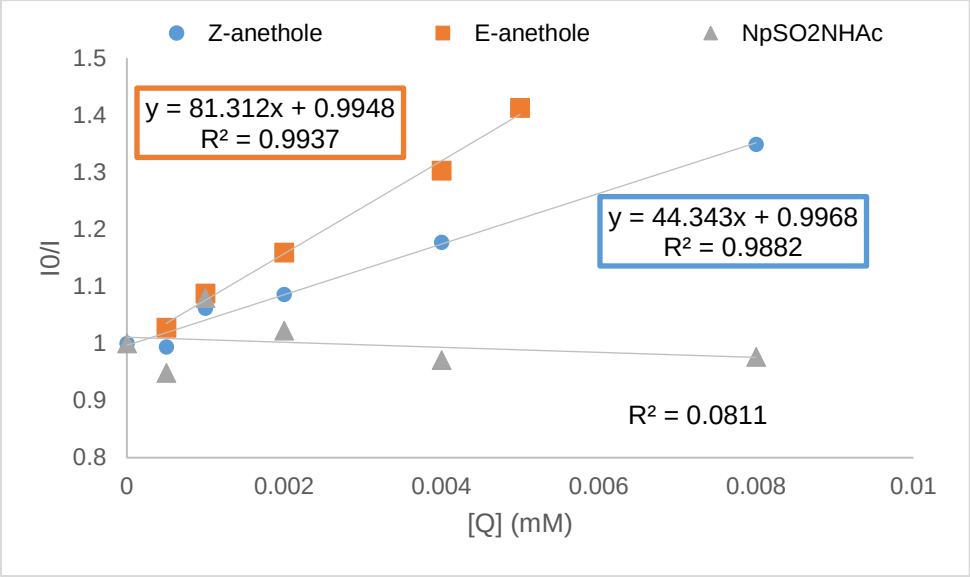

Figure 77: Stern-Volmer Quenching of $Ir(dF(CF_3)ppy)_2(5,5'd(CF_3)bpy)PF_6$

Table 2: Initial Rate of Reactivity for Aminoarylation Components

	Rate of reaction ($M \cdot min^{-1}$)		
	***E*-anethole**	**1-naphthylsulfonylacetamide**	**4.207**
1.2 equiv alkene	-0.0013	-0.0018	+0.0012
2.0 equiv alkene	-0.0007	-0.0011	+0.0012
Rate of cis to trans isomerization	> 0.0051 M min^{-1}	**Rate of trans to cis isomerization**	0.0009 M min^{-1}

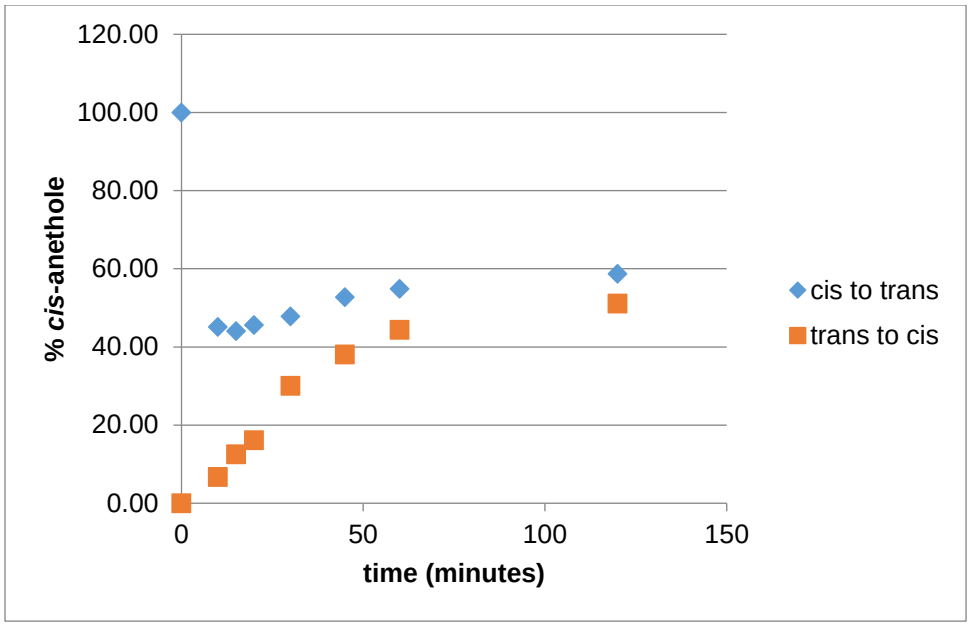

Figure 78: Anethole photoisomerization to photostationary state

The works of Norman Schepp and Linda Johnston on the rates of radical cation reactivity with nucleophiles and alkenes (aryl and aliphatic), lends significant evidence to the reactivity outcome of this reaction.[264,265] Arene electronics, and alkene sterics are the two most influential factors influencing the rate of bimolecular reactivity between a styrene radical cation derivative with another molecule. Table 3 is a compilation of rates that lends creedence to the justification that the kinetics of the reaction favor nucleophilic trapping of the alkene radical cation with the anionic sulfonamide in solution. Additional systematic study of photochemical anethole dimerization by Lewis and Kojima demonstrate that the relative speed of bond rotation is faster than bond formation, resulting in a stereospecific formation of **4.260**. The theoretical product of *cis*-anethole photocycloaddition is **4.261**, if the olefin geometry was preserved in the cycloaddition process. However, to form the C-C bond connecting each benzylic position, the intersystem crossing necessary for bond formation is a slower process than bond rotation, and thus the steric interaction between vicinal aryl groups causes rotation and bond formation resulting in **4.260**.

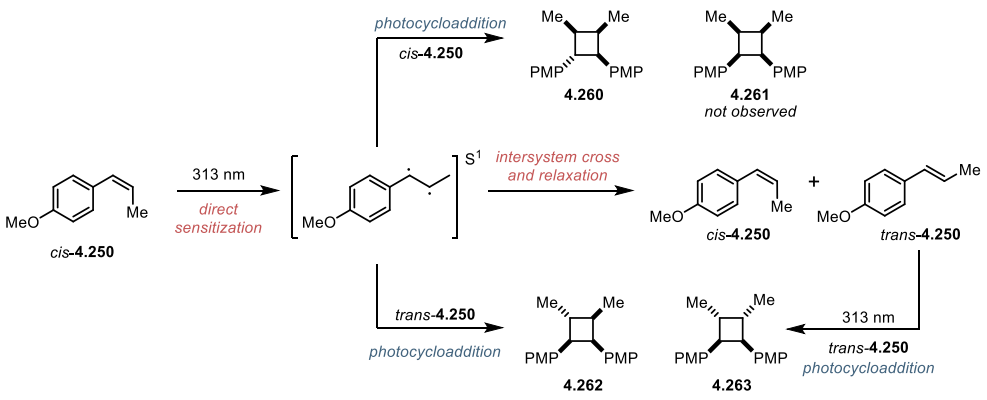

Figure 79: Photocycloaddition Dimerization of Anethole (4.250)

Table 3: Rates of Alkene Radical Cation Trapping

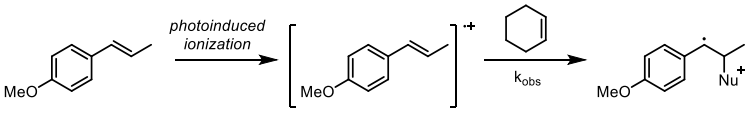

	nucleophile	rate		nucleophile	rate
4.196	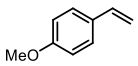	$<5 \times 10^5$	**4.252**		5×10^5
4.247	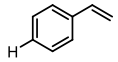	1.2×10^9	**4.253**		3.6×10^6
4.248	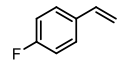	3.5×10^8	**4.254**	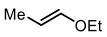	9.2×10^6
4.249	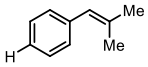	$<5 \times 10^5$	**4.255**	MeCN	4×10^4
			4.256	anethol	$<1 \times 10^8$
4.250	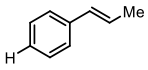	8.9×10^6	**4.257**	N_3^-	2.9×10^{10}
			4.258	CN^-	1.4×10^{10}
4.251	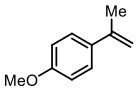	$<5 \times 10^5$	**4.259**	OH^-	2.0×10^{10}

4.3 Conclusion

Alkene difunctionalization challenges the preeminent catalytic designs for small molecule synthesis and provides excitingly efficient synthesis of medicinally relevant compounds. Aminoarylation, a small but profound class of alkene difunctionalizations, is challenged by identifying suitable precursors for C–N and C–C bond formation in a single step. Reaction designs

range from fully radical reactivity to stepwise metal catalyzed bond forming steps with impressive stereoselective control. Recent discoveries within the field of photoredox catalysis have demonstrated direct methods for generating reactive amines, amides and alkenes all competent in selective alkene difucntionalization reactions. The disclosed work herein establishes sulfonylacetamides as a competent class of bifunctional reagents for alkene aminoarylation in a single operation. This process is catalyzed by a highly oxidizing $Ir(III)^{+}$ photocatalyst in the presence of blue light at room temperature. Overall this approach is distinguished from previous methods of aminoarylation and can help address challenges in synthesizing stereodefined 2,2-arylethylamine products.

4.4 Experimental

4.4.1 General Information:

All chemicals were used as received and stored as recommended by the supplier. Reactions were monitored by thin layer chromatography (TLC) using glass-backed plates pre-coated with 230–400 mesh silica gel (250 mm thickness) with fluorescent indicator F254, available from EMD Millipore (cat. #: 1.05715.0001). Plates were visualized with a dual short wave/long wave UV lamp. Column flash chromatography was performed using 230-400 mesh silica (SiliCycle cat. #: R12030B). gel or via automated column chromatography. NMR spectra were recorded on Varian MR400, Varian Inova 500, Varian Vnmrs 500, or Varian Vnmrs 700 spectrometers. Chemical shifts for ^{1}H NMR were reported as δ, parts per million, relative to the signal of $CHCl_3$ at 7.26 ppm and for DMSO 2.50. Chemical shifts for ^{13}C NMR were reported as δ, parts per million, relative to the center line signal of the $CDCl_3$ triplet at 77.0 ppm and for DMSO 39.52 for center of septet.^{19}F NMR chemical shifts were reportd as δ, parts per million, relative to $CFCl_3$ at 0.0 ppm. The abbreviations s, br. s, d, dd, br. d, ddd, t, q, br. q, qi, m, and br. m stand for the resonance multiplicity singlet, broad singlet, doublet, doublet of doublets, broad doublet, doublet of doublet of doublets, triplet, quartet, broad quartet, quintet, multiplet and broad multiplet, respectively. IR spectra were recorded on a Perkin-Elmer Spectrum BX FT-IR spectrometer fitted with an ATR accessory. Mass Spectra were recorded at the Mass Spectrometry Facility at the Department of Chemistry of the University of Michigan in Ann Arbor, MI on an Agilent Q-TOF HPCL-MS with ESI high resolution mass spectrometer using electrospray ionization (ESI), positive ion mode, or electron impact ionization (EI). We thank Dr. James Windak and Dr. Paul Lennon at the University of Michigan Department of Chemistry instrumentation facility for conducting these experiments. X-Ray Crystallography work was done by Dr. Jeff. W. Kampf. UV-Vis measurements were obtained on a Shimadzu UV-1601 UV-Vis Spectrometer. Electrochemical data was collected on a

CHI600E potentiostat with the accompanying CH Instruments software. H150 Blue grow lights from Kessil were used as the visible light irradiation source.

4.4.2 Reaction Set-up:

Unless stated otherwise, all reactions were run on a 0.3 mmol scale in a 2-dram vial equipped with an oval shaped stir bar. 1 x H150 Kessil lamp sufficiently irradiated 1-3 reaction vials at one time, about 5 cm away (Figure 80AFigure 80: General reaction set-up for radical aminoarylation, side view). At this distance, with a fan dissipating the standing atmosphere (Figure 80B, top view), the air temperature surrounding the reactions did not exceed 30˚C.

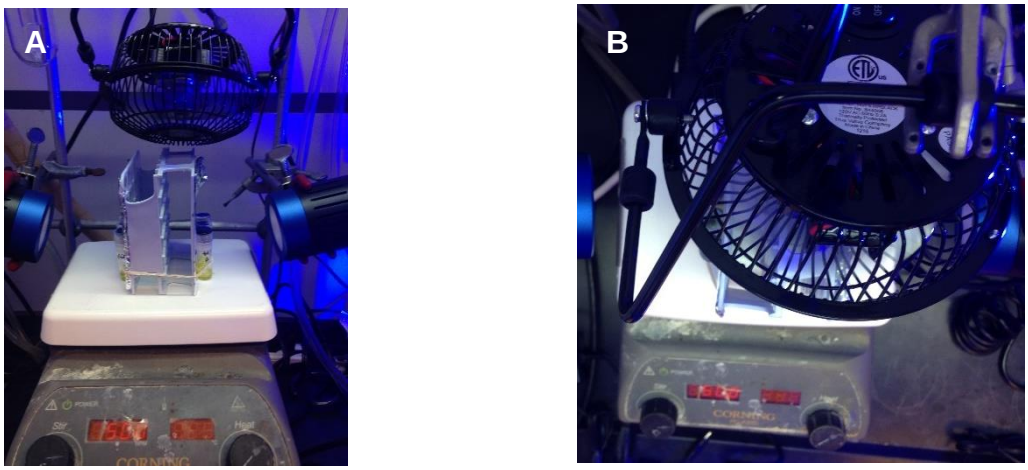

Figure 80: General reaction set-up for radical aminoarylation

4.4.2.1 General Procedure for Aminoarylation

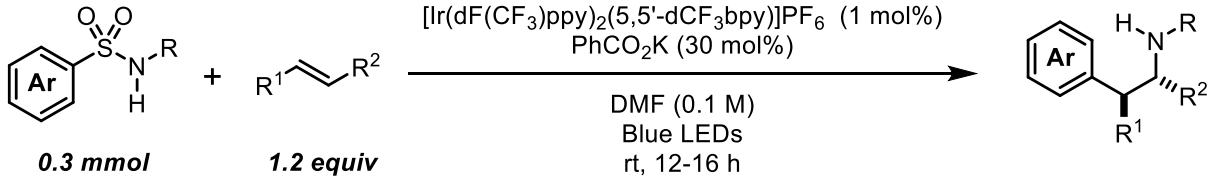

Unless otherwise noted, to a flame dried 2-dram vial, equipped with a teflon coated oval shaped stir bar, was added (aryl-sulfonyl)acetamide (1 equiv, 0.3 mmol), potassium benzoate (14.4 mg, 30 mol%), and $Ir(dF(CF_3)ppy)_2(5,5'd(CF_3)bpy)PF_6$ (3 mg, 1 mol%). The vial contents were then dissolved in anhydrous DMF (3 mL, 0.1 M). Finally, the alkene (1.2 equiv) was added to the reaction vial. The reaction was sparged under argon for 15 min, quickly capped and sealed with parafilm. Reactions were irradiated with 1 x blue H150 Kessil LED light and stirred (500 to 550 rpm) for 12 to 16 h at room temperature.

Reaction workup was performed by diluting the reaction with 15 mL dH_2O and extracting the aqueous layer with EtOAc (3 x 10 mL). The organic layer was combined, washed with 5 wt% LiCl (3 x 10 mL), brine (15 mL), dried over sodium sulfate, filtered and concentrated to provide the crude residue, which was purified by flash column chromatography.

4.4.2.3 Reaction Optimization Experiments:

Optimization reactions were conducted on 0.3 mmol scale according to **Aminoarylation General Procedure**. Yields reported are from isolation.

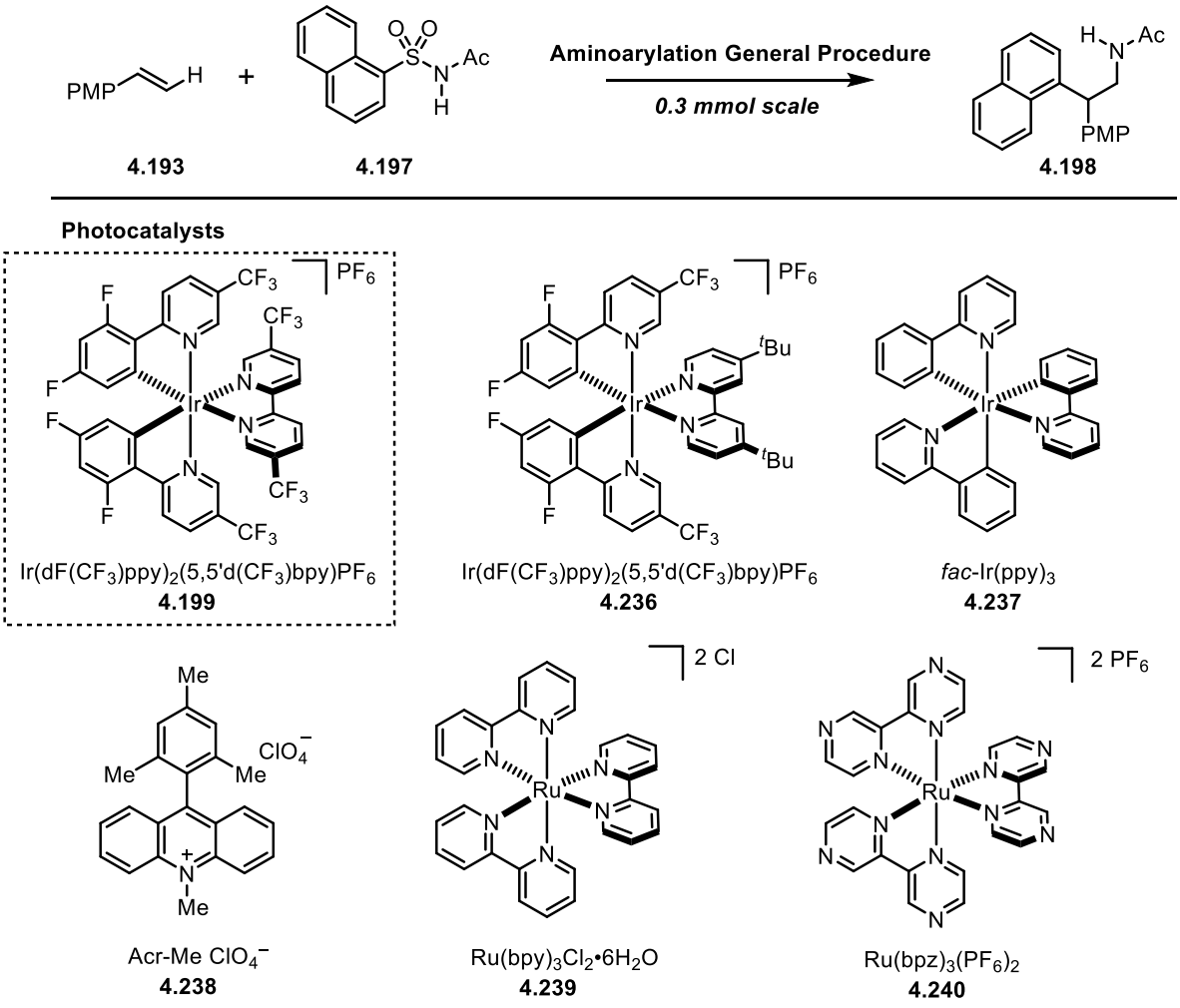

Figure 81: Reaction Optimization and Photocatalyst Screen

Table 4: Aminoarylation Reaction Optimization Results

	R	4.197 equiv	Base	Base equiv	Catalyst	Solvent [M]	Yield (%)
1	Ac	3	KOAc	3	4.199	DMF [0.1 M]	46
2	Ac	3	NaOAc	3	4.199	DMF [0.1 M]	42
3	Ac	3	K_2HPO_4	3	4.199	DMF [0.1 M]	23
4	Ac	3	K_2CO_3	3	4.199	DMF [0.1 M]	11
5	Ac	3	K_3PO_4	3	4.199	DMF [0.1 M]	41
6	Ac	3	Pyridine	3	4.199	DMF [0.1 M]	9
7	Ac	1	KOAc	0.3	4.199	DMF [0.1 M]	32
8	Ac	1	$PhCO_2K$	0.3	4.199	DMF [0.1 M]	38
9	Ac	1	CF_3CO_2K	0.3	4.199	DMF [0.1 M]	10
10	Ac	1	K_3PO_4	0.3	4.199	DMF [0.1 M]	30
11	Ac	1	Pyridine	0.3	4.199	DMF [0.1 M]	0
12	Ac	1	$PhCO_2K$	0.3	4.199	DMF [0.2 M]	7
13	Ac	1	$PhCO_2K$	0.3	4.199	DMF [0.4 M]	<5
14	Ac	1	K_3PO_4	0.3	4.199	DMSO [0.1 M]	10
15	Ac	1	K_3PO_4	0.3	4.199	MeCN [0.1 M]	11
16	Ac	1	K_3PO_4	0.3	4.199	THF [0.1 M]	0
17	Ac	1	$PhCO_2K$	0.3	4.199	THF:DMF [0.1 M]	30
18	Ac	1	K_3PO_4	0.3	4.236	DMF [0.1 M]	0
19	Ac	1	K_3PO_4	0.3	4.237	DMF [0.1 M]	0
20	Ac	1	K_3PO_4	0.3	4.239	DMF [0.1 M]	0
21	Ac	1	K_3PO_4	0.3	4.240	DMF [0.1 M]	0
22	Ac	1	Pyridine	0.3	4.238	DMF [0.1 M]	13
23	Ac	1	0.3 K_3PO_4 + 10 eq. ^{i}PrOH		4.199	DMF [0.1 M]	34
24	Ac	1	DABCO	0.3	4.199	DMF [0.1 M]	<10
25	Ac	1	Et_3N	0.3	4.199	DMF [0.1 M]	<10
26	Ac	1	$PhMe_2SiH$	1	4.199	DMF [0.1 M]	<10
27	Ac	1	$(EtO)_3SiH$	1	4.199	DMF [0.1 M]	<10
28	Ac	1	1,4-cyclohexadiene	0.6	4.199	DMF [0.1 M]	30

4.4.2.3.1 Aminoarylation Reaction Assembly

Table 5: Aminoarylation reaction assebly, a pictoral guide

 **Step 1:** Flame dried 2-dram vial and stir bar	 **Step 2:** Solid reagents loaded
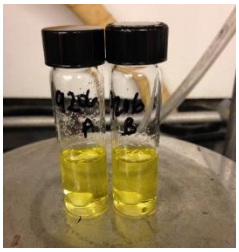 **Step 3:** Solid reagents diluted in DMF (0.1 M)	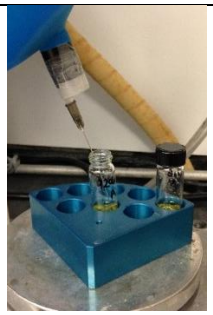 **Step 4:** Sparge degassing technique with argon balloon and 4” hypodermic needle
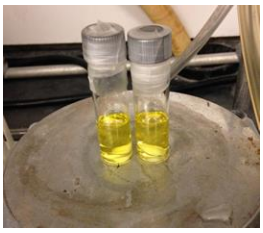 **Step 5:** Vial-cap juncture wrapped in parafilm immediately after argon sparging	 **Step 6:** Blue light irradiation with 1 x H150 blue Kessil grow lamp, 500 rpm, and fan for cooling

4.4.2.3.4 Photocatlyzed Alkene Isomerization

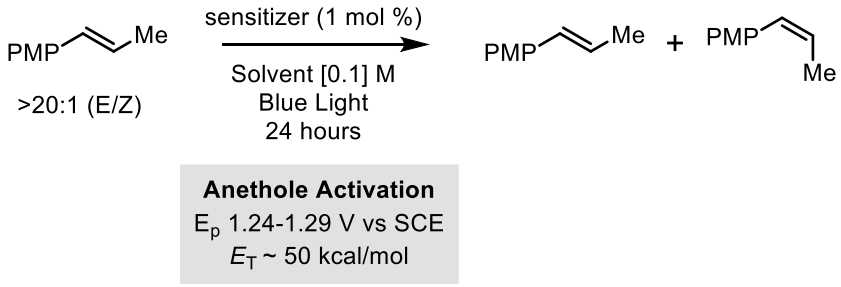

entry	Sensitizer	E_T	$E_{1/2}(M^*/M^+)$	Solvent	Result (E/Z)
1	4.239	47 kcal/mol	0.77 V	DMF	>20:1 (E/Z)
2	4.237	58 kcal/mol	0.31 V	DMF	1:1.1
3	4.199	43 kcal/mol	1.68 V	DMF	1:1.1
4	4.199	43 kcal/mol	1.68 V	Cyclohexane	1:1.6
5	4.199	43 kcal/mol	1.68 V	DCE	1:1.4

Figure 82: Background Anethole Epimerization Reaction

To a 1-dram vial equipped with a stir bar, solid photosensizer was added (≤1 mg) was added. Each photocatalyst was then diluted in the specified solvent (1 mL, 0.1 M) and 15 μL or *E*-anethole was added. Each reaction was degassed by 3 cycles of freeze-pump-thaw degas, and then sealed before irradiating by 1 H150 Blue Kessil light for 24 hours. After this irradiation period, reactions in DMF were extracted 2x times with pentanes and then concentrated for ^{1}H NMR analysis. Reactions run in cyclohexane and 1,2-DCE were simply concentrated and then analyzed by ^{1}H NMR (500 mHz). Olefin mixtures were identified by the signals 5.95 (m, 1H, *E*-anethole) and 5.56 (m, 1H, *Z*-anethole). These signals are shifted from the values of the neat material in chloroform, due to the large amounts of DMF in the sample, even when the anethole isomers are extracted into pentanes. The ratio obtained in entry 3 does not directly reflect the experimental observation of a 1:1.4 mixture obtained in the anethole isomer functionalization studies, however, the experiment was

run identically, and reflect the overall epimerization process occurring in the absence of nucleophile. Furthermore, this trend supports the hypothesis that this epimerization is redox enabled, and not a triplet sensitization reaction.

4.4.3 Preparation of Reagents

4.4.3.1 Preparation of $Ir(dF(CF_3)ppy)_2(5,5'd(CF_3)bpy)PF_6$ (**4.199**)

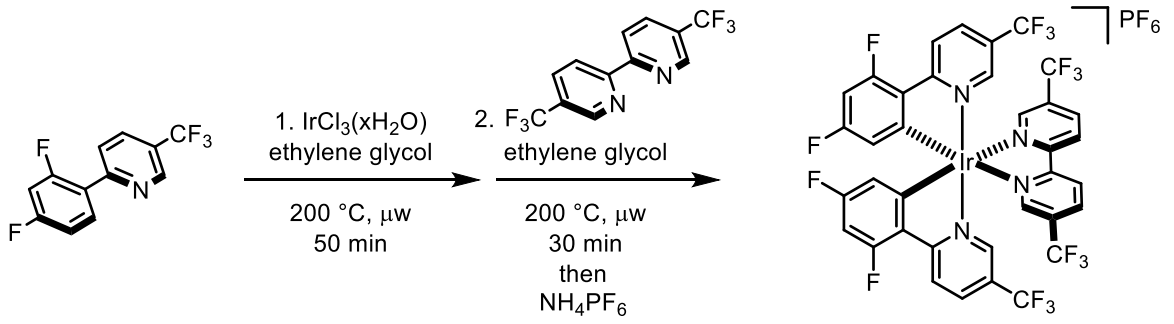

$Ir(dF(CF_3)ppy)_2(5,5'd(CF_3)bpy)PF_6$
4.199

The following procedure has been adopted from a two-step, one-pot literature procedure from our laboratory disclosing the synthesis of heteroleptiC–Ir(I) complexes through microwave irradiation.[266]

To an oven dried 20 mL microwave vial was charged a magnetic stirring bar, $IrCl_3$-xH_2O (507 mg, 1.6 mmol, 1 equiv), and 2-(2,4-difluorophenyl)-5-(trifluoromethyl)pyridine (1.04 g, 4.0 mmol, 2.5 equiv). The vial contents were dissolved in ethylene glycol (15 mL) and then the microwave vial capped. Then the reaction was sonicated for 3 minutes to increase homogeneity. The reaction was heated in a microwave reactor at 200 °C for 50 min with a 5 min pre-stir period. After the reaction had cooled to room temperature, 5-(trifluoromethyl)-2-[5-(trifluoromethyl)-2-pyridyl]pyridine (617 mg, 2.1 mmol, 2 equiv) was added, the vial re-capped, and the reaction was heated to 200 °C for 30 min with a 5 min pre-stir period.

After the reaction had cooled to room temperature, the solution was dissolved in dH_2O (50 mL) and extracted with CH_2Cl_2 (3 x 20 mL). The organic layer was combined and concentrated down, followed by the addition of NH_4PF_6 (10 g in ~50 mL dH_2O). The whole was placed in the freezer overnight to allow for maximum crystal formation. The yellow/orange crystals were filtered and

washed with cold Et_2O. Re-crystallization was performed with pentane and acetone (insoluble in pentane) to provide the title complex as a free-flowing yellow powder (1.08 g, 59%).

^{1}H and ^{19}F NMR characterization data corresponded to the literature reported values.[267]

^{1}H NMR (500 MHz, d_6-Acetone) δ = 9.32 (d, *J* = 8.6 Hz, 1H), 8.83 (d, *J* = 8.5 Hz, 1H), 8.61 (d, *J* = 8.7 Hz, 1H), 8.56 (s, 1H), 8.40 (d, *J* = 8.9 Hz, 1H), 8.19 (s, 1H), 6.91 (t, *J* = 11.7 Hz, 1H), 5.98 (dd, *J* = 8.4, 2.2 Hz, 1H) ppm

^{19}F NMR (471 MHz, d_6-Acetone) δ = -62.66 (d, *J* = 107.9 Hz), -71.75(d, J_{P-F} = 707.4 Hz), -103.14(dd, *J* = 20.1, 9.3 Hz), -106.81(t, *J* = 12.2 Hz) ppm

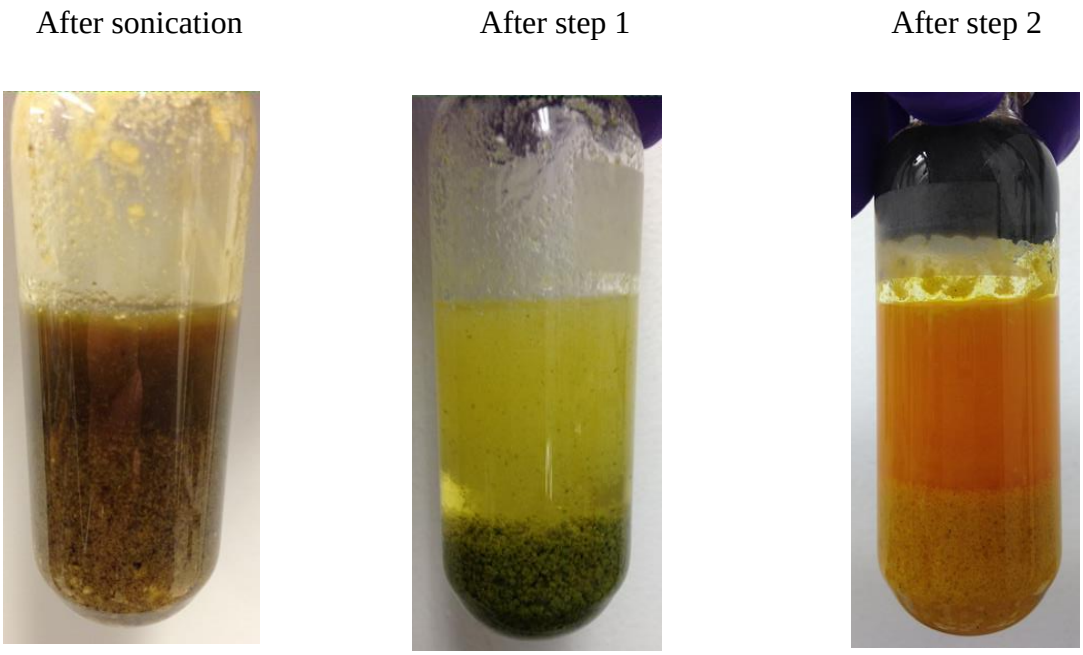

Figure 83: Photocatalyst synthesis, a pictoral guide

4.4.3.1.1 Strong base interaction with $Ir(dF(CF_3)ppy)_2(5,5'd(CF_3)bpy)PF_6$:

Experimental Procedure

UV-Vis: A 25 μM solution of 4.199 in 2 mL of DMF was prepared by weighing 1.6 mg of **4.199** into a volumetric flask and then diluting to 5 mL. The spectra of this solution was recorded. Separately, 1.7 mg of 4.199 was weighed intoa 5 mL volumetric flask followed by 7.7 mg of NaO*t*Bu. The solids were then diluted in 5 mL of DMF and homogenized using a pipette. The spectra of the homogeneous solution was recorded.

NMR titration: To a 1 dram vial 2 mL of DMSO-d6 and 5 mg of photocatalyst were mixed. Separately 3.36 mg of NaO*t*Bu in 1 mL of DMSO-d6 was prepared. Five solutions were prepared in standard NMR tubes by combining the following listed volumes.

Table 6: Base titration with $Ir(dF(CF_3)ppy)_2(5,5'd(CF_3)bpy)PF_6$ (4.199) set-up

4.199 volume (mL)	Base volume (mL)	Void Volume	total volume - 500 uL
0.4	0	0.1	0.5
0.4	0.0125	0.0875	0.5
0.4	0.025	0.075	0.5
0.4	0.0375	0.0625	0.5
0.4	0.05	0.05	0.5

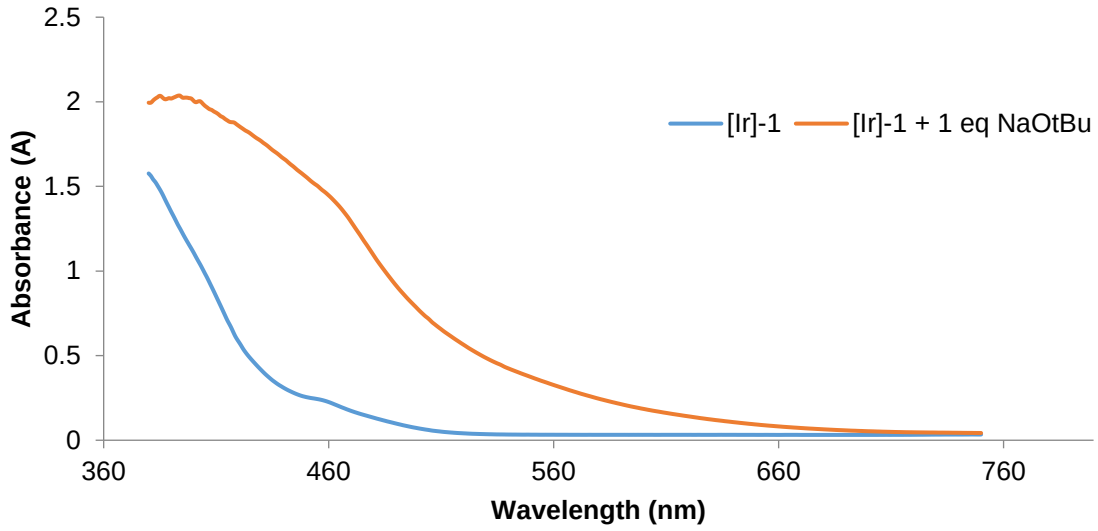

Figure 84: Ir(dF(CF$_3$)ppy)$_2$(5,5'd(CF$_3$)bpy)PF$_6$ [4.199] modification with strong base

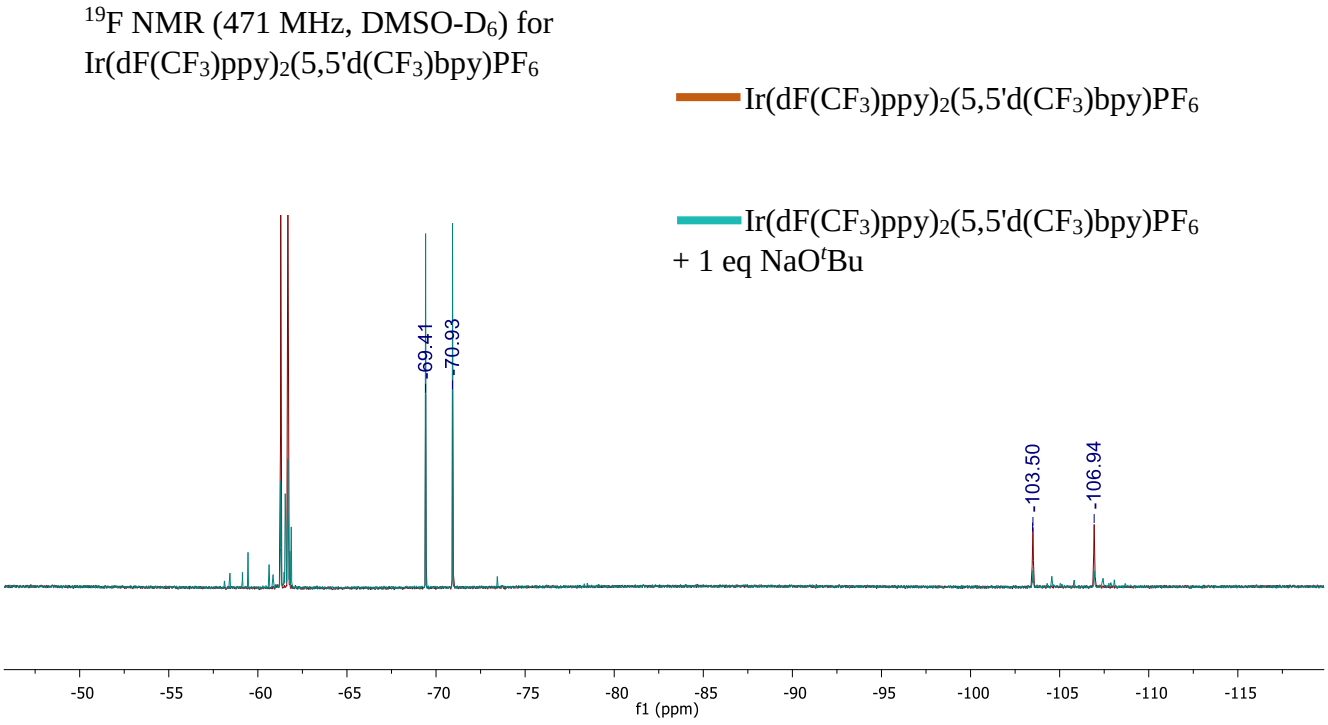

Figure 85: NMR Overlay of Ir(dF(CF$_3$)ppy)$_2$(5,5'd(CF$_3$)bpy)PF$_6$ in the presence and absence of NaO^{t}Bu

4.4.3.2 Acyl Sulfonamides

N-(naphthalen-1-ylsulfonyl)acetamide (S1)

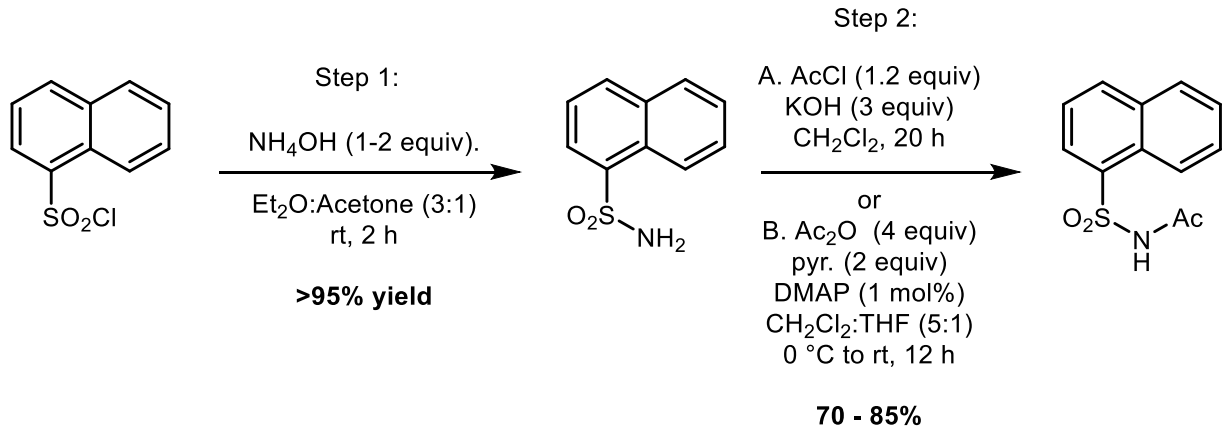

Step 1:

To a dry 250 mL round bottom flask equipped with a sizable oval shaped stir bar, a 3:1 mixture of Ether:Acetone was prepared (100 mL total). To this the solid naphthalene-1-sulfonyl chloride (10.0 g, 44.1 mmol), added into the flask. The solution is homogeneous at this point. Then by dropwise addition, saturated NH_4OH ((5809 µl) 44.1 mmol, 1 equiv) was added at 0 °C. The reaction was checked by TLC (4:6 EtOAc:Hexanes). If the reaction was not complete in 1 hour, an additional 1 equiv of NH_4OH was added to ensure full conversion.

The reaction was then neutralized to a pH of 6-7. Caution should be taken to not inhale the off gassing excess ammonia from the solution, and this will process faster if the reaction is under a continuous flush of nitrogen gas. Dilute the reaction in an equal volume of water and extract 2x with an equal amount of ethyl acetate. Combine the organic portions and dry over sodium sulfate, with a final concentration *in vacuo* to reveal a white powder.

Step 2 A:

To a dry 250 mL round bottom flask equipped with a sizeable oval shaped stir bar, KOH (4426 mg, 78.9 mmol – crushed fine powder) and naphthalene-1-sulfonamide (5.45 g, 26.3 mmol) were added. The flask was evacuated and backfilled with nitrogen 3 times, after which the contents were diluted in dichloromethane solvent (50 mL). After stirring for a few minutes, acetyl chloride (2244 µL, 31.6 mmol) was added dropwise at room temperature. During this addition, the reaction very noticeably goes heterogeneous, then homogeneous and then back to heterogeneous. After 2 hours this reaction is complete, but is stable if left under nitrogen for up to 24 hours. At this point the reaction was diluted with 100 mL of water and acidified past neutrality. These contents were then transferred to a 500 mL separatory funnel and the aqueous layer was extracted 2x times with 75 mL of CH_2Cl_2. The CH_2Cl_2 extracts were combined, and concentrated, and the product was recrystallized in methanol to yield dense white crystals.

Alternatively, the product can be separated from the starting material by first combining the CH_2Cl_2 extraction and concentrating *in vacuo* to take back up in a minimal amount of EtOAc (60 mL). This was then extracted 5x times with 60 mL of 5 % $NaHCO_3$ aq solution. These combined aqueous extracts were then acidified using 4 M HCl beyond neutrality (product becomes insoluble in solution. Finally, the desired product can be extracted from the acidic aqueous layer using EtOAc or CH_2Cl_2. Combination and drying over Na_2SO_4 and concentration *in vacuo* yields the desired product. The product can be further purified by recrystallization in MeOH. Non-recystallized material is lighter in density, and more difficult to handle.

Step 2 B:

To a flame dried 100 mL round bottom flask equipped with a magnetic stir bar was added naphthalene-1-sulfonamide (1 g, 4.83 mmol), DMAP (6 mg, 1 mol%), CH_2Cl_2 (35 mL), and THF (6 mL). The reaction mixture at this point appears mostly heterogeneous. Then the reaction was cooled to 0 °C and via syringe was added pyridine (777 μL, 9.65 mmol, 2 equiv) followed by acetic anhydride (1.82 mL, 19.3 mmol, 4 equiv). The whole slowly became more homogeneous over a few minutes. The reaction was slowly allowed to warm to rt while stirring overnight (12 h). Upon completion of the reaction as judged by TLC analysis (40% EtOAc in Hex), the reaction was diluted in 20 mL dH_2O, layers separated, and the aqueous layer washed with 20 mL CH_2Cl_2. The organic layer was combined and rinsed with 1 N HCl (2 x 20 mL), brine, dried over sodium sulfate, filtered and concentrated *in vacuo* to provide white, compact crystals. The product may be further purified via flash column chromatography (0 to 40% EtOAc in Hex elution gradient).

^{1}H NMR (700 MHz, $CDCl_3$): δ = 8.68 (bs, 1H), 8.59 (d, *J* = 8.5 Hz, 1H), 8.51 (d, *J* = 7.2 Hz, 1H), 8.16 (d, *J* = 8.1 Hz, 1H), 7.99 (d, *J* = 8.1 Hz, 1H), 7.70 (t, *J* = 7.6 Hz, 1H), 7.63 (dd, *J* = 12.5, 7.3 Hz, 2H), 2.03 (s, 3H) ppm

^{13}C NMR (176 MHz, $CDCl_3$): δ = 168.1, 135.8, 134.2, 133.0, 132.1, 129.4, 128.9, 128.0, 127.1, 124.2, 123.6, 23.4 ppm

R_f (4:6 – EtOAc:Hex) = 0.3

IR (*neat*): 3246, 1730, 1441, 1410, 1372, 1328, 1215, 1127, 760, 734 cm^{-1}

HRMS (ESI+) *m/z* calculated for $C_{12}H_{11}NO_3S$ $[M+H]^+$ 250.0532, found 250.0529

ethyl (naphthalen-1-ylsulfonyl)carbamate (S2)

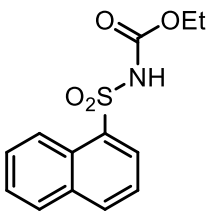

To a 100 mL round bottom flask charged with a magnetic stir bar was added naphthalene-1-sulfonamide (1 g, 4.83 mmol), DMAP (29.5 mg, 0.24 mmol), CH_2Cl_2 (30 mL), and ethyl chloroformate (0.59 mL, 6.27 mmol). The whole was cooled to 0 °C then triethylamine (0.74 mL, 5.31 mmol) was added dropwise via syringe. The reaction slowly went from a white, heterogeneous mixture to a clear colorless, homogenous solution. The reaction was gradually warmed to rt and monitored by TLC (50% EtOAc in Hex). After 2 h, the reaction was concentrated under reduced pressure to give a light yellow oil. This crude mixture was diluted with EtOAc (30 mL) then washed 3 x with 1 N HCl (10 mL). The organics were washed with brine, dried over sodium sulfate, and filtered to give a white solid. Purification by flash column chromatography (10 to 40% EtOAc in Hex elution gradient) provided the title substrate as a compact white solid (782 mg, 59%).

^{1}H NMR (700 MHz, $CDCl_3$): δ = 8.60 (d, *J* = 8.6 Hz, 1H), 8.49 (d, *J* = 7.4 Hz, 1H), 8.15 (d, *J* = 8.2 Hz, 1H), 7.98 (d, *J* = 8.1 Hz, 1H), 7.80 (s, 1H), 7.70 (t, *J* = 7.7 Hz, 1H), 7.62 (dt, *J* = 12.1, 7.5 Hz, 2H), 4.04 (q, *J* = 7.1 Hz, 2H), 1.11 (t, *J* = 7.1 Hz, 3H) ppm

^{13}C NMR (176 MHz, $CDCl_3$): δ = 150.2, 135.7, 134.1, 132.8, 132.4, 129.3, 128.8, 128.0, 127.0, 124.1, 123.9, 63.1, 13.9 ppm

R_f (5:5 – EtOAc:Hex) = 0.5

IR (*neat*): 3081, 1712, 1507, 1476, 1352, 1309, 1167, 1139, 917, 802, 766 cm^{-1}

HRMS (ESI+) *m/z* calculated for $C_{13}H_{13}NO_4S$ [M+H]+ 280.0368, found 260.0634.

tert-butyl (naphthalen-1-ylsulfonyl)carbamate (S3)

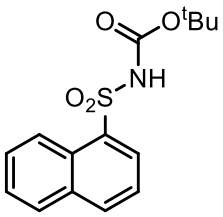

To a 50 mL round bottom flask charged with a magnetic stir bar was added naphthalene-1-sulfonamide (1 g, 4.83 mmol), DMAP (58.9 mg, 0.483 mmol), CH_2Cl_2 (30 mL), and BOC anhydride (1.22 mL, 5.31 mmol). The whole was cooled to 0 °C then triethylamine (0.74 mL, 5.31 mmol) was added dropwise via syringe. The reaction slowly went from a cloudy white color to clear. The whole was slowly warmed to rt and monitored by TLC (50% EtOAc in Hex). After 2 h, the reaction was concentrated under reduced pressure to give a light yellow oil. This crude mixture was diluted with EtOAc (30 mL) then washed 3 x with 1 N HCl (10 mL). The organics were washed with brine, dried over sodium sulfate, and filtered to give a white solid. Purification by flash column chromatography (10 to 40% EtOAc in Hex elution gradient) provided the title substrate as a compact white solid (1.02 g, 69%).

^{1}H NMR (700 MHz, $CDCl_3$): δ = 8.58 (d, *J* = 8.6 Hz, 1H), 8.45 (d, *J* = 7.2 Hz, 1H), 8.15 (d, *J* = 8.2 Hz, 1H), 7.97 (d, *J* = 8.1 Hz, 1H), 7.69 (t, *J* = 7.5 Hz, 1H), 7.63 − 7.59 (m, 3H), 1.27 (s, 9H) ppm

^{13}C NMR (176 MHz, $CDCl_3$): δ = 149.0, 135.4, 134.1, 133.2, 132.1, 129.2, 128.7, 128.0, 126.9, 124.0, 123.9, 84.3, 27.7 ppm

R_f (5:5 – EtOAc:Hex) = 0.5

IR (*neat*): 3073, 2982, 1701, 1354, 1332, 1134, 804, 777 cm^{-1}

HRMS (ESI+) *m/z* calculated for $C_{15}H_{17}NO_4S$ [M+H]+ 308.0951, found 308.0947.

2,2,2-trifluoro-N-(naphthalen-1-ylsulfonyl)acetamide (S4)

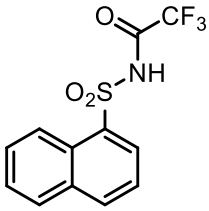

To a 100 mL round bottom flask charged with a magnetic stir bar was added naphthalene-1-sulfonamide (1 g, 4.83 mmol), DMAP (58.9 mg, 0.483 mmol), CH2Cl2 (40 mL), and TFAA (0.783 mL, 5.31 mmol). The whole was cooled to 0 °C then triethylamine (0.74 mL, 5.31 mmol) was added dropwise via syringe. The reaction slowly went from a cloudy white color to clear. The whole was slowly warmed to rt and monitored by TLC (50% EtOAc in Hex). After 4 h, the reaction was concentrated under reduced pressure to give a light yellow oil. This crude mixture was diluted with EtOAc (30 mL) then washed 3 x with 1 N HCl (10 mL). The organics were washed with brine, dried over sodium sulfate, and filtered to give a white solid. Purification by flash column chromatography (10 to 40% EtOAc in Hex elution gradient) provided the title substrate as a compact white solid (1.28 g, 88%)

^{1}H NMR (400 MHz, DMSO-d_6): δ = 11.06 (bs, 1H), 8.68 (d, *J* = 8.0 Hz, 1H), 8.14 – 8.01 (m, 2H), 7.98 (d, *J* = 7.4 Hz, 1H), 7.72 – 7.40 (m, 3H) ppm

^{13}C NMR (176 MHz, DMSO-d_6): δ = 159.9 (q, *J* = 32.9 Hz), 139.9, 133.6, 131.7, 128.3, 128.3, 127.4, 126.6, 126.1, 124.3, 117.6 (q, *J* = 291.4 Hz)

^{19}F NMR (377 MHz, DMSO-d_6) = δ -74.1 ppm

R_f (5:5 – EtOAc:Hex) = 0.3

IR (*neat*): 3209, 1762, 1508, 1452, 1362, 1201, 1108, 988, 765 cm^{-1}

HRMS (ESI+) *m/z* calculated for $C_{12}H_8F_3NO_3S$ [M+H]+ 326.0069, found 326.0066.

N-(thiophen-2-ylsulfonyl)acetamide (S5)

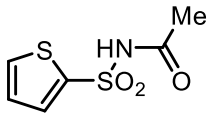

To a flame dried 250 mL round bottom flask charged with a magnetic stir bar was added thiophene-2-sulfonamide (3 g, 18.4 mmol), DMAP (22.5 mg, 0.184 mmol), CH_2Cl_2 (50 mL), and THF (10 mL). The reaction appears mostly heterogeneous. Then the reaction was cooled to 0 °C then via syringe was added pyridine (4.44 mL, 55.1 mmol) followed by acetic anhydride (6.95 mL, 73.5 mmol). The reaction was allowed to warm to rt and monitored by TLC (50% EtOAc in Hex). After 3 h, the reaction was concentrated under reduced pressure to give a light yellow oil. This crude mixture was diluted with EtOAc (30 mL) then washed 3 x with 1 N HCl (10 mL). The organics were washed with brine, dried over sodium sulfate, and filtered to give a white solid. Purification by flash column chromatography (10 to 50% EtOAc in Hex elution gradient) provided the title substrate as a compact white solid (2.57 g, 68%).

^{1}H NMR (700 MHz, $CDCl_3$): δ = 8.71 (s, 1H), 7.90 (dd, *J* = 3.8, 1.2 Hz, 1H), 7.71 (dd, *J* = 5.0, 1.2 Hz, 1H), 7.14 (dd, *J* = 4.9, 3.9 Hz, 1H), 2.13 (s, 3H) ppm

^{13}C NMR (176 MHz, $CDCl_3$): δ = 168.1, 138.6, 135.2, 134.2, 127.5, 23.6 ppm

R_f (5:5 – EtOAc:Hex) = 0.4

IR (*neat*): 3105, 1688, 1446, 1421, 1368, 1351, 1017, 999, 728 cm^{-1}

HRMS (EI) *m/z* calculated for $C_6H_7NO_3S_2$ [M^+] 204.9867, found 204.9871

methyl 3-(N-acetylsulfamoyl)thiophene-2-carboxylate (S6)

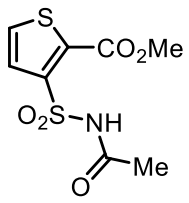

To a flame dried 100 mL round bottom flask charged with a magnetic stir bar was added methyl 3-sulfamoylthiophene-2-carboxylate (500 mg, 2.26 mmol), DMAP (2.76 mg, 0.0226 mmol), CH_2Cl_2 (35.0 mL), and THF (5.00 mL). The reaction appears mostly heterogeneous. The whole was cooled to 0 °C then via syringe was added pyridine (0.546 mL, 6.78 mmol) and acetic anhydride (0.854 mL, 9.04 mmol). The reaction was allowed to warm to rt and monitored by TLC (50% EtOAc in Hex). After 12 h, the reaction was concentrated under reduced pressure to give a light yellow oil. This crude mixture was diluted with EtOAc (30 mL) then washed 3 x with 1 N HCl (10 mL). The organics were washed with brine, dried over sodium sulfate, and filtered to give a white solid. Purification by flash column chromatography (10 to 50% EtOAc in Hex elution gradient) provided the title substrate as a compact white solid (512 mg, 86%).

^{1}H NMR (700 MHz, $CDCl_3$): δ = 8.92 (s, 1H), 7.72 (d, *J* = 5.2 Hz, 1H), 7.58 (d, *J* = 5.2 Hz, 1H), 3.95 (s, 3H), 2.15 (s, 3H) ppm

^{13}C NMR (176 MHz, $CDCl_3$): δ = 168.5, 160.3, 142.9, 132.6, 131.5, 130.4, 53.3, 23.6 ppm

R_f (5:5 – EtOAc:Hex) = 0.2

IR (*neat*): 3131, 1719, 1701, 1435, 1358, 1265, 1173, 1144, 898, 772 cm^{-1}

HRMS (ESI+) *m/z* calculated for $C_8H_9NO_5S_2Na$ $[M+Na]^+$ 285.9814, found 285.9818.

N-(quinolin-8-ylsulfonyl)acetamide (S7)

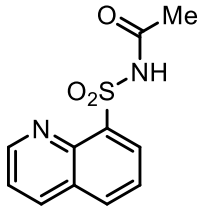

To a flame dried 250 mL round bottom flask charged with a magnetic stir bar was added quinoline-8-sulfonamide (1000 mg, 4.80 mmol), DMAP (5.87 mg, 0.0480 mmol), CH_2Cl_2 (35.0 mL), and THF (5.00 mL). The reaction appears mostly heterogeneous. The whole was cooled to 0 °C then via syringe was added pyridine (0.387 mL, 4.80 mmol) followed by acetic anhydride (1.82 mL, 19.2 mmol). The reaction was allowed to warm to rt and monitored by TLC (50% EtOAc in Hex). After 12 h, the reaction was diluted in 100 mL dH_2O. The white crystalline solid were filtered off and washed with cold acetone to provide the title substrate as a compact white solid (1.03 g, 86%).

^{1}H NMR (700 MHz, DMSO-d_3): δ = 12.32 (s, 1H), 9.10 (m, 1H), 8.57 (d, *J* = 8.1 Hz, 1H), 8.46 (d, *J* = 8.1 Hz, 1H), 8.35 (d, *J* = 8.1 Hz, 1H), 7.80 (t, *J* = 7.7 Hz, 1H), 7.72 (dd, *J* = 8.2, 4.1 Hz, 1H), 1.88 (s, 3H) ppm

^{13}C NMR (176 MHz, DMSO-d_3): δ = 169.0, 151.5, 142.8, 137.1, 135.2, 134.7, 133.1, 128.5, 125.6, 122.6, 23.1 ppm

R_f (5:5 – EtOAc:Hex) = 0.3

IR (*neat*): 3003, 2818, 1713, 1499, 1457, 1330, 1166, 1139, 995, 973 cm^{-1}

HRMS (ESI+) *m/z* calculated for $C_{11}H_{10}N_2O_3S$ $[M+H]^+$ 251.0485, found 251.0484.

N-(naphthalen-2-ylsulfonyl)acetamide (S8)

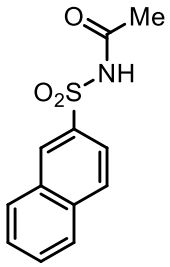

To a flame dried 100 mL round bottom flask equipped with a magnetic stir bar was added naphthalene-1-sulfonamide (1 g, 4.83 mmol), DMAP (6 mg, 1 mol%), CH_2Cl_2 (35 mL), and THF (6 mL). The reaction mixture at this point appears mostly heterogeneous. Then the reaction was cooled to 0 °C and via syringe was added pyridine (777 uL, 9.65 mmol, 2 equiv) followed by acetic anhydride (1.82 mL, 19.3 mmol, 4 equiv). The whole slowly became more homogeneous over a few minutes. The reaction was slowly allowed to warm to rt while stirring overnight (12 h). Upon completion of the reaction as judged by TLC analysis (40% EtOAc in Hex), the reaction was diluted in 20 mL dH2O, layers separated and the aqueous phase washed with 20 mL CH_2Cl_2. The organic layer was combined and rinsed with 1 N HCl (2 x 20 mL), brine, dried over sodium sulfate, filtered and concentrated *in vacuo* to provide a white powder. The material may be further purified via flash column chromatography (0 to 40% EtOAc in Hex elution gradient) to provide the title substrate as a compact white solid (848 mg, 78%).

^{1}H NMR (700 MHz, $CDCl_3$): δ = 8.67 (bm, 2H), 8.02 (d, *J* = 8.2 Hz, 1H), 7.99 (s, 2H), 7.93 (d, *J* = 8.2 Hz, 1H), 7.68 (t, *J* = 7.5 Hz, 1H), 7.63 (t, *J* = 7.5 Hz, 1H), 2.09 (s, 3H) ppm

^{13}C NMR (176 MHz, $CDCl_3$): δ = 168.0, 135.5, 135.1, 131.9, 130.5, 129.6, 129.5, 129.4, 127.9, 127.8, 122.5, 23.5 ppm

R_f (5:5 – EtOAc:Hex) = 0.3

IR (*neat*): 3274, 1719, 1436, 1412, 1328, 1150, 1126, 994, 877, 747 cm^{-1}

HRMS (ESI+) *m/z* calculated for $C_{12}H_{11}NO_3S$ $[M+H]^+$ 272.0352, found 272.0353.

methyl 5-(N-acetylsulfamoyl)furan-2-carboxylate (S9)

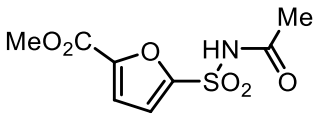

To a flame dried 100 mL round bottom flask equipped with a magnetic stir bar was added methyl 5-sulfamoylfuran-2-carboxylate (184 mg, 0.897 mmol), DMAP (1.10 mg, 0.00897 mmol), CH_2Cl_2 (20.0 mL), and THF (5.00 mL). The reaction mixture at this point appears mostly heterogeneous. Then the reaction was cooled to 0 °C and via syringe was added pyridine (0.217 mL, 2.69 mmol) followed by acetic anhydride (0.339 mL, 3.59 mmol). The whole slowly became more homogeneous over a few minutes. The reaction was slowly allowed to warm to rt while stirring for 3 h. Upon completion of the reaction as judged by TLC analysis (50% EtOAc in Hex), the reaction was concentrated under reduced pressure to give a light yellow oil. This crude mixture was diluted with CH_2Cl_2 (15 mL) then washed 3 x with 1 N HCl (10 mL). The organics were washed with brine, dried over sodium sulfate, and filtered to give a white solid. Purification by flash column chromatography (10 to 50% EtOAc in Hex elution gradient) provided the title substrate as a compact white solid (172 mg, 78%).

^{1}H NMR (700 MHz, $CDCl_3$): δ = 8.89 (s, 1H), 7.38 (d, *J* = 3.6 Hz, 1H), 7.24 (d, *J* = 3.6 Hz, 1H), 3.93 (s, 3H), 2.17 (s, 3H) ppm

^{13}C NMR (176 MHz, $CDCl_3$): δ = 168.0, 158.0, 148.9, 147.3, 120.3, 118.0, 52.8, 23.6 ppm

R_f (5:5 – EtOAc:Hex) = 0.2

IR (*neat*): 3303, 3159, 1732, 1574, 1431, 1355, 1040, 917 cm^{-1}

HRMS (ESI+) *m/z* calculated for $C_8H_9NO_6S$ $[M+H]^+$ 265.0489, found 265.0488.

N-(thiophen-3-ylsulfonyl)acetamide (S10)

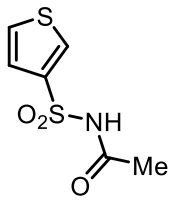

To a flame dried 100 mL round bottom flask equipped with a magnetic stir bar was added thiophene-3-sulfonamide (1000 mg, 6.13 mmol), DMAP (7.48 mg, 0.0613 mmol), CH_2Cl_2 (35.0 mL), and THF (5.0 mL). The reaction mixture at this point appears mostly heterogeneous. Then the reaction was cooled to 0 °C and via syringe was added pyridine (1.48 mL, 18.4 mmol) followed by acetic anhydride (2.32 mL, 24.5 mmol). The whole slowly became more homogeneous over a few minutes. The reaction was slowly allowed to warm to rt while stirring for 12 h. Upon completion of the reaction as judged by TLC analysis (50% EtOAc in Hex), the reaction was concentrated under reduced pressure to give a light yellow oil. This crude mixture was diluted with CH_2Cl_2 (25 mL) then washed 3 x with 1 N HCl (20 mL). The organics were washed with brine, dried over sodium sulfate, and filtered to give a white solid. Purification by flash column chromatography (10 to 50% EtOAc in Hex elution gradient) provided the title substrate as a compact white solid (1.12 g, 89%).

^{1}H NMR (700 MHz, $CDCl_3$): δ = 8.78 (s, 1H), 8.32 – 8.20 (m, 1H), 7.60 – 7.48 (m, 1H), 7.44 (dd, *J* = 5.1, 3.1 Hz, 1H), 2.11 (s, 3H) ppm

^{13}C NMR (176 MHz, $CDCl_3$): δ = 168.3, 138.0, 133.7, 127.8, 126.1, 23.6 ppm

R_f (5:5 – EtOAc:Hex) = 0.3

IR (*neat*): 3070, 2867, 1691, 1460, 1417, 1346, 1235, 1157, 788 cm^{-1}

HRMS (ESI+) *m/z* calculated for $C_6H_7NO_3S_2Na$ $[M+Na]^+$ 227.9760, found 227.9757.

N-((5-chlorothiophen-2-yl)sulfonyl)acetamide (S11)

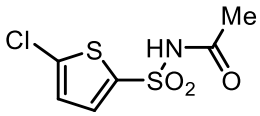

To a flame dried 100 mL round bottom flask equipped with a magnetic stir bar was added 5-chlorothiophene-2-sulfonamide (500 mg, 2.53 mmol), DMAP (3.09 mg, 0.0253 mmol), CH_2Cl_2 (35.0 mL), and THF (5.00 mL). Then the reaction was cooled to 0 °C and via syringe was added pyridine (0.611 mL, 7.59 mmol) followed by acetic anhydride (0.956 mL, 10.1 mmol). The whole slowly became more homogeneous over a few minutes. The reaction was slowly allowed to warm to rt while stirring for 12 h. Upon completion of the reaction as judged by TLC analysis (50% EtOAc in Hex), the reaction was concentrated under reduced pressure to give a light yellow oil. This crude mixture was diluted with CH_2Cl_2 (25 mL) then washed 3 x with 1 N HCl (20 mL). The organics were washed with brine, dried over sodium sulfate, and filtered to give a white solid. Purification by flash column chromatography (10 to 50% EtOAc in Hex elution gradient) provided the title substrate as a compact white powder (486 mg, 77%).

^{1}H NMR (700 MHz, $CDCl_3$): δ = 8.69 (s, 1H), 7.69 (d, *J* = 4.1 Hz, 1H), 6.97 (d, *J* = 4.1 Hz, 1H), 2.14 (s, 3H) ppm

^{13}C NMR (176 MHz, $CDCl_3$): δ = 168.1, 140.0, 136.0, 134.7, 126.8, 23.6 ppm

R_f (5:5 – EtOAc:Hex) = 0.4

IR (*neat*): 3076, 2874, 1689, 1463, 1409, 1357, 1235, 1162, 1004, 990 cm^{-1}

HRMS (ESI+) *m/z* calculated for $C_6H_6ClNO_3S_2$ $[M+H]^+$ 239.9550, found 239.9548.

N-((5-bromothiophen-2-yl)sulfonyl)acetamide (S12)

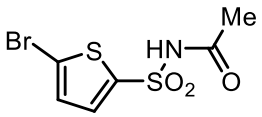

To a flame dried 100 mL round bottom flask equipped with a magnetic stir bar was added 5-bromothiophene-2-sulfonamide (1000 mg, 4.13 mmol), DMAP (5.05 mg, 0.0413 mmol), CH_2Cl_2 (35.0 mL), and THF (5.0 mL). Then the reaction was cooled to 0 °C and via syringe was added pyridine (1.0 mL, 12.4 mmol) followed by acetic anhydride (1.56 mL, 16.5 mmol). The whole slowly became more homogeneous over a few minutes. The reaction was slowly allowed to warm to rt while stirring for 12 h. Upon completion of the reaction as judged by TLC analysis (50% EtOAc in Hex), the reaction was concentrated under reduced pressure to give a light yellow oil. This crude mixture was diluted with CH_2Cl_2 (25 mL) then washed 3 x with 1 N HCl (20 mL). The organics were washed with brine, dried over sodium sulfate, and filtered to give a white solid. Purification by flash column chromatography (10 to 50% EtOAc in Hex elution gradient) provided the title substrate as a compact white powder (1.07 g, 91%).

^{1}H NMR (700 MHz, $CDCl_3$): δ = 8.62 (s, 1H), 7.64 (d, *J* = 4.1 Hz, 1H), 7.11 (d, *J* = 4.1 Hz, 1H), 2.13 (s, 3H) ppm

^{13}C NMR (176 MHz, $CDCl_3$): δ = 168.0, 138.9, 135.4, 130.4, 122.7, 23.6 ppm

R_f (5:5 – EtOAc:Hex) = 0.3

IR (*neat*): 3301, 1713, 1412, 1395, 1209, 1155, 1025, 799, 678 cm^{-1}

HRMS (ESI+) *m/z* calculated for $C_6H_6BrNO_3S_2$ $[M+Na]^+$ 305.8865, found 305.8869.

N-(benzo[d]thiazol-2-ylsulfonyl)acetamide (S13)

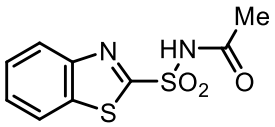

To a flame dried 100 mL round bottom flask equipped with a magnetic stir bar was added 1,3-benzothiazole-2-sulfonamide (294 mg, 1.37 mmol), DMAP (1.68 mg, 0.0137 mmol), CH_2Cl_2 (35.0 mL), and THF (5.0 mL). Then the reaction was cooled to 0 °C and via syringe was added pyridine (0.322 mL, 4.12 mmol) followed by acetic anhydride (0.519 mL, 5.49 mmol). The whole slowly became more homogeneous over a few minutes. The reaction was slowly allowed to warm to rt while stirring for 12 h. Upon completion of the reaction as judged by TLC analysis (50% EtOAc in Hex), the reaction was concentrated under reduced pressure to give a light yellow oil. This crude mixture was diluted with CH_2Cl_2 (25 mL) then washed 3 x with 1 N HCl (20 mL). The organics were washed with brine, dried over sodium sulfate, and filtered to give a white solid. Purification by flash column chromatography (10 to 50% EtOAc in Hex elution gradient) provided the title substrate as a compact white solid (443 mg, 99%).

^{1}H NMR (700 MHz, DMSO-d_6): δ = 13.06 (s, 1H), 8.31 (d, *J* = 7.8 Hz, 1H), 8.23 (d, *J* = 7.9 Hz, 1H), 7.75 – 7.61 (m, 2H), 2.04 (s, 3H) ppm

^{13}C NMR (176 MHz, DMSO-d_6): δ = 169.7, 165.4, 151.4, 136.3, 128.1, 127.9, 124.7, 123.3, 23.4 ppm

R_f (5:5 – EtOAc:Hex) = 0.1

IR (*neat*): 3022, 2855, 1726, 1484, 1358, 1162, 1132, 1094, 994 cm^{-1}

HRMS (ESI+) *m/z* calculated for $C_9H_8N_2O_3S_2$ $[M+H]^+$ 257.0049, found 257.0052.

4.4.3.3 *p*-methoxybenzene alkenes

1-methoxy-4-vinylbenzene (4.196)

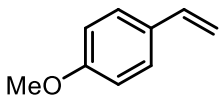

Vinyl-anisole was purchased from Sigma Aldrich (97%, item # 141003) and was distilled under hi-vac (~ 13 mbar), at 60 °C. It was then stored in the dark, under argon in a 4 dram vial for the remainder of the work.

***(*E)-1-methoxy-4-(prop-1-en-1-yl)benzene (A1)**

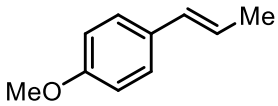

trans-Anethole was purchased from AK Scientific (98%, item # X8716) and was used as received. The material was stored in the dark and under argon when not in use.

1-(cyclopent-1-en-1-yl)-4-methoxybenzene (A2)

The following procedure was followed according to that reported in the literature for the preparation of the title substrate.

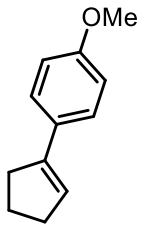

$CeCl_3 \cdot 7H_2O$ (2218 mg, 9.00 mmol) was quickly ground to a fine powder in a mortar, placed in a three-neck 250 mL round bottom flask and dried at 140 °C for 2 h. At rt, nitrogen gas was introduced, and anhydrous THF (25 mL) was added with vigorous stirring. The suspension was stirred for 1.5 h at rt. To a cold (-78 °C) and stirred solution of 4-Bromoanisole (0.828 mL, 6.60 mmol) in anhydrous THF (25 mL) was added 1.6 M nBuLi in hexanes (4.50 mL, 7.20 mmol). This solution was stirred at -78 °C for 1.5 h then added to the cold (-78 °C) suspension of $CeCl_3$ in THF. The resulting solution was stirred at -78 °C for 1 h. Cyclopentanone (0.531 mL) 6.00 mmol) dissolved in anhydrous THF (5 mL) was added to the corresponding organocerium reagent. The resulting mixture was stirred at -78 °C for 1h then at rt for 1 h. At -30 °C, after dilution with anhydrous THF (20 mL), DBU (2.32 mL, 10.5 mmol, 3 equiv) then MsCl (1.39 mL, 10.5 mmol, 3 equiv) were added dropwise. The reaction mixture was then allowed to warm to rt and stirred overnight. At 0 °C, aqueous HCl 1 M (15 mL) was added and the solution was stirred for 1 h. The aqueous layer was extracted with Et_2O (3 x 30 mL). The resulting organic layer was washed with aqueous NaOH 2 M (10 mL), water (10 mL), brine (10 mL), dried over sodium sulfate and the solvent evaporated to provide a light yellow oil. The residue was purified by flash column chromatography on silica gel using a 0 to 1% EtOAc in Hex elution gradient to provide the desired olefin as a white fluffy powder (616 mg, 59%).

All analytical data matches that reported in the literature.[268]

^{1}H NMR (700 MHz, $CDCl_3$): δ = 7.38 (d, *J* = 8.7 Hz, 2H), 6.86 (d, *J* = 8.7 Hz, 2H), 6.08 – 5.99 (m, 1H), 3.81 (s, 3H), 2.68 (td, *J* = 7.8, 2.1 Hz, 2H), 2.52 (td, *J* = 7.7, 2.3 Hz, 2H), 2.08 – 1.95 (m, 2H) ppm

^{13}C NMR (176 MHz, $CDCl_3$): δ = 158.5, 141.8, 129.7, 126.7, 123.9, 113.6, 55.3, 33.3, 33.2, 23.4 ppm

R_f (1:9 – EtOAc:Hex) = 0.6

IR (*neat*): 2951, 2894, 2841, 1707, 1601, 1510, 1309, 1252, 1180, 1030 cm^{-1}

HRMS (EI) *m/z* calculated for $C_{12}H_{14}O$ [M+] 174.1045, found 174.1042.

1-(4-methoxyphenyl)cyclohept-1-ene (A3)[1]

The following procedure was followed according to that reported in the literature for the preparation of the title substrate.

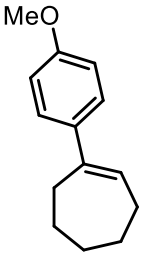

$CeCl_3 \cdot 7H_2O$ (2218 mg, 9.00 mmol) was quickly ground to a fine powder in a mortar, placed in a three-neck 250 mL round bottom flask and dried at 140 °C for 2 h. At rt, nitrogen gas was introduced, and anhydrous THF (25 mL) was added with vigorous stirring. The suspension was stirred for 1.5 h at rt. To a cold (-78 °C) and stirred solution of 4-Bromoanisole (0.828 mL, 6.60 mmol) in anhydrous THF (25 mL) was added 1.6 M nBuLi in hexanes (4.50 mL, 7.20 mmol). This solution was stirred at -78 °C for 1.5 h then added to the cold (-78 °C) suspension of $CeCl_3$ in THF. The resulting solution was stirred at -78 °C for 1 h. Cycloheptanone (0.709 mL, 6.00 mmol) dissolved in anhydrous THF (5 mL) was added to the corresponding organocerium reagent. The resulting mixture was stirred at -78 °C for 1 h then at rt for 1 h. At -30 °C, after dilution with anhydrous THF (20 mL), DBU (2.32 mL, 10.5 mmol, 3 equiv) then MsCl (1.39 mL, 10.5 mmol, 3 equiv) were added dropwise. The reaction mixture was then allowed to warm to rt and stirred overnight. At 0 °C, aqueous HCl 1 M (15 mL) was added and the solution was stirred for 1 h. The aqueous layer was extracted with Et_2O (3 x 30 mL). The resulting organic layer was washed with aqueous NaOH 2 M (10 mL), water (10 mL), brine (10 mL), dried over sodium sulfate and the solvent evaporated to provide a light yellow oil. The residue was purified by flash column chromatography on silica gel using a 0 to 1% EtOAc in Hex elution gradient to provide the desired olefin as a colorless oil (655 mg, 54%).

All analytical data matches that reported in the literature.[1]

^{1}H NMR (700 MHz, $CDCl_3$): δ = 7.27 (d, *J* = 8.7 Hz, 2H), 6.85 (d, *J* = 8.6 Hz, 2H), 6.03 (t, *J* = 6.7 Hz, 1H), 3.81 (s, 3H), 2.64 – 2.54 (m, 2H), 2.28 (dd, *J* = 11.0, 6.5 Hz, 2H), 1.84 (dt, *J* = 11.8, 6.0 Hz, 2H), 1.64 (dt, *J* = 11.3, 5.8 Hz, 2H), 1.56 (dt, *J* = 11.3, 5.9 Hz, 2H) ppm

^{13}C NMR (176 MHz, $CDCl_3$): δ = 158.2, 144.3, 137.5, 128.8, 126.7, 113.4, 55.3, 32.8, 32.7, 28.8, 26.9, 26.8 ppm

R_f (1:9 – EtOAc:Hex) = 0.8

IR (*neat*): 2916, 2834, 1606, 1509, 1489, 1286, 1242, 1177, 1032 cm^{-1}

HRMS (ESI+) *m/z* calculated for $C_{14}H_{18}O$ [M+H]+ 203.1430, found 203.1424.

N-[(E)-3-(4-methoxyphenyl)allyl]-4-methyl-N-phenacyl-benzenesulfonamide (A4)

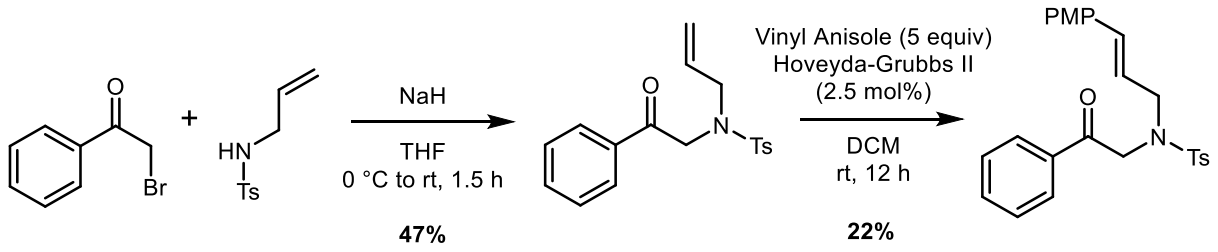

To a flame dried 50 mL round bottom flask charged with a magentic stir bar was added *N*-allyl-4-methyl-benzenesulfonamide (637 mg, 3.01 mmol, 1.2 equiv) 5 mL of DMF. To this, NaH (60.0 %, 86.6 mg, 2.26 mmol, 0.9 equiv) was added portion-wise to the flask and the sulfonamide was allowed to react at 0 °C for 30 minutes. After this time, 2-bromo-1-phenyl-ethanone (500 mg, 2.51 mmol, 1 equiv), was diluted separately in 6 mL of DMF and transferred to the reaction via syringe at 0 °C. The reaction was slowly allowed to warm to room temperature over 1 h, and then quenched with 7 mL of aqueous 5% citric acid and 7 mL of 10% sodium thiosulfate at 0 °C. The mixture was then transferred to a separatory funnel and extracted 3 times with 50 mL of diethyl ether. The combined ether extracts were washed with saturated sodium bicarbonate solution, followed by 5% LiCl wash (equal volume). The combined organic fractions were dried over sodium sulfate and then concentrated *in vacuo* to provide a crude dark oil which was purified by silica gel chromatography (30% EtOAc in Hexanes). *N*-allyl-4-methyl-*N*-phenacyl-benzenesulfonamide isolated in 47% yield (396 mg), and corresponded to literature characterization.[269]

To a flame dried 25 mL round bottom flask charged with a magnetic stir bar was added *N*-allyl-4-methyl-*N*-phenacyl-benzenesulfonamide (100 mg, 0.304 mmol), 6 mL of dry CH_2Cl_2, followed by 1-methoxy-4-vinyl-benzene (202 µL, 1.52 mmol, 5 equiv). The reaction was sparged by an argon line for 5 minutes. Then Hoveyda-Grubbs II (CAS No. 301224-40-8) (4.76 mg, 0.00759 mmol, 2.5 mol %) was added, the flask was flushed with argon and then the reaction was capped

and allowed to stir for 12 hours. Following this time, the crude mixture was pushed through a celite plug and concentrated to provide the crude residue. The material was purified by silica gel chromatography (3:7 ethyl acetate/Hexanes), and the stilbene impurity was triturated out with cold ether, after concentrating to yield 29 mg of the title product (22%).

^{1}H NMR (700 MHz, $CDCl_3$) δ = 7.89 (d, J = 8.0 Hz, 2H), 7.79 (d, J = 8.1 Hz, 2H), 7.58 (t, J = 7.4 Hz, 1H), 7.45 (t, J = 7.6 Hz, 2H), 7.33 (d, J = 8.2 Hz, 2H), 7.17 (d, J = 8.6 Hz, 2H), 6.33 (d, J = 15.8 Hz, 1H), 6.33 (d, J = 15.8 Hz, 1H), 5.88 (dt, J = 14.6, 7.0 Hz, 1H), 5.88 (dt, J = 14.6, 7.0 Hz, 1H), 4.76 (s, 2H), 4.05 (d, J = 7.0 Hz, 2H), 3.80 (s, 3H), 2.45 (s, 3H) ppm

^{13}C NMR (176 MHz, $CDCl_3$) δ = 194.2, 159.5, 143.4, 136.9, 134.9, 134.4, 133.7, 129.6, 128.7, 128.7, 128.0, 127.7, 127.5, 121.0, 113.9, 55.3, 51.9, 50.5, 21.6 ppm

R_f (3:7 – EtOAc:Hex) = 0.3

IR (*neat*): = 2932, 2836, 2254, 1699, 1606, 1579, 1510, 1448, 1420, 1334, 1304, 1249, 1224, 1174, 1154, 1092, 1059, 1032, 1001, 971, 906, 856, 839, 812, 729, 689, 668, 607

HRMS (ESI+): predicted $[M+Na]^+$ 458.1397, observed 458.1389.

4.4.3.4 Aminoarylation Products

N-(2-(4-methoxyphenyl)-2-(naphthalen-1-yl)ethyl)acetamide (4.201)

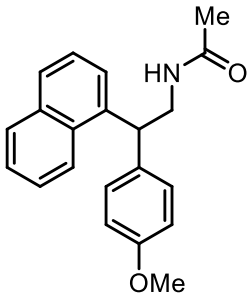

The **General Procedure** was followed performing the reaction with *N*-(1-naphthylsulfonyl)acetamide (75 mg, 0.3 mmol) and 1-methoxy-4-vinyl-benzene (48 μL, 0.36 mmol) and purification by flash column chromatography (SiO_2, 90:10→30:70 Hex:EtOAc) to furnish the title compound as a white fluffy powder (39 mg, 41%).

^{1}H NMR (700 MHz, $CDCl_3$): δ = 8.13 (d, *J* = 8.1 Hz, 1H), 7.88 – 7.81 (m, 1H), 7.77 (d, *J* = 8.1 Hz, 1H), 7.51 – 7.43 (m, 3H), 7.39 (d, *J* = 7.1 Hz, 1H), 7.19 (d, *J* = 8.6 Hz, 2H), 6.83 (d, *J* = 8.6 Hz, 2H), 5.53 (bs, 1H), 4.96 (t, *J* = 7.7 Hz, 2H), 4.03 (ddd, *J* = 13.6, 7.5, 6.0 Hz, 1H), 3.97 – 3.86 (m, 1H), 3.76 (s, 3H), 1.88 (s, 3H) ppm

^{13}C NMR (176 MHz, $CDCl_3$): δ = 170.1, 158.3, 137.5, 134.1, 133.9, 131.9, 129.1, 128.8, 127.6, 126.3, 125.7, 125.3, 124.2, 123.7, 114.1, 55.2, 45.1, 44.1, 23.3 ppm

R_f (5:5 – EtOAc:Hex) = 0.1

IR (*neat*): 2929, 1648, 1547, 1510, 1260, 1240, 1140, 1025, 781 cm^{-1}

HRMS (ESI) *m/z* calculated for $C_{21}H_{21}NO_2$ $[M+H]^+$ 320.1645, found 320.1645.

ethyl-(2-(4-methoxyphenyl)-2-(naphthalen-1-yl)ethyl)carbamate (4.202)

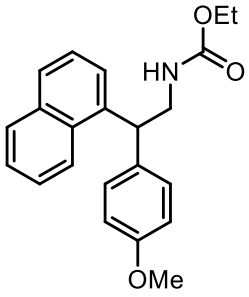

The **General Procedure** was followed performing the reaction with ethyl-*N*-(1-naphthylsulfonyl)carbamate (251 mg, 0.9 mmol) and 1-methoxy-4-vinyl-benzene (40 μL, 0.3 mmol) and purification by flash column chromatography (SiO_2, 90:10→30:70 Hex:EtOAc) to furnish the title compound as a light yellow fluffy powder (38 mg, 36%).

^{1}H NMR (500 MHz, $CDCl_3$): δ = 8.12 (d, *J* = 6.9 Hz, 1H), 7.84 (d, *J* = 8.5 Hz, 1H), 7.76 (d, *J* = 8.1 Hz, 1H), 7.46 (m, 3H), 7.38 (d, *J* = 7.0 Hz, 1H), 7.19 (d, *J* = 8.5 Hz, 2H), 6.83 (d, *J* = 8.6 Hz, 2H), 4.95 (bs, 1H), 4.73 (bs, 1H), 4.09 (m, 2H), 3.96 (dd, *J* = 13.4, 6.3 Hz, 1H), 3.90 – 3.79 (m, 1H), 1.19 (t, *J* = 6.5 Hz, 3H) ppm

^{13}C NMR (176 MHz, $CDCl_3$): δ = 158.3, 156.5, 137.5, 134.1, 133.9, 131.9, 129.2, 128.8, 127.6, 126.3, 125.6, 125.3, 124.1, 123.7, 114.1, 60.8, 55.2, 45.7, 45.5, 14.6 ppm

R_f (5:5 – EtOAc:Hex) = 0.1

IR (*neat*): 2931, 1693, 1609, 1509, 1244, 1177, 1032, 799, 729 cm^{-1}

HRMS (ESI+) *m/z* calculated for $C_{22}H_{23}NO_3$ $[M+H]^+$ 350.1751, found 350.1747.

tert-butyl-(2-(4-methoxyphenyl)-2-(naphthalen-1-yl)ethyl)carbamate (4.203)

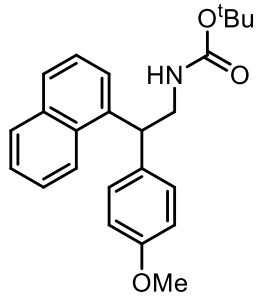

The **General Procedure** was followed performing the reaction with *t*-butyl-*N*-(1-naphthylsulfonyl)carbamate (277 mg, 0.9 mmol) and 1-methoxy-4-vinyl-benzene (40 μL, 0.3 mmol) and purification by flash column chromatography (SiO_2, 90:10→30:70 Hex:EtOAc) to furnish the title compound as a white fluffy powder (30 mg, 27%).

^{1}H NMR (700 MHz, $CDCl_3$): δ = 8.10 (d, *J* = 7.9 Hz, 1H), 7.84 (d, *J* = 8.0 Hz, 1H), 7.77 (d, *J* = 8.1 Hz, 1H), 7.50 – 7.44 (m, 3H), 7.42 (d, *J* = 6.6 Hz, 1H), 7.18 (d, *J* = 8.6 Hz, 2H), 6.82 (d, *J* = 8.3 Hz, 2H), 4.93 (t, *J* = 7.0 Hz, 1H), 4.62 (s, 1H), 3.89 (dd, *J* = 13.3, 6.3 Hz, 1H), 3.84 (dd, *J* = 12.9, 6.2 Hz, 1H), 3.76 (s, 3H), 1.41 (s, 9H) ppm

^{13}C NMR (176 MHz, $CDCl_3$): δ = 158.2, 155.8, 137.6, 134.1, 132.1, 129.2, 128.8, 127.5, 126.2, 125.6, 125.3, 124.1, 123.7, 114.0, 79.3, 55.2, 45.7, 45.2, 29.7, 28.4 ppm

R_f (5:5 – EtOAc:Hex) = 0.1

IR (*neat*): 2975, 1696, 1508, 1365, 1245, 1161, 1035, 799, 780 cm^{-1}

HRMS (ESI+) *m/z* calculated for $C_{24}H_{27}NO_3$ $[M+H]^+$ 378.2064, found 378.2049.

tert-butyl-1-(4-methoxyphenyl)-1-(naphthalen-1-yl)propan-2-yl)carbamate (4.203)

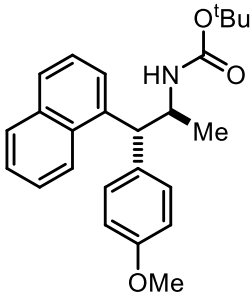

The **General Procedure** was followed performing the reaction with *t*-butyl-*N*-(1-naphthylsulfonyl)carbamate (277 mg, 0.9 mmol) and *trans*-anethole (45 μL, 0.3 mmol) and purification by flash column chromatography (SiO_2, 90:10→30:70 Hex:EtOAc) to furnish the title compound as a white fluffy powder (43 mg, 37%).

^{1}H NMR (700 MHz, $CDCl_3$): δ = 8.13 (d, *J* = 8.3 Hz, 1H), 7.82 (d, *J* = 7.9 Hz, 1H), 7.72 (d, *J* = 7.8 Hz, 2H), 7.50 (t, *J* = 7.6 Hz, 1H), 7.46 (t, *J* = 7.4 Hz, 1H), 7.42 (t, *J* = 7.3 Hz, 1H), 7.26 (d, *J* = 7.6 Hz, 2H), 6.78 (d, *J* = 8.2 Hz, 2H), 4.61 (s, 1H), 4.56 (d, *J* = 9.9 Hz, 1H), 4.33 (s, 1H), 3.72 (s, 3H), 1.33 (s, 9H), 1.18 (d, *J* = 5.7 Hz, 3H) ppm

^{13}C NMR (176 MHz, $CDCl_3$): δ = 158.1, 155.3, 137.5, 134.1, 132.0, 129.4, 128.9, 127.1, 125.9, 125.5, 125.2, 124.4, 123.3, 114.3, 113.9, 79.1, 55.1, 52.2, 49.3, 28.3, 21.1 ppm

R_f (5:5 – EtOAc:Hex) = 0.1

IR (*neat*): 2974, 2831, 1689, 1609 1509, 1452, 1365, 1247, 1162, 929, 782 cm^{-1}

HRMS (ESI+) *m/z* calculated for $C_{25}H_{29}NO_3$ $[M+H]^+$ 392.2220, found 392.2230.

N-1-(4-methoxyphenyl)-1-(naphthalen-1-yl)propan-2-yl)acetamide (4.207)

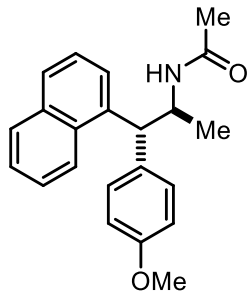

The **General Procedure** was followed performing the reaction with *N*-(1-naphthylsulfonyl)acetamide (75 mg, 0.3 mmol) and *trans*-anethole (54 μL, 0.36 mmol) and purification by flash column chromatography (SiO_2, 90:10→30:70 Hex:EtOAc) to furnish the title compound as a light yellow powder (82 mg, 82%).

^{1}H NMR (700 MHz, $CDCl_3$): δ = 8.14 (d, *J* = 8.5 Hz, 1H), 7.82 (d, *J* = 8.0 Hz, 1H), 7.73 (d, *J* = 8.2 Hz, 1H), 7.66 (d, *J* = 7.2 Hz, 1H), 7.50 (t, *J* = 7.7 Hz, 1H), 7.47 (td, *J* = 8.1, 7.1 Hz, 1H), 7.43 (t, *J* = 7.4 Hz, 1H), 7.25 (d, *J* = 8.5 Hz, 2H), 6.78 (d, *J* = 8.6 Hz, 2H), 5.22 (d, *J* = 7.8 Hz, 1H), 5.01 – 4.87 (m, 1H), 4.58 (d, *J* = 10.4 Hz, 1H), 3.72 (s, 3H), 1.74 (s, 3H), 1.17 (d, *J* = 6.3 Hz, 3H) ppm

^{13}C NMR (176 MHz, $CDCl_3$): δ = 169.4, 158.2, 137.1, 134.1, 133.7, 131.9, 129.5, 129.1, 127.3, 126.0, 125.6, 125.3, 124.2, 123.2, 113.9, 55.1, 51.9, 48.1, 23.4, 20.7 ppm

R_f (5:5 – EtOAc:Hex) = 0.1

IR (*neat*): 3089, 2929, 1637, 1509, 1370, 1302, 1249, 1177, 1031 cm^{-1}

HRMS (ESI+) *m/z* calculated for $C_{22}H_{23}NO_2$ $[M+H]^+$ 334.1802, found 334.1802.

N-1-(4-methoxyphenyl)-1-(naphthalen-2-yl)propan-2-yl)acetamide (4.208)

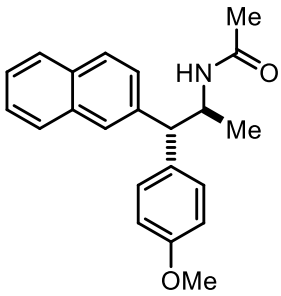

The **General Procedure** was followed performing the reaction with *N*-(2-naphthylsulfonyl)acetamide (75 mg, 0.3 mmol) and *trans*-anethole (54 μL, 0.36 mmol) and purification by flash column chromatography (SiO_2, 90:10→30:70 Hex:EtOAc) to furnish the title compound as a light yellow powder (78 mg, 78%).

^{1}H NMR (700 MHz, $CDCl_3$): δ = 7.79 (d, *J* = 8.0 Hz, 1H), 7.77 (d, *J* = 7.9 Hz, 1H), 7.75 (d, *J* = 8.6 Hz, 1H), 7.73 (m, 1H), 7.45 (td, *J* = 11.0, 3.9 Hz, 1H), 7.42 (t, *J* = 6.9 Hz, 1H), 7.38 (dd, *J* = 8.5, 1.2 Hz, 1H), 7.23 (d, *J* = 8.6 Hz, 2H), 6.82 (d, *J* = 8.7 Hz, 2H), 5.22 (d, *J* = 8.4 Hz, 1H), 5.01 – 4.87 (m, 1H), 3.97 (d, *J* = 9.7 Hz, 1H), 3.76 (s, 3H), 1.77 (s, 3H), 1.17 (d, *J* = 6.4 Hz, 3H) ppm

^{13}C NMR (176 MHz, $CDCl_3$): δ = 169.3, 158.3, 139.6, 134.2, 133.4, 132.2, 129.3, 128.3, 127.8, 127.5, 126.5, 126.4, 126.1, 125.6, 114.1, 57.2, 55.2, 47.5, 23.5, 20.3 ppm

R_f (5:5 – EtOAc:Hex) = 0.1

IR (*neat*): 3268, 2971, 1636, 1509, 1371, 1247, 1178, 1032, 915 cm^{-1}

HRMS (ESI+) *m/z* calculated for $C_{22}H_{23}NO_2$ $[M+H]^+$ 334.1802, found 334.1805.

N-1-(4-methoxyphenyl)-1-(thiophen-3-yl)propan-2-yl)acetamide (4.209)

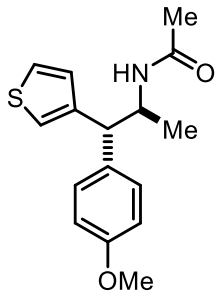

The **General Procedure** was followed performing the reaction with *N*-(3-thienylsulfonyl)acetamide (62 mg, 0.3 mmol) and *trans*-anethole (54 μL, 0.36 mmol) and purification by flash column chromatography (SiO_2, 90:10→30:70 Hex:EtOAc) to furnish the title compound as a light yellow powder (26 mg, 30%).

^{1}H NMR (700 MHz, $CDCl_3$): δ = 7.24 – 7.21 (m, 1H), 7.14 (d, *J* = 8.4 Hz, 2H), 7.09 (s, 1H), 6.93 (d, *J* = 4.8 Hz, 1H), 6.83 (d, *J* = 8.4 Hz, 2H), 5.20 (d, *J* = 8.1 Hz, 1H), 4.83 – 4.66 (m, 1H), 3.94 (d, *J* = 8.7 Hz, 1H), 3.78 (s, 3H), 1.87 (s, 3H), 1.07 (d, *J* = 6.5 Hz, 3H) ppm

^{13}C NMR (176 MHz, $CDCl_3$): δ = 169.2, 158.4, 142.8, 133.4, 129.5, 127.8, 125.6, 120.9, 113.9, 55.2, 52.2, 48.2, 23.6, 19.6 ppm

R_f (5:5 – EtOAc:Hex) = 0.1

IR (*neat*): 3325, 3000, 1628, 1511, 1373, 1251, 1032, 849, 796, 708 cm^{-1}

HRMS (ESI+) *m/z* calculated for $C_{16}H_{19}NO_2S$ $[M+H]^+$ 290.1209, found 290.1211.

methyl-2-acetamido-1-(4-methoxyphenyl)propyl)thiophene-2-carboxylate (4.210)

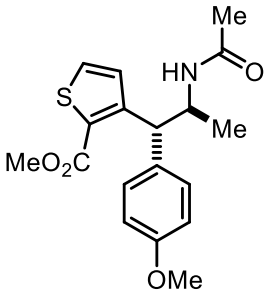

The **General Procedure** was followed performing the reaction with methyl 3-(acetylsulfamoyl)thiophene-2-carboxylate (79 mg, 0.3 mmol) and *trans*-anethole (54 μL, 0.36 mmol) and purification by flash column chromatography (SiO_2, 90:10→30:70 Hex:EtOAc) to furnish the title compound as a light yellow powder (92 mg, 89%).

^{1}H NMR (700 MHz, $CDCl_3$): δ = 7.36 (d, *J* = 5.2 Hz, 1H), 7.27 (d, *J* = 8.7 Hz, 2H), 7.15 (d, *J* = 5.2 Hz, 1H), 6.83 (d, *J* = 8.6 Hz, 2H), 5.86 (d, *J* = 9.0 Hz, 1H), 4.93 (d, *J* = 11.5 Hz, 1H), 4.86 – 4.65 (m, 1H), 3.89 (s, 3H), 3.77 (s, 3H), 1.75 (s, 3H), 1.12 (d, *J* = 6.4 Hz, 3H) ppm

^{13}C NMR (176 MHz, $CDCl_3$): δ = 169.1, 163.9, 158.4, 151.8, 133.1, 130.9, 129.5, 129.0, 126.2, 114.0, 55.2, 52.0, 49.6, 49.1, 23.3, 20.7 ppm

R_f (5:5 – EtOAc:Hex) = 0.1

IR (*neat*): 3289, 2941, 1718, 1639, 1585, 1512, 1445, 1226, 1104, 1075, 829 cm^{-1}

HRMS (ESI+) *m/z* calculated for $C_{18}H_{21}NO_4S$ $[M+H]^+$ 348.1264, found 348.1265.

N-1-(4-methoxyphenyl)-1-(thiophen-2-yl)propan-2-yl)acetamide (4.211)

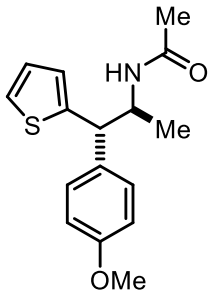

The **General Procedure** was followed performing the reaction with *N*-(2-thienylsulfonyl)acetamide (62 mg, 0.3 mmol) and *trans*-anethole (54 μL, 0.36 mmol) and purification by flash column chromatography (SiO_2, 90:10→30:70 Hex:EtOAc) to furnish the title compound as a light yellow powder (69 mg, 79%).

^{1}H NMR (700 MHz, $CDCl_3$): δ = 7.21 (d, *J* = 8.6 Hz, 2H), 7.15 (d, *J* = 4.9 Hz, 1H), 6.93 – 6.91 (m, 2H), 6.85 (d, *J* = 8.6 Hz, 2H), 5.31 (d, *J* = 8.3 Hz, 1H), 4.73 – 4.67 (m, 1H), 4.15 (d, *J* = 8.1 Hz, 1H), 3.79 (s, 3H), 1.89 (s, 3H), 1.11 (d, *J* = 6.6 Hz, 3H) ppm

^{13}C NMR (176 MHz, $CDCl_3$): δ = 169.3, 158.6, 145.6, 133.2, 129.5, 126.7, 124.9, 124.1, 113.9, 55.2, 51.6, 49.1, 23.5, 19.5 ppm

R_f (5:5 – EtOAc:Hex) = 0.1

IR (*neat*): 2987, 2983, 1638, 1538, 1512, 1373, 1282, 1030 cm^{-1}

HRMS (ESI+) *m/z* calculated for $C_{16}H_{19}NO_2S$ $[M+H]^+$ 290.1209, found 290.1209.

N-1-(5-chlorothiophen-2-yl)-1-(4-methoxyphenyl)propan-2-yl)acetamide (4.212)

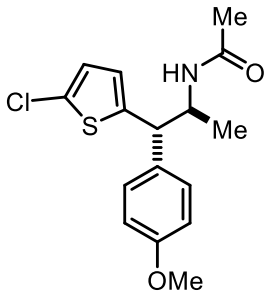

The **General Procedure** was followed performing the reaction with *N*-[(5-chloro-2-thienyl)sulfonyl]acetamide (72 mg, 0.3 mmol) and *trans*-anethole (54 μL, 0.36 mmol) and purification by flash column chromatography (SiO_2, 90:10→30:70 Hex:EtOAc) to furnish the title compound as a light yellow powder (67 mg, 69%).

^{1}H NMR (700 MHz, $CDCl_3$): δ = 7.17 (d, *J* = 8.6 Hz, 2H), 6.86 (d, *J* = 8.6 Hz, 2H), 6.71 (d, *J* = 3.8 Hz, 1H), 6.68 (d, *J* = 3.6 Hz, 1H), 5.30 (d, *J* = 8.5 Hz, 1H), 4.71 – 4.58 (m, 1H), 4.03 (d, *J* = 8.2 Hz, 1H), 3.79 (s, 3H), 1.92 (s, 3H), 1.09 (d, *J* = 6.6 Hz, 3H) ppm

^{13}C NMR (176 MHz, $CDCl_3$): δ = 169.3, 158.8, 144.6, 132.4, 129.5, 128.3, 125.6, 124.2, 114.1, 55.2, 51.9, 48.7, 23.6, 19.3 ppm

R_f (5:5 – EtOAc:Hex) = 0.1

IR (*neat*): 3275, 2985, 1652, 1585, 1511, 1484, 1249, 1034 cm^{-1}

HRMS (ESI+) *m/z* calculated for $C_{16}H_{18}ClNO_2S$ $[M+H]^+$ 324.0820, found 324.0819.

N-1-(5-bromothiophen-2-yl)-1-(4-methoxyphenyl)propan-2-yl)acetamide (4.213)

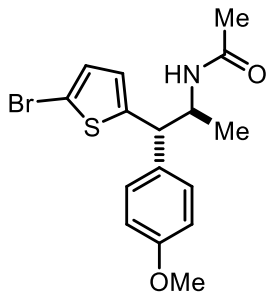

The **General Procedure** was followed performing the reaction with *N*-[(5-bromo-2-thienyl)sulfonyl]acetamide (85 mg, 0.3 mmol) and *trans*-anethole (54 μL, 0.36 mmol) and purification by flash column chromatography (SiO_2, 90:10→30:70 Hex:EtOAc) to furnish the title compound as a light yellow foam (49 mg, 45%).

^{1}H NMR (700 MHz, $CDCl_3$): δ = 7.17 (d, *J* = 8.5 Hz, 2H), 6.86 – 6.85 (m, 3H), 6.67 (d, *J* = 3.6 Hz, 1H), 5.27 (d, *J* = 7.4 Hz, 1H), 4.77 – 4.55 (m, 1H), 4.06 (d, *J* = 8.1 Hz, 1H), 3.79 (s, 3H), 1.92 (s, 3H), 1.09 (d, *J* = 6.6 Hz, 3H) ppm

^{13}C NMR (176 MHz, $CDCl_3$): δ = 169.3, 158.8, 147.5, 132.4, 129.5, 129.4, 125.2, 114.1, 110.5, 55.3, 51.9, 48.7, 23.6, 19.3 ppm

R_f (5:5 – EtOAc:Hex) = 0.1

IR (*neat*): 3313, 2930, 1627, 1511, 1446, 1372, 1281, 1222, 1175, 801 cm^{-1}

HRMS (ESI+) *m/z* calculated for $C_{16}H_{18}BrNO_2S$ $[M+H]^+$ 368.0314, found 368.0315.

Methyl-2-acetamido-1-(4-methoxyphenyl)propyl)furan-2-carboxylate (4.214)

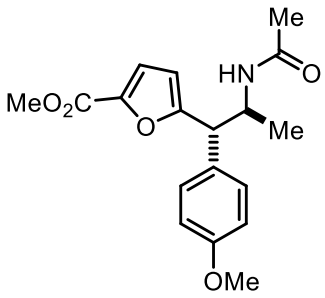

The **General Procedure** was followed performing the reaction with methyl 5-(acetylsulfamoyl)furan-2-carboxylate (74 mg, 0.3 mmol) and *trans*-anethole (54 μL, 0.36 mmol) and purification by flash column chromatography (SiO_2, 90:10→30:70 Hex:EtOAc) to furnish the title compound as a white solid (79 mg, 80%).

^{1}H NMR (700 MHz, $CDCl_3$): δ = 7.19 (d, *J* = 8.7 Hz, 2H), 7.09 (d, *J* = 3.5 Hz, 1H), 6.86 (d, *J* = 8.7 Hz, 2H), 6.29 (d, *J* = 3.4 Hz, 1H), 5.53 (d, *J* = 9.3 Hz, 1H), 4.77 – 4.60 (m, 1H), 4.05 (d, *J* = 8.2 Hz, 1H), 3.86 (s, 3H), 3.79 (s, 3H), 1.89 (s, 3H), 1.07 (d, *J* = 6.7 Hz, 3H) ppm

^{13}C NMR (176 MHz, $CDCl_3$): δ = 169.3, 160.4, 159.1, 158.9, 143.5, 130.1, 129.5, 119.1, 114.1, 109.3, 55.2, 51.8, 50.4, 48.2, 23.5, 19.5 ppm

R_f (5:5 – EtOAc:Hex) = 0.1

IR (*neat*): 3294, 2989, 1721, 1634, 1628, 1515, 1308, 1251, 1126, 1031, 826 cm^{-1}

HRMS (ESI+) *m/z* calculated for $C_{18}H_{21}NO_5$ $[M+H]^+$ 332.1492, found 332.1491.

N-1-(4-methoxyphenyl)-1-(quinolin-8-yl)propan-2-yl)acetamide (4.215)

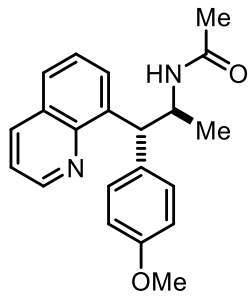

The **General Procedure** was followed performing the reaction with methyl *N*-(8-quinolylsulfonyl)acetamide (62 mg, 0.25 mmol) and *trans*-anethole (44 μL, 0.3 mmol) and purification by flash column chromatography (SiO_2, 90:10→30:70 Hex:EtOAc) to furnish the title compound as a light yellow foam (47 mg, 58%).

^{1}H NMR (700 MHz, $CDCl_3$): δ = 8.95 (d, *J* = 2.7 Hz, 1H), 8.16 (d, *J* = 8.1 Hz, 1H), 7.67 (d, *J* = 7.3 Hz, 1H), 7.65 (d, *J* = 8.0 Hz, 1H), 7.47 (t, *J* = 7.7 Hz, 1H), 7.42 (dd, *J* = 8.2, 4.1 Hz, 1H), 7.35 (d, *J* = 8.6 Hz, 2H), 6.83 (d, *J* = 8.6 Hz, 2H), 6.44 (s, 1H), 5.45 (d, *J* = 11.1 Hz, 1H), 4.89 – 4.76 (m, 1H), 3.76 (s, 3H), 1.48 (s, 3H), 1.25 (d, *J* = 6.3 Hz, 3H) ppm

^{13}C NMR (176 MHz, $CDCl_3$): δ = 169.1, 158.1, 149.2, 146.6, 141.1, 136.9, 134.2, 129.8, 128.8, 128.4, 126.8, 126.5, 120.8, 113.8, 55.2, 49.6, 48.9, 23.1, 21.0 ppm

R_f (5:5 – EtOAc:Hex) = 0.1

IR (*neat*): 3259, 2965, 1664, 1638, 1495, 1369, 1302, 1230, 1031, 930 cm^{-1}

HRMS (ESI+) *m/z* calculated for $C_{21}H_{22}N_2O_2$ $[M+H]^+$ 335.1754, found 335.1752.

N-1-(benzothiazol-2-yl)-1-(4-methoxyphenyl)propan-2-yl)acetamide (4.216)

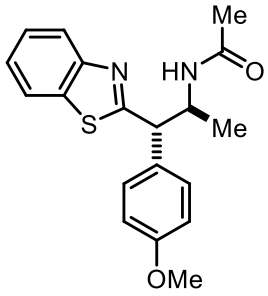

The **General Procedure** was followed performing the reaction with *N*-(1,3-benzothiazol-2-ylsulfonyl)acetamide (77 mg, 0.3 mmol) and *trans*-anethole (54 μL, 0.36 mmol) and purification by flash column chromatography (SiO_2, 90:10→30:70 Hex:EtOAc) to furnish the title compound as a light yellow solid (43 mg, 42%).

^{1}H NMR (700 MHz, $CDCl_3$): δ = 8.03 (d, *J* = 8.2 Hz, 1H), 7.83 (d, *J* = 8.0 Hz, 1H), 7.49 (t, *J* = 7.7 Hz, 1H), 7.38 (t, *J* = 7.6 Hz, 1H), 7.27 (d, *J* = 8.7 Hz, 2H), 6.90 (d, *J* = 8.3 Hz, 1H), 6.85 (d, *J* = 8.6 Hz, 2H), 4.76 (dq, *J* = 13.0, 6.4 Hz, 1H), 4.48 (d, *J* = 5.9 Hz, 1H), 3.78 (s, 3H), 1.91 (s, 3H), 1.27 (d, *J* = 6.7 Hz, 3H) ppm

^{13}C NMR (176 MHz, $CDCl_3$): δ = 171.9, 169.4, 159.0, 152.9, 134.9, 130.9, 129.4, 126.1, 125.1, 122.9, 121.6, 114.1, 55.2, 53.8, 49.7, 23.6, 20.1 ppm

R_f (5:5 – EtOAc:Hex) = 0.1

IR (*neat*): 3309, 2924, 1639, 1531, 1515, 1247, 1183, 1038, 832, 757 cm^{-1}

HRMS (ESI+) *m/z* calculated for $C_{19}H_{20}N_2O_2S$ $[M+H]^+$ 341.1318, found 341.1320.

N-(3-(4-methoxyphenyl)-5-phenylpent-4-en-2-yl)acetamide (4.217)

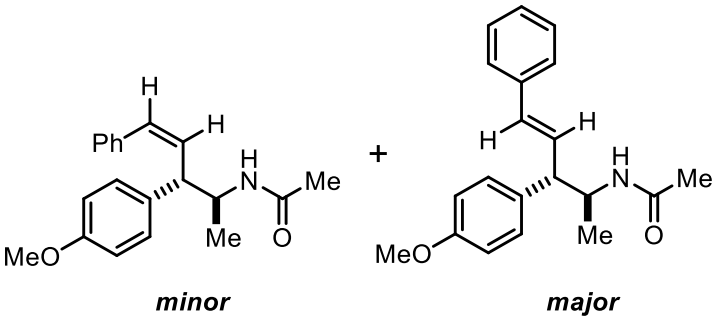

minor ***major***

The **General Procedure** was followed performing the reaction with N-[(E)-styryl]sulfonylacetamide (20.1 mg, 0.0894 mmol) and trans-anethole (13.3 mg, 0.0894 mmol)and purification by flash column chromatography (SiO_2, 30:70 Hex:EtOAc) to furnish the title compound (23 mg, 84%).

Major Diastereomer:

^{1}H NMR (700 MHz, $CDCl_3$) δ 1.94 (s, 3H), 1.06 (d, J=6.6 Hz, 3H), 3.39 (t, J= 8.2 Hz, 3H), 3.80 (s, 3H), 4.43-4.36 (m, 1H), 5.39 (d, J=6.2 Hz, 1H), 6.39 (dd,J = 15.8, 8.1 Hz, 1H), 6.44 (d, J = 15.8 Hz, 1H), 7.18-7.37 (m, 9H)

Minor diastereomer:

^{1}H NMR (700 MHz, CDCl3) δ 0.94 (d, J = 6.6 Hz, 3H), 1.92 (s, 3H), 3.66 (t, J = 9.83, 1H), 3.80 (s, 3H), 4.27 (m, 1H), 5.16 (d, J=8.45, 1H), 5.99 (t, J=11.2 Hz, 1H), 6.59 (d, J=11.6 Hz, 1H), 7.18-7.37 (m, 9H)

^{13}C NMR (mixture): ^{13}C NMR (176 mHz) = 169.4, 158.5, 158.4, 137.1, 137.0, 133.5, 133.0, 133.0, 131.3, 131.0, 130.1, 129.6, 129.1, 128.7, 128.5, 128.3, 127.3, 127.0, 126.2, 114.2, 114.1, 55.3, 54.9, 50.0, 49.5, 49.1, 23.6, 23.5, 18.8, 18.6.

R_f (7:3 – EtOAc:Hex) = 0.5

IR (*neat*): 3283.49, 2969.75, 2836.83 2244.71, 1651.05, 1610.54, 1550.33, 1511.58, 1449.98, 1372.41, 1301.84, 1250.84, 1178.35, 1147.47, 1034.90, 964.96, 908.96, 829.34, 732.09, 696.78, 650.44, 624.59, 607.50

HRMS (ESI+) *m/z* calculated for $C_{20}H_{23}NO_2$ $[M+H]^+$ was 310.1807, found 310.1805 m/z.

N-(1-(4-methoxyphenyl)-3-((4-methyl-N-(2-oxo-2-phenylethyl)phenyl)sulfonamido)-1-(naphthalen-1-yl)propan-2-yl)acetamide (4.218)

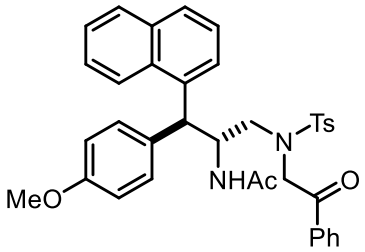

The **General Procedure** was followed performing the reaction with N-(1-naphthylsulfonyl)acetamide (18.9 mg, 0.0758 mmol) and *N*-[(*E*)-3-(4-methoxyphenyl)allyl]-4-methyl-*N*-phenacyl-benzenesulfonamide (33.0 mg, 0.0758 mmol) and purification by flash column chromatography (SiO_2, 30:70 Hex:EtOAc) to furnish the title compound (10 mg, 27%).

^{1}H NMR (700 MHz, $CDCl_3$) δ 8.16 (d, J = 8.6 Hz, 1H), 7.83 (d, J = 8.0 Hz, 2H), 7.80 (d, J = 8.0 Hz, 1H), 7.69 (d, J = 8.1 Hz, 1H), 7.62 – 7.55 (m, 4H), 7.45 (m, 5H), 7.22 (d, J = 8.2 Hz, 2H), 7.20 (d, J = 8.6 Hz, 2H), 6.69 (d, J = 8.6 Hz, 2H), 5.71 (d, J = 9.2 Hz, 1H, N-H), 5.13 (ddd, J = 20.1, 9.8, 3.8 Hz, 1H), 4.96, 4.81 (ABq, 2H, J_{AB} = 18.9) 4.87 (d, J = 9.9 Hz, 1H), 3.64 (dd, J = 15.1, 10.1 Hz, 1H), 3.31 (dd, J = 15.1, 3.7 Hz, 1H).

^{13}C NMR (mixture): (176 MHz, $CDCl_3$) δ 193.7, 171.1, 158.3, 143.4, 137.2, 137.0, 134.8, 134.1, 133.9, 132.8, 131.7, 129.5, 129.1, 128.8, 127.9, 127.4, 127.3, 126.2, 125.5, 125.3, 124.6, 123.1, 114.2, 55.1, 52.4, 50.7, 49.3, 48.2, 23.3, 21.5.

R_f (7:3 – EtOAc:Hex) = 0.5

IR (*neat*): 2833, 2790, 2752, 2730, 2709, 1699, 1658,

1597, 1511, 1449, 1333, 1304, 1253, 1226, 1157, 1033, 980, 812, 785 cm^{-1}

HRMS (ESI+) *m/z* calculated for $C_{37}H_{36}N_2O_5S$ $[M+H]^+$ 621.23, found 621.2418 m/z.

Methyl-2-acetamido-1-(4-methoxyphenyl)cyclopentyl)thiophene-2-carboxylate (4.219)

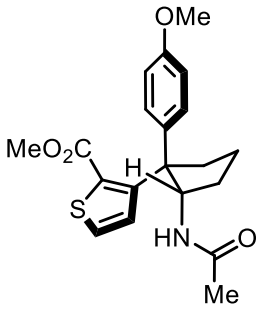

The **General Procedure** was followed performing the reaction with methyl 3-(acetylsulfamoyl)thiophene-2-carboxylate (79 mg, 0.3 mmol) and 1-(cyclopenten-1-yl)-4-methoxy-benzene (63 mg, 0.36 mmol) and purification by flash column chromatography (SiO_2, 90:10→30:70 Hex:EtOAc) to furnish the title compound as an off white foam (62 mg, 55%).

^{1}H NMR (700 MHz, $CDCl_3$): δ = 7.43 (d, *J* = 5.2 Hz, 1H), 7.21 (d, *J* = 5.2 Hz, 1H), 7.16 (d, *J* = 8.7 Hz, 2H), 6.77 (d, *J* = 8.7 Hz, 2H), 6.39 (d, *J* = 6.3 Hz, 1H), 5.03 (q, *J* = 6.6 Hz, 1H), 3.76 (s, 3H), 3.59 (s, 3H), 2.44 – 2.40 (bm, 1H), 2.39 – 2.33 (bm, 2H), 1.89 – 1.80 (bm, 4H), 1.77 – 1.67 (bm, 1H), 1.67 – 1.55 (bm, 2H) ppm

^{13}C NMR (176 MHz, $CDCl_3$): δ = 169.8, 163.3, 157.6, 150.4, 137.5, 131.2, 129.0, 128.4, 127.8, 113.2, 56.5, 56.3, 55.2, 52.4, 39.9, 31.0, 23.4, 20.6 ppm

R_f (5:5 – EtOAc:Hex) = 0.2

IR (*neat*): 3290, 2949, 1719, 1649, 1510, 1434, 1371, 1246, 1182, 1031, 780 cm^{-1}

HRMS (ESI+) *m/z* calculated for $C_{20}H_{23}NO_4S$ $[M+H]^+$ 374.1421, found 374.1428.

N-(2-(4-methoxyphenyl)-2-(thiophen-2-yl)cyclopentyl)acetamide (4.220)

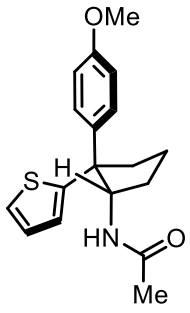

The **General Procedure** was followed performing the reaction with *N*-(2-thienylsulfonyl)acetamide (62 mg, 0.3 mmol) and 1-(cyclopenten-1-yl)-4-methoxy-benzene (63 mg, 0.36 mmol) and purification by flash column chromatography (SiO_2, 90:10→30:70 Hex:EtOAc) to furnish the title compound as a light yellow foamy oil (55 mg, 58%).

^{1}H NMR (700 MHz, $CDCl_3$): δ = ^{1}H NMR (700 MHz, cdcl$_3$) δ 7.25 – 7.17 (m, 3H), 6.98 (dd, *J* = 4.8, 3.7 Hz, 1H), 6.81 (d, *J* = 8.7 Hz, 2H), 6.75 (d, *J* = 3.0 Hz, 1H), 5.36 (d, *J* = 9.4 Hz, 1H), 5.01 (dd, *J* = 17.3, 9.9 Hz, 1H), 3.78 (s, 3H), 2.63 (ddd, *J* = 13.9, 9.5, 4.4 Hz, 1H), 2.25 – 2.13 (m, 2H), 2.03 – 1.94 (m, 1H), 1.92 (s, 3H), 1.81 (ddd, *J* = 17.8, 11.3, 4.5 Hz, 1H), 1.60 – 1.51 (m, 1H) ppm

^{13}C NMR (176 MHz, $CDCl_3$): δ = 169.3, 158.0, 149.8, 139.4, 128.0, 126.7, 126.1, 124.7, 113.5, 55.1, 54.7, 54.6, 41.3, 30.4, 23.7, 19.5 ppm

R_f (5:5 – EtOAc:Hex) = 0.1

IR (*neat*): 3292, 2927, 1651, 1607, 1510, 1372, 1248, 1181, 1032, 827 cm^{-1}

HRMS (ESI+) *m/z* calculated for $C_{18}H_{21}NO_2S$ $[M+H]^+$ 316.1366, found 316.1364.

N-(2-(4-methoxyphenyl)-2-(naphthalen-1-yl)cyclopentyl)acetamide (4.221)

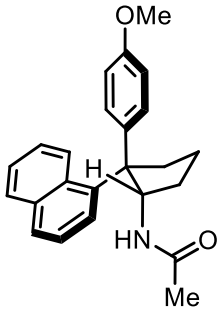

The **General Procedure** was followed performing the reaction with *N*-(1-naphthylsulfonyl)acetamide (75 mg, 0.3 mmol) and 1-(cyclopenten-1-yl)-4-methoxy-benzene (63 mg, 0.36 mmol) and purification by flash column chromatography (SiO_2, 90:10→30:70 Hex:EtOAc) to furnish the title compound as a light yellow powder (40 mg, 37%).

^{1}H NMR (700 MHz, $CDCl_3$): δ = 7.80 (d, *J* = 8.2 Hz, 1H), 7.77 (t, *J* = 7.3 Hz, 2H), 7.66 (d, *J* = 8.7 Hz, 1H), 7.51 (t, *J* = 7.7 Hz, 1H), 7.31 (t, *J* = 7.4 Hz, 1H), 7.19 (d, *J* = 8.8 Hz, 2H), 7.16 (t, *J* = 7.7 Hz, 1H), 6.75 (d, *J* = 8.8 Hz, 2H), 5.47 (dd, *J* = 13.3, 7.3 Hz, 1H), 4.88 (d, *J* = 7.4 Hz, 1H), 3.73 (s, 3H), 2.67 – 2.59 (m, 1H), 2.59 – 2.50 (m, 1H), 2.17 (s, 1H), 1.84 (dd, *J* = 19.9, 10.0 Hz, 1H), 1.78 – 1.66 (m, 1H), 1.60 (dd, *J* = 20.6, 9.5 Hz, 1H), 1.40 (s, 3H) ppm

^{13}C NMR (176 MHz, $CDCl_3$): δ = 168.8, 157.6, 139.9, 139.1, 134.7, 131.9, 128.7, 128.6, 127.4, 126.8, 126.0, 125.4, 125.3, 124.7, 113.7, 58.9, 55.1, 54.9, 41.6, 34.0, 23.1, 20.7 ppm

R_f (5:5 – EtOAc:Hex) = 0.1

IR (*neat*): 2954, 1642, 1609, 1508, 1372, 1249, 1183, 1034, 827, 776 cm^{-1}

HRMS (ESI+) *m/z* calculated for $C_{24}H_{25}NO_2$ $[M+H]^+$ 360.1958, found 360.1962.

N-(4-methoxyphenyl)-2-(naphthalen-1-yl)cycloheptyl)acetamide (4.222)

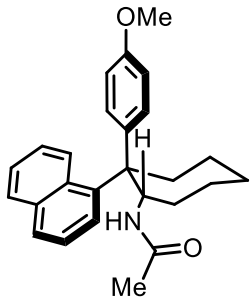

The **General Procedure** was followed performing the reaction with *N*-(1-naphthylsulfonyl)acetamide (75 mg, 0.3 mmol) and 1-(4-methoxyphenyl)cycloheptene (73 mg, 0.36 mmol) and purification by flash column chromatography (SiO_2, 90:10→30:70 Hex:EtOAc) to furnish the title compound as a light yellow powder (36 mg, 31%).

^{1}H NMR (700 MHz, $CDCl_3$): δ = 7.80 – 7.72 (m, 2H), 7.50 (d, *J* = 8.8 Hz, 1H), 7.48 (t, *J* = 7.8 Hz, 1H), 7.31 (t, *J* = 7.4 Hz, 1H), 7.20 – 7.04 (m, 3H), 6.73 (d, *J* = 8.4 Hz, 2H), 5.22 (bs, 1H), 5.15 (bs, 1H), 3.74 (s, 3H), 2.61 (dd, *J* = 15.0, 9.2 Hz, 1H), 2.51 – 2.40 (m, 1H), 2.36 (d, *J* = 22.7 Hz, 1H), 2.21 – 2.12 (m, 1H), 1.90 (s, 1H), 1.75 (dd, *J* = 14.2, 6.6 Hz, 1H), 1.71 – 1.61 (m, 1H), 1.56 (bs, 2H), 1.49 (dd, *J* = 12.7, 8.6 Hz, 1H), 1.35 (s, 3H) ppm

^{13}C NMR (176 MHz, $CDCl_3$): δ = 168.5, 157.4, 142.1, 140.9, 135.0, 132.3, 128.8, 128.5, 127.4, 125.6, 125.2, 125.1, 124.2, 113.6, 56.9, 55.1, 55.0, 42.1, 32.0, 29.7, 24.8, 24.6, 22.8 ppm

R_f (5:5 – EtOAc:Hex) = 0.1

IR (*neat*): 2928, 2859, 1650, 1608, 1508, 1462, 1247, 1183, 726 cm^{-1}

HRMS (ESI+) *m/z* calculated for $C_{26}H_{29}NO_2$ $[M+H]^+$ 388.2271, found 388.2268.

4.4.4 Crystallographic data

4.4.4.1 N-(2-(4-methoxyphenyl)-2-(naphthalen-1 yl)cyclopentyl)acetamide (4.221)

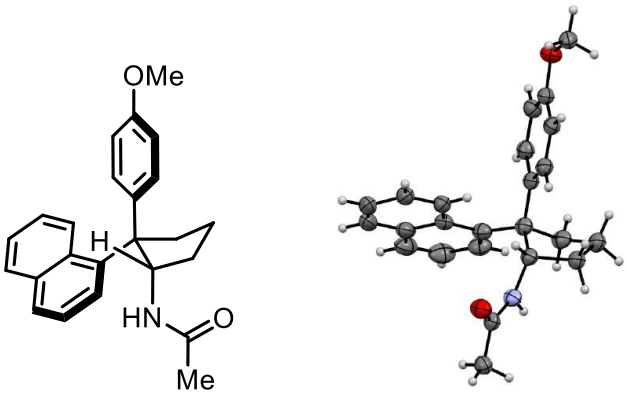

Structural figure of compound **4.20.3**, with 50% probability ellipsoids

Accession Number

The structure of **27** has been deposited in the Cambridge Crystallographic Data Center under accession number CCDC: 1572214.

Structure Determination

Colorless blocks of **27** were grown by vapor diffusion of diethyl ether into a pentane solution of the compound at 22 deg. C. A crystal of dimensions 0.10 x 0.10 x 0.09 mm was mounted on a Rigaku AFC10K Saturn 944+ CCD-based X-ray diffractometer equipped with a low temperature device and Micromax-007HF Cu-target micro-focus rotating anode (λ = 1.54187 A) operated at 1.2 kW power (40 kV, 30 mA). The X-ray intensities were measured at 85(1) K with the detector placed at a distance 42.00 mm from the crystal. A total of 2028 images were collected with an oscillation width of 1.0° in ω The exposure times were 1 sec. for the low angle images, 4 sec. for high angle. Rigaku d*trek images were exported to CrysAlisPro for processing and corrected for absorption. The integration of the data yielded a total of 28115 reflections to a maximum 2θ value

of 138.62° of which 6933 were independent and 5766 were greater than 2σ(I). The final cell constants (Table 1) were based on the xyz centroids of 8542 reflections above 10σ(I). Analysis of the data showed negligible decay during data collection. The structure was solved and refined with the Bruker SHELXTL (version 2016/6) software package, using the space group P1bar with Z = 4 for the formula $C_{24}H_{25}NO_2$. All non-hydrogen atoms were refined anisotropically with the hydrogen atoms placed in a combination of refined and idealized positions. Full matrix least-squares refinement based on F^2 converged at R1 = 0.0537 and wR2 = 0.1504 [based on I > 2sigma(I)], R1 = 0.0634 and wR2 = 0.1646 for all data. Additional details are presented in Table 1 and are given as Supporting Information in a CIF file. Acknowledgement is made for funding from NSF grant CHE-0840456 for X-ray instrumentation.

G.M. Sheldrick (2015) "Crystal structure refinement with SHELXL", Acta Cryst., C71, 3-8 (Open Access).

CrystalClear Expert 2.0 r16, Rigaku Americas and Rigaku Corporation (2014), Rigaku Americas, 9009, TX, USA 77381-5209, Rigaku Tokyo, 196-8666, Japan.

CrysAlisPro 1.171.38.41 (Rigaku Oxford Diffraction, 2015).

4.4.4.1.1 Crystal data and structure refinement for 4.221.

Empirical formula	C24 H25 N O2
Formula weight	359.45
Temperature	85(2) K
Wavelength	1.54184 A
Crystal system, space group	Triclinic, P-1
Unit cell dimensions	a = 9.3165(6) A alpha = 88.002(3) deg.

b = 12.6453(6) A beta = 76.578(4) deg.

c = 16.9508(5) A gamma = 83.003(5) deg.

Volume 1927.92(17) A^3

Z, Calculated density 4, 1.238 Mg/m^3

Absorption coefficient 0.613 mm^-1

F(000) 768

Crystal size 0.100 x 0.100 x 0.090 mm

Theta range for data collection 2.680 to 69.309 deg.

Limiting indices -11<=h<=11, -15<=k<=15, -20<=l<=20

Reflections collected / unique 28115 / 6933 [R(int) = 0.0461]

Completeness to theta = 67.684 97.5 %

Absorption correction Semi-empirical from equivalents

Max. and min. transmission 1.00000 and 0.76174

Refinement method Full-matrix least-squares on F^2

Data / restraints / parameters 6933 / 0 / 500

Goodness-of-fit on F^2 1.046

Final R indices [I>2sigma(I)] R1 = 0.0537, wR2 = 0.1504

R indices (all data) R1 = 0.0634, wR2 = 0.1646

Extinction coefficient 0.0040(5)

Largest diff. peak and hole 0.273 and -0.248 e.A^-3

4.4.4.2 N-1-(5-bromothiophen-2-yl)-1-(4-methoxyphenyl)propan-2-yl)acetamide (4.213)

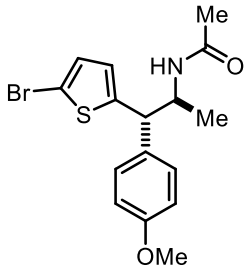

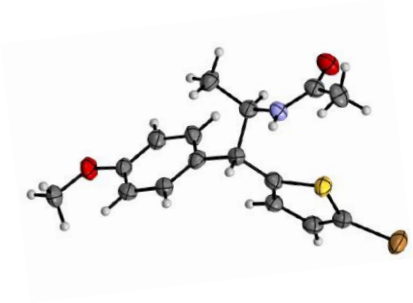

Structural figure of compound **4.20.5**, with 50% probability ellipsoids.

Accession Number

The structure of **16** has been deposited in the Cambridge Crystallographic Data Center under accession number CCDC: 1572215.

Structure Determination

Colorless plates of **16** were grown from by diethyl ether/pentane vapor diffusion at 22 deg. C. A crystal of dimensions 0.04 x 0.02 x 0.01 mm was mounted on a Rigaku AFC10K Saturn 944+ CCD-based X-ray diffractometer equipped with a low temperature device and Micromax-007HF Cu-target micro-focus rotating anode (λ = 1.54187 A) operated at 1.2 kW power (40 kV, 30 mA). The X-ray intensities were measured at 85(1) K with the detector placed at a distance 42.00 mm from the crystal. A total of 2028 images were collected with an oscillation width of 1.0° in ω The exposure times were 15 sec. for the low angle images, 80 sec. for high angle. Rigaku d*trek images were exported to CrysAlisPro for processing and corrected for absorption. The integration of the data yielded a total of 24869 reflections to a maximum 2θ value of 138.84° of which 3075 were independent and 2171 were greater than 2σ(I). The final cell constants (Table 1) were based on the xyz centroids of 3709 reflections above 10σ(I). Analysis of the data showed

negligible decay during data collection. The structure was solved and refined with the Bruker SHELXTL (version 2016/6) software package, using the space group P2(1)/c with Z = 4 for the formula $C_{16}H_{18}NO_2SBr$. All non-hydrogen atoms were refined anisotropically with the hydrogen atoms placed in a combination of refined and idealized positions. Full matrix least-squares refinement based on F^2 converged at R1 = 0.0599 and wR2 = 0.1512 [based on I > 2sigma(I)], R1 = 0.0894 and wR2 = 0.1732 for all data. Additional details are presented in Table 1 and are given as Supporting Information in a CIF file. Acknowledgement is made for funding from NSF grant CHE-0840456 for X-ray instrumentation.

G.M. Sheldrick (2015) "Crystal structure refinement with SHELXL", Acta Cryst., C71, 3-8 (Open Access).

CrystalClear Expert 2.0 r16, Rigaku Americas and Rigaku Corporation (2014), Rigaku Americas, 9009, TX, USA 77381-5209, Rigaku Tokyo, 196-8666, Japan.

CrysAlisPro 1.171.38.41 (Rigaku Oxford Diffraction, 2015).

4.4.4.2.1 Crystal data and structure refinement for 4.213

Empirical formula	C16 H18 Br N O2 S
Formula weight	368.28
Temperature	85(2) K
Wavelength	1.54184 A
Crystal system, space group	Monoclinic, P2(1)/c
Unit cell dimensions	a = 16.2401(10) A alpha = 90 deg.
	b = 10.9158(5) A beta = 101.798(7) deg.
	c = 9.5079(6) A gamma = 90 deg.

Volume 1649.89(17) A^3

Z, Calculated density 4, 1.483 Mg/m^3

Absorption coefficient 4.607 mm^-1

F(000) 752

Crystal size 0.040 x 0.020 x 0.010 mm

Theta range for data collection 2.780 to 69.421 deg.

Limiting indices -19<=h<=19, -13<=k<=13, -11<=l<=11

Reflections collected / unique 24869 / 3075 [R(int) = 0.1138]

Completeness to theta = 67.684 99.9 %

Absorption correction Semi-empirical from equivalents

Max. and min. transmission 1.00000 and 0.81698

Refinement method Full-matrix least-squares on F^2

Data / restraints / parameters 3075 / 0 / 197

Goodness-of-fit on F^2 1.042

Final R indices [I>2sigma(I)] R1 = 0.0599, wR2 = 0.1512

R indices (all data) R1 = 0.0894, wR2 = 0.1732

Extinction coefficient n/a

Largest diff. peak and hole 1.452 and -0.856 e.A^-3

Chapter 5: Trifluoromethylation of Arene using an Electron Donor-Acceptor Complex

5.1 Significance

Small molecule fluorination chemistry is a critical strategy for a variety of medicinal chemistry applications including bioisosteric functional group replacement, drug optimization and radiolabeling.[270] Fluorine is a xenobiotic element despite being located at the vertex of the non-metal elements, all of which are more commonly observed in bio-organic chemistry. Fluorine exhibits the highest electronegativity of the non-metals, a feature that manifests many unique properties.[271] The atomic radius of fluorine is smaller than oxygen or nitrogen (1.47 to 1.52 and 1.57 Å), making fluorine a minimal steric perturbation in the replacement of C–H bonds with C–F bonds. Yet, organofluorine bonds are distinctly stronger than C–O or C–N bonds (107 kcal/mol vs 84 and 69 kcal/mol, respectively), suggesting an ionic nature to this bond. The polarization of C–F bonds can drastically change the stereoelectronics of a functional group from electron donating to electron withdrawing. One such stereoelectronic effect is the alignment of an alkylfluoride in a gauche orientation to a vicinal polar group ("gauche effect"). This effect was documented by Mascitti et. al. at Pfizer in the optimization of GPR119 receptor (Figure 86). [272] Replacement of the central methyl group on **5.1** with a fluorine minimized the lipophilicity and directed the orientation of the fluoride and amide groups gauche. While the fluorinated compound exhibited an improved oxidative resistance, reactive metabolite formation suspended further development of this molecule into a drug. Extrapolation of the fundamental bonding properties of

organofluorine motifs rationalizes the efficacy of small molecule drugs and supports the continued investigation of organofluorination for improved drug development.

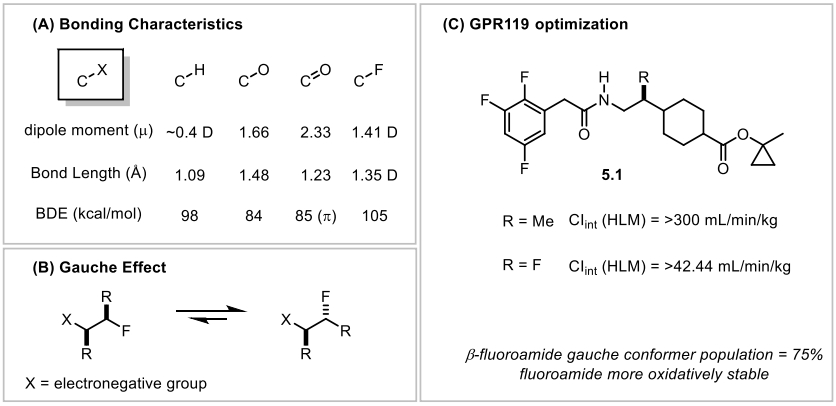

Figure 86: Organofluorine Physical Chemistry Basics

Among the many organofluorine motifs, trifluoromethylated arenes are commonly pursued in both development phase and late stage drug optimization.[273,274]Many trifluoromethylated drugs have come to market included blockbusters such as Prozac (Fluoxetine), Januvia (Sitagliptin) and Celebrex (Celecoxib) (Figure 87). Synthesis of trifluoromethyled arenes is possible in two complementary strategies. Building block trifluoromethylation is possible, whereby early stage starting materials incorporate the trifluoromethyl functionality through nucleophilic displacement of alkyl chlorides (Swarts process[275]), or cyclodehydration for heterocycle synthesis using trifluoroacetic anhydride (TFAA).[276] Alternatively, as biological assays implicate certain functional groups within a small molecule drug as metabolic liabilities or lacking lipophilicity, late-state trifluoromethylation can remedy such targets. To accomplish a late stage trifluoromethylation, a number of reagents have been developed (Figure 88).[277] While many of these reagents were originally developed for polar reaction mechanisms, redox activation renders many of these reagents reactive in a radical mechanism.

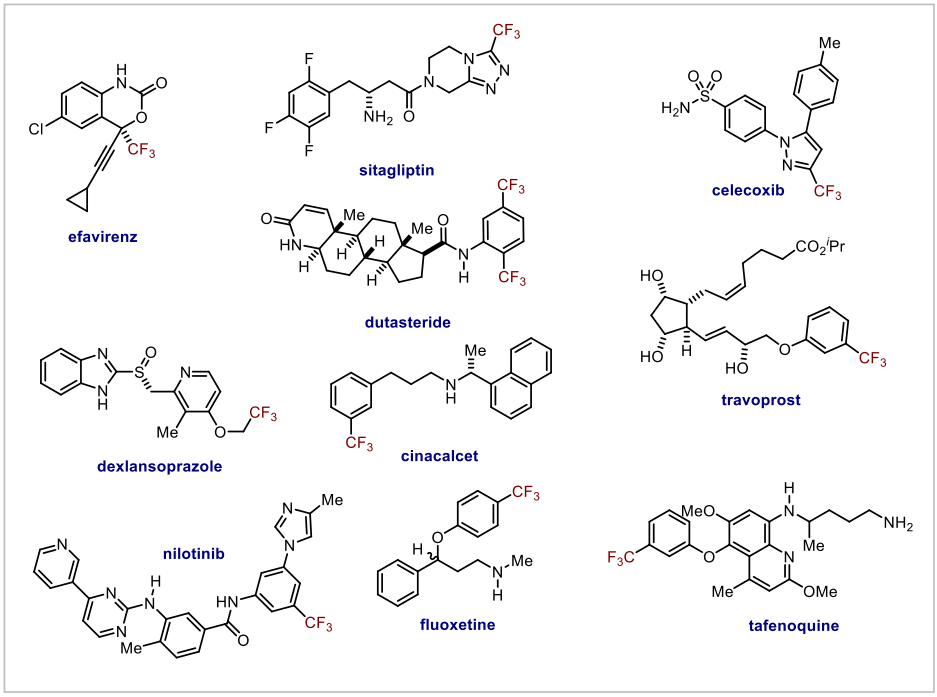

Figure 87: Drugs containing the Trifluoromethyl group

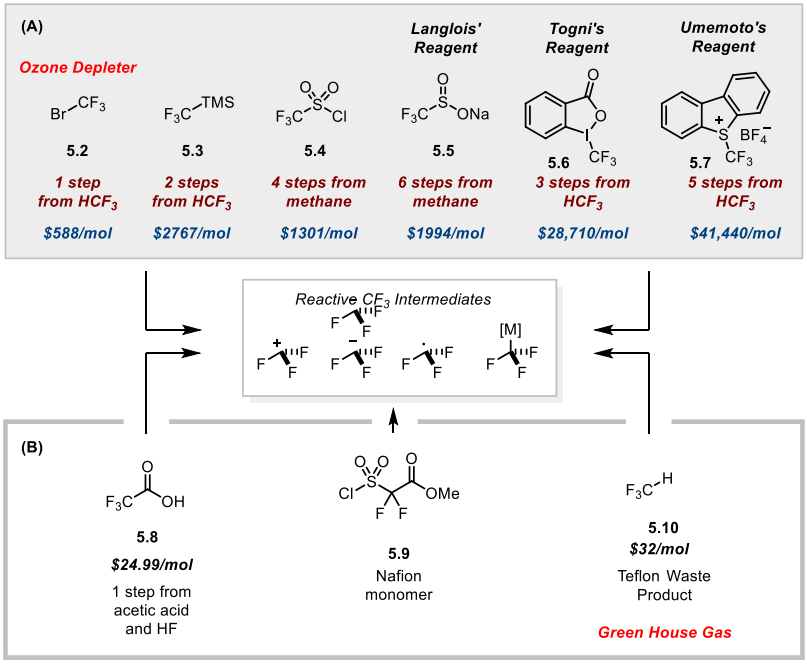

Figure 88: Cost and Diversity of Trifluoromethylation Reagents

Furthering the use of radical trifluoromethylation strategies hinges on the scalability and economic feasibility of the reactive trifluoromethylation reagent. Highlighting this issue, Senanayake and co-workers described cost-benefit analysis of this challenge, realizing stoichiometric copper-trifluoromethylation for the advanced intermediate **5.14** for an anti-infectives campaign was the best choice (Figure 89). The reagents depicted in Figure 88 benefit the operator by creating more reactive trifluoromethyl groups (in comparison to trifluoromethyliodide), as well as existing as bench stable solid reagents; however, these reagents require multistep synthetic preparation, as reflected in the cost. Moreover, these syntheses start from fluoroform, yet funnel through bromotrifluoromethane, a documented ozone-depleter with a reported atmospheric half-life of 110 years in the troposphere.[278]

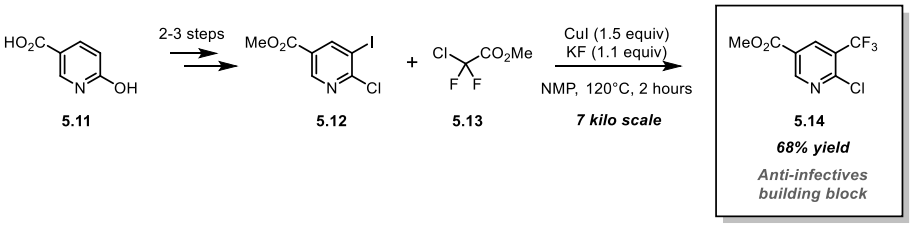

Figure 89: Synthesis of Methyl 6-chloro-5-(trifluoromethyl)nicotinate

To improve access to trifluoromethylation reagents, reaction development using molecules that do not rely upon trifluoromethyl halide derivatives is imperative. Sources such as trifluoroacetate, fluoroform and difluoro β-sultone acetate derivatives (**5.9**)[279] meet this requirement. Trifluoroacetate is obtainable in a single step through the electrochemical oxidation of trifluoroacetate in the presence of HF (Simons process).[280] **5.10** and **5.9** derivatives are produced at an estimated 20,000 tons/year as byproducts of the manufacturing of Teflon and Nafion, making these reagents available less than $0.10/mol.[281][282] Additionally, fluoroform is a greenhouse gas with a warming potential 11,700 times that of carbon dioxide as well as a 254 year atmospheric lifetime, making it critical to remove from manufacturing waste streams.[283]

To sequester fluoroform and create useful chemical entities, strongly deprotonating conditions must be used. Towards this end, Shono and co-workers creatively approached this challenge by developing an electrogenerated amide base for fluoroform deprotonation and trapping with ketone substrates.[284] This reaction is designed to operate by an initial amide reduction to form an equivalent of H_2 gas and pyrrolidinone anion (**5.16**). This base generated *in situ* can deprotonate fluoroform, which is a miscible liquid in DMF at -50°C. After deprotonation, rapid reactivity with ketones and aldehydes was observed (Figure 90A). The addition of hexamethyldisalizane increased the yield of the reaction, purportedly by trapping out the alkoxide intermediates as the silyl ethers and releasing an equivalent of trimethylsilylamine. Comparably, these conditions were more effective than hydride or alkoxide bases under similarly low temperature conditions, highlighting the kinetic challenge of deprotonating fluoroform in the liquid state.

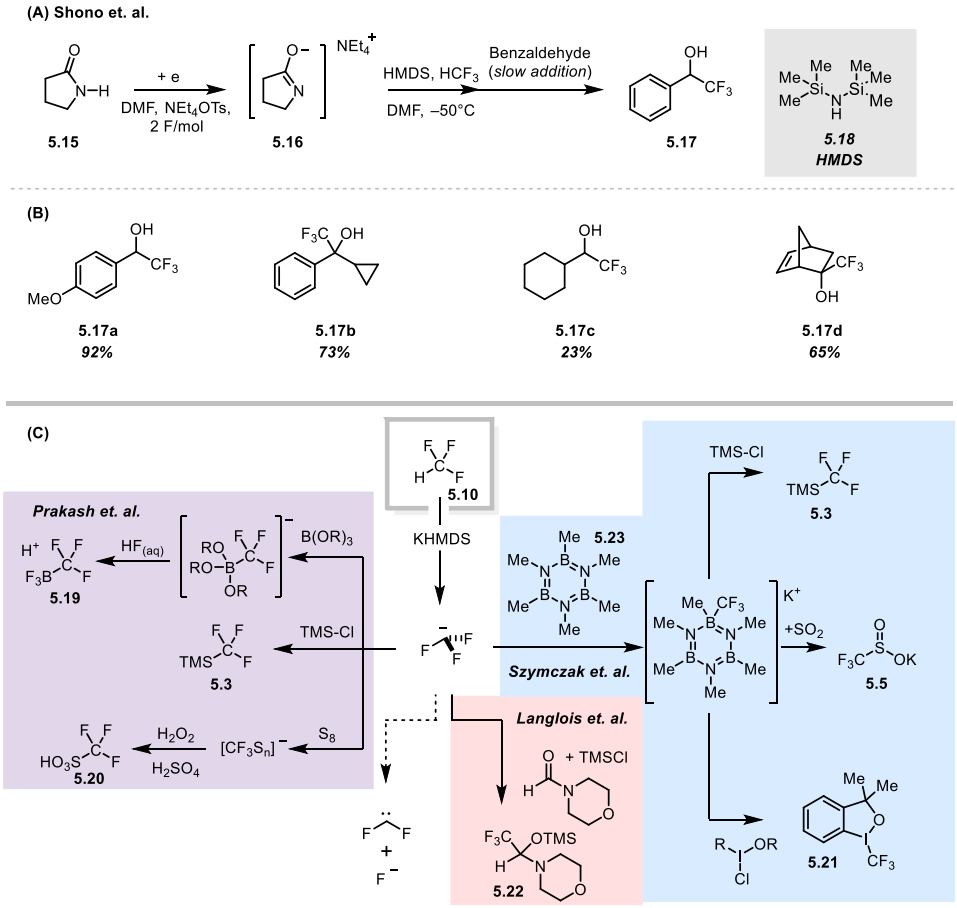

Figure 90: Harnessing the Trifluoromethyl Anion

Other approaches taken by Langlois and co-workers, highlight some of the underlying processes benefitting Shono.[285] Firstly, the solvent, DMF, is a competent shuttle for fluoroform anion formed in the reaction. Secondly, the critical equilibrium between trifluoromethyl anion and difluoromethyl carbene suggests an alternative pathway for the HMDS additive in the reaction: generation of difluoromethyl carbene and fluoride promotes silyl transfer and formation of monosilylamide base in the reaction to further generate more fluoroform anion. Moreover, hexamethyldisalizide is a competent base for the deprotonation of fluoroform, suggesting this is the active base for Shono's conditions. Regardless of the serendipity of the electrogenerated basic conditions, further work storing the fluoroform anion with several p-block elements has been carried out by Prakash[286] and most recently Szymczak and Geri (Figure 90C).[282] These approaches

notably provide direct one-pot reactions for the generation of a number of activated trifluoromethyl groups (**5.3**, **5.5**, **5.19**-**5.21**) at operationally simple reaction temperatures (–5 to 25°C).[282, 286]

The activation of trifluoroacetate is an entirely different challenge to that of fluoroform. Trifluoroacetic acid (TFA) is a strong acid (pK_a = 0.23 in water)[287], yet the salt form is challenging to oxidize or decarboxylate (Figure 91).[288] Matsui et. al. recorded an early demonstration of the oxidation of sodium trifluoroacetate using copper iodide at 160 °C in *N*-methylpyrrolidine.[289] This process is hampered by the formation of fluoroform at high temperature. To safely heat a copper promoted trifluoromethylation reaction, Buchwald and co-workers developed conditions using continuous flow processing, in combination with 20 mol% copper and 60 mol% silver.[290] This process was conducted at 200°C, focusing on faster decarboxylation conditions, to trifluoromethylate a range of simple arenes in short reaction times. Other oxidizing conditions such as Hunsdiecker decarboxylation and xenon difluoride have been shown to decarboxylate TFA and trifluoromethylate arenes.[291,292]

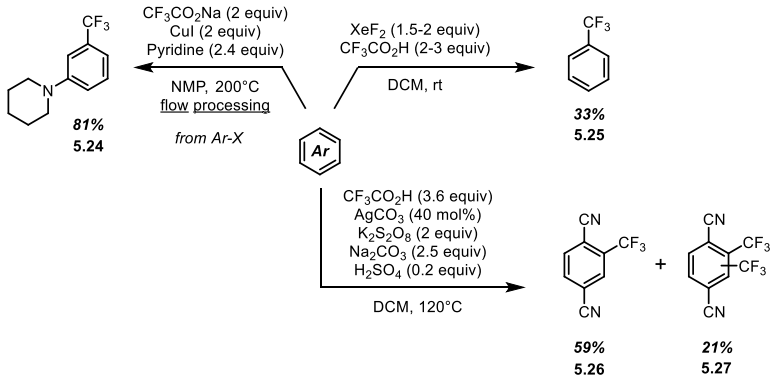

Figure 91: Oxidative Methods for TFA activation to Trifluoromethylate Arenes

Oxidative decarboxylation is a challenging reaction design to generalize as many solvents and aromatic substrates will oxidatively decompose prior to the activation of TFA. Reductive generation of the CF_3 radical circumvents this issue and has also been explored extensively with

trifluoromethyl iodide. Dolbier has outlined the multitude of low valent metals demonstrated for reductively activated trifluoromethylation reactions. [288] These conditions also commonly operate at elevated temperatures (>60 °C).

5.2. Visible Light Enabled Trifluoromethylation Reactions

The interest in radical trifluoromethylation reactivity was substantially increased during the revival of visible light photocatalysis. Photochemical methods for radical trifluoromethylation were demonstrated in the 1940s using trifluoromethyl sources such as trifluoromethylsulfonyl bromide, trifluoromethyl iodide and trifluoroacyl Barton esters.[293] These derivatives could be activated with UV light for homolysis, revealing the trifluoromethyl radical after one or multiple radical fragmentation reactions. These reagents were demonstrated for simple alkene polymerization. The reintroduction of photoredox catalysis warranted a secondary investigation of radical trifluoromethylation due to both the promise of the sustainability of visible light photochemistry and the photoexcited reduction potentials of Ru(II) and Ir(III) catalysts exhibit. As a first demonstration, Scott, Nagib, and MacMillan showcased an enantioselective trifluoromethylation of aldehydes using a chiral iminium catalyst and photocatalysis (Figure 92).[294] This reaction is hypothesized to begin with a sacrificial reductive quenching event between a photoexcited $Ir(III)^{+}$ complex and the chiral iminium catalyst (**5.31**). The resultant Ir(II) (–1.55 V vs SCE) can reduce trifluoromethyl iodide (–1.22 V vs SCE). Steady-state catalysis is justified by a reductive quenching event between the trifluoromethyl–α–amino radical (**5.33**) and photoexcited $Ir(III)^{+}$ complex, while CF_3I reduction drives catalytic turnover. This reaction impressively works at –20°C and generates α–aldehyde stereocenters in greater than 90% ee in many cases. The α–chiral aldehydes are excellent building blocks for other enantioenriched trifluoromethylated molecules such as amines, carboxylic acids and alcohols (Figure 92C).

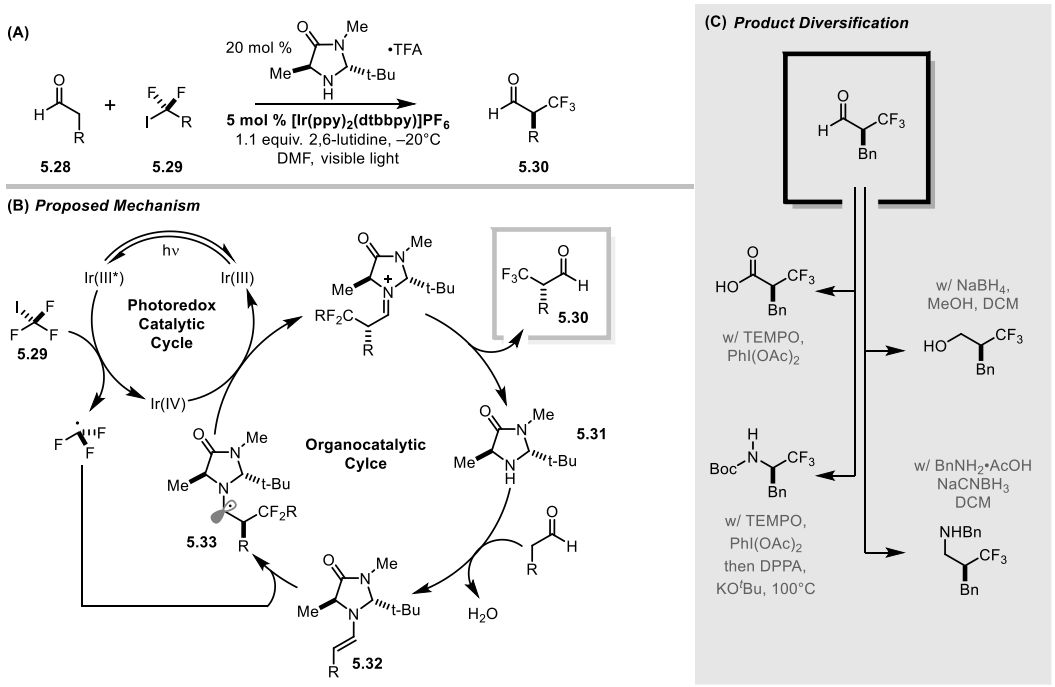

Figure 92: Enantioselective Trifluoromethylation of Aldehydes

Nagib and MacMillan further work proved the utility of photoredox catalysis for radical trifluoromethylation by activating trifluoromethylsulfonyl chloride for arene functionalization.[295] Trifluoromethylsulfonyl chloride (–0.18 V vs SCE) exhibits a significantly lower reduction potential than trifluoromethyliodide, thus $Ru(phen)_3^{3+}$ (–0.90 V vs SCE) was discovered as the optimal photocatalyst for this process. The reaction is proposed to begin with an oxidative quenching event between Ru(II)* and trifluoromethylsulfonyl chloride to reveal the trifluoromethyl radical after de-sulfonylation. Catalyst turn-over is enabled through oxidation of the arene radical adduct (**5.37**) to replenish the electronic valence of the Ru(II) photocatalyst and re-aromatize the arene. This strategy was broadly general for a large number of 5- and 6-member arenes, particularly, pyridine aromatics. The authors additionally investigated the feasibility of pharmaceutical trifluoromethylation; this protocol afforded high yields of trifluoromethylated regio isomers of methyluracil, ibuprofen and atorvastatin. These substrates demonstrated the

concept of the "late stage functionalization" paradigm as each isomer can be separated and individually evaluated in medicinal performance.

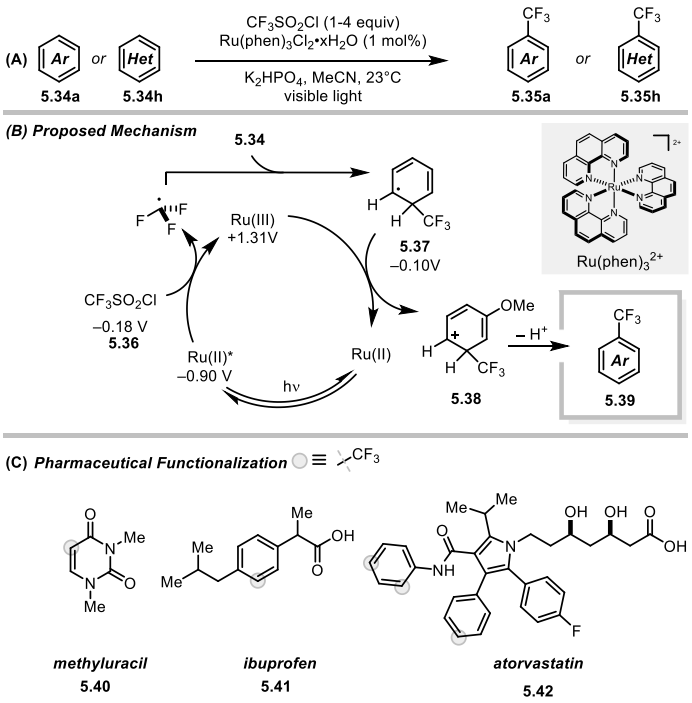

Figure 93: Photoredox Catalyzed Trifluoromethylation with Trifluoromethylsulfonyl chloride

Langlois' reagent is also competent for photoredox activation and π–system functionalization. Utilizing the oxidatively biased acridinium photocatalysts for alkene difunctionalization, Wilger, Gesmundo, and Nicewicz discovered a method for *anti*-Markovnikov selective hydrotrifluoromethylation (Figure 94).[296] The original reaction design focused on a reductive quenching event between photoexcited *N*-methyl acridinium tetrafluoroborate and Langlois' sodium sulfonate salt. Photooxidation of Langlois reagent followed by a rapid loss of SO_2 gas generates the highly reactive trifluoromethyl radical. Alkene functionalization followed by H-atom transfer completes the product formation, and the photocatalyst regenerates through thiyl radical reduction. Reaction scope evaluation revealed moderate to good yields of this catalytic process on both terminal and internal alkenes. Interestingly, in contrast to the majority of Nicewicz's

acridinium photocatalysis,[241] thiol H-atom transfer catalysis was not necessary to furnish the product. Alternative proposals involving 2,2,2-trifluoroethanol H-atom transfer to the key β-trifluoromethyl radical intermediate are suggested, citing the bond strength of the α–oxo C–H bond, in addition to the captodative stabilization of a α–trifluoromethyl-α-oxo methine radical. Under the same rationale, chloroform solvent could also provide the terminal H-atom necessary to the reaction.

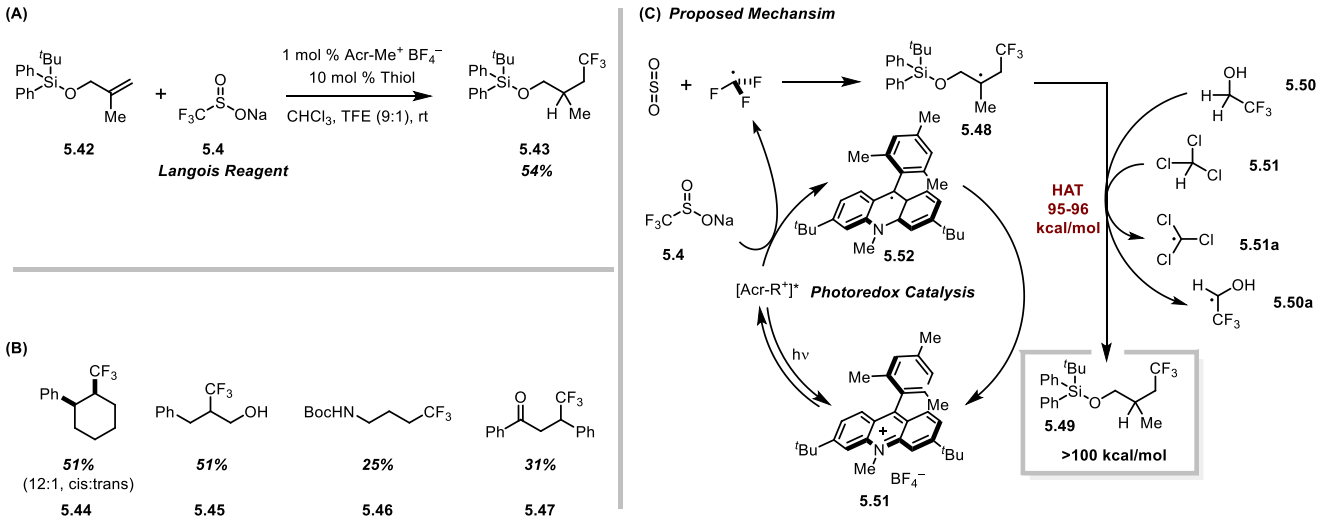

Figure 94: Photoredox Catalyzed Trifluoromethylation using Langlois Reagent

Other photochemical methods for arene trifluoromethylation using de-sulfonylation processes have been demonstrated by Li (Figure 95).[297] In one design, diacetyl was photoactivated at 420 nm to oxidize Langlois' reagent through a ketyl radical intermediate. This method is not catalytic, yet, the reagents are simple organic solvents weakly activated by 400-430 nm light. In a second design, radical desulfonylation of α–sulfoxoarylketones was photopromoted resulting in a multistep fragmentation to reveal a trifluoromethyl radical (Figure 95C).[298] The optimal ketone for this process was **5.55**, which was then used to trifluoromethylated a standard scope of electron rich arene substrates.

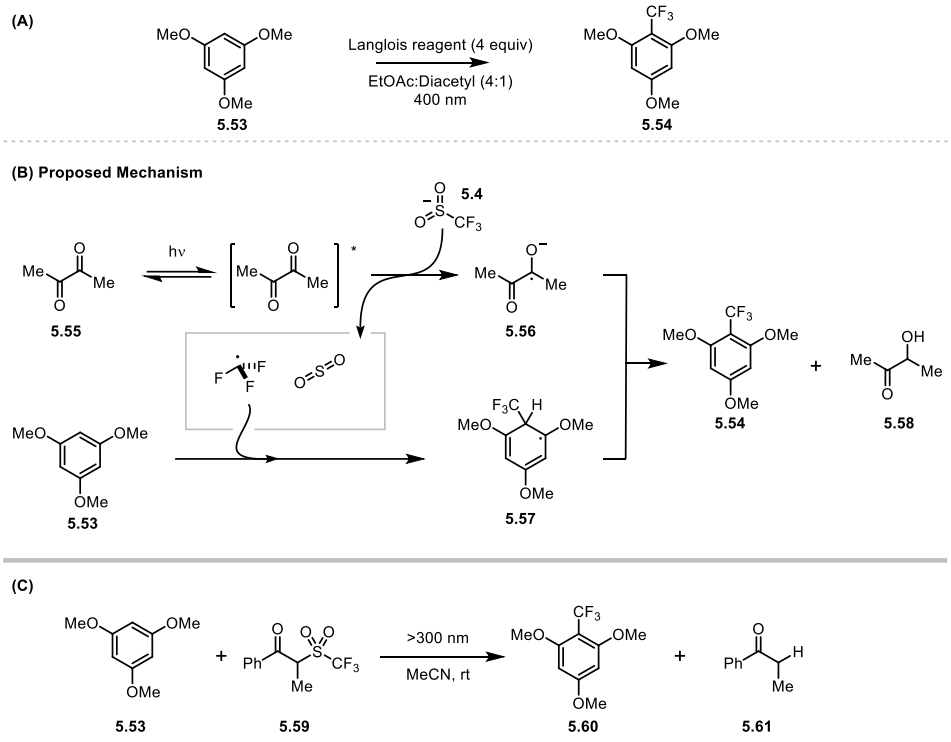

Figure 95: Ketyl Enabled Desulfonylative Trifluoromethylation of Arenes

Reductive atom transfer radical addition (ATRA) of the trifluoromethyl radical to alkenes is another methodology paradigm. Trifluoromethyl iodide, perfluoroiodoalkanes, and both Umemoto's and Togni's reagent all participate as photochemical oxidative quenchers for Ir(III) based photocatalysis. In ATRA, both portions of the photoredox-activated substrate are incorporated across the alkene. This is particularly useful in alkene functionalization reactivity. For instance, Stephenson showed ATRA of terminal alkenes with trifluoromethyl iodide to form β–iodo trifluoroalkanes of which a distal nucleophilic functionality could displace the secondary iodide in an intramolecular cyclization reaction, or elimination reaction (Figure 96A).[299,300] Koike and Akita leveraged photocatalytic ATRA reactivity first with Umemoto's reagent to form 1-phenyl-3,3,3-trifluropropanols (Figure 96B).[301] This reaction was designed to turn-over through the oxidation of the trifluoromethyl adduct (**5.68**) via either a catalytic oxidation by the Ir(IV) catalyst or a propagative electron transfer with the trifluoromethylation reagent. Both pathways

converge on a benzylic–stabilized carbocation, which is trapped with water co-solvent (**5.65**). This approach was equally effective using a Ritter trapping process to generate the corresponding acetamide (**5.66**).[302] Photocatalytic activation of Togni's reagent performed differently than Umemoto's despite the same reaction design. The key difference between the two is that reduction of Togni's reagent generates o-iodobenzoate (**5.72**), a reactive base in solution. This phenomenon, in combination with DMSO, enabled a Kornblum oxidation of the common benzylic carbocation intermediate (**5.69)** to generate β–trifluoromethyl ketones.[303] The CF_3 halide derivatives have provided interesting mechanistic designs to photocatalytic reactivity in order to generate a variety of trifluoromethylated small molecules.

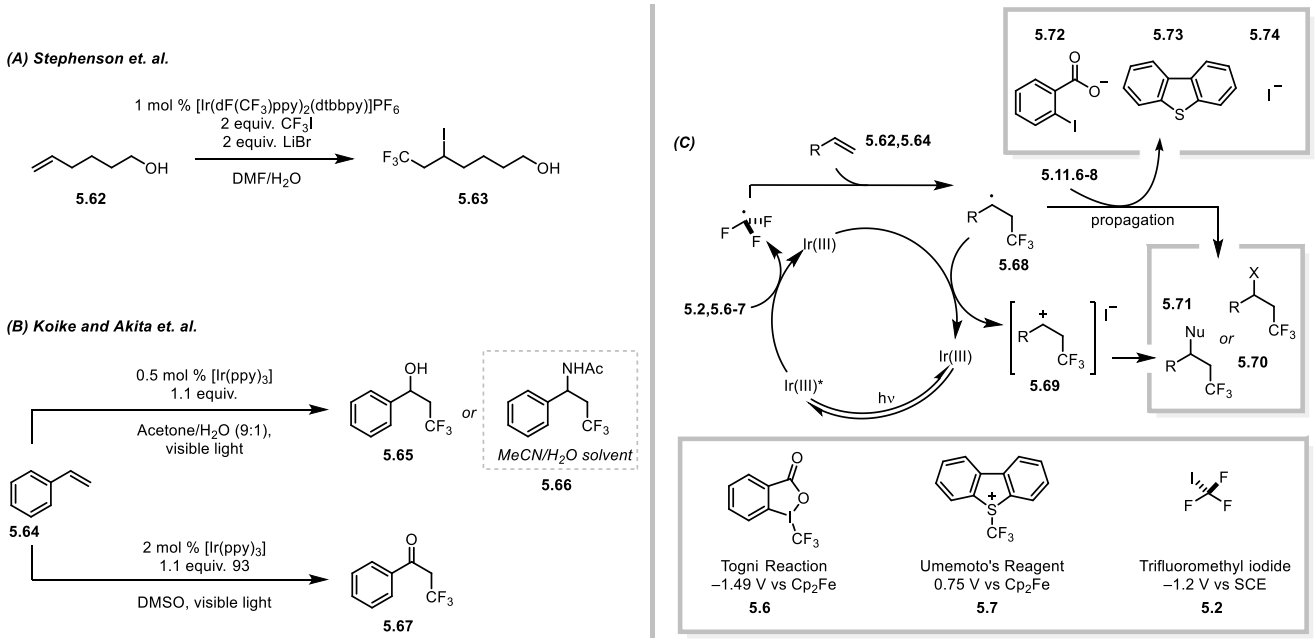

Figure 96: Trifluoromethyl Atom Transfer Radical Addition (ATRA) Reactions

Motivated to contribute a chemoselective TFA based trifluoromethylation[304,305], Stephenson and co-workers have demonstrated the reductive activation of TFA using pyridine *N*-oxide (Figure 97). To accomplish this, trifluoroacetic anhydride, an equally inexpensive CF_3 source is acylated with pyridine *N*-oxide (PNO).[306] This acylation process is rapid and results in a salt adduct that

exhibits a reduction potential of –1.1 V vs. SCE (MeCN). The acylated PNO reagent is similarly activated like Togni and Umemoto's reagent in just two steps, pyridine N-oxidation and acylation. To realize a catalytic trifluoromethylation, a reaction was designed to begin with the oxidative quenching of a photocatalyst with the acylated PNO intermediate. Fragmentation of the reduced acylated intermediate is kinetically estimated as a near barrierless process,[307,308] occurring within a single vibration of **5.75a**. A double radical fragmentation process can then occur releasing CF_3 radical. At this point, arene trifluoromethylation can occur with photocatalyst turn-over occurring during arene oxidation to furnish the trifluoromethylated product (**5.77**). Employment of PNO as a redox auxiliary for trifluoromethylation works because pyridine is electronically mismatched with the trifluoromethyl radical. Rather, the trifluoromethyl radical prefers bonding with an electron rich arene, such as *tert*-butyl anisole, where both the radical and the arene can participate in charge transfer in the transition state.[53] This was additionally demonstrated by Barton and co-workers in the reductive decarboxylation of TFAA using a thiohydroxamic ester. Moreover, this process was efficient for the trifluoromethylation for a variety of arenes include MIDA-boronate substituted thiophenes and bromoarenes useful for cross coupling reactions (Figure 97F). Additionally, access to BI intermediate (**5.4**) was demonstrated in 64% yield. In collaboration with Eli Lilly, flow processing of this reaction afforded a 50% yield on kilo scale.

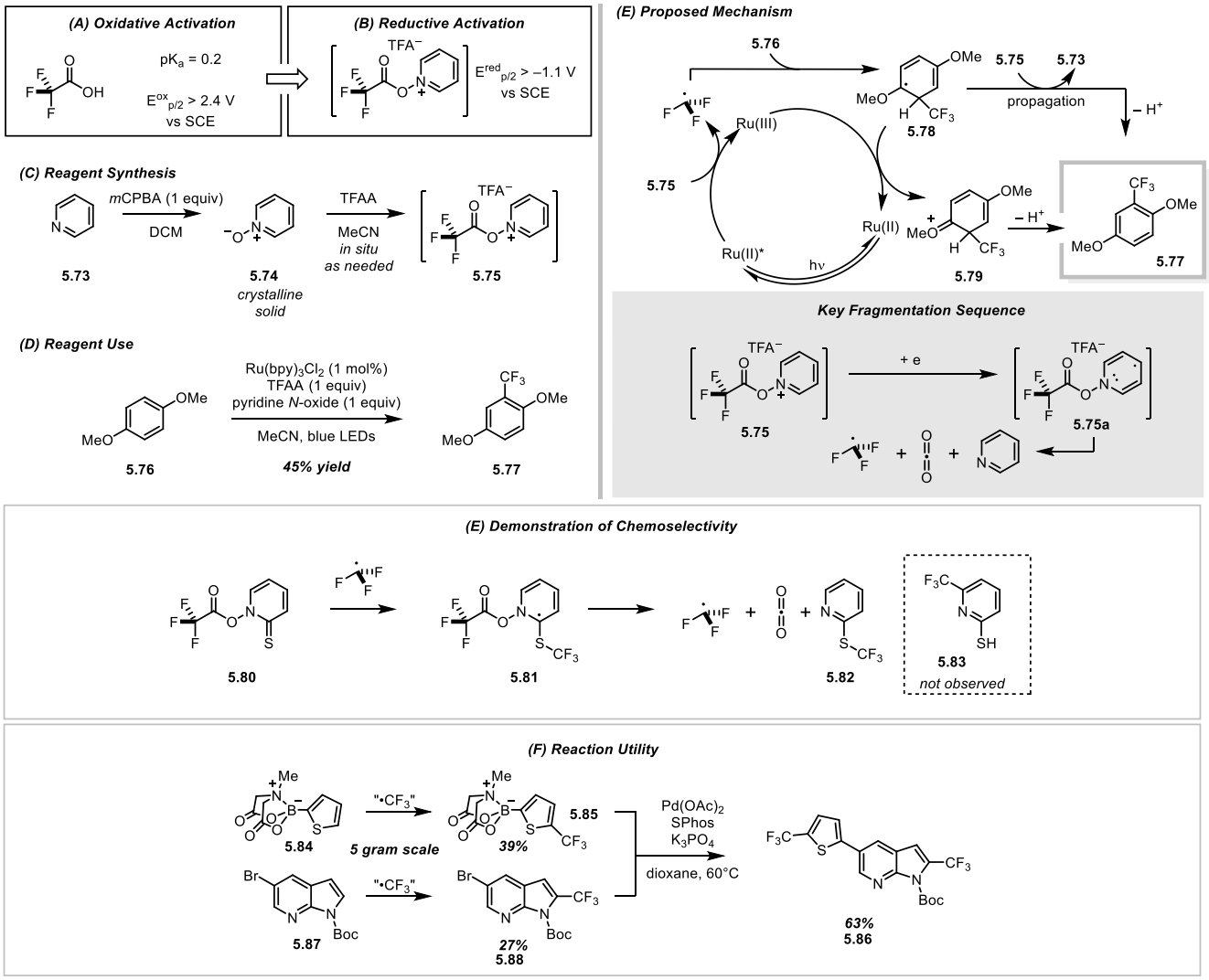

Figure 97: Reductive Decarboxylation of TFAA for Arene Trifluoromethylation

Further investigation of the PNO reagent revealed *para*-derivatization produced higher yields of trifluoromethylated product.[309] Qualitatively, this was realized as in minimization of reaction time from 15 hours to 3 hours, but quantitatively, the 4-Ph-PNO (**5.87**) reacted as an oxidative quencher 10-fold faster than the PNO. In the absence of $Ru(bpy)_3Cl_2$ photocatalyst, the 4-Ph-PNO reagent was capable of trifluoromethylating mesitylene in 74% yield when irradiated with blue visible light. The 4-Ph-PNO reagent, when acylated, uniquely forms an electron donor-acceptor complex (EDA) complex with electron donating arenes and exhibits the linear Mulliken

relationship.[310] Moreover, the yield of mesitylene trifluoromethylation could be controlled through selection of excitation wavelength. When the reaction mixture was irradiated with green light, a 10% yield was measured, as compared to the 74% yield using blue light. A further discussion of photochemically labile EDA complexes for trifluoromethylation will frame the context of this discovery and future work completed in this chapter.

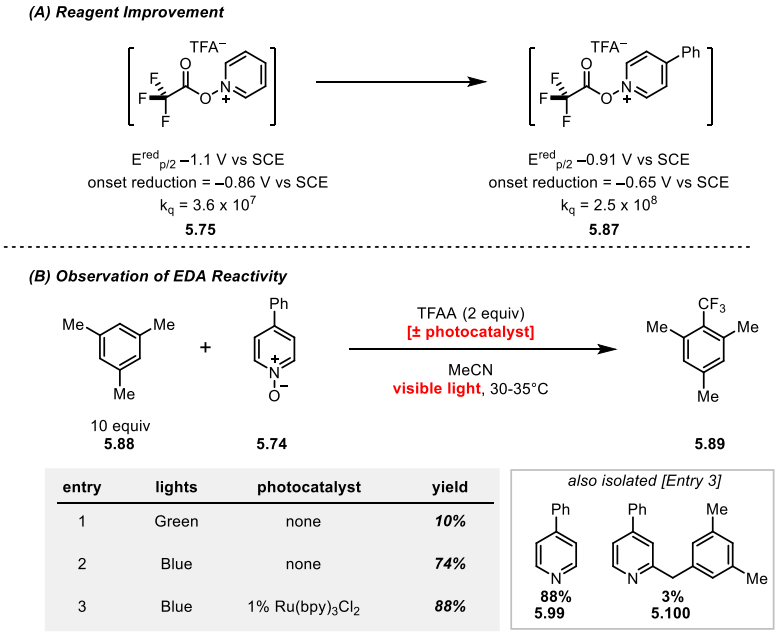

entry	lights	photocatalyst	yield
1	Green	none	*10%*
2	Blue	none	*74%*
3	Blue	1% $Ru(bpy)_3Cl_2$	*88%*

Figure 98: EDA Trifluoromethylation Result

5.3 Electron Donor-Acceptor Complexes and Trifluoromethylation Reactivity

Many trifluoromethylation reactions have been developed with the various named CF_3-X reagents. These reagents champion operational simplicity as each exists as a bench stable solid or liquid at room temperature in comparison to trifluoroiodide or bromide. Additionally, based on the identity of the activator each trifluoromethylation reagent is uniquely activated for single electron reduction or oxidation by an electrochemical cell or photoredox catalyst. While these reagents are reactive in the radical manifold, nearly every trifluoromethylation reagent, aside from trifluoroacetate, participates in a weak intermolecular complexation with a sufficiently electron

donating molecule (Figure 99). For example, *N*-donors including solvents commonly associated with trifluoromethyl iodide reactions such as DMSO and DMF for dense liquids with trifluoromethyl iodide. Optimizing this interaction, Ritter and co-workers found the complexation of trifluoromethyl iodide and tetramethylguanidine forms a bench stable liquid capable of holding the gas for two months.[311] Other σ-hole donors include enolates, silyl enol ethers and both tertiary and secondary amines. This complexation event is often characterized by the observation of a uniquely colored species in solution, noted as the electron donor-acceptor (EDA) complex.

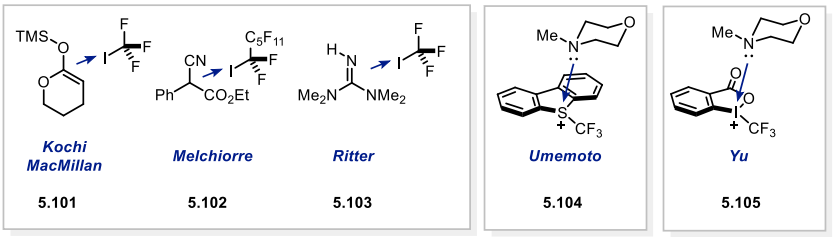

Figure 99: Donor-Acceptor Interactions with Trifluoromethylation Reagents

Theory on the existence of electron donor-acceptor complexes dates as early as the [4,2] cycloaddition reaction between acrolein and 1,3-butadiene.[312] In 1952, Mulliken founded a simple theory about the existence of EDA complexes after witnessing the complexation between iodine and benzene (Figure 100).[313] The energy gap observed as a visible light absorbance (λ) is linearly related to both the electron donor (IP, ionization potential), the acceptor (EA, electron affinity) as well as a work function to account for the columbic attraction between the two species in a given solvent polarity. Importantly, this linearly relates the energetic gap of a given acceptor with a variety of donors, and vice-verse, allowing for an element of photochemical tunability when designing reactivity.

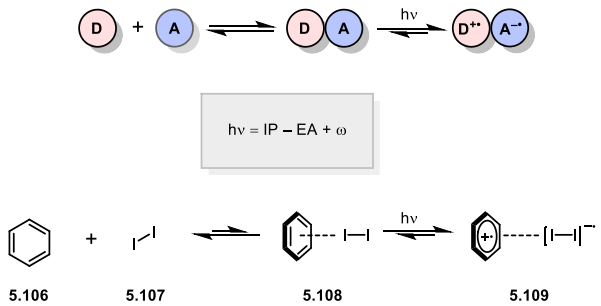

Figure 100: Mulliken EDA Theory

The realization of photochemical reactivity of EDA complexes has largely been reserved to the stoichiometric manifold.[314] This is caused by several factors, most notably back electron transfer. From a given photoexcited state, EDA complexes do not undergo the same internal conversion and intersystem crossing processes harnessed in photocatalysts. Rahter, photoexcitation from a ground state results in a charge transfer ionization event to generate the corresponding radical-ion of both the donor and acceptor. To observe divergent reactivity, a polar solvent must solvate one or both ions to prevent back electron transfer from occurring. Back electron transfer occurs on the picosecond scale, long enough to be observed, but too short for ion separation in many cases.

An early realization of EDA photochemical trifluoromethylation was disclosed by Melchiorre and co-workers (Figure 101A). In this reaction, benzylic enolates react with trifluoromethyl iodide, or perfluorohexyliodide, when excited by a broad spectrum white light.[315] The enolate donor is proposed to act as an σ–hole activator to the perfluoroalkyl iodide. After charge transfer and ion pair separation, the trifluoromethyliodide radical anion fragments to deliver the perfluoroalkyl radical and iodide anion. The perfluoroalkyl radical preferentially reacts with the aryl enolate *para* to the enolate species, and this radical adduct can reduce another molecule of perfluoroalkyl iodide to propagate the cycle and form more product. The key design element to maximize yields was performing this reaction in a biphasic mixture of nitromethane and perfluorohexane. The

perfluorohexane preferentially extracts the fluorinate products into the fluorous phase to maximize production formation based on Le Chatelier's principle. This same approach could be applied in an asymmetric sense, with chiral cinchonidine alkaloid cations to furnish perfluorohexyl quaternary substation of β–ketoester enolates.[316]

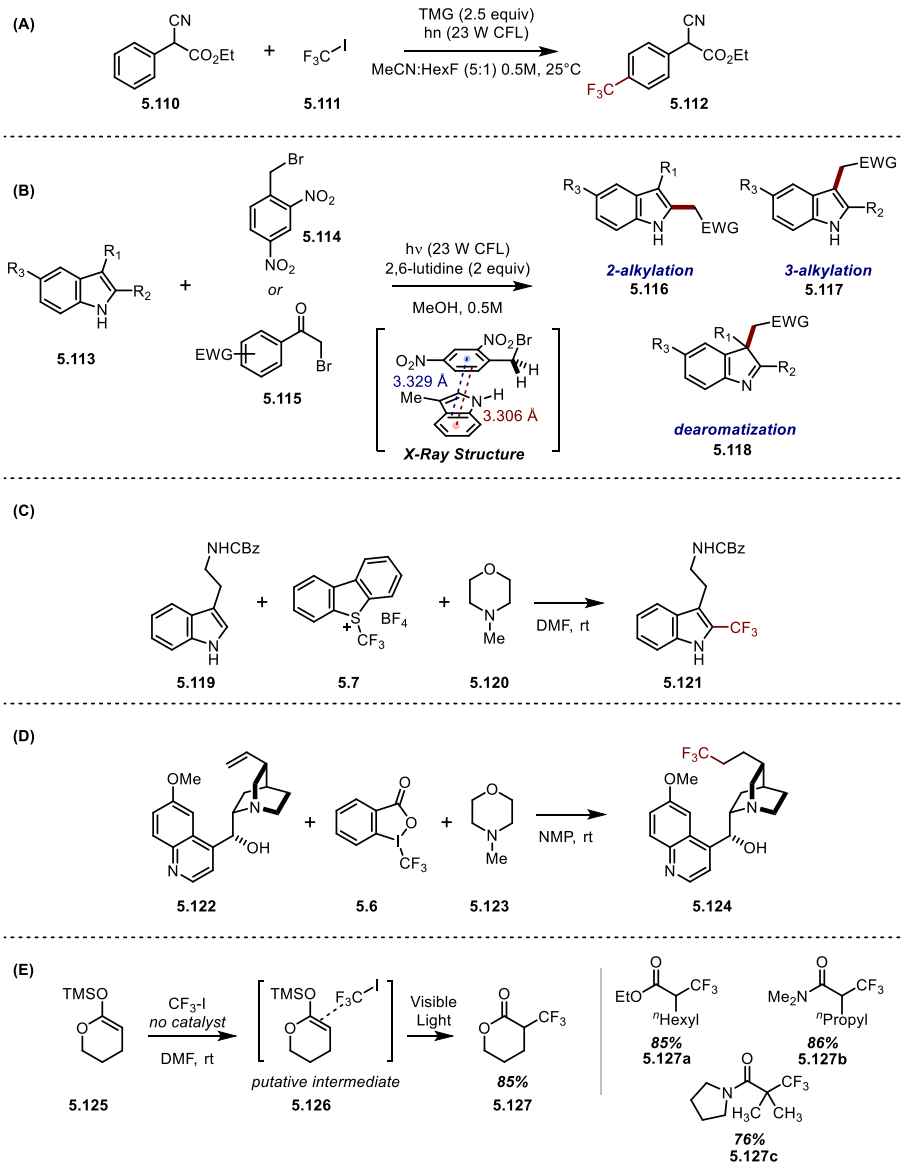

Figure 101: EDA Enabled Stoichiometric Trifluoromethylation

Further work was completed by Melchiorre in the area of EDA photochemistry for the alkylation of indoles, in which the key EDA complex was crystallographically characterized

(Figure 101B).[317] The solid state structure revealed an interplanar spacing between the donor and accepter was significantly closer than by van der Waals attraction and this complex existed in a 1:1 stoichiometry. While crystallographic analysis has proven fundamental for the characterization of a variety of EDA complexes, there is no direct translation between crystal structure and efficient reactivity for synthesis.[318] Lastly, Melchiorre and co-workers have also identified phenolate photochemical reactions for trifluoromethylation.[319] In this instance, no additional photochromic shift is observed between the phenolate in the presence and absence of accepter, thus, the authors characterize this reaction as proceeding through the direct excitation of the donor molecule.

Yu and co-workers have also investigated amine promoted EDA reactivity using a variety of trifluoromethylation reagents. In the instances of EDA complexation between Togni's reagent or Umemoto's reagent and *N*-methylmorphoroline (NMM), the reaction is not photo-promoted (Figure 101C, D). The EDA complex is stable enough to allow for NMR monitoring to generate equilibrium constants, however, allowing the combination of a tertiary amine and these reagents stir will result in radical decomposition. The authors were able to leverage this reactivity for the trifluoromethylation of terminal alkenes and alkynes. [320, 321]

In contrast to Umemoto's and Togni's reagent, the σ–hole activation of iodo-perfluoroalkanes with an amine donor is photo-regulated.[322] Comparably, the σ* orbital of the C–I bond is smaller than the π* orbitals of both Togni and Umemoto's reagents and thus increases the energy barrier of activation. To study the EDA activation of perfluorohexyl iodide, Yu and co-workers used a double radical isocyanide insertion reaction. Perfluorohexyliodide was optimally activated by dibenzylamine in acetonitrile solvent, in comparison to DABCO and DIPEA. This process was efficient for forming a variety of 2-perfluoroalkyl-3-iodoquinoxalines with no regioselectivity

when bearing an asymmetrically positioned aryl substituent. The binding energy of this EDA complex was calculated, using a 6-311+G(d,p) basis set, to –2.7 kcal/mol.

EDA reactivity is not often not targeted but discovered through mechanistic investigation of catalytic photoredox reactivity. This was the instance for Pham, Nagib, and MacMillan investigating the photocatalytic trifluoromethylation of esters and amides (Figure 101E).[323,324] While the photoredox catalyzed mechanism is consistent for the α–trifluoromethylation of ketones and aldehydes, silyl ketene acetals and aminals were observed to trifluoromethylate in comparable yields without the Ru(II) photocatalyst. Comparably, silylketene acetals and aminals are more electron donating and exhibit an oxidation potential of 1.2 V vs SCE (in MeCN), which is very close to the reduction potential of trifluoromethyl iodide (–1.22 V vs SCE, in DMF)(ΔG = -55.3 kcal/mol). Prior work by Kochi, Mariano, and Yoon support this EDA reactivity hypothesis.[325,326]

5.4 Photoinitiated Arene Trifluoromethylation Using an EDA π-π Complex

Several factors about EDA complex photochemistry piqued our interest to further investigate the capabilities of a chemoselectively unique EDA complex for a general arene trifluoromethylation reaction. Firstly, the cost comparison between Ru(II) (124.5/gram) and EDA photocatalysis ($0.37/gram – 2-methoxynapthalene) was distinct. Secondly, organic photoredox catalysis, or non-transition metal photochemistry, is often valued for wider availability and avoidance of transition metal impurities in manufactured products.[327] Finally, the operative photochemical mechanism of EDA reactivity is inner sphere electron transfer, implying that trifluoromethylation could occur in the presence of other reductively labile functional groups such as benzylic bromides and trichloroacetyl groups.[14] The corollary of this statement is that EDA photochemistry looks to harness the full potential of the excited state of a charge-transfer species, as fragmentation, and not intersystem crossing and other relaxation processes are operative in a

non-covalent complex (Figure 102). Noburu Mataga best described this exciting notion by writing[328]:

"*Whereas photoionization requires that the excitation photon have an energy larger than the ionization potential of the molecule in solution, ionic photo dissociation can occur by low-energy photons available from sunlight, indicating a wide utility.*"

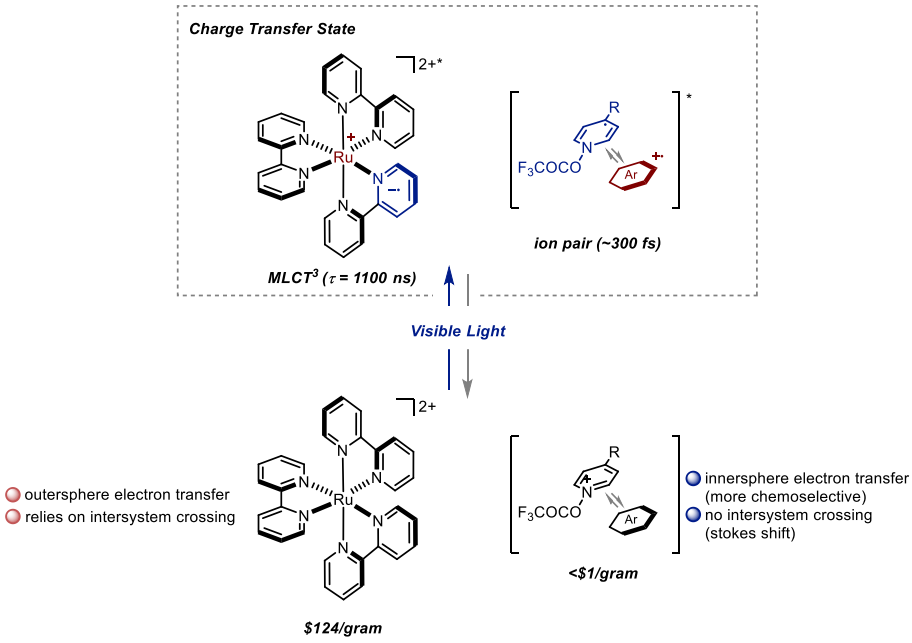

Figure 102: Comparing Ru(II) to EDA Complex Photoexcitation

While the reduction of acylated pyridine *N*-oxides was a unique disclosure in the literature, the kinetics of N-O bond fragmentation as a function of PNO structure have been elucidated by Gould and co-workers.[307,308] Through studying the photochemical fragmentation of alkoxypyridines with tris-anisyl amine, illuminating conclusions on the minutia of the thermodynamic and kinectic characteristics of electron transfer arising from a photoexcited EDA complex were reached. For *N*-methoxylpyridinium tetrafluoroborate, electron withdrawing groups including *para*-cyano slow

the rate of N-O bond fragmentation and allow for back electron transfer to the amine donor. This is attributed to a resonance stabilization effect in the fleeting pyridyl radical intermediate. Interestingly, phenyl substitution at C_2-C_4 increased fragmentation rates relative to the unsubstituted PNO suggesting phenyl substituents lack resonance contribution an act solely as an electron withdrawing substituents. Electron donating substituents exert the most positive accelerating influence on N-O bond fragmentation. These substituents are energetically destabilizing to the EDA complex by reducing the acceptor's electron affinity in the ground and excited states. Thus, when irradiation promotes photoionization, the geminate radical-ion pair is higher in energy compared to *para*-cyano *N*-methoxypyridine. The ensuing fragmentation occurs from this maximally unstable ionized state, in comparison to the other derivatives. Back electron transfer is additionally avoided because the enthalpy of this process is large enough to kinetically slow the rate of back electron transfer (Marcus inverted region).[329] Kochi and co-workers have also investigated the EDA complexes of pyridinium oxidants and studied the kinetics of EDA photolysis.[330] Through these studies, Kochi characterizes the radical transients of the functionalized molecules with UV-Vis spectroscopy, and demonstrates pyridinium oxidants can productively functionalize molecules when photoexcited in the presence of an arene donor.

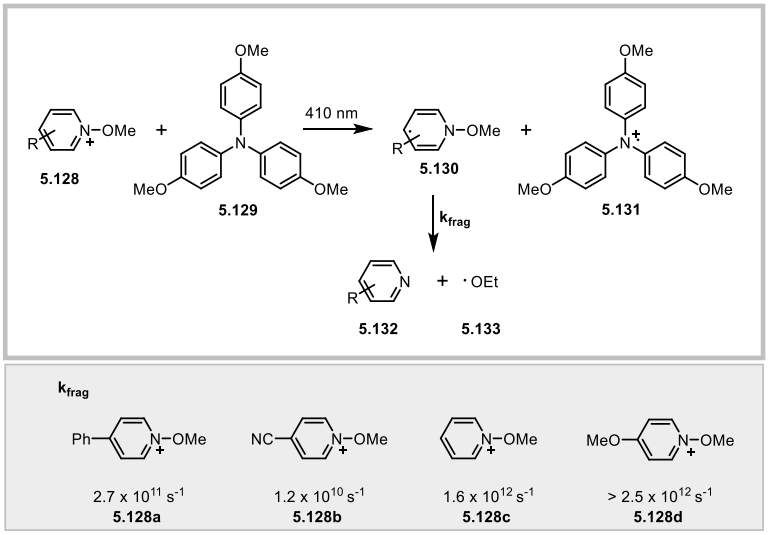

Figure 103: Fragmentation kinetics of single electron reduced *N*-methoxypyridinium cations

Emboldened by these fundamental studies, we set out to discover an efficient EDA photochemical method that not only fragmented the acylated pyridine N-oxides, but also produced desirable amounts of trifluoromethylated arenes, exogenous to the EDA complex. An initial screen of arene donors ranging in ionization potential of 6.86 eV (triphenylamine) to 8.12 (naphthalene) with acylated 4-Ph-PNO was conducted. Assay yield of this reaction trended with donor ionization potential, however, this yield unsatisfyingly peaked at 18%. Changing the 4-Ph substituent to 4-CO_2Et increased the reaction yield, despite the Gould's reports. Furthermore, this second donor

screen qualitatively produced higher yields, as nitromethane was utilized as a more polar solvent to promote separation of the radical ion pair.

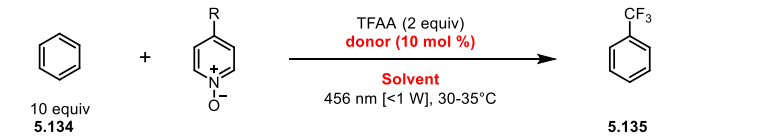

PNO derivative	Solvent	Donor	Ionization Potential (eV)	Yield (%)
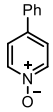 5.136	MeCN [0.4 M]	naphthalene	8.12	1
		1,3,5-trimethoxybenzene	7.96	1
		hexamethylbenzene	7.85	5
		N-trifluoroacetylcarbazole	--	2
		2-methoxynaphthalene	7.8	8
		N-methylcarbazole	7.57	6
		4-bromophenyl-diphenylamine	--	15
		triphenylamine	6.86	18
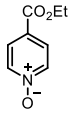 5.137	$MeNO_2$ [0.2 M]	naphthalene	8.12	10
		1,3,5-trimethoxybenzene	7.96	0
		hexamethylbenzene	7.85	12
		N-trifluoroacetylcarbazole	--	-
		2-methoxynaphthalene	7.8	**28**
		N-methylcarbazole	7.57	0
		4-bromophenyl-diphenylamine	--	15
		triphenylamine	6.86	10

Figure 104: Donor Screen for EDA reactivity with 4-Ph-PNO and 4-CO_2-PNO

Broadening the screening scope to three different arene substrates (**5.88, 5.134, 5.139**), and four different pyridine N-oxides (**5.75, 5.136, 5.137, 5.138**), 2-methoxynaphthalene was tested as a donor in search of an efficient EDA trifluoromethylation process (Figure 105). Control reactions supported the hypothesis of an EDA complex between substoichiometric donor and acylated PNO and not the title substrates (**5.88, 5.134, 5.139**). For 4-Ph-PNO this was not true, blue light excitation in the absence of 2-methoxynaphthalene produced yields ranging from 10-50%. This background reaction could be minimized by using green light, an irradiation wavelength the pyridinium EDA complexes absorb significantly less. In this sense, trifluoromethylation of *N*-Boc–pyrrole-2-carboxylate was the most chemoselective process and was selected for further study.

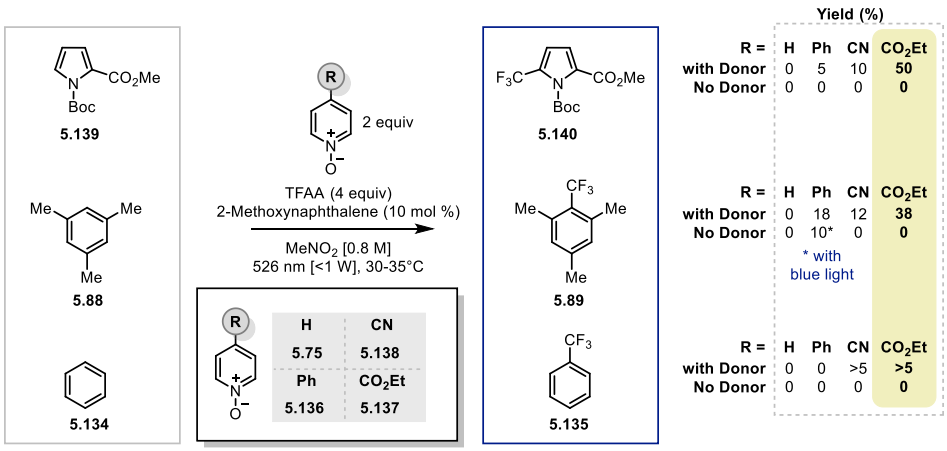

Figure 105: Substrate and PNO reagent Optimization

Additional reaction parameters were chosen for optimal reactivity for the reaction screen in Figure 105. Firstly, the reaction temperature was lowered using a jacketed beaker and methanol bath. EDA complexation is enthalpically favored as the entropy is decreased. To prove this, variable temperature UV-Vis studies confirmed that the EDA complex between 2-methoxynaphthalene and 4CO_2Et-PNO at 0.4 M absorbed 100% more green light at 15°C than at 50°C (Figure 106). Secondly, the reaction concentration was doubled to 0.8 M to additionally promote EDA complexation. Lastly, a two-fold excess of TFAA was consistently employed to ensure full acylation of the pyridine N-oxide. While simply mixing 1.1 equivalents of TFAA with PNO was sufficient to trifluoromethylate arenes using Ru(II) photocatalysis, a charge-transfer absorption is observable when a single equivalent of TFAA is mixed with ethyl isonicotinate *N*-oxide in the absence of donor. This is qualitatively assigned to an $O_{\text{non-bonding}}$ to $\pi^*_{\text{pyridinium}}$ interaction.[309] Finally, a screen of reagent stoichiometry revealed that for all reactions, one and two equivalents of reagent give comparable yields (~50%), while three equivalents of reagent underperformed this mark. Nearly identical results using 2 equivalents of reagent was obtained using either blue or green lights. Overall, excessive loading of the reagent, or use of higher energy light resulted in reagent trifluoromethylation which is a foreseeable issue for product isolation.

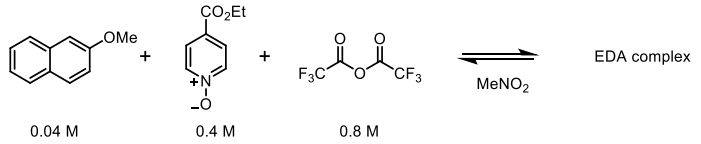

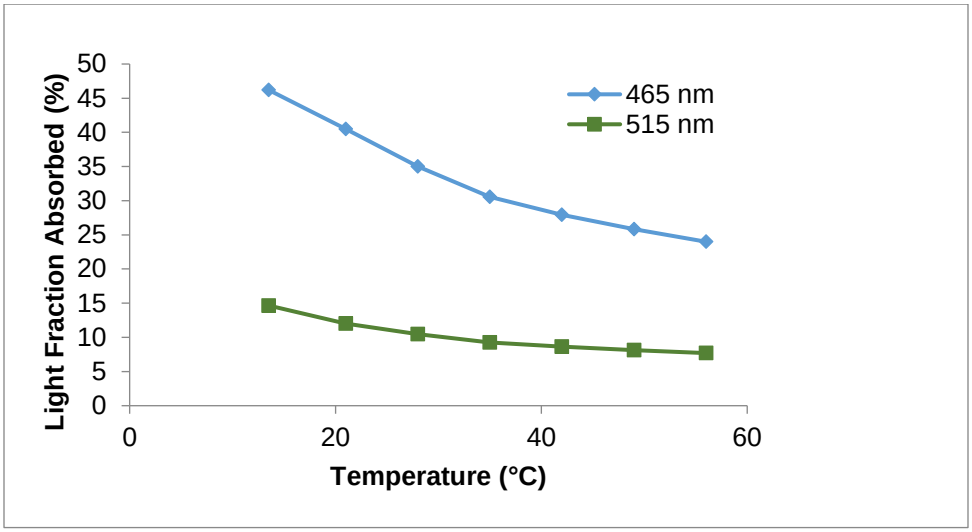

Figure 106: Temperature Dependence on Absorptivity of EDA complex

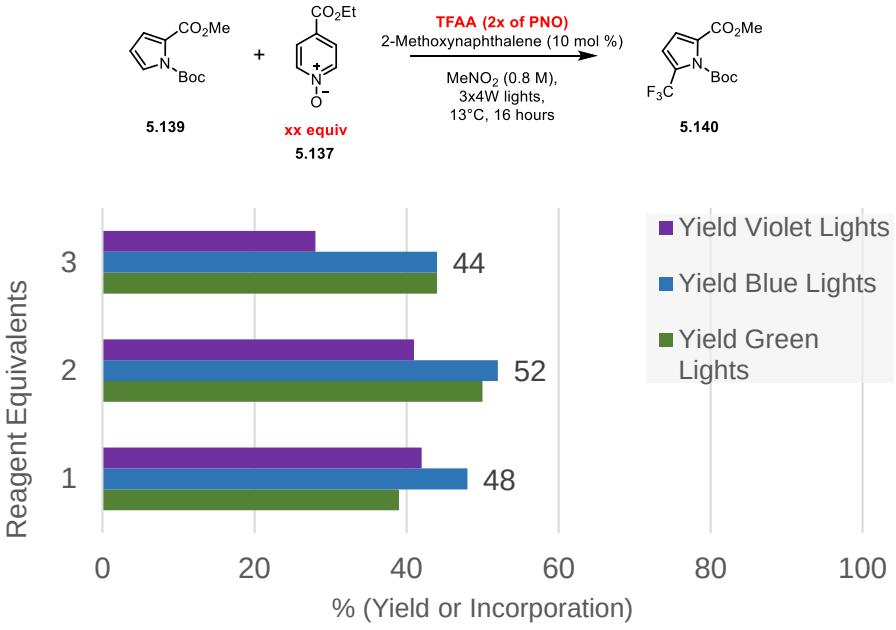

Figure 107: Reagent Stoichiometry Optimization

Interested in further mechanistic study of this reaction prior to evaluating a substrate scope, several experiments were conducted were conducted in hopes of observing higher yields of . Probing the substitution of 2-methoxynaphthalene with other dimethoxylated naphthalenes was unsuccessful (Figure 108). Sequential loading of the donor over two reaction periods was not productive in increasing the yield after the initial irradiation period (Figure 109). Additionally, slow addition of various reaction components was not effective for increasing the yield of **5.140**. Inspired by Kochi's work noting the radical transients formed following N-oxide fragmentation, benzene was added as a trifluoromethyl radical shuttle. This idea was unsuccessful and simply resulted in the trifluoromethylation of benzene along with **5.140.**

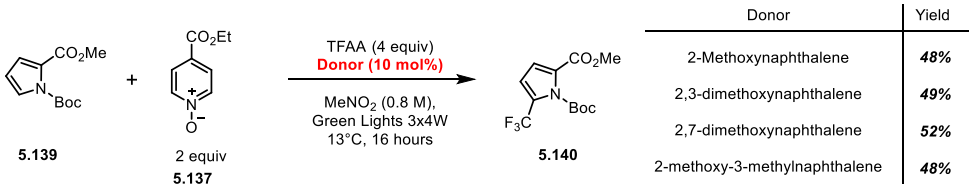

Donor	Yield
2-Methoxynaphthalene	***48%***
2,3-dimethoxynaphthalene	***49%***
2,7-dimethoxynaphthalene	***52%***
2-methoxy-3-methylnaphthalene	***48%***

Figure 108: Other Methoxynaphthalenes as EDA donors

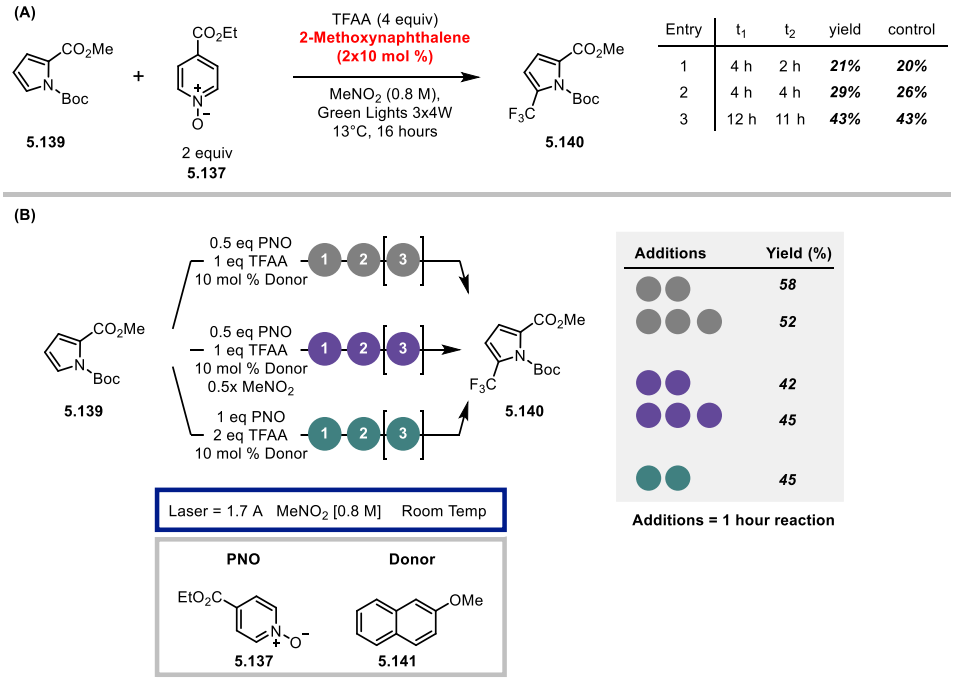

Figure 109: Sequential Addition of 2-Methoxynaphthalene Experiments

Sufficiently perplexed by the lack of improvement in reactivity, reaction termination processes were investigated. Given that 2-methoxynapthalene acts as both a donor and a competent substrate for trifluoromethylation, 2-methoxytrifluoromethylnaphthalene was tested for EDA reactivity (Figure 110). Subjecting a mixture of trifluoromethylated naphthalene as the donor in the title reaction resulted in a a 2% yield of product and a 10% yield in pyridine. Additionally, pyridine was investigated as an inhibitor of the reaction (Figure 111). Comparing separate reactions containing an increasing amount of pyridine from 0-200 mol% supported the inhibitor hypothesis. Furthermore, a charge transfer band at 370 nm was observed for an equimolar mixture of ethylisonicotinate, trifluoroacetic acid an 2-methoxynaphthalene at 0.8 M. This charge transfer band can absorb blue light, however, a productive electron transfer is not envisioned; rather it offers a sequestration pathway for 2-methoxynaphthalene.

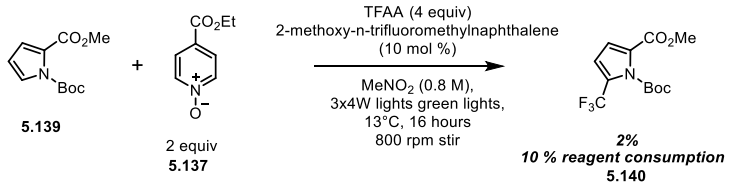

Figure 110: Trifluoromethylated 2-Methoxynaphthalene does not promote EDA reaction

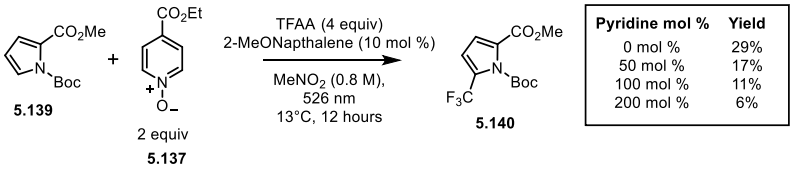

Pyridine mol %	Yield
0 mol %	29%
50 mol %	17%
100 mol %	11%
200 mol %	6%

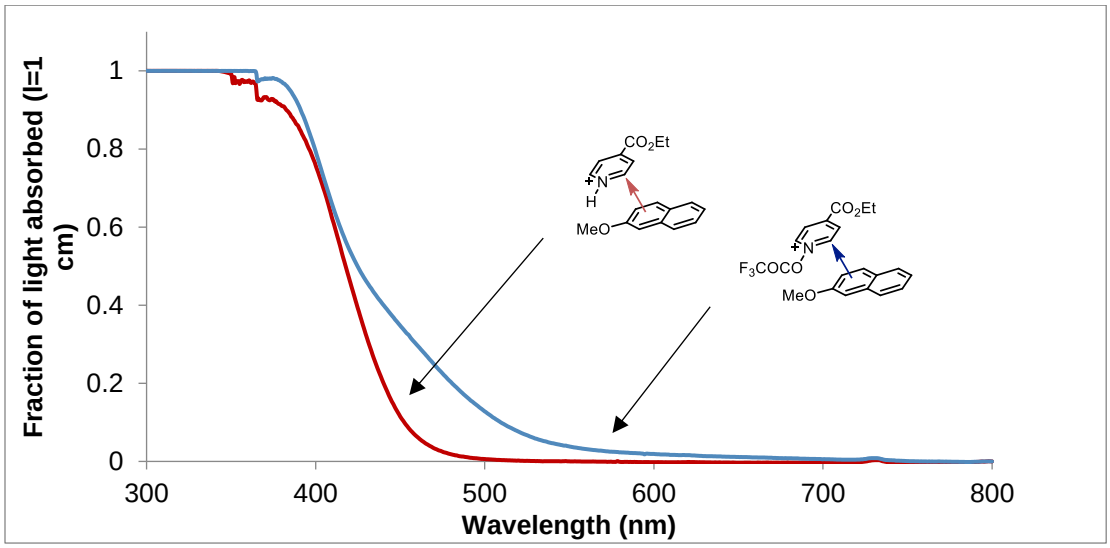

Figure 111: Pyridine Inhibition of EDA Reaction

The wealth of data generated suggested this reaction design was optimally suited for pyrroles, the fastest reacting heterocycles with perfluoroalkyl radicals.[331] Discussing this chemistry with Dr. Kaid Harper and others at Abbvie,[332] it became apparent the light sources used in the initial investigation were not sufficiently bright for optimally photolyzing the reaction solution. To better access a higher concentration of photoexcited EDA complex, laser irradiation sources, boasting a photon flux 10-100 times more intense than the standard LED light source could effect a higher yielding reaction (Figure 112).

Lasers, in comparison to light emitting diodes (LEDs), are directional light sources. Lasers provide an engineering advantage to LED irradiation because solutions can be irradiated with a focused beam of light at a uniform range of excitation wavelengths. LED lights, based on the supplier, can vary in emission wavelength, and non-directionally irradiate a solution volume. LED irradiation is sufficient in photoredox catalysis because Ru(II) and Ir(III) photocatalysts exhibit molar absorptivity on the order of 14,000 $M^{-1}s^{-1}$.[18] This translates to a volume of 1 mL of solvent requiring 1.5 mg of $Ru(bpy)_3Cl_2•6H_2O$ in order to achieve full irradiation across the maximum path length of the vial. Separately, flow photochemistry aids reactions requiring high catalyst loadings and challenging reaction volume irradiation.[333] EDA complexes, are by nature, less photoabsorbing because of the requisite pre-equilibration process. Yet, this lack of absorptivity benefits the use of laser irradiation because the equilibration avoids the occurrence of radiative and thermal excited state decay, characteristic of molecular photocatalysts. Thus, a laser source, operated at a high optical density can safely irradiate a solution of pyridinium EDA complex without detrimental thermal degradation an optimal photoexcitation.

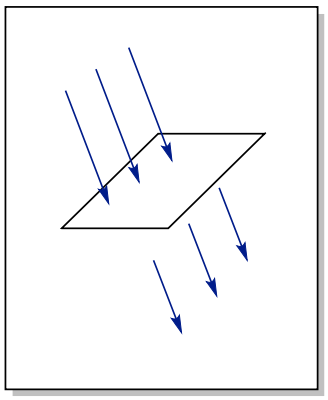

Photon Flux = photons/area/time

LED Strips = 9.1 x 10^{-8} E/s

Kessil H150 lamp [LED] = 1.6 x 10^{-7} E/s

0.71A, 450 nm Laser Diode = 2.9 x 10^{-6} E/s

1.7 A, 450 nm Laser Diode =5.4 x 10^{-6} E/s

Figure 112: Photon Flux Comparison Between LED and Laser Irradiation Sources

With a renewed interest in the success of acylated pyridinium EDA reaction, we pursued reaction development with a laser irradiation source. An optimally performing reactor was

assembled using a chemglass (CG-1318) adapter and an aluminum heatsink to mount the laser to a variable set of vial sizes (see experimental). A more elaborate solvent screen, confirmed the initial result of the superiority of nitromethane as a solvent. Additional UV-Vis studies of the complex showcased the effect of solvent polarity on the formation of the EDA complex. Interestingly, the slight increase in polarity between acetonitrile and nitromethane (0.10 μ difference in dipole moment) causes a large increase in absorbance of the solution (Figure 114). To ensure reproducible yields, $CaCl_2$, a desiccant used to dry organic solvents, was necessary to include. This was realized when the highest yields of trifluoromethylation were recorded just after solvent purification, with diminishing returns as time progressed.

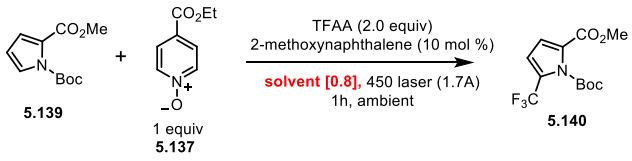

entry	Solvent	Yield (%)	entry	Solvent	Yield (%)
1	$MeNO_2$	***43***	10	Hexafluoroisopropanol (HFIP)	***0***
2	MeCN	***33***	11	DCE	***0***
3	DMF	***18***	12	$MeNO_2$ + HFIP (1eq)	***9***
4	THF	***12***	13	Cyclohexane	***9***
5	DMSO	***0***	14	$PhCF_3$:$MeNO_2$= 1:1	***42***
6	$MeNO_2$	***35***	15	$PhCF_3$:$MeNO_2$= 2:1	***35***
7	DMA	***0***	16	$PhCF_3$:$MeNO_2$= 5:1	***20***
8	AcOEt	***22***	17	$PhCF_3$:$MeNO_2$= 1:2	***24***
9	Trifluoroethanol	***0***			

Figure 113: Solvent Screen with Laser Irradiation Set-up

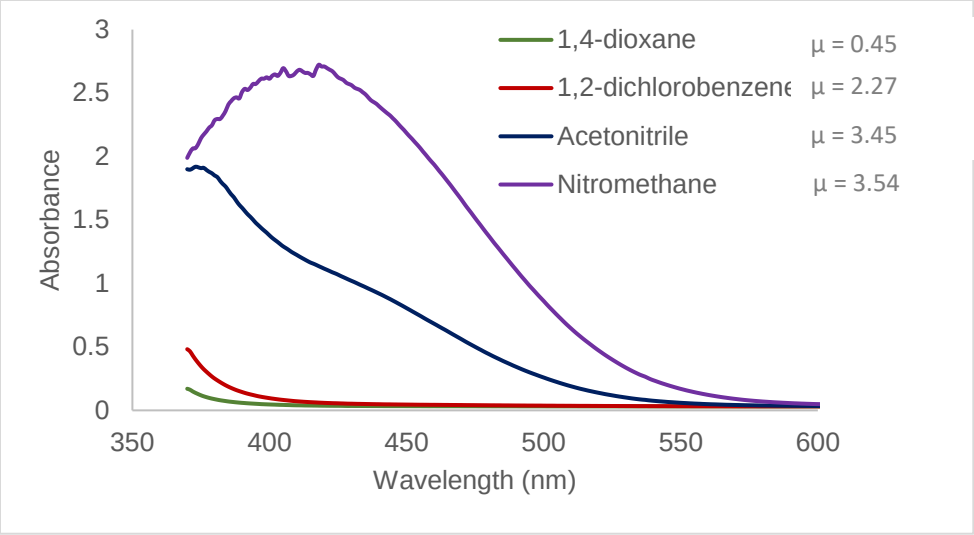

Figure 114: EDA complex formation as a function of solvent polarity

The laser irradiation EDA reaction now performs comparably to the Ru(II) catalyzed variant across a variety of substrates (Figure 115). Mesitylene and vetraldehyde reacted in high yield (**5.149-5.150**), showing this method is general to benzene based substrates. *tert*-Butylanisole (**5.148**) performed identically in the presence and absence of 2-methoxynaphthalene, proving this substrate to also be a competent donor initiator. Other heterocycles such as *N*-methyl nudifluorate methyl ester and benzothiophene (**5.144, 5.147**) also trifluoromethylated in moderate yield, surviving the excess loading of TFAA. Interesting pyrrole **5.145** failed to trifluoromethylate, highlighting the rapidity of background H-atom abstraction occurring in the reaction. Scaling the reaction to 1 mmol in target substrate has not matched the test scale optimization experiments (Figure 115B). Further work investigating continuous batch processing with overhead irradiation, or thin film irradiation will be conducted to assess the value of flow on EDA photochemical reactivity.

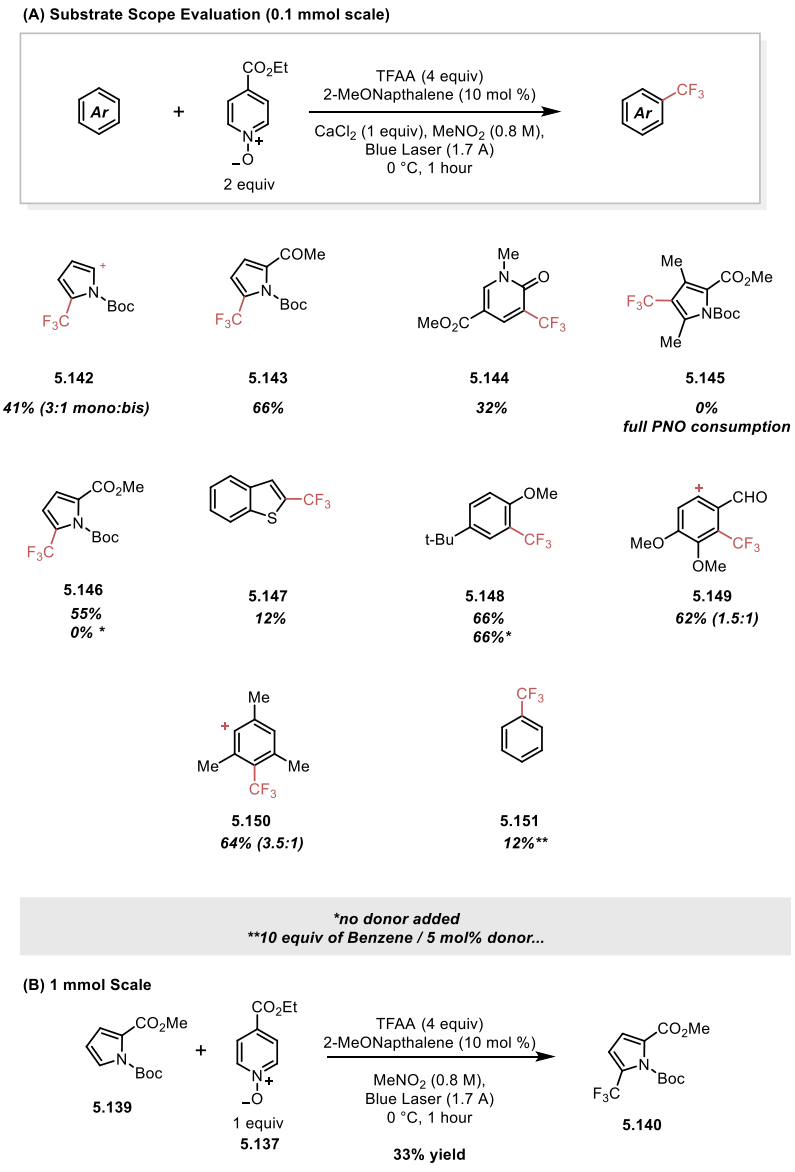

Figure 115: EDA Reaction Scope Evaluation

5.5 Discussion of EDA Complexation and Reaction Mechanism.

Realizing an EDA mediated photochemical method for the trifluoromethylation of arene small molecules beckons the question of what is the structure of this EDA complex? An initial investigation of the equilibrium constant revealed the title EDA complex exhibits a non-linear correlation between concentration and absorbance (Figure 117A-B), one that complicates standard equilibrium constant calculations based on Beer's law and the Benesi-Hildebrand equation.[334]

Investigating the stoichiometry of the EDA complex with Job's method (Figure 116), a maximally absorbing species exhibiting a 4:2:1 stoichiometry between TFAA, ethyl isonicotinate and 2-methoxynaphthalene in nitromethane was identified. The 2:1:1 stoichiometry also absorbs a significant fraction of light. Early studies using Job's method[335] also exhibited a 2:1 complexation in acetonitrile, suggesting that with sufficiently polar solvent an acylated pyridine N-oxide derivative will maximally saturate by binding a donor molecule as well as a counter ion. Counter ion studies using Job's method were not conducted.

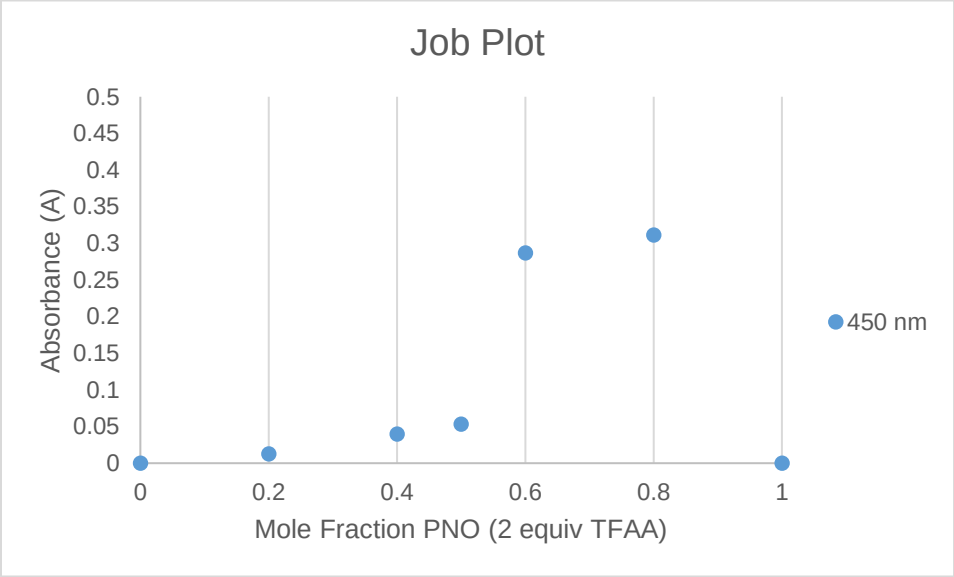

Figure 116 Job plot for optimal binding stoichiometry

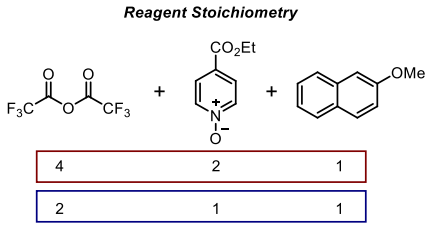

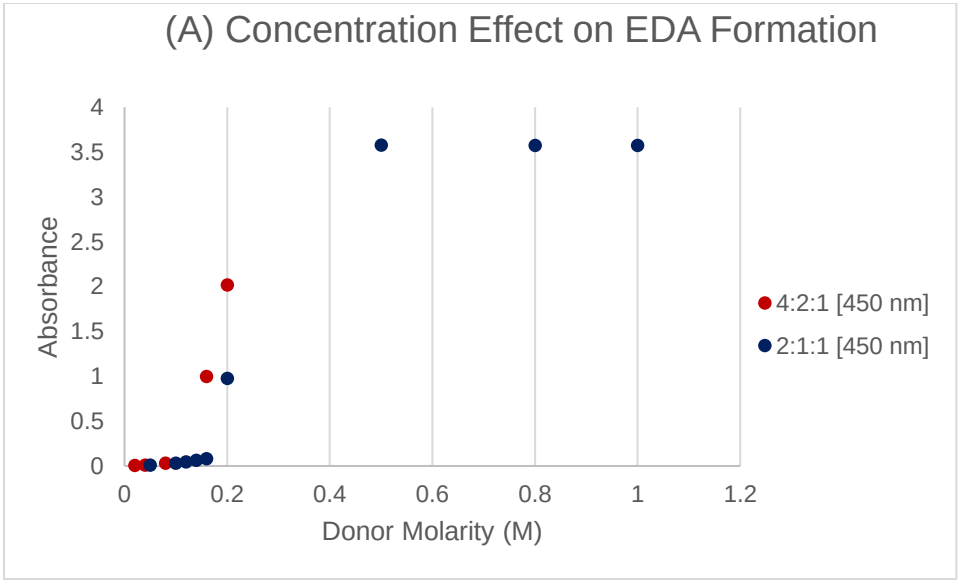

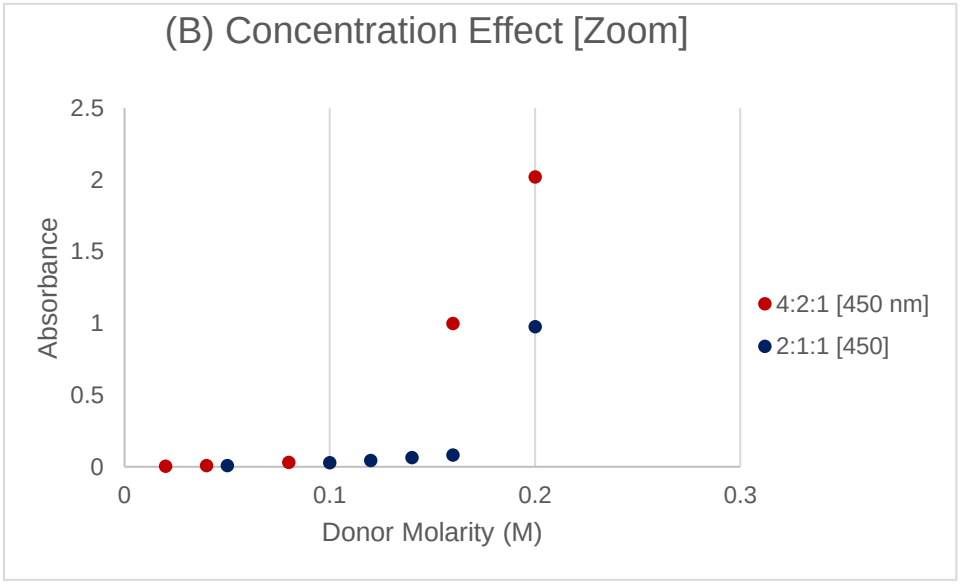

Figure 117 Concentration Effect on EDA Complex Formation

In addition to the slow addition experiments, an on-off irradiation experiment further supports a mechanistic hypothesis of a photoinitiated trifluoromethyl radical generation followed by a

sufficiently propagative chain process to afford the observed trifluoromethylated products. Failure to increase the yield after the second irradiation period, showcases the mechanistic likelihood of donor trifluoromethylation in competition with substrate trifluoromethylation during the reaction. The 2:1 EDA complex assists this picture, as not only can photoionization be maximized with the intercalation of a donor between two acceptors, but columbic repulsion from the radical ion state can facilitate solvent separation of the radical and ions. Solvent polarity works to maximize acylation and complexation, while temperature minimization and reaction concentration further facilitate EDA formation.

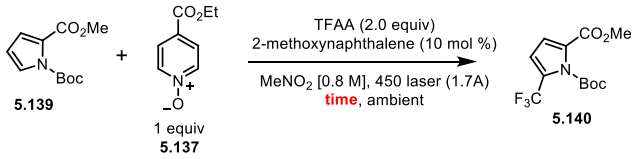

Time	15 min	30 min	1 h	2 h
Yield (%)	***30***	***41***	***48***	***49***

On/Off Experiment	On 10 min	Off 10 min	On 50 min
Yield (%)	***14%***		***18%***

Figure 118: On-Off Irradiation Experiment

5.6 Conclusion:

The following studies describe a photochemically initiated trifluoromethylation arising from the non-covalent binding of acylated pyridinium *N*-oxide derivatives and electron donating arenes. Specifically, the substoichiometric binding of 2-methoxynaphthalene with trifluoroacylated ethyl isonicotinate *N*-oxide afforded a productive source of trifluoromethyl radicals to functionalize a variety of exogenous arenes. This reaction was optimized through maximizing the formation of a target EDA complex, while laser irradiation ensured rapid conversion of the weakly associated complex to radical and ion degradation components. This study offers fundamental knowledge in

promoting simple, economically inexpensive and sustainable radical arene functionalization reactions using photochemistry.

Many EDA complexes have been characterized and investigated for stoichiometric reactivity. The described photochemically regulated EDA complex offers a unique reaction design while intricately balancing several factors to enable reactivity. Firstly, the described EDA complex consists of two aromatic molecules likely interacting a π-π stacking interaction. This is in contrast to the work of Melchiorre[315], Lenori[321,322], and Yu[94], all who have documented EDA complexes of n-donors (enolates and trialkylamines) with activated π or σ acceptors. In the lattermost case, the EDA interaction between hypervalent iodine or sulfonium accepters and trialkylamine donors is not photochemically regulated and occurs via thermal electron transfer in the ground state. This example represents the farthest extreme of a non-covalent bonding interaction prior to chemical change. In contrast, the acylated pyridine-*N*-oxide EDA complexes were stable up to 60 °C. Additionally, activation of TFA using TFAA and PNO is incompatible with many n-donors due to trifluoroacylation of anions and heteroatomic lone pairs; thus, it was central to the design of the EDA reagent that a π-donor was identified.

At the outset, investigation of the reactive efficiency of an EDA initiated trifluoromethylation reaction was a strong curiosity. It is now impressive to note that this method is comparable in yield to the Ru(II) catalyzed process, but also illuminating in the chemical processes of photochemical radical trifluoromethylation. The rate of Ru(II) excited state quenching with trifluoroacylated PNO and trifluoroacylated 4-Ph-PNO was measured at 3.6×10^7 and 2.5×10^8 s^{-1}, respectively.[336] The rate of pyridinium N-O bond fragmentation, as measured by Gould, is 2.7×10^{11}-1.7×10^{12} s^{-1}, 3-4 orders of magnitude faster than electronic quenching. This data, along with the qualitative knowledge that the Ru(II) catalyzed process progresses with a photochemically limiting darkening of the

reaction solution, demonstrates that Ru(II) photocatalyst trifluoromethylation is a significantly prevalent catalyst degradation pathway.[337] In the context of degrative trifluoromethylation, the EDA initiated is as notable as the Ru(II) catalysis because each method has the same limiting design parameter, and the EDA method is far simpler and cheaper. The success of the EDA process also influences one to think about reagent design, photocatalysis and reaction mechanism in a sobering fashion – how many photoredox catalyzed are solely enabled by the photocatalyst? For trifluoromethylation arising from an acylated PNO derivative, substrate supported background reactivity, or the lack thereof, is undeniably a contributing factor.

5.7 Experimental Methods:

All chemicals were used as received. Reactions were monitored by TLC and visualized with a dual short wave/long wave UV lamp. Column flash chromatography was performed using 230-400 mesh silica gel or via automated column chromatography. Preparative TLC purifications were run on silica plates of 1000 μm thickness. NMR spectra were recorded on Varian MR400, Varian Inova 500, Varian Vnmrs 500, or Varian Vnmrs 700 spectrometers. Chemical shifts for ^{1}H NMR were reported as δ, parts per million, relative to the signal of CHCl3 at 7.26 ppm. Chemical shifts for ^{13}C NMR were reported as δ, parts per million, relative to the center line signal of the CDCl3 triplet at 77.0 ppm. Chemical shifts for ^{19}F NMR were reported as δ, parts per million, relative to the signal of a trifluorotoluene internal standard at -63.72 ppm. The abbreviations s, br. s, d, dd, br. d, ddd, t, q, br. q, qi, m, and br. m stand for the resonance multiplicity singlet, broad singlet, doublet, doublet of doublets, broad doublet, doublet of doublet of doublets, triplet, quartet, broad quartet, quintet, multiplet and broad multiplet, respectively. IR spectra were recorded on a Perkin-Elmer Spectrum BX FT-IR spectrometer fitted with an ATR accessory. Mass Spectra were recorded at the Mass Spectrometry Facility at the Department of Chemistry of the University of Michigan in Ann Arbor, MI on an Agilent Q-TOF HPCL-MS with ESI high resolution mass spectrometer. TFAA was purified by distillation prior to usage. $MeNO_2$ was distilled over $CaCl_2$ prior to usage. Both TFAA and $MeNO_2$ were stored in individual desiccators in between reactions.

LED and laser irradiation sources:

Creative Lighting Solutions:

- Emerald Green LED Flexstrip, UV Reactive LED Flexstrip and Blue LED Flexstrip (all: 12 inch, 12vDC, w/JST connector (CL-FRS5050-12WP-12V)).

- Other associated parts: CL-PS94670-25W (25 W power supply), CL-PS16020-150W (150 W power supply), CL-PC6FT-PCW (power cord), CL-TERMBL-5P 182

Kessil LED lamp: H150N Blue (http://www.kessil.com/horticulture/H150.php).

Blue Laser Diode:

- Eagle Pair(R) 190-540 nm OD5 standard laser safety goggles
- 450 laser diode w/ 12mm copper module and G2 lens (Nachia: NUBM44 450(6W)). Purchased from: https://sites.google.com/site/dtrlpf/home/diodes/6w-nubm44-445nm-laser-diode (visited Sept 2017).
- Power meter: Costway EP20570 – 110 V
- Aluminium cooling shank: aluminum radiator heatsink 20x27x50mm for 12-13 mm laser diode module, golden from Flip Electrical.
- Vial adapter: CG-1318
- Septum Stopper, 24/40, CG302228 (available from Fisher):

5.7.1 Laser Irradiation Set-up:

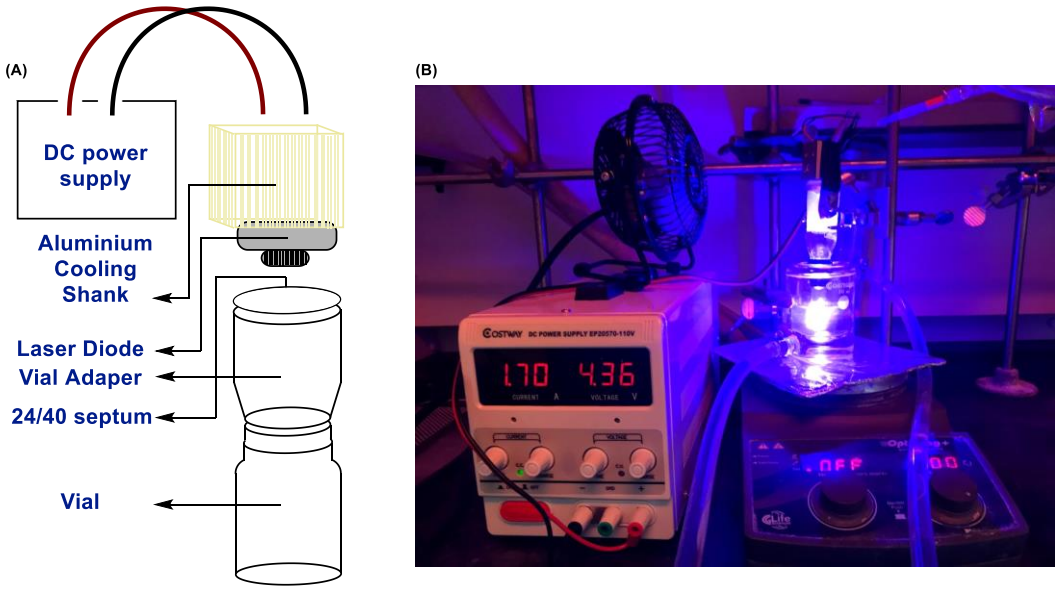

Laser Irradiation Set-up

Safety notice: The laser diode used in these studies is a Class 4 (>0.5 W light intensity). Permanent retinal damage can occur if ANSI compliant safety glasses are not worn. This reaction set up was operated in a fume hood with 3 layers of blue-light filtering amber film (available: UVprocess.com – accessed Oct 2017) along with laser compliant safety glasses. Consult local OSEA laser specific training prior to assembling and operating this set-up.

5.7.2 General Reaction Procedure A

Unless stated otherwise, all reactions were run on a 0.1 mmol scale in a 1-dram vial equipped with an oval shaped stir bar. 6W+ NUBM44-81 450 nm laser diode, set to 1.7 A current, sufficiently irradiated a reaction vial at one time. A fan placed perpendicular to the laser heatsink was used to dissipate the heat of the standing atmosphere A nitrogen inlet was threaded through the septum interface to maintain a dry and O_2 minimal atmosphere. To a flame dried vial with stir bar, substrate (0.1 mmol, 1 equiv) was weighed out. Then solid reagents included 4-CO_2Et PNO (2 equiv, 33.4 mg), 2-Methoxynaphthalene (0.1 equiv, 1.5 mg) and $CaCl_2$ (1 equiv, 11.1 mg) were

added to the vial. The whole was taken up in 125 μL of $MeNO_2$. Lastly, TFAA (56 μL, 4 equiv) was added to the solution changed from colorless to yellow-orange. The reaction was then attached to the laser module and stirred at 0°C for 5 minutes, prior to irradiation. Following this time, the reaction was irradiated for 60 minutes, and then the laser was turned off. To quench and analyze the reaction, 125 μL of MeOH was added, followed by 12.5 μL of benzotrifluoride. A sample of this mixture was taken for ^{1}H and ^{19}F NMR analysis, with the benzotrifluoride signal referenced to δ -63.72. T1 delay on ^{19}F NMR analysis was set to 5 seconds to ensure good integration fidelity in measuring reaction yields.

5.7.3 Reaction Optimization:

This followed the General Reaction Procedure A utilizing 1-(*tert*-butyl) 2-methyl 1*H*-pyrrole-1,2-dicarboxylate as the model substrate. Product peaks in the ^{19}F NMR were integrated with 1-(*tert*-butyl) 2-methyl 5-(trifluoromethyl)-1*H*-pyrrole-1,2-dicarboxylate observed at δ -59.6 (s, 3F).

5.7.4: Product Characterization

tert-butyl 2-(trifluoromethyl)-1_H_-pyrrole-1-carboxylate and _tert_-butyl 2,5-bis(trifluoromethyl)-1_H_-pyrrole-1-carboxylate (5.142)

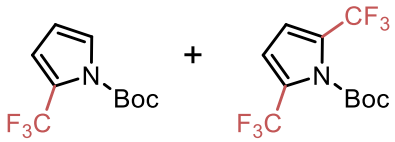

Following General Procedure A, *tert*-butyl-1*H*-pyrrole (0.100 mmol, 16.7 mg, 1 equiv) was reacted with ethyl isonicotinate *N*-oxide (33.4 mg, 2 equiv), 2-methoxynaphthalene (1.58 mg, 0.1 equiv), TFAA (56.4 µL, 4 equiv) and $CaCl_2$ (11.1 mg, 1 equiv) in 125 µL of solvent for 1 hour at 1.70 A 450 nm laser irradiation. ^{19}F NMR analysis of the crude reaction mixture referenced to benzotrifluoroide revealed the volatile title compound *tert*-butyl 2-(trifluoromethyl)-1*H*-pyrrole [^{19}F NMR ($CDCl_3$, 388 MHz): δ -59.28 (s, 3F, ***32%***)] and *tert*-butyl 2,5-bis(trifluoromethyl)-1*H*-pyrrole [^{19}F NMR ($CDCl_3$, 388 MHz): δ -59.36 (s, 3F, ***23%***)]. The isolation and characterization of these compounds has been previously reported. [306, 309]

tert-butyl 2-acetyl-5-(trifluoromethyl)-1_H_-pyrrole-1-carboxylate (5.143)

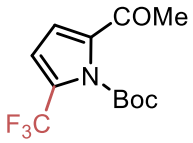

Following General Procedure A, *tert*-butyl 2-acetyl-1*H*-pyrrole-1-carboxylate (0.100 mmol, 26.3, 1 equiv) was reacted with ethyl isonicotinate *N*-oxide (33.4 mg, 2 equiv), 2-methoxynaphthalene (1.58 mg, 0.1 equiv), TFAA (56.4 μL, 4 equiv) and $CaCl_2$ (11.1 mg, 1 equiv) in 125 μL of solvent for 1 hour at 1.70 A 450 nm laser irradiation. ^{19}F NMR analysis of the crude reaction mixture referenced to benzotrifluoroide revealed the volatile title compound *tert*-butyl 2-acetyl-5-(trifluoromethyl)-1*H*-pyrrole [^{19}F NMR ($CDCl_3$, 388 MHz): δ -59.8 (s, 3F, ***68%***)]. The isolation and characterization of these compounds has been previously reported. [306, 309]

1-methyl-5-trifluoromethyl nudifluorate (5.144)

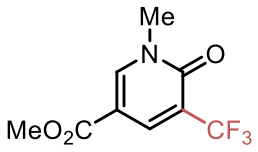

Following General Procedure A, 1-methylnudifluorate methyl ester (0.100 mmol, 16.7 mg, 1 equiv) was reacted with ethyl isonicotinate *N*-oxide (33.4 mg, 2 equiv), 2-methoxynaphthalene (1.58 mg, 0.1 equiv), TFAA (56.4 μL, 4 equiv) and $CaCl_2$ (11.1 mg, 1 equiv) in 125 μL of solvent for 1 hour at 1.70 A 450 nm laser irradiation. ^{19}F NMR analysis of the crude reaction mixture referenced to benzotrifluoroide revealed the volatile title compound 1-methyl-5-trifluoromethyl nudifluorate methyl ester [^{19}F NMR ($CDCl_3$, 388 MHz): δ -67.2 (s, 3F, ***32%***)]. The isolation and characterization of these compounds has been previously reported.[306, 309]

1-(*tert*-butyl) 2-methyl 5-(trifluoromethyl)-1*H*-pyrrole-1,2-dicarboxylate (5.146)

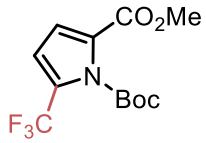

Following General Procedure A, 1-(*tert*-butyl) 2-methyl 1*H*-pyrrole-1,2-dicarboxylate (0.100 mmol, 26.3 mg, 1 equiv) was reacted with ethyl isonicotinate *N*-oxide (33.4 mg, 2 equiv), 2-methoxynaphthalene (1.58 mg, 0.1 equiv), TFAA (56.4 μL, 4 equiv) and $CaCl_2$ (11.1 mg, 1 equiv) in 125 μL of solvent for 1 hour at 1.70 A 450 nm laser irradiation. ^{19}F NMR analysis of the crude reaction mixture referenced to benzotrifluoroide revealed the volatile title compound 1-(*tert*-butyl) 2-methyl 5-(trifluoromethyl)-1*H*-pyrrole-1,2-dicarboxylate [^{19}F NMR ($CDCl_3$, 388 MHz): δ -59.6 (s, 3F, ***55%***)]. The isolation and characterization of these compounds has been previously reported.[306, 309]

2-(trifluoromethyl)benzo[*b*]thiophene (5.147)

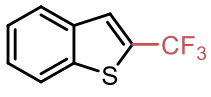

Following General Procedure A, benzothiophene (1.0 mmol, 134 mg, 1 equiv) was reacted with ethyl isonicotinate *N*-oxide (167 mg, 1 equiv), 2-methoxynaphthalene (1.58 mg, 0.1 equiv), TFAA (282 μL, 4 equiv) and $CaCl_2$ (111 mg, 1 equiv) in 1.25 mL of solvent for 1 hour at 1.70 A 450 nm laser irradiation. ^{19}F NMR analysis of the crude reaction mixture referenced to benzotrifluoroide revealed the volatile title compound 2-trifluoromethylbenzothiophene [^{19}F NMR ($CDCl_3$, 388 MHz): δ -57.3 (s, 3F, ***66%***)]. The isolation and characterization of these compounds has been previously reported. [338]

4-(*tert*-butyl)-1-methoxy-2-(trifluoromethyl)benzene (5.148)

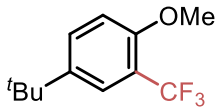

Following General Procedure A, 4-*tert*-butylanisole (0.100 mmol, 17.5 µL, 1 equiv) was reacted with ethyl isonicotinate *N*-oxide (33.4 mg, 2 equiv), 2-methoxynaphthalene (1.58 mg, 0.1 equiv), TFAA (56.4 µL, 4 equiv) and $CaCl_2$ (11.1 mg, 1 equiv) in 125 µL of solvent for 1 hour at 1.70 A 450 nm laser irradiation. ^{19}F NMR analysis of the crude reaction mixture referenced to benzotrifluoroide revealed the volatile title compound 4-(*tert*-butyl)-1-methoxy-2-(trifluoromethyl)benzene [^{19}F NMR ($CDCl_3$, 388 MHz): δ -63.12 (s, 3F, ***66%***)]. The isolation and characterization of these compounds has been previously reported.[306, 309]

The procedure was repeated with the omission of 2-Methoxynaphthalene to obtain a yield of ***66***% signifying a competitive binding and reaction between the 4-*tert*-butylanisole and acylated PNO reagent, as compared to the 2-Methoxynaphthalene enabled reaction.

2-trifluoromethylveratraldehyde and 2,5-bistrifluoromethylveratraldehyde3,4-dimethoxy-2-(trifluoromethyl)benzaldehyde (5.149)

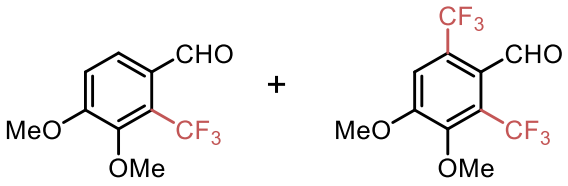

Following General Procedure A, 3,4-dimethoxybenzaldehyde (0.100 mmol, 16.6 mg, 1 equiv) was reacted with ethyl isonicotinate *N*-oxide (33.4 mg, 2 equiv), 2-methoxynaphthalene (1.58 mg, 0.1 equiv), TFAA (56.4 µL, 4 equiv) and $CaCl_2$ (11.1 mg, 1 equiv) in 125 µL of solvent for 1 hour at 1.70 A 450 nm laser irradiation. ^{19}F NMR analysis of the crude reaction mixture referenced to benzotrifluoroide revealed the volatile title compounds 3,4-dimethoxy-2-(trifluoromethyl)benzaldehyde [^{19}F NMR ($CDCl_3$, 388 MHz): δ -54.67 (s, 3F, ***42%***)] and 3,4-dimethoxy-2,5-bis(trifluoromethyl)benzaldehyde [^{19}F NMR ($CDCl_3$, 388 MHz): δ -53.87 (s, 3F, ***28%***)]. The isolation and characterization of these compounds has been previously reported. [339]

1,3,5-trimethyl-2-(trifluoromethyl)benzene and 1,3,5-trimethyl-2,4-bis(trifluoromethyl)benzene (5.150)

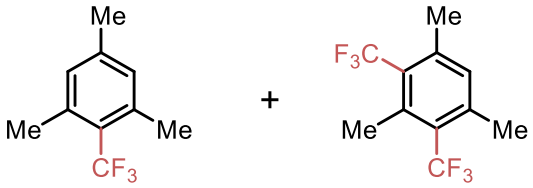

Following General Procedure A, mesitylene (0.100 mmol, 13.9 μL, 1 equiv) was reacted with ethyl isonicotinate *N*-oxide (33.4 mg, 2 equiv), 2-methoxynaphthalene (1.58 mg, 0.1 equiv), TFAA (56.4 μL, 4 equiv) and $CaCl_2$ (11.1 mg, 1 equiv) in 125 μL of solvent for 1 hour at 1.70 A 450 nm laser irradiation. ^{19}F NMR analysis of the crude reaction mixture referenced to benzotrifluoroide revealed the volatile title compounds 1,3,5-trimethyl-2-(trifluoromethyl)benzene [^{19}F NMR ($CDCl_3$, 388 MHz): δ -54.7 (s, 3F, ***49%***)] and 1,3,5-trimethyl-2,4-bis(trifluoromethyl)benzene [^{19}F NMR ($CDCl_3$, 388 MHz): δ -53.9 (s, 3F, ***14%***)]. The isolation and characterization of these compounds has been previously reported.[306, 309]

1,1,1-trifluorotoluene (5.151)

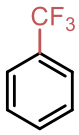

Following General Procedure A, benzene (2.0 mmol, 178 μL, 10 equiv) was reacted with ethyl isonicotinate *N*-oxide (33.4 mg, 2 equiv), 2-methoxynaphthalene (1.58 mg, 0.1 equiv), TFAA (56.4 μL, 4 equiv) and $CaCl_2$ (11.1 mg, 1 equiv) in 125 μL of solvent for 1 hour at 1.70 A 450 nm laser irradiation. ^{19}F NMR analysis of the crude reaction mixture referenced to 2,2,2-trifluoroethanol revealed the volatile title compound 1,1,1-trifluoromethyltoluene [^{19}F NMR ($CDCl_3$, 388 MHz): δ -63.7 (s, 3F, ***12%***)]. The isolation and characterization of these compounds has been previously reported.[306, 309]

5.7.5: Photon Flux Experiment

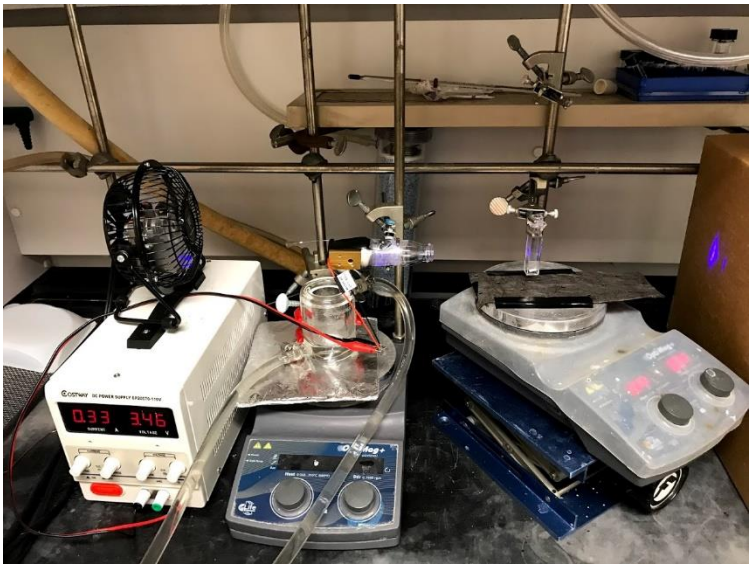

Figure 119: Flux Experiment Set-up

Standard Sample preparation[340]:

0.05 M stock solution: To a 100 mL volumetric flask, 0.281 mL of concentrate H_2SO_4 was added to 90 mL of deionized water. Then the remainder of volume was filled with deionized water to the 100 mL graduation mark.

0.15 M potassium ferrioxolate solution: This solution was prepared by dissolving solid $K_3FeC_2O_4 \cdot 3H_2O$ (1.842 g, 3.75 mmol) in 20 mL of 0.05 M $H_2SO_{4\,(aq)}$ solution. The remainder of the 25 mL volume was then filled with 0.05 M $H_2SO_{4\,(aq)}$ after ensuring the ferrioxylated had fully dissolved. This solution was stored in an amber bottle and kept in the dark except for the brief time it was in use.

Developer solution: 225 g of sodium acetate trihydrate was dissolved in 1 liter of 0.5 M sulfuric acid. 10 g of 1,10-phenantroline was added to this solution. This was stored in a 1 L clear glass bottle, but stored in the dark when not in use.

Experiment preparation: Prior to running the experiment, 5x3 2 dram amber vials were filled with 5x0.9 mL with a 1 mL repeater pipette and capped. The laser was aligned and pre-set to the desired input current by irradiating an empty cuvette to ensure the beam was not reflecting off the stir bar, or stir plate below. After alignment the laser was turned off. In the dark, to a 1 mL quartz cuvette was charged with 3x0.9 mL of the 0.15 M potassium ferrioxolate solution. This was stirred at 700 rpm for 1 minute prior to extracting 10 uL and adding it to a vial of developer solution. To being the reaction, an object used to block the laser beam was placed in between the laser and the stirring reaction. Then the laser was turned on and allowed to settle on the desired light output (this takes 10-15 seconds, often over-shoots the programmed amperage). Then the barrier was removed and the reaction began. 10 μL aliquots were extracted and added to individual vials of developer solution. Each light setting was repeated three times.

Data Analysis:

To calculate the photon flux, first determine the number of Fe^{2+} ions produced in the reaction:

$$moles\ Fe^{2+} = \frac{\Delta A_{510\ nm} V_1 V_3}{\varepsilon_{510\ nm} l V_2}$$

ΔA = difference in absorbance at 510 nm between sample and t_0 time point

l = pathlength of cuvette (1 cm)

$\varepsilon_{510\ nm}$ = Extinction coefficient of $Fe(phen)_3$ complex at 510 nm (11,100 M^{-1} cm^{-1})

V_1 = total volume of irradiated solution (3x0.9 mL = 2.7 mL)

V_2 = volume of aliquot extracted from V_1 (0.01 mL)

V_3 – volume that V_2 is diluted to (5x0.9 mL = 4.5 mL)

Photon flux is then determined as

$$photon\ flux = \frac{moles\ of\ Fe^{2+}}{\emptyset_{405\ nm} \bullet t \bullet F}$$

$\emptyset_{450} = 0.93$[341]

t = time evolved (seconds)

F = mean fraction of light absorbed by the ferrioxalate solution (F = 0.986)

0.71 A 450 nm Laser Irradiation: Flux = 2.98×10^{-6} mol photons/second

Table 7: Photon flux data for 0.71A 450 nm laser irradiation

time of irr	1	2	3	mean	std dev	rel dev	dA
0	0.266846	0.280273	0.265259	0.270793	0.008248	3%	0
15	0.466064	omit	0.450806	0.458435	0.010789	2%	0.187642
30	0.727173	0.701782	0.671997	0.700317	0.027617	4%	0.429525
45	0.86731	0.907837	0.85437	0.876506	0.027894	3%	0.605713
60	omit	0.949219	0.994507	0.971863	0.032023	3%	0.70107
75	1.005737	1.236328	1.178955	1.14034	0.120047	11%	0.869547

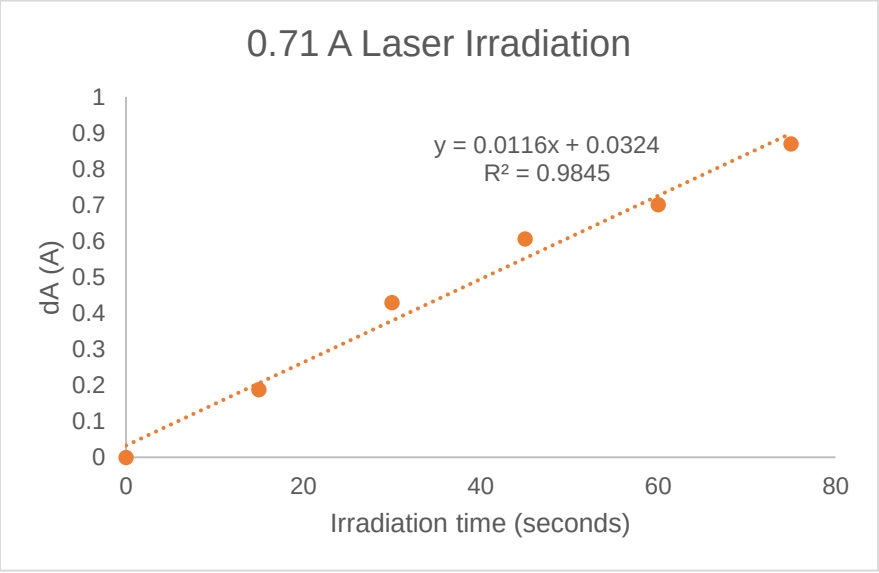

Figure 120: Photon flux using 0.71A 450 nm Laser irradiation

1.70 A 450 nm Laser Irradiation: Flux = 5.44 x 10^{-6} mol photon/second

Table 8: Photon flux data for 1.70 A 450 nm laser irradiation

time of irr	1	2	3	mean	std dev	rel dev	dA
0	0.285889	0.281006	0.293945	0.286946667	1%	0.022771	0
10	0.79895	0.791016	0.757202	0.782389333	2%	0.028337	0.495443
20	1.216553	1.107666	1.074097	1.132772	7%	0.065744	0.845825
30	1.06311	1.392578	0.775879	1.077189	31%	0.286478	0.790242

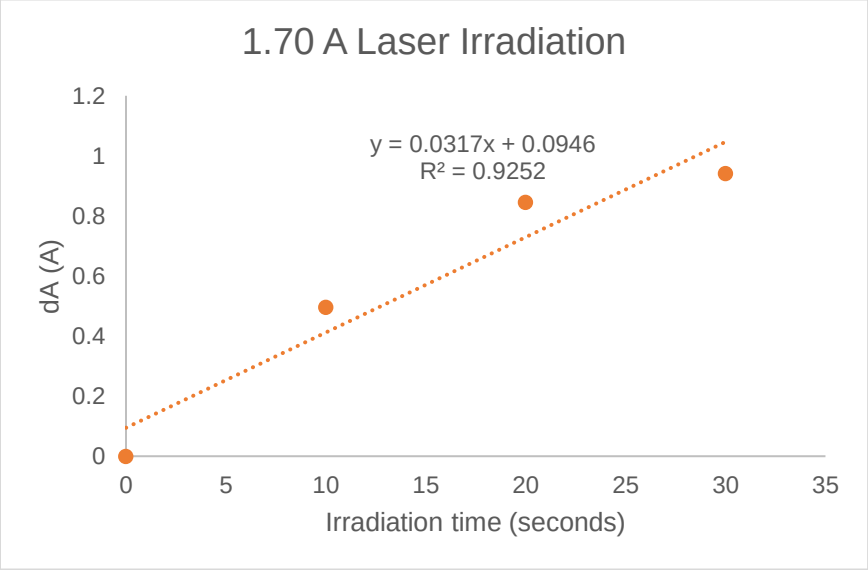

Figure 121: Photon Flux time using 1.70 A 450 nm laser irradiation

H150N Blue Kessil Light Irradiation: Flux = 1.57 x 10^{-7} mol photons/second

Two of the sides of the vial were taped off with black electrical tape to ensure a single path length of 1 cm.

Table 9: Photon flux data for H150N Blue Kessil lamp irradiation

time of irr	1	2	3	mean	std dev	rel dev	dA
0	0.362915	0.333496	0.331543	0.342651	0.017576	5%	0
1.5	0.492065	0.466064	0.474487	0.477539	0.013266	3%	0.134887
3	0.543335	0.590332	0.608398	0.580688	0.033586	6%	0.238037
4.5	0.698486	0.680176	0.658203	0.678955	0.020169	3%	0.336304
6	0.754517	0.824341	0.737061	0.771973	0.046184	6%	0.429322

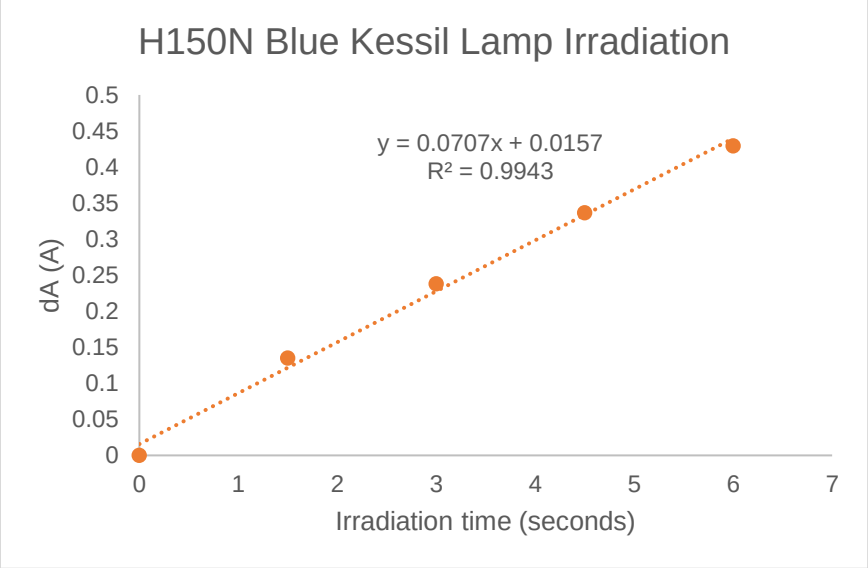

Figure 122: Photon flux time using H150 Kessil Blue lamp irradiation

5.7.6: UV-Vis studies of EDA complex mixture.

UV-Vis analysis was carried out on a Shimadzu UV-1601 UV-Vis spectrometer with accompanying Peltier temperature controller set to 23°C. Solutions were made to 2.5 mL in a 1x1 cm quartz cuvette.

The following concentrations were used for each of the reported UV-Vis spectra

Table 10: Conditions for Provided UV-Vis Data of EDA Complexes

Figure	Solvent	2-methoxynaphthalene	4-CO_2Et PNO	TFAA
Figure 106	$MeNO_2$	0.04 M	0.4 M	0.8 M
Figure 111	MeCN	0.04 M	0.4 M	0.4 M
Figure 114	1,4-dioxane	0.2 M	0.2 M	0.4 M
Figure 114	1,2-dichlorobenzene	0.2 M	0.2 M	0.4 M
Figure 114	MeCN	0.2 M	0.2 M	0.4 M
Figure 114	$MeNO_2$	0.2 M	0.2 M	0.4 M
Figure 116	$MeNO_2$	0.2 M-X	X Where $0 < x < 0.2M$	2X

Figure 117	$MeNO_2$ (4:2:1 complex)	0.02, 0.04, 0.08, 0.16, 0.20 M	0.03, 0.06, 0.12, 0.24, 0.30 M	0.06, 0.12, 0.24, 0.48, 0.60 M
Figure 117	$MeNO_2$ (2:2:1 complex)	0.05, 0.12, 0.14, 0.16, 0.1, 0.2, 0.3, 0.5, 0.8, 1.0 M	0.05, 0.12, 0.14, 0.16, 0.1, 0.2, 0.3, 0.5, 0.8, 1.0 M	0.10, 0.24, 0.28, 0.32, 0.20, 0.40, 0.60, 1.0, 1.6, 2.0 M

Bibliography

[1] Nicolaou, K.C.; Montagnon, T. *Molecules That Changed The World*. Wiley-VCH. Weinheim, 2008.

[2] Tucker, J.L. *Org. Process Res. Dev.* **2006**, *10*, 315–319.

[3] Albini, A.; Fagnoni, M. *ChemSusChem* **2008**, *1*, 63-66.

[4] Ciamicin, G. *Science* **1912**, *36*, 385-394.

[5] Ciamician, G.; Silber, P. Chemische Lichtwirkungen. *Ber. Dtsch. Chem. Ges*. **1908**, *41*, 1928−1935.

[6] Yoon, T.P.; Ischay, M.A.; Juana, D. *Nature Chem.* **2010**, *2*, 527-532.

[7] Kärkäs, M.D.; Porco, J.A.; Stephenson, C.R.J. *Chem. Rev.* **2016**, *116*, 9683-9747.

[8] Noyes Jr., W.A.; Porther, G.B.; Jolley, J.E. *Chem. Rev.* **1956**, *56*, 49-94.

[9] Corey, E.J.; Bass, J.D.; LeMahieu, R.; Mitra, R.B. *J. Am. Chem. Soc.* **1964**, *86*, 5570-5583.

[10] Platz, M.S. Nitrenes. In *Reactive Intermediates Chemistry*; Moss, R.A.; Platz, M.S.; Jones, M., Eds.; Wiley & Sons, Inc.: Hoboken, 2003.

[11] Cornelisse, J.; *Chem. Rev.* **1993**, *93*, 615-669.

[12] Narayanam, J.M.R.; Stephenson, C.R.J. *Chem. Soc. Rev.* **2011**, *40*, 102-113.

[13] Tucker, J.W.; Stephenson, C.R.J. *J. Org. Chem.* **2011**, *77*, 1617-1622.

[14] Prier, C.K.; Rankic, D.A.; MacMillan, D.W.C. *Chem. Rev.* **2013,** *113*, 5322-5363.

[15] Romero, N.A.; Nicewicz, D.A. *Chem. Rev.* **2016**, *116*, 10075-10166.

[16] Photochemistry and Photophysics of Coordination Compounds I. In *Topics in Current Chemistry*; Balzani, V.; Campagna, S. Ed.; Springer-Verlag Berlin Heidelberg, 2007; Vol. 280, p. 1-273.

[17] Photochemistry and Photophysics of Coordination Compounds II. In *Topics in Current Chemistry*; Balzani, V.; Campagna, S. Ed.; Springer-Verlag Berin Heidelberg, 2007; Vol. 281, p. 1-327.

[18] Damrauer, N. H.; Cerullo, G.; Yeh, A.; Boussie, T. R.; Shank, C. V.; McCusker, J. K. *Science* **1997**, *275*, 54-57.

[19] Wrighton, M.; Markham, J. *J. Phys. Chem.* **1973**, *77*, 3042-3044.

[20] Lu, Z.; Yoon, T.P. *Angew. Chem. Int. Ed.* **2012**, *51*, 10392-10332.

[21] Skubi, K.L.; Kidd, J.B.; Jung, H.; Guzei, I.A.; Baik, M-H.; Yoon, T.P. *J. Am. Chem. Soc.* **2017**, *139*, 17186-17192.

[22] Hörmann, F.M.; Chung, T.S.; Rodriguez, E.; Jakob, M.; Bach, T. *Angew. Chem. Int. Ed.* **2018**, *57*, 827-831.

[23] Zhao, J.; Brosmer, J.L.; Tang, Q.; Yang, Z.; Houk, K.N.; Diaconescu, P.L.; Kwon, O. *J. Am. Chem. Soc.* **2017**, *139*, 9807-9810.

[24] Wang, C.; Lu, Z. *Org. Lett.* **2017**, *19*, 5888-5891.

[25] Farney, E.P.; Yoon, T.P. *Angew. Chem. Int. Ed.* **2014**, *53*, 793-797.

[26] Scholz, S.O.; Farney, E.P.; Kim, S.; Bates, D.M.; Yoon, T.P. *Angew. Chem. Int. Ed.* **2016**, *55*, 2239-2242.

[27] Welin, E.R.; Le, C.; Arias-Rotondo, D.M.; McCusker, J.K.; MacMillan, D.W.C. *Science*, **2017**, *355*, 380-385.

[28] Assumes entropic considerations are negligible in MLCT.

[29] Green, N.J.; Pimblott, S.M.; Tachiya, M. *J. Phys. Chem.* **1993**, *97*, 196-202.

[30] Arias-Rotondo, D. M.; McCusker, J. K. *Chem. Soc. Rev.* **2016**, *45*, 5803-5820.

[31] Darwent, J.R.; Kalyanasundaram, K. *J. Chem. Soc., Faraday Trans. 2.* **1981**, *77*, 373-382.

[32] Prantz, K.; Mulzer, J. *Chem Rev.* **2010**, *110*, 3741-3766.

[33] Moad, G.; Rizzard, E.; Thang, S.H. *Polymer* **2008**, *49*, 1079-1131.

[34] Perrier, S. *Macromolecules* **2017**, *50*, 7433-7447.

[35] Sternbach, D.; Jaisli, F.; Bonetti, M.; Eschenmoser, A.; Shibuya, M. *Angew. Chem. Int. Ed.* **1979**, *18*, 634-636.

[36] Shibuya, M.; Jaisli, F., Eschenmoser, A. *Angew. Chem. Int. Ed.* **1979**, *18*, 636-637

[37] Barton, D.H.R.; Crich, D.; Motherwell, W.B. *J. Chem. Soc. Chem. Commun.* **1983**, *0*, 939-941.

[38] Barton, D. H. R.; Parekh, S. I. and Tse, C.-L. *Tetrahedron Lett*. **1993**, *34*, 2733-2736.

[39] Spiegel, D.A.; Wiberg, K.B.; Schacherer, L.N.; Medeiros, M.R.; Wood, J.L. *J. Am. Chem. Soc.* **2005**, *127*, 12513-12515.

[40] Fukuzumi, S.; Koumitzu, S.; Hironaka, K.; Tanaka, T. *J. Am. Chem. Soc.* **1987**, *109*, 305-316.

[41] Connelly, N.G.; Geiger, W.E. *Chem. Rev.* **1996**, *96*, 877-910.

[42] Anne, A.; Hapiot, P.; Meiroux, J.; Neta, P.; Savéant, J-M. *J. Am. Chem. Soc.* **1992**, *114*, 4694-4701.

[43] Hedstrand, D.M.; Kruizinga, W.H.; Kellogg, R.M. *Tetrahedron Lett.* **1978**, *14*, 1255-1258.

[44] Pac, C.; Ihama, M.; Yasuda, M.; Miyauchi, Y.; Sakurai, H. *J. Am. Chem. Soc.* **1981**, *103*, 6495-6497.

[45] Ishitani, O.; Yanagida, S.; Takamuku, S.; Pac, C. *J. Org. Chem.* **1987**, 52, 2790–2796.

[46] Ishitani, O.; Ihama, M.; Miyauchi, Y.; Pac, C. *J. Chem. Soc. Perkin. Trans. 1* **1985**, 1527-1537.

[47] Fukuzumi, S.; Mochizuki, S.; Tanaka, T. *J. Phys. Chem.* **1990**, *94*, 722-726.

[48] Hasebe, M.; Tsuchiya, T. *Tetrahedron Lett.* **1987**, *28*, 6207-6210.

[49] Okada, K.; Okamoto, K.; Oda, M. *J. Chem. Soc., Chem. Commun.* **1989**, *0*, 1636-1637.

[50] Okada, K.; Okamoto, K.; Oda, M. *J. Am. Chem. Soc.* **1988**, *110*, 8736-8738.

[51] Okada, K.; Okamoto, K.; Morita, N.; Okubo, K.; Oda, M. *J. Am. Chem. Soc.* **1991**, *113*, 9401-9402.

[52] Okada, K.; Okubo, K.; Morita, N.; Oda, M. *Tetrahedron Lett.* **1992**, *33*, 7377-7380.

[53] Roberts, B.P. *Chem. Soc. Rev.* **1999**, *28*, 25-35.

[54] Cano-Yelo, H.; Deronzier, A. *J. Chem. Soc., Perkin Trans. 2* **1984**, *0*, 1093-1094

[55] Cox, A.; Kemp, T.J.; Payne, D.R.; Symons, M.C.R.; Allen, D.M.; Pinot de Moira, P. *J. Chem. Soc., Chem. Commun.* **1976**, 693-694.

[56] Cano-Yelo, H.; Deronzier, A. *Tetrahedron Lett.* **1984**, *25*, 5517-5520.

[57] Cano-Yelo, H.; Deronzier, A. *J. Photochem.* **1987**, *37*, 315-321.

[58] Ischay, M.A.; Anzovino, M.E.; Du, J.; Yoon, T.P. *J. Am. Chem. Soc.* **2008**, *130*, 12886-12887.

[59] Nicewicz, D.A.; MacMillan, D.W.C. *Science*, **2008**, *322*, 77-80.

[60] Narayanam, J.M.R.; Tucker, J.W.; Stephenson, C.R.J. *J. Am. Chem. Soc.* **2009**, *131*, 8756-8757.

[61] Pause, L.; Robert, M.; Savéant, J-M. *J. Am. Chem. Soc.* **1999**, *121*, 7158-7159.

[62] Costentin, C.; Robert, M.; Savéant, J-M. *J. Am. Chem. Soc.* **2004**, *126*, 16051-16057.

[63] Maslak, P. Fragmentations by photoinduced electron transfer. Fundamentals and practical aspects. In *Photoinduced Electron Transfer V.* Mattay, J., Ed.; Springer, Berlin Heidelberg, 1993; Vol. 168, p. 1-47.

[64] Even in the instance of rapid electron transfer – decarboxylation of α–anilino carboxylate is slower than the generation of MV• : Su, Z.; Falvey, D.E.; Yoon, U.C.; Mariano, P.S. *J. Am. Chem. Soc.* **1997**, *119*, 5261-5262.

[65] Schnermann, M.J.; Overman, L.E. *Angew. Chem. Int. Ed.* **2012**, *51*, 9576-9580.

[66] Lackner, G.L.; Quasdorf, K.W.; Overman, L.E. *J. Am. Chem. Soc.* **2013**, *135*, 15342-15345

[67] Lackner, G.L.; Quasdorf, K.W.; Pratsch, G.; Overman, L.E. *J. Org. Chem.* **2015**, *80*, 6012-6024.

[68] Narwat, C.C.; Jamison, C.R.; Slutskyy, Y.; MacMillan, D.W.C.; Overman, L.E. *J. Am. Chem. Soc.* **2015**, *137*, 11270-11273.

[69] Chu, L.; Ohta, C.; Zuo, Z.; MacMillan, D.W.C. *J. Am. Chem. Soc.* **2014**, *136*, 10886-10889.

[70] Zhang, L; Jiao, L. *J. Am. Chem. Soc.* **2017**, *139*, 607-610.

[71] Qin, T.; Cornella, J.; Li, C.; Malins, L.R.; Edwards, J.T.; Kawamura, S.; Maxwell, B.D.; Eastgate, M.D.; Baran, P.S. *Science* **2016**, *352*, 801-805.

[72] Cornella, J.; Edwards, J.T.; Quin, T.; Kawamura, S.; Wang, J.; Pan, C–M.; Giantassio, R.; Schmidt, M.; Eastgate, M.D.; Baran, P.S. *J. Am. Chem. Soc.* **2016**, *138*, 2174-2177.

[73] Huihui, K.M.M.; Caputo, J.A.; Melchor, Z.; Olivares, A.M.; Spiewak, A. M.; Johnson, K.A.; Dibenedetto, T.A.; Kim, S.; Ackerman, L.K.G.; Weix, D.J. *J. Am. Chem. Soc.* **2016**, *138*, 5016-5019.

[74] Candish, L.; Teders, M.; Glorius, F. *J. Am. Chem. Soc.* **2017**, *139*, 7440-7443.

[75] Additional examples include: (A) Wang, D.; Chen, P.; Lin, Z.; Liu, G. *J. Am. Chem. Soc.* **2017**, *139*, 15632-15635. (A) Sherwood, T.C.; Li, N.; Yazdani, A.N.; Dhar, T.G.M. *J. Org. Chem.* **2018**, *83*, 3000-3012. (b) Tlahuext-Aca, A.; Candish, L.; Garza-Sanchez, R.A.; Glorius, F. *ACS Catalysis*, 2018, 8. 1715-1719. (c) Tlahuext-Aca, A.; Candish, L.; Garza-Sanchez, R.A.; Schafer, M.; Glorius, F. *Org. Lett.* ***2018****, 20*, 1546-1549.

[76] Gutiérrez-Bonet, Á.; Remur, C.; Matsui, J.K.; Molander, G.A. *J. Am. Chem. Soc.* **2017**, *139*, 12251-12258.

[77] Chen, W.; Liu, Z.; Tian, J.; Li, J.; Ma, J.; Cheng, X.; Li, G. *J. Am. Chem. Soc.* **2016**, *138*, 12312-12315.

[78] Gutiérrez-Bonet, A.; Tellis, J.C.; Matsui, J.K.; Bara, B.A.; Molander, G.A. *ACS Catal*. **2016**, *6*, 8004-8008.

[79] Buzzetti, L.; Prieto, A.; Roy, S.R.; Melchiorre, P. *Angew. Chem. Int. Ed.* **2017**, *56*, 15039-15043.

[80] Verrier, C.; Alandini, N.; Pezzetta, C.; Moliterno, M.; Buzzetti, L.; Hepbrun, H.B.; Vega-Peñaloza, A.; Silvi, M.; Melchiorre, P. *ACS Catalysis* **2018**, *8*, 1062-1066.

[81] C. Punta, F. Minisci, *Trends Heterocycl. Chem*. **2008**, *13*, 1 – 68.

[82] Cernak, T.; Dykstra, K.D.; Tyagarajan, S.; Vachal, P.; Krska, S.W. *Chem. Soc. Rev.* **2016**, *45*, 546-576.

[83] DiRocco, D.A.; Dykstra, K.; Krska, S.; Vachal, P.; Conway, D.V.; Tudge, M. *Angew. Chem. Int. Ed.* **2014**, *53*, 4802-4806.

[84] Properties of Atoms, Radicals and Bonds. In *Lange's Handbook of Chemistry*; Dean, J.A., Ed.; McGraw-Hill: New York, 1999; p 439 .

[85] Data from Scaiano, Ingold and Fouassier suggest that energy transfer is a more likely energetic event between a visible light photosensitizer and a diacyl peroxide: (a) Ingold, K.U.; Johnston, L.J.; Lusztyk, J.; Scaiano, J.C. *Chem. Phys. Lett.* **1984**, *110*, 433-436. (b) Morlet-Savary, F.; Wieder, F.; Fouassier, J.P. *J. Chem. Soc., Faraday Trans.* **1997**, *93*, 3931-3937.

[86] Fujiwara, Y.; Dixon, J.A.; O'Hara, F.; Funder, E.D.; Dixon, D.D.; Rodriguez, R.A.; Baxter, R.D.; Herlé, B.; Sach, N.; Collins, M.R.; Ishihara, Y.; Baran, P.S. *Nature*, **2012**, *492*, 95-99.

[87] Molander, G.A.; Colombel, V.; Braz, V.S. *Org. Lett.* **2011**, *13*, 1852-1855.

[88] Zard, S.Z.; *Chem. Soc. Rev.* **2008**, *37*, 1603-1618.

[89] Allen, L.J.; Cabrera, P.J.; Lee, M.; Sanford, M.S. *J. Am. Chem. Soc.* **2014**, *136*, 5607-5610.

[90] Quin, Q.; Yu, S. *Org. Lett.* **2014**, *16*, 3504-3507.

[91] Song, L.; Zang, L.; Luo, S.; Cheng, J-P. *Chem. Eur. J.* **2014**, *20*, 14231-14234.

[92] Kim, H.; Kim, T.; Lee, D.G.; Roh, S.W.; Lee, C. *Chem. Comm.* **2014**, *50*, 9273-9276.

[93] Cecere, G.; König, C.M.; Alleva, J.L.; MacMillan, D.W.C. *J. Am. Chem. Soc.* **2013**, *135*, 11521-11524.

[94] Davies, J.; Booth, S.G.; Essafi, S.; Dryfe, R.A.W.; Leonori, D. *Angew. Chem. Int. Ed.* **2015**, *54*, 14017-14021.

[95] Davies, J.; Svejstrup, T.D.; Reina, D.F.; Sheikh, N.S.; Leonori, D. *J. Am. Chem. Soc.* **2016**, *138*, 8092-8095.

[96] Davies, J.; Sheikh, N.S.; Leonori, D. *Angew. Chem. Int. Ed.* **2017**, *56*, 13361-13365.

[97] Jiang, H.; Studer, A. *Angew. Chem. Int. Ed.* **2017**, *56*, 12273-12276.

[98] Zhu, Q.; Gentry, E.C.; Knowles, R.R. *Angew. Chem. Int. Ed.* **2016**, *55*, 9969-9973.

[99] Gentry, E.C.; Rono, L.J.; Hale, M.E.; Matsuura, R.; Knowles, R.R. *J. Am. Chem. Soc.* **2018**, *140*, 3394-3402.

[100] Nonoyama, M. *Bull. Chem. Soc. Jpn.* **1974**, *47*, 767-768.

[101] King, K.A.; Watts, R.J. *J. Am. Chem. Soc.* **1986**, *109*, 1589-1590.

[102] Konno, H..; Sasaki, Y. *Chem. Lett.* **2003**, *32*, 252-253.

[103] Davies, D.L.; Lowe, M.P.; Ryder, K.S.; Singh, K.; Singh, S. *Dalton Trans.* **2011**, *40*, 1028-1030.

[104] Lowry, M.S.; Goldsmith, J.I.; Slinker, J.D.; Rohl, R.; Pascal, R.A.; Malliaras, G.G.; Bernhard, S. *Chem. Mater.* **2005**, *17*, 5712-5719.

[105] Henwood, A.F.; Zysman-Coleman, E. *Chem. Comm.* **2017**, *53*, 807-826.

[106] Hayes, B. L. Microwave Synthesis: Chemistry at the Speed of Light; CEM Publishing: Matthews, NC, 2002.

[107] Singh, A., Teegardin, K., Kelly, M., Prasad, K.S., Krishnan, S., Weaver, J.D. *J. Organomet. Chem.* **2015**, *776*, 51-59.

[108] United Nations: Climate Change. Kyoto Protocol. http://unfccc.int/kyoto_protocol/items/2830.php (accessed Mar 20, 2018).

[109] Bajpai, P. Structure of Lignocellulosic Biomass. In: *Pretreatment of Lignocellulosic Biomass for Biofuel Production.* SpringerBriefs in Molecular Science. Springer: Singapore, 2016.

[110] Holladay, J.E.; White, J.F.; Bozell, J.J.; Johnson, D. Top Value-Added Chemicals from Biomass: Volume II–Results of Screening for Potential Candidates from Biorefinery Lignin. Pacific Northwest National Laboratory. PNNL-16983; Department of Commerce: Springfield, 2007; 1-77.

[111] Budzinski, M.; Nitzsche, R. *Bioresource Tech.* **2016**, *216*, 613-621.

[112] Ragauskas, A.J.; Williams, C.K.; Davison, B.H.; Britovsek, G.; Cairney, J.; Eckert, C.A.; Frederick Jr., W.J.; Hallett, J.P.; Leak, D.J.; Liotta, C.L.; Mielenz, J.R.; Murphy, R.; Templer, R.; Tschaplinski, T. *Science*, **2006**, *27*, 484-489.

[113] Kamm, B.; Kamm, M. *Appl. Microbiol. Biotechnol.* **2004**, *64*, 137-145.

[114] Tyson, K.S.; Bozell, J.; Wallace, R.; Petersen, E.; Moens, L. Biomass Oil Analysis: Research Needs and Recommendations. NREL/TP-510-34796; Department of Commerce: Springfield, 2004; 1-87.

[115] Fernando, S.; Adhikari, S.; Chandrapal, C.; Murali, N. *Energy & Fuel* **2006**, *20*, 1727-1737.

[116] Cheali, P.; Posada, J.A.; Gernaey, K.V.; Sin, G. *Biofuel Bioprod. Bioref.* **2016**, *10*, 435-445.

[117] Fernando, S.; Adhikari, S.; Chandrapal, C.; Murali, N. *Energy & Fuel* **2006**, *20*, 1727-1737.

[118] Perlack, R.D.; Wright, L.L.; Turhollow, A.F.; Graphm, R.L.; Stokes, B.J.; Erbach, D.C. A Bioenergy and bioproducts industry: the technical feasibility of a billion-ton annual supply. DOE/GO-102005-2135; Department of Commerce: Springfield, 2005; 1-38.

[119] Zakzeski, J.; Bruijnincz, P.C.A.; Jongerius, N.A.; Weckhuysen, B.M. *Chem. Rev.* **2010**, *110*, 3552-3599.

[120] Gierer, J. *Wood Sci. Technol.* **1980**, *14*, 241-266.

[121] Zhu, J.Y.; Pan, X.J.; Wang, G.S.; Gleisner, R. *Bioresour Technol.* **2009**, *100*, 2411-2418.

[122] Zhu, J.Y.; Pan, X.J.; Wang, G.S.; Gleisner, R. *Bioresource Tech.* **2009**, *100*, 2411-2418.

[123] Boerjan, W.; Ralph, J.; Baucher, M. *Ann. Rev. Plant Biol.* **2003**, *54*, 519-543.

[124] Kärkäs, M.D.; Matsuura, B.S.; Monos, T.M.; Magallanes, G.; Stephenson, C.R.J. *Org. Biomol. Chem.* **2016**, *14*, 1853-1914.

[125] Deuss, P.J.; Barta, K.B. *Coord. Chem. Rev.* **2016**, *306*, 510-532.

[126] Sun, Z.; Fridrich, B.; de Santi, A.; Elangovan, S.; Barta, K. *Chem. Rev.* **2018**, *118*, 614-678.

[127] Li, C.; Zhao, X.; Wang, A.; Huber, G.W.; Zhang, T. *Chem. Rev.* **2015**, *115*, 11559-11624.

[128] Tien, M.; Kirk, T.K.; *Proc. Natl. Acad. Sci. U.S.A.* **1984**, *3*, 1612-1616.

[129] Meunier, B. *Chem. Rev.* **1992**, 92, 1411-1456.

[130] Huynh, V-B. *Biochem. Biophys. Res. Commun.* **1986**, *139*, 1104-1110.

[131] Specific to pinacol dimers: Davis, H.F.; Das, P.K.; Reichel, L.W.; Griffin, G.W. *J. Am. Chem. Soc.* **1984**, *106*, 6968-6973.

[132] Directly analogous to photochemical electron transfer: Nave, P.M.; Trahanovsky, W.S. *J. Am. Chem. Soc.* **1971**, *93*, 4536-4540.

[133] Pardini, V.L.; Smith, C.Z.; Utley, J.H.P.; Vargas, R.R.; Viertler, H. *J. Org. Chem.* **1991**, *56*, 7305-7313.

[134] Pardini, V.L.; Vargas, R.R.; Viertler, H. *Tetrahedron,* **1992**, *48*, 7221-7228.

[135] Cho, D.W.; Parthasarathi, R.; Pimentel, A.S.; Maestas, G.D.; Park, H.J.; Yoon, U.C.; Dunaway-Mariano, D.; Gnanakaran, S.; Langan, P.; Mariano, P.S. *J. Org. Chem.* **2010**, *75*, 6549-6562.

[136] Cho, D.W.; Latham, J.A.; Park, H.J.; Yoon, U.C.; Langan, P.; Dunaway-Mariano, D.; Mariano, P.S. *J. Org. Chem.* **2011**, *76*, 2840-2852.

[137] Popielarz, R.; Arnold, D.R.; *J. Am. Chem. Soc.* **1990**, *112*, 3068-3082.

[138] Biannic, B.; Bozell, J.J. *Org. Lett.* **2013**, *15*, 2730-2733.

[139] Bozell, J.J.; Hames, B.R.; Dimmel, D.R. *J. Org. Chem.* **1995**, *60*, 2398-2404.

[140] Mulder, P.; Saastad, O.W.; Griller, D. *J. Am. Chem. Soc.* **1988**, *110*, 4090-4092.

[141] Alternative hypothesis of direct Co binding to increase the population of the Co(III)OO• complex was disproven in: Cedeno, D.; Bozell, J.J. *Tetrahedron Lett.* **2012**, *53*, 2380-2383.

[142] Sedai, B.; Díaz-Urrutia, C.; Baker, R.T.; Wu, R.; Silks, L.A.; Hanson, S.K. *ACS Catal.* **2011**, *1*, 794-804.

[143] Hanson, S.K.; Wu, R.; Silks, L.A. *Angew. Chem. Int. Ed.* **2012**, *51*, 3410-3413.

[144] γ hydroxy refers to the canocial lignin nomenclature, where the benzylic position is the β carbon, and the homobenzylic position is the γ carbon.

[145] Son, S.; Toste, F.D. *Angew. Chem. Int. Ed.* **2010**, *49*, 3791-3794.

[146] Chan, J.M.W.; Bauer, S.; Sorek, Sreekumar, S.; Wang, K.; Toste, F.D. *ACS Catal.* **2013**, *3*, 1369-1377.

[147] Nichols, J.M.; Bishop, L.M.; Bergman, R.G.; Ellman, J.A. *J. Am. Chem. Soc.* **2010**, *132*, 12554-12555.

[148] Wu, A.; Patrick, B.O.; Chung, E.; James, B.R. *Dalton Trans.* **2012**, *41*, 11093-11106.

[149] Galkin, M.V.; Samec, J.S.M. *ChemSusChem* **2014**, *7*, 2154-2158.

[150] Zhou, X.; Mitra, J.; Rauchfuss, T.B. *ChemSusChem* **2014**, *7*, 1623-1626.

[151] Hoover, J.M.; Steves, J.E.; Stahl, S.S. *Nat. Protoc.* **2012**, *7*, 1161-1166/

[152] Rahimi, A.; Azarpira, A.; Kim, H.; Ralph, J.; Stahl, S.S. *J. Am. Chem. Soc.* **2013**, *135*, 6415-6418. And the references therein.

[153] Bobbitt, J.M.; *J. Org. Chem.* **1998**, *63*, 9367-9374.

[154] Mercadante, M.A.; Kelly, C.B.; Bobbitt, J.M.; Tilley, L.J.; Leadbeater, N.E. *Nat. Protoc.* **2013**, *8*, 666-676.

[155] Rahimi, A.; Ulbrich, A.; Coon, J.J.; Stahl, S.S. *Nature* **2014**, *515*, 249-252.

[156] Das, A.; Rahimi, A.; Ulbrich, A.; Alherech, M.; Motagamwala, A.H.; Bhalla, A.; DaCosta Sousa, L.; Balan, V.; Dumesic, J.A.; Hegg, E.L.; Dale, B.E.; Ralph, J.; Coon, J.J.; Stahl, S.S. *ACS Sustainable Chem. Eng.* **2018**, *6*, 3367-3374.

[157] Wenkert, E.; Michelotti, E.L.; Swindell, C.S. *J. Am. Chem. Soc.* **1979**, *101*, 2246-2247.

[158] Dankwardt, J.W. *Angew. Chem. Int. Ed.* **2004**, *43*, 2428-2432.

[159] Kelley, P.; Lin, S.; Edouard, G.; Day, M.W.; Agapie, T. *J. Am. Chem. Soc.* **2012**, *134*, 5480-5483.

[160] Álvarez-Bercedo, P.; Martin, R.; *J. Am. Chem. Soc.* **2010**, *132*, 17352-17353.

[161] Cornella, J.; Gómez-Bengoa, E.; Martin, R. *J. Am. Chem. Soc.* **2013**, *135*, 1997-2009.

[162] Sergeev, A.G.; Hartwig, J.F. *Science* **2011**, *332*, 439-443.

[163] Sergeev, A.G.; Webb, J.D.; Hartwig, J.F. *J. Am. Chem. Soc.* **2012**, *134*, 20226-20229.

[164] Saper, N.I.; Hartwig, J.F. *J. Am. Chem. Soc.* **2017**, *139*, 17667-17676.

[165] The original measurement was –2.27 to –2.34 V. Experimental conditions: epoxide [0.005 M] in DMF, [0.1] M Bu4NClO4, reference electrode 0.1 M Ag/AgI/0.1 M I^-, hanging mercury drop working electrode. AgI/Ag + I^- = –0.152 vs. SHE. Boujlel, K.; Simonet, J. *Electrochimica Acta*. **1979**, *24*, 481–487.

[166] The original measurement reported was –2.10 V vs. SCE. Experimental conditions: 0.1 M tetraethylammonium perchlorate supporting electrolyte in acetonitrile at 20 °C. Ag/AgCl (–0.042 V vs SCE) reference electrode, mercury hanging drop working electrode. Martens, F. M.; Verhoeven, J.W.; Gase, R.A.; Pandit, U.K.; De Boer, TH.J. *Tetrahedron*, **1978**, *34*, 443-446.

[167] Fukuzumi, K.; Ishikawa, K.; Hironaka, T.; Tanaka, T. *J. Chem. Soc., Perkin Trans. 2* **1987**, *0*, 751-760.

[168] Fukuzumi, S.; Mochizuki, S.; Tanaka, T. *J. Phys. Chem.* **1990**, *94*, 722-726.

[169] Hasegawa, E.; Takizawa, S.; Seida, T.; Yamaguchi, A.; Yamaguchi, N.; Chiba, N.; Takahashi, T.; Ikeda, H.; Akiyama, K. *Tetrahedron*, **2006**, *62*, 6581-6588.

[170] Larraufie, M-H.; Pellet, T.; Fensterbank, L.; Goddard, J-P.; Lacôte, E.; Malacria, M.; Ollivier, C. *Angew. Chem. Int. Ed.* **2011**, *50*, 4463-4466.

[171] Tarantino, K.T.; Knowles, R.R. *J. Am. Chem. Soc.* **2013**, *135*, 10022-10025.

[172] Rono, L.J.; Yayla, H.G.; Wang, D.Y.; Armstrong, M.F.; Knowles, R.R. *J. Am. Chem. Soc.* **2013**, *135*, 17735-17738.

[173] Kim, S.; Chmely, S.C.; Minlos, M.R.; Bomble, Y.J.; Foust, T.D.; Paton, R.S.; Beckham, G.T. *J. Phys. Chem. Lett.* **2011**, *2*, 2846-2852.

[174] Nguyen, J.D.; Matsuura, B.S.; Stephenson, C.R.J. *J. Am. Chem. Soc.* **2014**, *136*, 1218-1221.

[175] Nakajima, M.; Fava, E.; Loescher, S.; Jiang, Z.; Rueping, M. *Angew. Chem. Int. Ed.* **2015**, *54*, 8828-8832.

[176] Monos, T.M.; Magallanes, G.; Sebren, L.J.; Stephenson, C.R.J. *J. Photochem. Photobio. A* **2016**, *328*, 240-248.

[177] Bosque, I.; Magallanes, G.; Rigoulet, M.; Kärkäs, M.D.; Stephenson, C.R.J. *ACS Cent. Sci.* **2017**, *3*, 621-628.

[178] Kärkäs, M.D.; Bosque, I.; Matsuura, B.S.; Stephenson, C.R.J. *Org. Lett.* **2016**, *18*, 5166-5169.

[179] Wu, A.; Patrick, B. O.; Chung, E.; James, B. R. *Dalton Trans.* **2012**, *41*, 11093–11106.

[180] Nguyen, J. D.; Matsuura, B. S.; Stephenson, C. R. J. *J. Am. Chem. Soc.* **2014**, *136*, 1218–1221.

[181] Hanson, S. K.; Wu, R.; Silks, L. A. *Angew. Chem. Int. Ed.* **2012**, *51*, 3410–3413.

[182] Nichols, J. M.; Bishop, L. M.; Bergman, R. G.; Ellman, J. A. *J. Am. Chem. Soc.* **2010**, *132*, 12554–12555.

[183] Tang, G.; Ji, T.; Hu, A.-F.; Zhao, Y.-F. *Synlett* **2008**, *2008*, 1907–1909.

[184] Tayama, E.; Yanaki, T.; Iwamoto, H.; Hasegawa, E. *Eur. J. Org. Chem.* **2010**, *2010*, 6719–6721.

[185] Bastug, G.; Dierick, S.; Lebreux, F.; Markó, I. E. *Org. Lett.* **2012**, *14*, 1306–1309.

[186] Teo, Y.-C.; Yong, F.-F.; Ithnin, I. K.; Yio, S.-H. T.; Lin, Z. *Eur. J. Org. Chem.* **2013**, *2013*, 515–524.

[187] Arisawa, M.; Suwa, K.; Yamaguchi, M. *Org. Lett.* **2009**, *11* (3), 625–627.

[188] Kumar, R.; Sharma, N.; Sharma, U. K.; Shard, A.; Sinha, A. K. *Adv. Synth. Catal.* **2012**, *354*, 2107–2112.

[189] Moriyama, K.; Takemura, M.; Togo, H. *Org. Lett.* **2012**, *14*, 2414-2417.

[190] Banfield, S. C.; Omori, A. T.; Leisch, H.; Hudlicky, T. *J. Org. Chem.* **2007**, *72*, 4989–4992.

[191] Rodriguez-Ruiz, V.; Carlino, R.; Bezzenine-Lafolée, S.; Gil, R.; Prim, D.; Schulz, E.; Hannedouche, J. *Dalton Trans.* **2015**, *44*, 12029-12059.

[192] Beller, M.; Seayad, J.; Tillack, A.; Jiao, H. *Angew. Chem. Int. Ed.* **2004**, *43*, 3368-3398.

[193] Zeng, X. *Chem. Rev.* **2013**, *113*, 6864-6900.

[194] Zhang, A.; Neumeyer, J.L.; Baldessarini, R.J. *Chem. Rev.* **2007**, *107*, 274-302.

[195] Muci, A.R.; Buchwald, S.L.; *Top. Curr. Chem.* **2002**, *291*, 131-209.

[196] Hartwig, J.F. *Pure Appl Chem.* **1999**, *71*, 1417-1423.

[197] Early example of Pd mediated C–N bond formation: Billaneuva, LA.; Abboud, K.A.; Boncella, J.M. **1992**, *11*, 2963-2965.

[198] Ney, J.E.; Wolfe, J.P. *Angew. Chem. Int. Ed.* **2004**, *43*, 3605-3608.

[199] Full organometallic investigation of the *syn*-aminopalladation process was disclosed in: Neukom, J.D.; Perch, N.S.; Wolfe, J.P. *Organometallics,* **2011**, *30*, 1269-1277.

[200] Lira, R.; Wolfe, J.P. *J. Am. Chem. Soc.* **2004**, *126*, 13906-13907.

[201] Yang, Q.; Ney, J.E.; Wolfe, J.P. *J. Am. Chem. Soc.* **2005**, *7*, 2575-2578.

[202] Bertrand, M.B.; Leathen, M. L.; Wolfe, J.P. *Org. Lett.* **2007**, *9*, 457-460.

[203] Ney, J.E.; Wolfe, J.P. *J. Am. Chem. Soc.* **2005**, *127*, 8644-8651.

[204] Wolfe, J.P. *Synlett* **2008**, *19*, 2913-2937.

[205] Mai, D.N.; Wolfe, J.P. *J. Am. Chem. Soc.* **2010**, *132*, 12157-12159.

[206] Fornwald, R.M.; Fritz, J.A.; Wolfe, J.P. *Angew. Chem. Int. Ed.* **2014**, *20*, 8782-8790.

[207] White, D.R.; Hutt, J.T.; Wolfe, J.P. *J. Am. Chem. Soc.* **2015**, *137*, 11246-11249.

[208] Sibbald, P.A.; Rosewall, C.F.; Swartz, R.D.; Michael, F.E. *J. Am. Chem. Soc.* **2009**, *131*, 15945-15951.

[209] Liu, Z.; Wang, Y.; Wang, Z.; Zeng, T.; Liu, P.; Engle, K. M. *J. Am. Chem. Soc.* **2017**, *139*, 11261-11270.

[210] Zaitsev, V.G.; Shabashov, D.; Dauglis, O. *J. Am. Chem. Soc.* **2005**, *127*, 13154-13155.

[211]Gurak, J. A., Jr.; Yang, K. S.; Liu, Z.; Engle, K. M. *J. Am. Chem. Soc*. **2016**, *138*, 5805–5808.

[212] O'Duill, M. L.; Matsuura, R.; Wang, Y.; Turnbull, J. L.; Gurak, J. A., Jr.; Gao, D.-W.; Lu, G.; Liu, P.; Engle, K. M. *J. Am. Chem. Soc*. **2017**, *139*, 15576–15579.

[213] Derosa, J.; Tran, V. T.; Boulous, M. N.; Chen, J. S.; Engle, K. M. *J. Am. Chem. Soc.* **2017**, *139*, 10657–10660.

[214] Liu, Z.; Derosa, J.; Engle, K. M. *J. Am. Chem. Soc*. **2016**, *138*, 13076–13081.

[215] Tasker, S.Z.; Jamison, T.F. *J. Am. Chem. Soc.* **2015**, *137*, 9531-9534.

[216] Twilton, J.; Le, C.; Zhang, P.; Shaw, M.H.; Evans, R.W.; MacMillan, D.W.C. *Nature Rev.* **2017**, 0052.

[217] Larock, R.C.; Berrios-Peña, N.; Narayanan, K. *J. Org. Chem.* **1990**, *55*, 3447-3450.

[218] Zeng, W.; Chemler, S.R. *J. Am. Chem. Soc.* **2007**, *129*, 12948-12949.

[219] Liwosz, T. W.; Chemler, S.R.; *J. Am. Chem. Soc.* **2012**, *134*, 2020-2023.

[220] Paderes, M.C.; Keister, J.B.; Chemler, S.R.; *J. Org. Chem.* **2013**, *78*, 506-515.

[221] Wang, D.; Wu, L.; Wang, F.; Wan, X.; Chen, P.; Lin, Z.; Liu, G. *J. Am. Chem. Soc.* **2017**, *139*, 6811-6814.

[222] Brezovich, W.E.; Benitez, D.; Lackner, A.D.; Shunatona, H.P.; Tkatchouk, E.; Goddard III, W.A.; Toste, F.D. *Angew. Chem. Int. Ed.* **2010**, *49*, 5519-552.

[223] Hamilton, G.L.; Kang, E.J.; Mba, M.; Toste, F.D. *Science* **2007**, *317*, 496-499.

[224] Widenhoefer, R.A.; Ha, X. *Eur. J. Org. Chem.* **2006**, 4555-4563.

[225] Tkatchouk, E.; Mankad, N.P.; Benitez, D.; Goddard III, W.A.; Toste, F.D. *J. Am. Chem. Soc.* **2011**, *133*, 14293-14300.

[226] Zhang, G.; Peng, Y.; Cui, L.; Zhang, L. *Angew. Chem. Int. Ed.* **2009**, *48*, 3112-3115.

[227] Helhado, A.D.; Brenzovich Jr., W.E.; Lackner, A.D.; Toste, F.D. *J. Am. Chem. Soc.* **2010**, *132*, 8885-8887.

[228] Kindt, S.; Heinrich, M.R. *Synthesis* **2016**, *48*, 1597-1606.

[229] Hari, D.P.; Hering, T.; König, B. *Angew. Chem. Int. Ed.* **2014**, *53*, 725-728.

[230] Sahoo, B.; Hopkinson, M.N.; Glorius, F. *J. Am. Chem. Soc.* **2013**, *135*, 5505-5508.

[231] Kärkäs, M. D. *ACS Catal.* **2017**, *7*, 4999-5022.

[232] Zard, S.Z. *Chem. Soc. Rev.* **2008**, *37*, 1603-1618.

[233] Gentry, E. C.; Knowles, R. R. *Acc. Chem. Res.* **2016**, *49*, 1546–1556.

[234] Choi, G.J.; Knowles, R.R. *J. Am. Chem. Soc.* **2015**, *137*, 9226-9229.

[235] Miller, D.C.; Choi, G.J.; Orbe, H.S.; Knowles, R.R. *J. Am. Chem. Soc.* **2015**, *137*, 13492-13495.

[236] Musacchio, A.J.; Lainhart, B.C.; Zhang, Z. Naguib, S.G.; Sherwood, T.C.; Knowles, R.R. *Science*, **2017**, *355*, 727-730.

[237] Zhu, Q.; Graff, D.E.; Knowles, R.R. *J. Am. Chem. Soc.* **2018**, *140*, 741-747.

[238] Nicewicz, D.A.; Hamilton, D.S. *Synlett* **2014**, 1191-1196.

[239] Fukuzumi, S.; Ohkubo, K.; Suenobu, T.; Kato, K.; Fujitsuka, M.; Ito, O. *J. Am. Chem. Soc*. **2001**, *123*, 8459-8467.

[240] Romero, N.A.; Nicewicz, D.A. *Chem. Rev.* **2016**, *116*, 10075-10166.

[241] Margrey, K. A.; Nicewicz, D. A. *Acc. Chem. Res.* **2016**, 49, 1997-2006.

[242] Romero, N.A.; Nicewicz, D.A. *J. Am. Chem. Soc.* **2014**, *136*, 17024-17035.

[243] Piou, T.; Rovis, T. *Nature* **2015**, *527*, 86-90.

[244] Douglas, J.J.; Albright, H.; Sevrin, M.J.; Cole, K.P.; Stephenson, C.R.J. *Angew. Chem. Int. Ed.* **2015**, *54*, 14898-14902.

[245] Douglas, J.J.; Sevrin, M.J.; Cole, K.P.; Stephenson, C.R.J. *Org. Proc. Res. Dev.* **2016**, *20*, 1148-1155.

[246] Plesniak, K.; Zarecki, A.; Wicha, J. *Top. Curr. Chem*. **2007**, *275*, 163–250.

[247] Truce, W.E.; Raw, W.J.; Norman, O. Eickemeyer, D.B. *J. Am. Chem. Soc.* **1958**, *80*, 3625-3629.

[248] Motherwell, W.B.; Pennell, A.M.K. *J. Chem. Soc. Chem. Commun.* **1991**, *13*, 877-879.

[249] Snape, T.J. *Chem. Soc. Rev.* **2008**, *37*, 2452-2458.

[250] Holden, C.M.; Greaney, M.F. *Chem. Eur. J.* **2019**, *23*, 8992-9008.

[251] Motherwell, W.B.; Vázquez, S. *Tetrahedron Lett.* **2000**, *41*, 9667-9671.

[252] Bacqué, E.; Qacemi, M.E.; Zard, S.Z. *Org. Lett*. **2005**, *7*, 3817-3820.

[253] Kong, W.; Casimiro, M.; Merino, E.; Nevado, C. *J. Am. Chem. Soc*. **2013**, *135*, 14480-14483.

[254] Kong, W.; Merino, E.; Nevado, C. *Angew. Chem. Int. Ed*. **2014**, *53*, 5078-5082.

[255] Fuentes, N.; Kong, W.; Fernández-Sánchez, L.; Merino, E.; Nevado, C. *J. Am. Chem. Soc.* **2015**, *137*, 14480-14483.

[256] Kong, W.; Fuentes, N.; García-Domínguez, A.; Merino, E.; Nevado, C. *Angew. Chem. Int. Ed.*, **2015**, *54*, 2487-2491.

[257] Brachet, E.; Marzo, L.; Selkti, M.; König, M.; Belmont, P. *Chem. Sci.* **2016**, *7*, 5002-5006.

[258] Fukazawa, Y; Kato, N. Itô, S. *Tetrahedron Lett*. **1982**, *4*, 437-438.

[259] Studer, A.; Bossart, M. *Tetrahedron* **2001**, *57*, 9649-9667.

[260] Chen, Z.-M.; Zhang, X.-M.; Tu, Y.-Q. *Chem. Soc. Rev*. **2015**, *44*, 5220–5245.

[261] Amii, H.; Kondo, S.; Uneyama, K. *Chem. Comm.* **1998**, 1844-1846.

[262] DeBaillie, A.C.; Jones, C.D.; Magnus, N.A.; Mateos, C.; Torrado, A.; Wepsiec, J.P.; Tokala, R.; Raje, P. *Org. Process Res. Dev.* **2015**, *19*, 1568-1575.

[263] Wang, L.; Wu, F.; Chen, J.; Nicewicz, D.A.; Huang, Y. *Angew. Chem. Int. Ed.* **2017**, *56*, 6896-6900.

[264] Johnston, L.J.; Schepp, N.P. *J. Am. Chem. Soc.* **1993**, *115*, 6564-6571.

[265] Schepp, N.P.; Johnston, L.J. *J. Am. Chem. Soc.* **1996**, *118*, 2872-2881.

[266] Monos, T.M.; Sun, A.C.; McAtee, R.C.; Devery, J.J.; Stephenson, C.R.J. *J. Org. Chem.* **2016**, *81*, 6988-6994.

[267] Choi, G.J. ; Zhu, Z. ; Miller, D.C. ; Gu, C.J. ; Knowles, R.R. *Nature*, **2016**, *239*, 268-271.

[268] Tallineau, J.; Bashiardes, G.; Coustard, J.-M.; Lecournué, F. Synlett, **2009**, *17*, 2761-2764.

[269] Tarantino, K.T.; Liu, P.; Knowles, R.R. *J. Am. Chem. Soc.* **2013**, *135*, 10022−10025.

[270] Fluorine in Pharmaceutical and Medicinal Chemistry: From Biophysical Aspects to Clinical Applications; Gouverneur, V., Müller, K., Eds.; ICP: London, 2011.

[271] O'Hagan, D.; *Chem. Soc. Rev.* **2008**, *37*, 308-319.

[272] Mascitti, V.; Stevens, B. D.; Choi, C.; McClure, K. F.; Guimarães, C. R. W.; Farley, K. A.; Munchhof, M. J.; Robinson, R. P.; Futatsugi, K.;Lavergne, S. Y.; Lefker, B.; Cornelius, A. P.; Bonin, P. D.; Kalgutkar, A.S.; Sharma, R.; Chen, Y. *Bioorg. Med. Chem. Lett*. **2011**, *21*, 1306−1309.

[273] Zhu, W.; Wang, J.; Wang, S.; Gu, Z.; Aceña, J.L.; Izawa, K.; Liu, H.; Soloshonok, V.A. *J. Fluor. Chem.* **2014**, *167*, 37-54.

[274] Cernak, T.;Dykstra, K. D.; Tyagarajan, S.; Vachal, P.; Krska, S. W. *Chem. Soc. Rev*. **2016**, *45*, 546-576.

[275] Swarts, F.; *Bull. Acad. Roy. Belg.* **1892**, *24*, 474.

[276] Schlosser, M. *Angew. Chem. Int. Ed.* **2006**,*45*, 5432-5446.

[277] Alonso, C.; Martínez de Marigorta, E.; Rubiales, G.; Palacios, F. *Chem. Rev.* **2015**, *115*, 1847-1935.

[278] Banks, R. E. *J. Fluorine Chem*. **1994**, *67*, 193–203.

[279] Ni, C.; Hu, J. *Synthesis* **2014**, *46*, 0842-0863.

[280] Simons, J.H.; Francis, H.T.; Hogg, J.A. *J. Electrochem. Soc.* **1949**, *95*, 53-55.

[281] Mazloomi, Z.; Bansode, A.; Benavente, P.; Lishchynskyi, A.; Urakawa, A.; Grushin, V.V. *Org. Process. Res. Dev.* **2014**, *18*, 1020-1026.

[282] Geri, J.B.; Szymczak, N.K. *J. Am. Chem. Soc.* **2017**, *139*, 9811-9814.

[283] McCulloch, A.; Lindley, A.A. *Atmospheric Environment* **2007**, *41*, 1560-1566.

[284] Shono, T.; Ishifune, M.; Okada, T.; Kashimura, S. *J. Org. Chem.* **1991**, *56*, 2-4.

[285] Langlois, B.R.; Billard, T. *Synthesis*, **2003**, *2*, 185-194.

[286] Prakash, G.K.S.; Jog, P.V.; Batamack, P.T.D.; Olah, G.A. *Science* **2012**, *338*, 1324-1327.

[287] Milne, J.B.; Parker, T.J. *J. Sol. Chem.* **1981**, *10*, 479-487.

[288] Dolbier, W. R. Jr. *Chem. Rev.* **1996**, *96*, 1557–1584.

[289] Matsui, K.; Tobita, E.; Ando, M.; Kondo, K. *Chem. Lett.* **1981**, *12*, 1719-1720.

[290] Chen, M.; Buchwald, S.L. *Angew. Chem. Int. Ed.* **2013**, *52*, 11628-11631.

[291] Shi, G.; Shao, C.; Pan, S.; Yu, J.; Zhang, Y. *Org. Lett.* **2015**, *17*, 38-41.

[292] Tanabe, Y.; Matsuo, N.; Ohno, N. *J. Org. Chem.* **1988**, *53*, 4582-4585.

[293] Haszeldine, R.N. *J. Chem. Soc.* **1949**, *0*, 2856-2861.

[294] Nagib, D.A.; Scott, M.E.; MacMillan, D.W.C. *J. Am. Chem. Soc.* **2009**, *131*, 10875-10877.

[295] Nagib, D.A.; MacMillan, D.W.C. *Nature* **2011**, *480*, 224-228.

[296] Wilger, D.J.; Gesmundo, N.J.; Nicewicz, D.A. *Chem. Sci.* **2013**, *4*, 3160-3165.

[297] Li, L.; Mu, X.; Liu, W.; Wang, Y.; Mi, Z.; Li, C–J. *J. Am. Chem. Soc.* **2016**, *138*, 5809-5812.

[298] Liu, P.; Liu, W.; Li, C–J. *J. Am. Chem. Soc.* **2017**, *139*, 14315-14321.

[299] Nguyen, J.D.; Tucker, J.W.; Konieczynska, M.D.; Stephenson, C.R.J. *J. Am. Chem. Soc.* **2011**, *133*, 4160-4163.

[300] Wallentin, C–J.; Nguyen, J.D.; Finkbeiner, P.; Stephenson, C.R.J. *J. Am. Chem. Soc.* **2012**,*134*, 8875-8884.

[301] Yasu, Y.; Koike, T.; Akita, M.; *Angew. Chem. Int. Ed.* **2012**, *51*, 9567-9571.

[302] Yasu, Y.; Koike, T.; Akita, M.; *Org. Lett.* **2013**, *15*, 2136-2139.

[303] Tomita, R.; Yasu, Y.; Koike, T.; Akita, M. *Angew. Chem. Int. Ed.* **2014** ,*53*, 7144-7148.

[304] Lai, C.; Mallouk, T.E. *J. Chem. Soc., Chem. Commun.* **1993**, *0*, 1359-1361.

[305] Lin, J.; Li, Z.; Kan, Huang, S.; Su, W.; Li, Y. *Nature Comm.* **2016**, *8*, 14353.

[306] Beatty, J.W.; Douglas, J.J.; Cole, K.P.; Stephenson, C.R.J. *Nature Comm.* **2015**, *6*, 7179.

[307] Lorance, E.D.; Kramer, W.H.; Gould, I.R. *J. Am. Chem. Soc.* **2002**,*124*, 15225-15238.

[308] Lorance, E.D.; Kramer, W.H.; Gould, I.R. *J. Am. Chem. Soc.* **2004**, *126*,14071-14078.

[309] Beatty, J.W.; Douglas, J.J.; Miller, R.; McAtee, R.C.; Cole, K.P.; Stephenson, C.R.J. *Chem*, **1**, 456-472.

[310] Lee, K.Y.; Kochi, J.K. *J. Chem. Soc. Perkin. Trans. 2* **1992**, 1011-1017.

[311] Sladojevich, F.; McNeill, E.; Börgel, J.; Zheng, S-L.; Ritter, T. *Angew. Chem. Int. Ed.* **2015** , *54*, 3712-3716.

[312] Woodward, R.B. *J. Am. Chem. Soc.* **1942**, *64*, 3058-3059.

[313] Mulliken, R.S. *J. Am. Chem. Soc.* **1952**, *74*, 811-824.

[314] Lima, C.G.S.; Lima, T.M.; Duarte, M.; Jurberg, I.D.; Paixão M.W. *ACS Catalysis* **2016**, *6*, 1389-1407.

[315] Nappi, M.; Bergonzini, G.; Melchiorre, P. *Angew. Chem. Int. Ed.* **2014**,*53*, 4921-4925.

[316] Woźniak, Ł.; Murphy, J.; Melchiorre, P. *J. Am. Chem. Soc.* **2015**,*137*, 5678-5681.

[317] Kandukuri, S.R.; Bahamonde, A.; Chatterjee, Jurberg, I.D.; Escudero-Adán, Melchiorre, P. *Angew. Chem. Int. Ed.* **2015**, *54*, 1485-1489.

[318] Rosokha, S.V.; Kochi, J.K. *Acc. Chem. Res.* **2008**, *41*, 641-653.

[319] Filippini, G.; Nappi, M.; Melchiorre, P. *Tetrahedron*, **2015**, *71*. 4535-4542.

[320] Cheng, Y.; Yu, S. *Org. Lett.* **2016**, *18*. 2962-2965.

[321] Cheng, Y.; Yuan, X.; Ma, J.; Yu, S. *Chem. Eur. J.* **2015**, *21*, 8355-8359.

[322] Sun, X.; Wang, W.; Li, Y.; Ma, J.; Yu, S. *Org. Lett.* **2016**, *18*, 4638-4641.

[323] Pham, P.V.; Nagib, D.A.; MacMillan, D.W.C. *Angew. Chem. Int. Ed.* **2011**, *50*, 6199-6122.

[324] Pham, P.V.; Nagib, D.A.; MacMillan, D.W.C. *Angew. Chem. Int. Ed.* **2011**, *50*, 9232.

[325] Sankararaman, S.; Haney, W.A.; Kochi, J.K.; *J. Am. Chem. Soc.* **1987**, *109*, 7824–7838.

[326] Cho, D.W.; Lee, H-Y.; Oh, S.W.; Choi, J.H.; Park, H.J.; Mariano, P.S.; Yoon, U.C. *J. Org. Chem.* **2008**, *73*, 4539-4547.

[327] Nicewicz, D.A.; Nguyen, T.M. *ACS. Catalysis* **2014**, *4*, 355-360.

[328] Masuhara, H.; Mataga, N. *Acc. Chem. Res.* **1981**, *14*, 312-318.

[329] Gould, I.R.; Ege, D.; Moser, J.E.; Farid, S. *J. Am. Chem. Soc.* **1990**, *112*, 4290-4301.

[330] Bockman, T. M.; Lee, K.Y.; Kochi, J.K. *J. Chem. Soc., Perkin Trans. 2* **1992**, *0*, 1581-1594.

[331] Bravo, A.; Bjørsvik, H-R.; Fontana, F.; Liguori, L.; Mele, A.; Minisci, F. *J. Org. Chem.* **1997**, *62*, 7128-7136.

[332] Harper, K. C.; Abbvie Inc. Personal Communication, January 2018.

[333] Garlets, Z.J.; Nguyen, J.D.; Stephenson, C.R.J. *Isr. J. Org. Chem.* **2014**, *54*, 351-360.

[334] Hirose, K. *J. Inc. Phenom. Macro. Chem.* **2001**, *39*, 139-209.

[335] Job, P. *Justus Liebigs Ann. Chem*. **1928**, 9, 113

[336] Beatty, J.W. Redox Activation of C–C and C–H Bonds Using Visible Light. Ph.D. Dissertation, University of Michigan, Ann Arbor, MI, 2016.

[337] Photocatalyst functionalization as a result of redox activation has been characterized and thoughtfully analyzed in: Devery, J.J.III. Douglas, J.J.; Nguyen, J.D.; Cole, K.P.; Flowers, R.A.; Stephenson, C.R.J. *Chem. Sci.* **2015**, 6, 537-541.

[338] Xu, J.; Luo, D-F.; Xiao, B.; Liu, Z-J.; Gong, T-J.; Fu, Y.; Liu, L. *Chem. Comm.* **2011**, *47*, 4300-4302.

[339] Markovich, K.M.; Tantishaiyakul, V.; Hamada, A.; Miller, D.D.; Rostedt, K.J.; Shams, G.; Shin, Y.; Fraundorfer, P.F.; Doyle, K.; Feller, D.R. *J. Med. Chem.* **1992**, *35*, 466-479.

[340] Yayla, H.G.; Peng, F.; Magnion, I.K.; McLaughlin, M.; Campeau, L-C.; Davies, I.W.; DiRocco, D.A.; Knowles, R.R. *Chem. Sci.* **2016**, *7*, 2066-2073.

[341] Hatchard, C. G.; Parker, C.A. *Proc. Royal Soc. Lond. A* **1956**, *235*, 518-536.